Simulation and modelling of water spray in the 3D explosion simulation program FLACS

Elin Kristin Dale

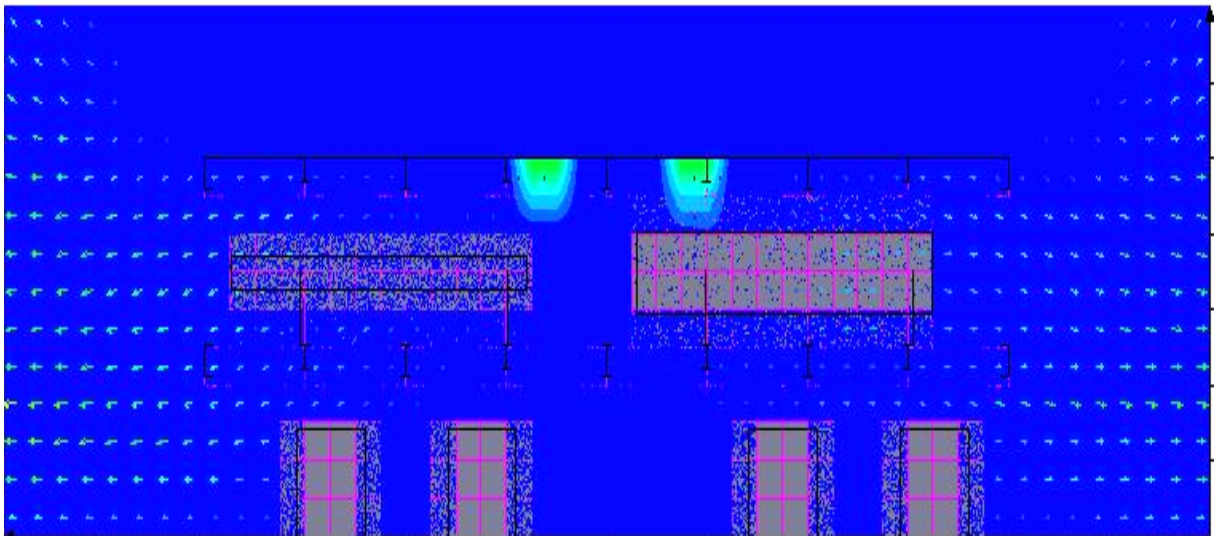

The University of Bergen
2004

1. Foreword

This report is submitted in the partial fulfilment of the requirements for a Master degree in process technology – safety technology at The University of Bergen. The theme for this report was established in cooperation with my instructor Bjørn Arntzen at UIB, and was proposed to Finn Roar Berg at Statoil. With his approval the study was mainly performed at Kårstø, Statoil Nord-Rogaland.

Several people have contributed with help to this study, and I would like to thank:

- Bjørn Artnzen at UIB/GexCon for guiding my work and giving professional and technical assistance.
- Finn Roar Berg at Kårstø for guiding my work and contributing with material and equipment.
- Kjetil Sverdrupsen at Kårstø who contributed with IT-assistance.
- Olav Roald Hansen at GexCon for lending me reports on experiments performed with gas explosions.
- Ole Jacob Tharadset at UIB/GexCon who gave me guidance in using the program FLACS.
- Joar Dalheim at DNV for sending me a copy of the Kårstø geometry, and for answering my questions about the technical report of Kårstø written by DNV [1].

Bergen, 20.november 2004

Elin Kristin Dale

2. Summary

In a gas processing plant and in offshore platforms a gas explosion could have serious consequences, and it is therefore essential to have mitigation systems that can prevent and/or reduce unwanted scenarios. One such mitigating technique that has proved to be effective is water spray and deluge systems. Since such systems often already are installed in most industries to use in a fire-situation, this has become an attractive method in fighting gas explosions. Experimental work has been done with the use of water spray, and the main results are that activation of water spray before an ignition can reduce rapid flame acceleration that otherwise could result in high-pressure build-up.

Because the consequences of a gas explosion depends on many different parameters, a numerical model was developed that could handle different scenarios and give good results. The model was named FLACS (FLame ACceleration Simulator), and is a tree-dimensional gas explosion and gas-dispersing tool. FLACS is a Computational Fluid Dynamics (CDF) code. FLACS 2.2.5 (2001) is the current version, where the water spray is defined by a simplified box-model that assumes uniform parameters inside each box area. This model doesn't include transport of droplets with the flow, reduction in burning velocity due to a temperature drop caused by the water spray, and turbulence and temperature changes due to break-up and evaporation of droplets. A new model, FLACS 2.2.6 (2004), is developed that takes into account the transport and break-up of droplets. An equation connecting the reduction in burning velocity to the amount of water spray over the amount of gas was therefore developed, and a setup file determining evaporation of droplets of different sizes was included to the model. This model is called FLACS 2.2.6*.

Results from the simulations show that water spray will have the best mitigating effect:

- In scenarios with sufficient ventilation openings and obstructions
- When it is activated at the accelerating phase of the explosion
- When the ignition occurs at the end of the cloud
- When not activated only near ignition

FLACS 2.2.5 does in most cases give a good representation of a real situation, but one weakness is that in scenarios where the water spray normally would be transported with the flow FLACS 2.2.5 has a tendency to under predicate the results.

FLACS 2.2.6* without the setup-file gives a good representation of the explosion pressure with the explosion box, but does in most cases over predicate the time of arrival. The tendencies are although the same as in the experiments. FLACS 2.2.6* with the setup-file over predicates both the explosion pressure and the time of arrival. The deviations are probably because the flow doesn't reach high enough values to fulfil the critical droplet velocity, and the evaporation and extraction of energy is thereby not effective. With the M24-25 module the results with the setup-file gives much better results. In this geometry the flow propagates over a larger distance, and thereby the break-up and evaporation of droplets will influence the results. A general source to deviation in the results is that the water spray is also exiting the nozzle as a narrow jet instead of a broad cone, as it would do in real life, and the lack of initial water spray turbulence gives a over predication in the time of arrival.

A report written by DNV concerning a detailed probabilistic explosion analysis at Kårstø states that due to the high explosion loads that is calculated, it is recommended to consider mitigating measures [1]. Explosion simulations performed with the Kårstø geometry show

that the explosion pressure is significantly reduced when water spray is activated at gas detection, if the water spray is located far from ignition or over a large area.

The formation of a large flammable gas cloud and the spreading of gas to other areas would result in a stronger explosion and more serious consequences. Simulations were performed to investigate the effect of water spray on gas dispersion at the Kårstø facility. The water spray will have a negative effect on the gas dispersion because the activation of water spray will cause turbulence and then increased mixing of gas and air. The water spray will have a positive effect by limiting the spreading of the gas to other areas.

3. Introduction

3.1 Theme

An explosion is a complex phenomenon where the outcome depends on many parameters and circumstances. The general definition of an explosion is an event that leads to a rapid increase of pressure, and a gas explosion is defined as a process where combustion of a premixed gas cloud is causing rapid increase of pressure. The first step to a gas explosion is a release of gas/liquid. Then a combustible cloud of fuel and air has to form and ignite, which then results in an explosion. See Figure 3.1.1.

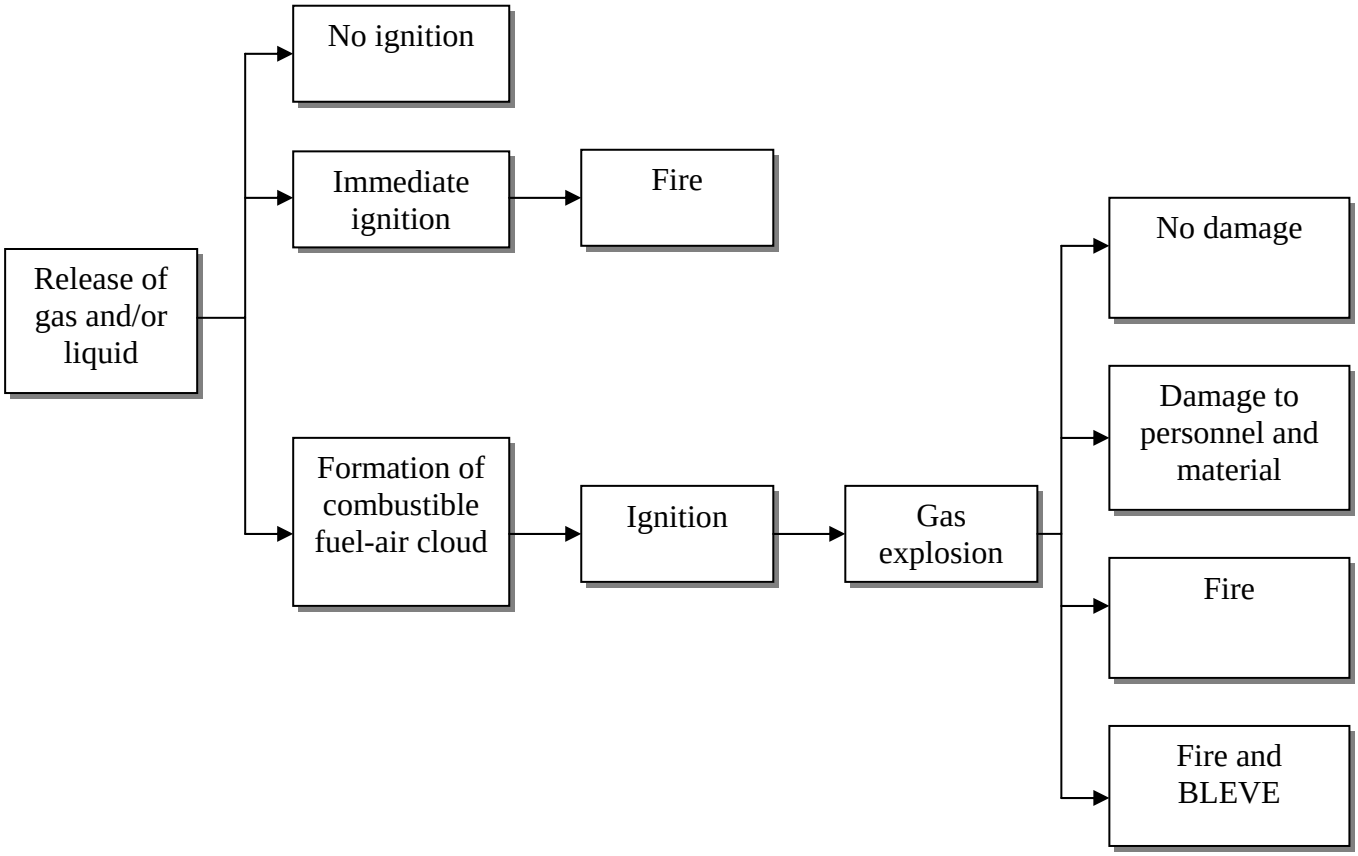

Figure 3.1.1: An event tree that shows different scenarios and outcomes of an accidental release of combustible gas and/or an evaporating liquid in air.

The consequences of a gas explosion can according to Figure 3.1.1 be damage to personnel and material, and depends on several factors:

- Type of fuel and oxidiser
- Size and fuel concentration of the combustible cloud
- Strength and location of the ignition source
- Size, location and type of explosion vent areas
- Location and size of obstructions
- Mitigation schemes

In a gas processing plant and in offshore platforms a gas explosion could have serious consequences, and it is therefore essential to have mitigation systems that can prevent and/or reduce unwanted scenarios. One such mitigating technique that has proved to be effective is water spray and deluge systems. Since such systems often already are installed in most industries to use in a fire-situation, this has become an attractive method in fighting gas explosions. Experimental work has been done with the use of water spray, and the main results are that activation of water spray before an ignition can reduce rapid flame acceleration that otherwise could result in high-pressure build-up.

Because the consequences of a gas explosion depends on many different parameters, a numerical model was developed that could handle different scenarios and give good results. The model was named FLACS (FLame ACceleration Simulator), and is a tree-dimensional gas explosion and gas-dispersing tool. FLACS is a Computational Fluid Dynamics code (CDF).The first version of the model was used in the 1980`s, and was very simple. Since then a continual improvement has taken place, and in 1994 a model that described water spray as a mitigating effect was implemented in FLACS-93. An improvement of this water spray model was done in 1997 and was implemented in FLACS-96. This is still the existing variant including water spray.

3.2 Purpose and activities

The main purpose of this report is to study the current water spray model in FLACS, FLACS 2.2.5, and to perform simulations including water spray. The water spray model is a simplified box-model that assumes uniform parameters inside each box-area. This current variant of the model does not take into account important parameters like generation of turbulence and temperature changes as a result of break-up and evaporation of droplets, and the influence this might have on explosion overpressure, gas dispersion and burning velocity. In addition the model does not include transport of droplets with the flow, which can result in misleading results. FLACS 2.2.6 has recently been developed where these parameters is taken into account, but the model does not behave physically correct when it comes to evaporation of droplets and reduction in burning velocity. An equation connecting the reduction in burning velocity to the amount of water spray over the amount of gas will therefore be developed, and a setup file for evaporation of droplets of different sizes will be included to the model. This model is called FLACS 2.2.6*.

At first the geometry of an explosion chamber, which has been used in explosion experiments at the British Gas Spadeadam test facility, will be created in the program CASD. Gas explosion simulations with FLACS 2.2.5 will be performed with and without water spray, and the results will be compared with reports written about the experiment to see that the simulation is acceptable.

Then there will be a thorough study of the physical parameters that are present in the interaction between a gas explosion and water spray, and suggested changes and supplements to improve the water spray model in FLACS 2.2.6. Changing different parameters as droplet-size to confirm that the model is behaving logically will test this improved model. The improved model, FLACS 2.2.6*, will then be used to do a new simulation of the explosion chamber. A discussion of differences in the two simulations will be done.

Two more advanced geometries will then be used to perform simulations with both the FLACS 2.2.5 and 2.2.6*, to see how the model will tackle a more complex scenario. A discussion of differences in simulation-results will be done.

At last there will be performed simulations with the geometry of the process-plant Kårstø. Explosion simulations will be performed with FLACS 2.2.5 and dispersion simulations will be performed with FLACS 2.2.6*. A report written by DNV concerning a detailed probabilistic explosion analysis at Kårstø states that due to the high explosion loads that is calculated, it is recommended to consider mitigating measures. An effective “blow down” system would have a significant impact on the explosion risk at the Kårstø facility. The effect of water spray on explosion pressure and gas dispersion will be discussed.

3.3 Definitions

Blast wave	an airwave set in motion by an explosion.
BLEVE	Boiling Liquid Expanding Vapour Explosion, an explosion due to flashing of liquid when a vessel with a substance of high vapour pressure sustains a failure.
Burning velocity	the velocity of the flame front (combustion wave) relative to the unburned gas immediately ahead of the flame.
Burning rate	the amount of fuel consumed by the combustion process per unit time.
CASD	Computer Aided Scenario Design
CMR	Christian Michelsen Research.
DDT	Deflagration to Detonation Transit, a sudden transition from deflagration to detonation
Deflagration	Subsonic combustion wave, i.e. a combustion wave that propagates at a velocity lower than the speed of sound relative to the unburned gas ahead of the flame.
Deluge	Water spray system where all of the nozzles are activated simultaneously at gas detection.
Detonation	Supersonic combustion wave, i.e. the detonation front propagates into unburned gas at a velocity higher than the speed of sound in front of the wave.
DNV	Det Norske Veritas

Explosion	An event that leads to a rapid increase of pressure.
FLACS	Flame Acceleration Simulator
Flame speed	the velocity of the flame relative to a stationary observer.
Gas explosion	a process where combustion of a premixed gas cloud is causing rapid increase of pressure.
GexCon	CMR’s Gas Explosion Consultancy
LFL	Lower flammable limit
LEL	Lower explosion limit
UFL	Upper flammable limit
UEL	Upper explosion limit

4. Literary analysis

This chapter will contain a description and discussion of the different methods used for estimating blast waves from gas explosions, and of the existing material about gas explosions and water spray.

4.1 Different methods

A strong gas explosion will result in blast waves that can cause damage to the area surrounded by the explosion. The magnitude of these blast waves will depend on the source of the explosion, i.e. the strength and duration, and the distance from the explosion. An ideal pressure-time curve for a blast wave is shown in Figure 4.1.1. The side-on pressure (initial atmospheric pressure) denoted p_o jumps suddenly to a shock value of $p_o + p_s$, where p_s is called side-on peak pressure and denotes the overpressure. It is usually the overpressure that is used to characterize a blast wave. The pressure is then gradually reduced to a much lower negative value before it then is stabilized to the original pressure p_o. It is often just the positive phase that is associated with destruction after a blast wave, but the negative suction phase can also contribute. Experiments done by CMR show that a gas explosion can cause blast waves with high pressures far away from the origin of the explosion, and when a evaluation of safety is to be made one have to consider free field blast [2].
Different methods have been developed over the years to estimate blast pressures, and they all have advantages and disadvantages. Some of these methods will now be described.

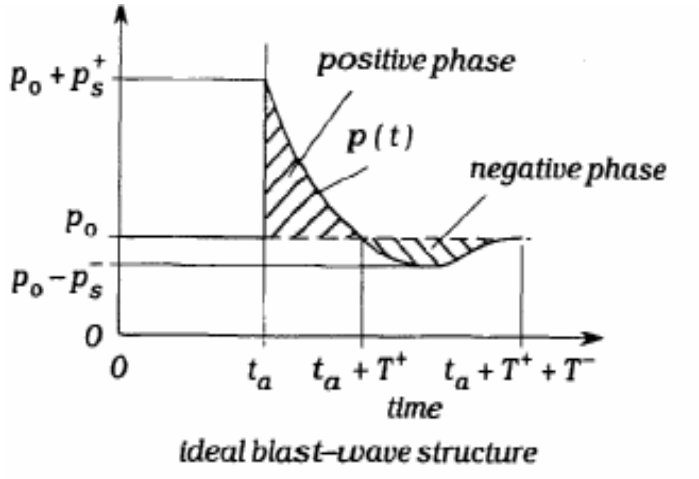

4.1.1: An ideal pressure - time curve for a blast wave.

4.1.1 TNT-method

One of the most frequently used methods for estimating blast pressures is the TNT-Method. This method is based on the well-documented blasts from different charges of high explosive TNT (trinitrotoluene). The peak pressure as a function of distance for different charges of TNT is shown in Figure 4.1.2.

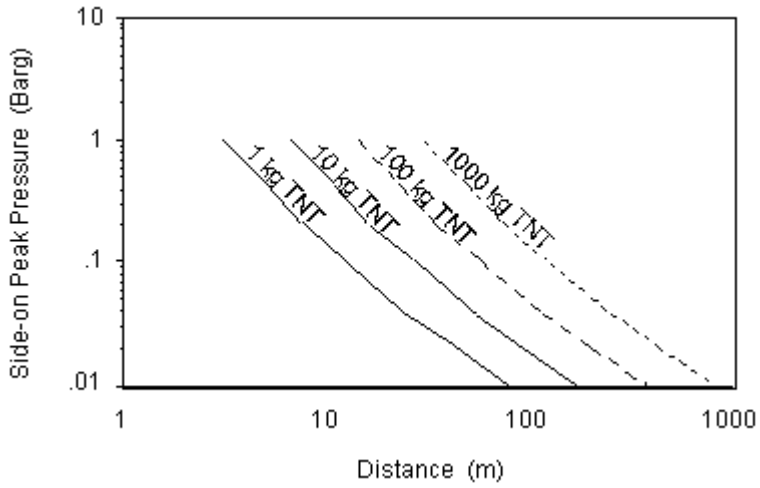

Figure 4.1.2: Peak explosion pressure versus distance for different TNT-charges.

A correlation between the mass of hydrocarbons and TNT is established based on the energy content of the exploding gas cloud by following formula:

$$W_{TNT} = \frac{\Delta H_{gas}}{\Delta H_{TNT}} \times \eta \times W_{HC} \approx 10 \times \eta \times W_{HC} \qquad (4.1.1)$$

ΔH_{gas} = Enthalpy; release of energy from gas [J/kg]
ΔH_{gas} = Enthalpy; release of energy from TNT (ca $4.52*10^6$ J/kg)
W_{TNT} = mass of TNT [kg]
W_{HC} = mass of hydrocarbon [kg]
η = Yield factor (empirical efficiency) based on experiments.

This formula is based on the fact that the heat of combustion for typical hydrocarbons is 10 times higher than the heat of reaction of TNT; hence the ratio of energy release becomes 10. This equivalent TNT charge is then used in the diagram shown in Figure 4.1.2 to estimate peak pressure of the explosion.

This original TNT-method has some drawbacks that are significant when calculating a gas explosion:

- The mass of hydrocarbons used is often the whole mass released in an accident, but normally just a part of the released gas cloud will contribute in the explosion as a consequence of geometry. The geometrical conditions are therefore not taken into account with this approach. A dispersion model could be used to estimate the probable mass and extent of the cloud, and the outcomes would then be more correct than the

over prediction that would be made using the total mass of release, though this approach also has errors.

- The explosion yield factor is based on experiments. It ranges from 1-10%, and will give a large differing in the predicted distances for the overpressures that is used. This would then be the larges potential source to error. A factor between 3-5% is normally used.

- An error that is smaller compared to the other two is that the heat of combustion for TNT varies with approximately 5 %, and an energy release factor would then become incorrect.

- It must also be noted that there are differences between a gas explosion and a TNT explosion. The blast pressure from a TNT detonation is much higher closer to the charge than a gas explosion, but as the distance increases it approaches the characteristics of a gas explosion. It is therefore recommended only to use the method when there is a sufficient distance from the gas-cloud.

Harris and Wickens (1989) did some improvement of the model to take geometrical conditions into account. The mass of hydrocarbons should represent a stoichiometric proportion in a severely congested region of a plant, and a yield factor of 20% was suggested instead of 3-5%. For natural gas the equation then becomes as followed:

$W_{TNT} = 0.16V$ (4.1.2)
V = volume of gas [m^3]

The results from this analysis approach compared with results from an experiment done by CMR is shown in Figure 4.1.3, and shows a good coherence as long as the pressures not are below 1 bar.

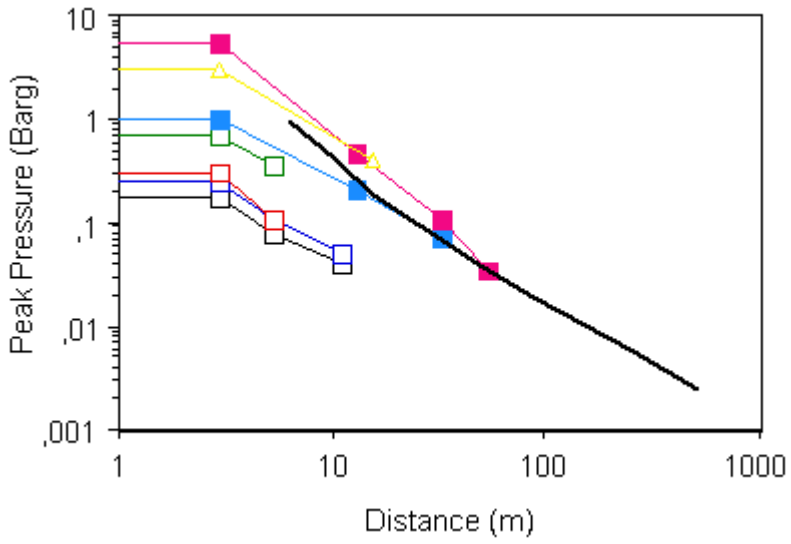

Figure 4.1.3: Comparison of peak explosion pressure versus distance from TNT-method (black curve) and CMR experiments from 50m^3 test.

When summarised the model has following drawbacks:

- A non-unique yield factor is needed.
- Weak gas explosions are not represented well.
- The process of a gas explosion is not represented well.
- It is problematic to choose an accurate blast centre.
- It represents only positive phase durations.

The strengths of this model are that it is easy to use, and it would give a prediction of which overpressures to expect from an explosion. This method will therefore be useful to give a rough estimate of a blast that is not to weak, as long as a yield factor of 20% is used and the mass or volume of the gas has a correct approximation.

4.1.2 Scaling of experiments

Another method that would give a rough estimation of explosion pressure is a scaling of experimental results. The data from experiments performed by CMR with a $50m^3$ compartment is scaled with a dimensionless length scale, and a pressure distance diagram containing curves from an explosion with different strengths in a $1000m^3$ compartment is made. This diagram can then be used in combination with the equivalent distance R_{Eq1000} found from formula 4.1.3 to estimate blast waves at different distances and compartments.

$$R_{Eq1000} = R \times \left[\frac{1000m^3}{V} \right]^{\frac{1}{3}} \qquad (4.1.3)$$

R = Distance from explosion centre.
V = Volume of confinement.

4.1.3 The Multi-energy method

The Multi-energy method (van den Berg, 1985) is an improvement of the TNT-method. It is based on the same principal with blast curves from explosions with variable strength (pressure), but the curves have their outcome from numerical simulations from a spherical cloud that is ignited in the centre and has a constant flame velocity. The curves for different strengths are then found by varying the flame velocity. A “charge strength value” is defined that ranges from unity to 10, where unity represents insignificant blast strength and 10 represents a detonation. See Figure 4.1.4.

To find the maximum overpressure from the curves one has to define the charge strength and the combustion energy. The charge strength has to be estimated from experiments or numerical simulations, and depends on the degree of confinement. The combustion energy for a stoichiometric hydrocarbon-air mixture can be found by following formula:

$$E = 3.5\ (MJ/m^3) * V \qquad (4.1.4)$$

V = volume of stoichiometric hydrocarbon-air mixture $[m^3]$

This value is then used in formula 4.1.5, to find the combustion energy-scaled distance to use in the left diagram in Figure 4.1.4.

$$\bar{R} = \frac{R}{\left(\frac{E}{p_0}\right)^{\frac{1}{3}}} \qquad (4.1.5)$$

R = distance from the charge
E = combustion energy
P_0 = atmospheric pressure

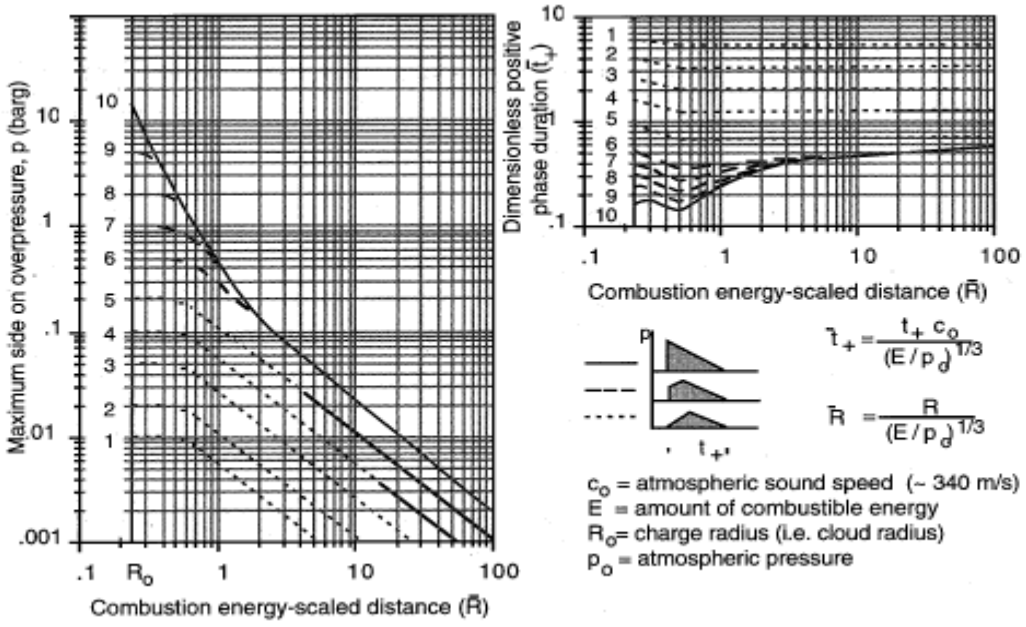

Figure 4.1.4: Explosion pressure curves used in the multi energy method.

The method takes into account that it is only the part of a gas cloud that is obstructed and partial confined that most likely will contribute to the explosion, and a better estimate of the blast energy will be found by the ratio between the partially confined to the total gas volume. This method is an improvement of the TNT-method, but there is a source to error in choosing the charge strength and combustion energy.

4.1.4 FLACS

FLACS is an advanced numerical fluid dynamic code, i.e. a Computational Fluid Dynamics (CFD) code, which can calculate explosion pressures and flow parameters as a function of time and space. It can simulate the interaction between advanced geometries, gas flow and blast waves, and gives a quantitative information output usually in the form of pressure-time curves. Important information about local pressure-build up or decay will be identified using this method. FLACS gives a good picture of how a given scenario develops, and is much more detailed than the methods described earlier.

The FLACS-3D code was originally developed to perform gas explosion simulations on offshore platforms. The code was then extended to performing dispersion simulations and combined gas explosion and blast simulations on onshore plants. A simulation of an onshore process plant requires a higher computer capacity and is more time demanding due to the more complex geometry. In order to compensate for this it is possible to use smaller control volumes, but this can result in important local information being lost.

In order to get a good communication between the simulation program and the user a program called CASD (Computer Aided Scenario Design) was developed. The interaction between FLACS and CASD is shown in the flow diagram in Figure 4.1.5.

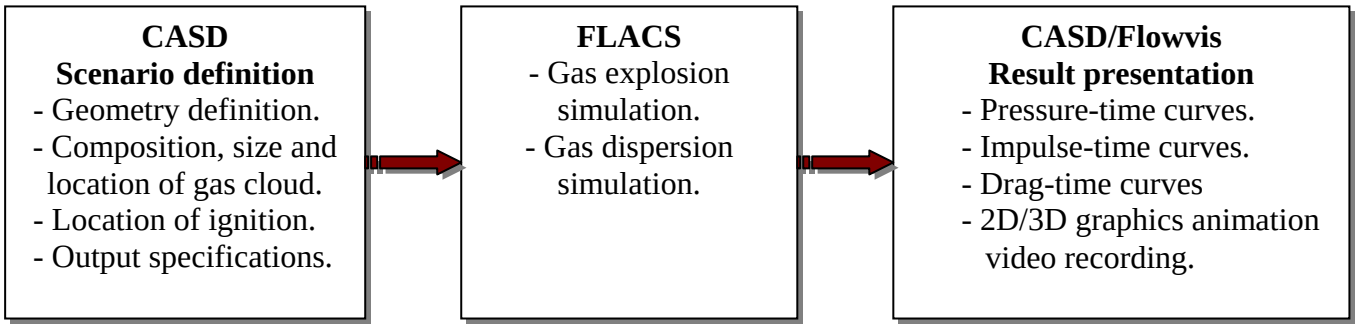

Figure 4.1.5: Flow diagram showing the progress of a FLACS simulation.

The first thing that has to bee done when performing a FLACS simulation is to create the geometry that is to bee investigated. The geometry is build up as detailed as possible by a number of boxes and cylinders representing piping, walls and equipment, to give a realistic picture of the real project. It is important to define whether a wall, floor or roof is solid, porous or open. A numerical grid is drawn surrounding the geometry to limit the area to bee investigated, and the grid is then divided in to many control volumes. Before the FLACS simulation can begin a scenario must be defined by determining different initial parameters and output specifications. The simulation then solves the three dimensional partial differential Navier-Stokes equations for each control volume in the area defined by the grid, and a program in CASD called Flowvis represents the output. If the geometry is complex the simulation can require a large computational time because of the extensive numerical calculations. A more detailed explanation of the performing of a FLACS simulation will be described in chapter 5: Methodology.

The FLACS code is based upon the latest knowledge from gas explosion research, and is continually being upgraded to relate with new information. FLACS is getting widely used by industry both national and international, and courses in using the program are frequently being held. When summarised FLACS has following strengths:

- Good physical and numerical models.
- High functionality and wide application range.
- Explosion simulations are efficiently solved.
- Validations of the models are extensive.
- User-friendly interfaces and output information.

As most numerical codes there exist limitations, like the need to predefine parameters and the need of large computational capacity. The limitations of FLACS are as followed:

- Detonations and Deflagration to Detonation Transition (DDT) can't be modelled.
- There exists limited validation for very reactive gases like ethylene, acetylene and hydrogen.
- FLACS may under predict pressures in scenarios with no confinement.
- Grid dependency has been seen in special situations.

The FLACS code has been thoroughly validate against experiments with different geometries and initial parameters performed by CMR and other institutes like British Gas, and gives good results ranging within 30-40% of the experimental data. Figure 4.1.6 shows a comparison between the results from experiments and FLACS [2]. There is still some validating with full-scale experiments that has to bee done, but so far the results from scaling seem to give adequate results.

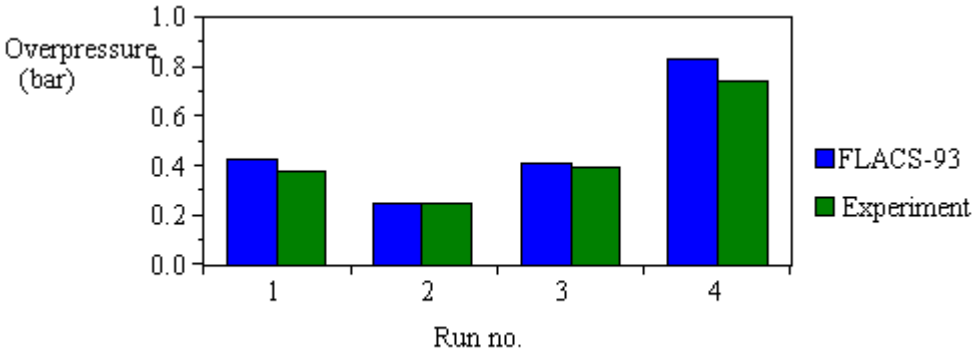

Figure 4.1.6: Comparison of FLACS93 results and experimental results for a 1:5 compressor module. (Storvik og Hansen, 1993)
Run 1: central ignition lower deck (methane)
Run 2: central ignition upper deck (methane)
Run 3: central ignition upper deck (propane)
Run 4: central ignition lower deck (propane)

4.2 Gas explosions versus water spray

4.2.1 The physics of a gas explosion

Figure 3.1.1 in chapter 3 shows the path that must take place, for a release of a combustible gas or evaporating liquid to result in a gas explosion. For a gas cloud to ignite there must be a sufficiently strong ignition source present, and the gas must be within its flammable limits. If ignition occurs a combustible wave will appear pushing the unburned gas ahead of the flame front. This is illustrated in Figure 4.2.1:

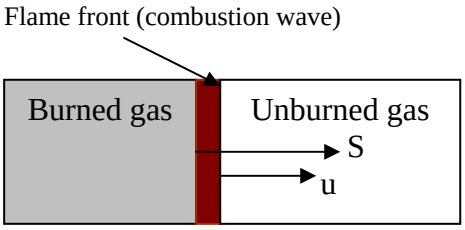

$$S = U + u$$

Figure 4.2.1: Illustration of flame propagation, S denotes the flame speed, U the burning velocity and u the velocity of the unburned gas.

Combustion releases energy, hence the temperature will rise in the burned gas. Due to the ideal gas law a rise in temperature will lead to a pressure increase and expansion, and the unburned gas flow (u) will increase. If the flow then interacts with obstacles it will create a turbulent flow field, and when the flame front reaches this field the burning rate will be enhanced and the burning velocity (U) and following the flame velocity (S) is increased. This again leads to increasing explosion pressure, expansion, increasing flow velocity and turbulence. This positive feedback process can be illustrated by the flow diagram in Figure 4.2.2 on the following page.

The value of the pressure generated by a combustion wave will depend on how fast the flame propagates and how the pressure is able to expand away from the combustible gas cloud. High pressures will be created in the presence of fast flame propagation due to rapid expansion, turbulence created by obstacles and total or partly confinement. A gas cloud that is totally unconfined will propagate slowly and only create insignificant overpressures.

The combustion wave can propagate in two different ways:

- Deflagration: A combustion wave propagating at subsonic velocity relative to the unburned gas immediately ahead of the flame, i.e. lower than the speed of sound.
- Detonation: A combustion wave propagating at supersonic velocity relative to the unburned gas immediately ahead of the flame, i.e. larger than the speed of sound.

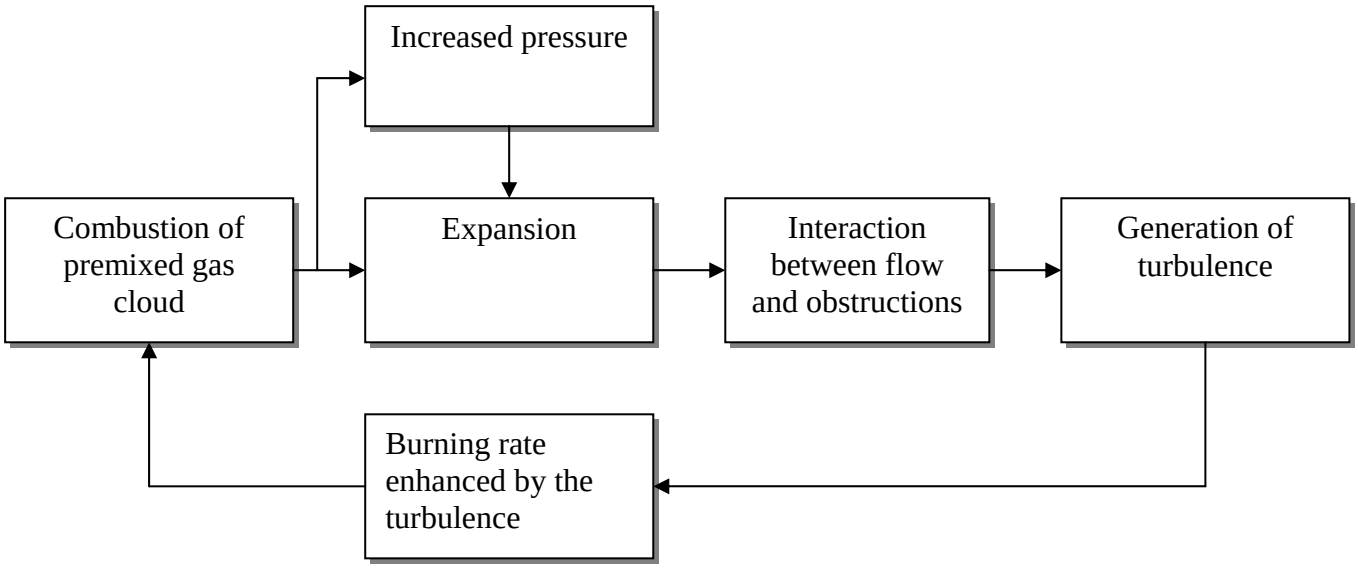

Figure 4.2.2: Flow diagram illustrating a positive feedback process causing rising explosion pressure.

4.2.2 Water spray as a mitigating effect

The effect of water spray on gas explosions has been tested in experiments performed by CMR and British gas, and they generally show that this will give an effective mitigating effect on the explosion [2]. Experiments with water spray showed that it did not have a mitigating effect on a centrally ignited gas cloud explosion, in fact it increased the overpressure in some cases, but the results from an end ignited gas cloud showed positive effects. In real life a gas cloud is ignited at the end in most situations. The positive effect on end ignited gas clouds is illustrated in Figure 4.2.3, where the overpressure is reduced by a factor of 3 when using water deluge.

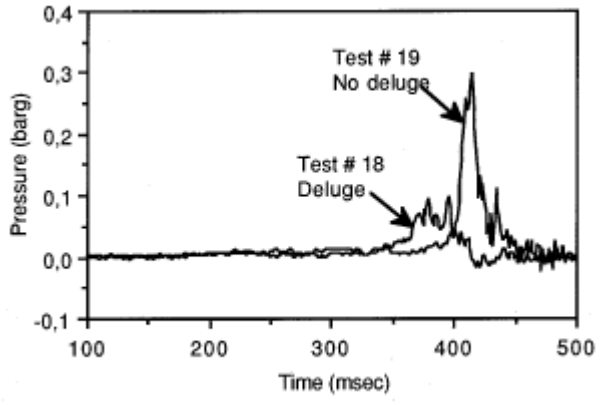

Figure 4.2.3: Pressure-time curve showing the results of two identical experiment with and without water deluge, using end ignition.

The main results from several experiments performed by British gas with an 180m^3 explosion box showed that the main factor determining whether the water spray would have a mitigating effect was if droplet break-up would occur [2]. For the water droplets to evaporate in the flame front the droplet diameter has to be 1-50μm or less. Large sized droplets will not be able to extract sufficient heat from the combustion in the time of the explosion, and since the droplet size in typical deluge nozzles usually are higher than 100μm a droplet break-up is necessary. The droplet break-up occurs if there is high gas acceleration in front of the flame, which is the case in geometries with a sufficient vent opening and obstructions to create fast flow. In the early stage of an explosion the pressure build-up will enhance due to the turbulence from the water spray, but after a while the flow turbulence from obstacles will become dominant and the explosion will be mitigated efficiently. This can be illustrated by the pressure-time curve with water deluge in Figure 4.8, where the pressure peak comes earlier but has a lower maximum value. For more confined geometries where the flow will be restricted by small vent opening, the turbulence from the water spray will be dominant through the whole explosion and the pressure will be higher than in the case of no water spray.

The two main results from the experiments showed a competing effect in using water spray, and can be summarised as following:

- In the initial phase of a gas explosion the water spray actually enhanced the explosion, due to turbulence caused by the flow of the water spray. The turbulence causes increasing flame velocity and following faster pressure build-up, hence the pressure-peak will come earlier.

- When the water droplets evaporate in the flame this process will extract energy and thereby reduce the temperature and the process of pressure build-up. The evaporation of droplets will also create a water mist that dilutes the gas mixture and thereby the reaction rate. For the droplets to evaporate they have to be smaller than the size they have in a water spray system, hence they have to be separated in smaller droplets after release for the water spray to have a mitigating effect. The break up of droplets requires a strong and accelerating flow surrounding the droplets, because there has to be a sufficient velocity difference between the gas and the droplets to produce strong hydrodynamic forces. This is the case in geometries that has a sufficient vent openings and obstructions.

The disadvantage of using water deluge is that it has to be activated on gas detection, because the reaction time of a standard deluge system is larger than the duration of an explosion. This can cause trouble and in the worst-case ignition of the gas if the electrical equipment in the area not is waterproof.

4.2.3 Water spray in FLACS 2.2.5

The FLACS code has a relative simple water spray model implemented, where a number of regions containing water spray are defined. It is important that these areas don't overlap each other. Within each region a water droplet size (D) and a water volume fraction (WVF) is determined, based on the water pressure, region, droplet velocity and specific parameters characteristic for the chosen nozzle type. The acceleration of the water droplet is defined by following formula:

$$a_D = \frac{F_D}{m_D} = \frac{3\rho_a C_D}{4\rho_W D} V_{rel} \times |V_{rel}| \qquad (4.2.1)$$

F_D = drag force acting on the droplet
m_D = droplet mass
ρ_a = density of air
ρ_W = density of water
D = droplet diameter
C_D = drag coefficient
V_{rel} = velocity of air stream relative to the droplet

A critical break-up velocity is defined based on the droplet diameter, and it is assumed that the droplets will break if the relative velocity between the droplet and the gas flow exceeds this value:

$$V_{critical} = \sqrt{\frac{0.505}{D}} \qquad (4.2.2)$$

Two non-dimensional factors called F1 and F2 are implemented in the numerical model. F1 is used to increase the burning rate due to initial turbulence at the presence of water spray, and ranges from 0 (no water spray) to 10 (high velocity water spray). F2 is used to reduce the burning rate if the conditions for droplet break-up are present, and ranges from 1 (no water spray) to 0 (total quenching). These factors are connected to the effective burning velocity (S_{water}) by following formula:

$$S_{water} = (S_{turbulent} + F1 \times S_{laminar})\, F2 \qquad (4.2.3)$$

$S_{turbulent}$ = ordinary burning velocity (without water spray)
$S_{laminar}$ = laminar burning velocity
F1 = accelerating factor
F2 = quenching factor

The input in the FLACS scenario file for the water spray contains following aspects:
Position: The position of the lower left corner of a water spray region: X_{min} Y_{min} Z_{min}.
Size: The size of the water spray region: X_{len} Y_{len} Z_{len}.
Droplet diameter: The mean diameter in mm of water droplets before break-up, defined by the Sauter diameter in formula 4.2.4:

$D = P^{-0.333}$ [mm] (4.2.4)
P = water pressure [bar]

Water Volume fraction (WVF): Volume of liquid water in litre divided by total volume in cubic meter inside water spray region. It is not used in the current version of FLACS, but must be set higher than the minimum value of 0.01. The WVF must still be calculated because it is needed to find the factors F1 and F2, and is found by equation 4.2.5:

$$WVF = \frac{n \times \frac{k \times \sqrt{P}}{60}}{X_{len} \times Y_{len} \times U_z} = \frac{n \times \frac{Q}{60}}{X_{len} \times Y_{len} \times U_z} \quad (4.2.5)$$

n = number of nozzles
k = characteristic nozzle factor (water flow rate)
P = water pressure [bar]
X_{len} = size of water spray region in x-direction [m]
Y_{len} = size of water spray region in y-direction [m]
U_z = average droplet velocity vertically downwards [m/s], defined by formula 4.2.6:

$U_z = 2.5D^{0.94}$ (4.2.6)
D = mean droplet diameter [mm]

Q = water flow from one nozzle [l/min], defined by formula 4.2.7:
$Q = k \times \sqrt{P}$ (4.2.7)

The droplet velocity vertically downwards becomes constant after a while because of the balance between drag forces and gravity forces, but if the droplets have a significant vertical velocity from the nozzles (High velocity nozzles) a typical greater velocity should be estimated.

Nozzle type ("Factors: F1 , F2"): Two non-dimensional factors characteristic for each nozzle type for a specified water pressure. The factors F1 and F2 are defined by following formulas:

$F1 = 14U_z \times WVF$ (4.2.8)

$$F2 = \frac{0.03}{D \times WVF} \quad (4.2.9)$$

It must be noted that the model doesn't take into account the transportation of water droplets with the gas flow, and one therefore has to identify water spray in areas where the gas is expected to flow as a result of expansion during the explosion. A typical area would be outside a vent opening. There are also done some simplifications according the shape of the droplets, and the assumptions of a uniform distribution of droplets inside the water spray region and that all the droplets have the same size.

4.2.4 Water spray in FLACS 2.2.6

In FLACS 2.2.6 two-phase flow is implemented, requiring a whole set of governing equations for the liquid flow in addition to the gaseous phase. The model was created based on modelling of oil mist, but is converted to water mist to be able to simulate water spray. The water mist usually consists of a whole range of different droplet sizes, which vary in time and space. In FLACS 2.2.5 a water region was defined with uniform values for droplet size and droplet speed. No transport of droplets with the fluid flow occurred. In FLACS 2.2.6 the droplets move with the main gaseous fluid flow, and as in two-phase flow these will affect each other in many ways. It is validated that FLACS predict the motion of aerosol particles with more than 90% accuracy [3]. The varying droplet size distribution is modelled by defining a set of droplet classes, where each class has a local representative value. The droplets belonging to a specific droplet class are assumed to have the same diameter within the same control volume of the numerical grid.

The model also takes into account break-up and coalescence of droplets. Break-up of droplets will occur when the relative speed between a droplet and the surrounding gaseous fluid flow is sufficiently large. When droplets are broken down the new diameter is typically 5% of the original diameter for 68% of the volume of broken droplets, and less than 5μm for the remaining 32%. The droplet break-up is determined by a Weber number criterion, where break-up occurs when We > ≈12:

$$\mathrm{We} = \frac{\rho_g (U_{rel})^2 d_j}{\sigma_j} \qquad (4.2.10)$$

ρ_g = density of gaseous phase surrounding the droplet [kg/m^3]
U_{rel} = relative speed between the surrounding gaseous phase and the droplet [m/s]
d_j = droplet diameter for droplet class j [m]
σ_j = surface tension between the droplet and the surrounding gaseous phase for droplet class j [N/m]

Coalescence of droplets means collision of droplets forming larger droplets. The collision is assumed to mainly appear between droplets of different sizes, and therefore collision between droplets belonging to the same droplet class is not modelled. If one considers collision between two droplet classes, the increase in volume for the largest droplet size per unit time can be modelled by:

$$\dot{V}_{large} = A_{proj} \times V_{small} \times U_{rel} \qquad (4.2.11)$$

$\dot{V}_{large}$ = Increase per unit time for the specific volume of the larger droplet class [1/s]
A_{proj} = Projected area of the largest droplet per unit open volume [1/m]
U_{rel} = Velocity difference between the to classes considered [m/s]

Evaporation of droplets is also modelled. According to an energy balance a certain amount of a droplet will boil of when net energy is transported to the droplet, and the model specifies the evaporation rate. However the evaporation of water droplets gives an incorrect physical result giving no heat transfer at zero droplet velocity. As a result of this a relation between the reduction in flame temperature and burning velocity due to the presence of water droplets has to be modelled.

4.3 Gas dispersion versus water spray

4.3.1 Gas dispersion

If flammable gas is accidentally released or leaks into the atmosphere, a combustible fuel-air cloud can be formed. If the cloud is outside the flammable concentration area, i.e. not between LFL and UFL, or there is no ignition source present, the gas cloud will simply dilute and disappear without causing any hazard. On the other hand if a large flammable gas cloud is formed and ignited this can cause a large and destructive explosion. Figure 3.1.1 shows typical consequences of an accidental release of flammable gas.

The size of a flammable gas cloud after a release in a congested area depends on the following factors:

- The size of the release
- The type and orientation of the release
- The properties of the released gas
- The degree of congestion
- The degree of ventilation

A gas release is divided into two different types: jet release and diffuse release. A jet release has a high momentum and will create a strong flow field due to additional air entrainment. This can result in a generation of recirculation zones than can create large combustible gas clouds. A diffuse release is an evaporating pool and will have a much lower flow velocity. Wind and buoyancy forces will therefore dominate the dispersion. If this evaporating liquid forms a dense gas, a combustible cloud can be established at ground level. The gas will then have a tendency to intrude into confined spaces (buildings), which can cause a large explosion.

The explosion area of the gas cloud will determine the size of the cloud, and the density of the gas will influence the location and spreading of the gas cloud. Congestion will affect the flow patterns in the gas cloud and therefore shape of the cloud. Obstructions can create turbulent flow fields and enhance the mixing of gas and air.

Ventilation will have a large effect on the size of the flammable gas cloud. The results from an experiment performed in a 1:5 offshore module show the effect of forced ventilation [2]. Figure 4.2.4 shows the change in the concentration as a result of different wind speeds. Higher wind speed will give a lower concentration.

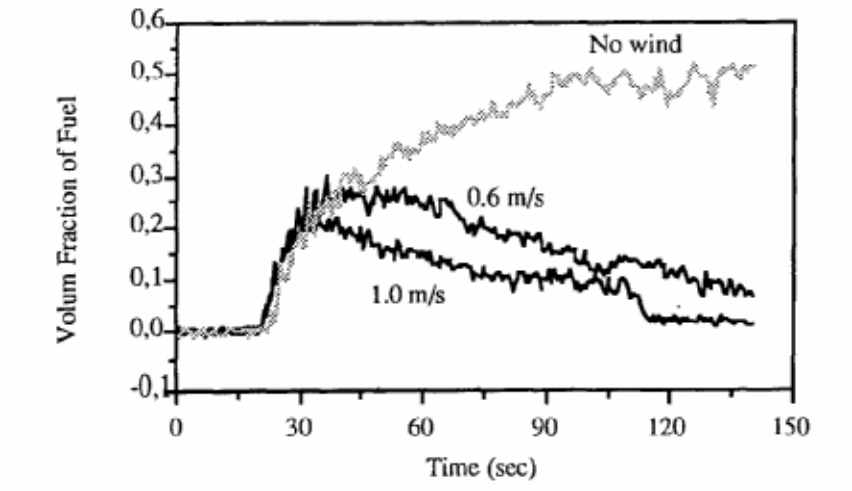

Figure 4.3.1 Concentration as a function time for different wind velocities.

4.3.2 The effect of water spray

It is known that water spray will have an effect on the propagation and the outcome of an explosion. In most cases the maximum explosion pressure will be significantly reduced with water spray present. Water spray can also have an effect on gas dispersion. A water spray curtain can prohibit a gas cloud from spreading to other areas, and thereby preventing the build-up of a large gas cloud. A large gas cloud would result in a powerful explosion if ignited. Water spray can also give a negative impact on the gas dispersion. In experiments performed by GexCon in 2003 it is seen that the water spray can enhance the mixing of the gas, and spread the gas to lower levels in geometries with several floors [4]. With diffusive release water spray gives a more effective mixing than mixing only due to buoyancy, and convection due to water spray dominates compared to convection due to buoyancy. With a jet release and external wind forces, the forces due to water spray did not dominate in the same way. If the gas is released at the upper deck the water spray contributes with the transport of fuel to the lower deck.

4.3.2 Water droplets in FLACS

In order to investigate the effect of water spray on gas dispersion a model for droplets had to be included in FLACS, FLACS 2.2.6, where it is possible to model liquid droplets in addition to the gaseous phase. Hans-Christen Salvesen has performed a study on simulations with gas dispersion and water spray, and a comparing of experimental and simulated results [5]. In general the same tendencies were seen in both experiments and simulations. Some differences were seen between the experiments and the simulations with water spray. Neither the simulations nor the experiments are perfectly representing an ideal situation, and therefore some deviations are unavoidable. One significant difference is that the water spray is released as a narrow jet in the simulations, but in the experiments a more broader and uniform jet is seen. There should therefore be developed a more complex model concerning the release of the water spray.

5. Methodology

This chapter will include the performance of explosion simulations with different geometries using FLACS 2.2.5, modelling of an improved model called FLACS 2.2.6, and explosion and dispersion simulations with the changed FLACS 2.2.6 model called FLACS 2.2.6*.

5.1 Explosion simulation with FLACS 2.2.5

The following simulations will be performed by FLACS- version 2.2.5 (2001).

5.1.1 Explosion box

This simulation of the 180m^3 explosion box filled with stoichiometric natural gas/air mixture was based on a rapport of experiments performed with this geometry by British Gas [6].

Geometry
The first step in performing the simulation was to create the geometry of the explosion box. The dimensions of the box are 9m × 4.5m × 4.5m, and a square ventilation opening is located in the centre of the left end wall. Pipes with a length of 4.5m and a diameter of 0.18m are located inside the box, where they are placed horizontally and perpendicular to the direction of flame propagation. Simulations are performed with two different vent openings of 1.5m × 1.5m (Kv=9) or 4.5m × 4.5m (Kv=1), and five different pipe congestions of 0, 20, 40, 56 or 80 pipes. The location of each pipe in the different congestions is shown in appendix 1, and the simulation configurations in appendix 2. The Kv-value is defined by the area of the vented side of the chamber divided by the area of the vent opening. Figure 5.1.1 shows an example of the geometry of the explosion box.

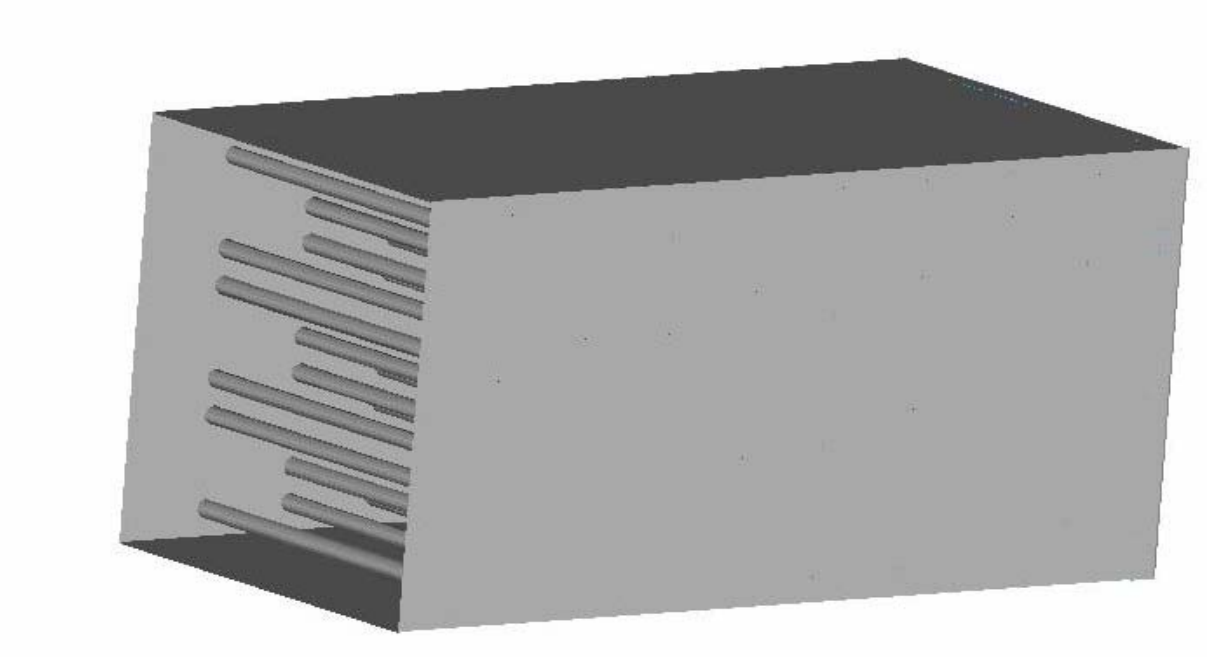

Figure 5.1.1: Explosion box with large ventilation opening and a congestion of 56 pipes.

Grid
A grid was drawn to define the size of the area that is to be calculated by FLACS. The simulation volume was set to 19m × 4.5m × 4.5m, and was stretched in the x-direction with a factor of 1.19375 outside the vent opening in the left end wall. The grid size was set to 0.5m in all directions. The number of control volumes in x-direction is then set to 38 (becomes 27 when stretched), and 9 in y-and z-direction. In a number of simulations a finer and extended grid was used, to see if this would have any influence on the results.

Calculating porosities
The porosities have to be calculated before beginning to define a scenario, and a text box reminding you to do this pops up if you don't activate the calculation. The porosity calculation is necessary to define if a wall or floor is open, solid or porous.

Scenario: Most of the scenario input is described in appendix 3.

- WATER SPRAY:
  In this example we have 3 scenarios where the box contains no nozzles, 8 nozzles of the type HV60 or 8 nozzles of the type MV57. The characteristic k-values for the nozzles are given. The position and size of the water spray regions are shown in Table 5.1.1, where "position" is the Cartesian coordinates of the corner of the box-shaped water spray region with the lowest value and "size" is the dimensions of the water spray region. The water spray is expected to cover the whole volume of the box. One large water spray region covering the whole box can be defined since the different regions of water spray have the same properties and are all activated. In a number of simulations the water spray was extended outside the ventilation opening to see if this could cause any deviations in the results.

	Position			**Size**		
Nozzle number (water region)	$\mathbf{X_{min}}$	$\mathbf{Y_{min}}$	$\mathbf{Z_{min}}$	$\mathbf{X_{len}}$	$\mathbf{Y_{len}}$	$\mathbf{Z_{len}}$
1	0	0	0	2.25	2.25	4.5
2	2.25	0	0	2.25	2.25	4.5
3	4.5	0	0	2.25	2.25	4.5
4	6.75	0	0	2.25	2.25	4.5
5	0	2.25	0	2.25	2.25	4.5
6	2.25	2.25	0	2.25	2.25	4.5
7	4.5	2.25	0	2.25	2.25	4.5
8	6.75	2.25	0	2.25	2.25	4.5

Table 5.1.1: Location of water spray regions.

The operating water pressure is set to 3.5 or 5 bar, and by using formula 4.2.4 the mean droplet diameter is calculated. The average droplet velocity for the MV57 nozzle is calculated by formula 4.2.6, but for the HV60 nozzle it is necessary to estimate a value because of the high velocity. X_{len} and Y_{len} are found from Table 5.1.1. The water volume fraction, F1 and F2 is calculated by formulas 4.2.5, 4.2.8 and 4.2.9. The characteristic parameters for the two different nozzles are displayed in table 5.1.2:

Nozzle	**Number of nozzles**	**k**	**P [bar]**	**D [μm]**	**Uz [m/s]**	**WVF [l/m^3]**	**F1**	**F2**
HV60	8	93	3.5	658.9	4	0.14	8.01	0.32
HV60	8	93	5.0	585.1	4	0.17	9.52	0.30
MV57	8	99.5	3.5	658.9	1.7	0.36	8.58	0.13

Table 5.1.2: Different parameters for the HV60 and MV57 nozzles.

5.1.2 1:5 offshore module, M24-25

The experiments with the 1:5 offshore module was performed at the CMR large-scale gas explosion test site at Sotra outside Bergen [7]. The geometry used in the experiments is a $50m^3$ small-scale version, combining the to modules M24 (compressor module) and M25 (separator module) at Gullfaks-A. The module is based on the M24 module, but with the exceptions that some large cylindrical separator tanks replace the equipment at the mezzanine deck, and the solid deck is removed so that water can fall through the mezzanine deck. The gases used in the experiments were slightly over-stoichiometric gas mixtures of methane (9.8%) or propane (4.2%) in air.

Geometry

The dimensions of the module is 8.00m × 2.50m × 2.50m. There are ventilation openings at each end of the module, and these can respectively be defined as a vent opening, louvered wall or solid wall. The geometry is shown in Figure 5.1.2. One of the long sidewalls is blanked in order to show the equipment inside the module better. A more detailed drawing of the geometry is shown in appendix 6 and the simulation configurations are described appendix 7.

Grid

The simulation volume of the grid was set to 12m × 4.5m × 3.5m, with 2 meters outside each end of the module in x-direction, 1 meter out on each side in y-direction and 1 meter upwards in z-direction. The size of one grid cells was set to 0.25 meters, which corresponds to 48 × 18 × 14 grid cells.

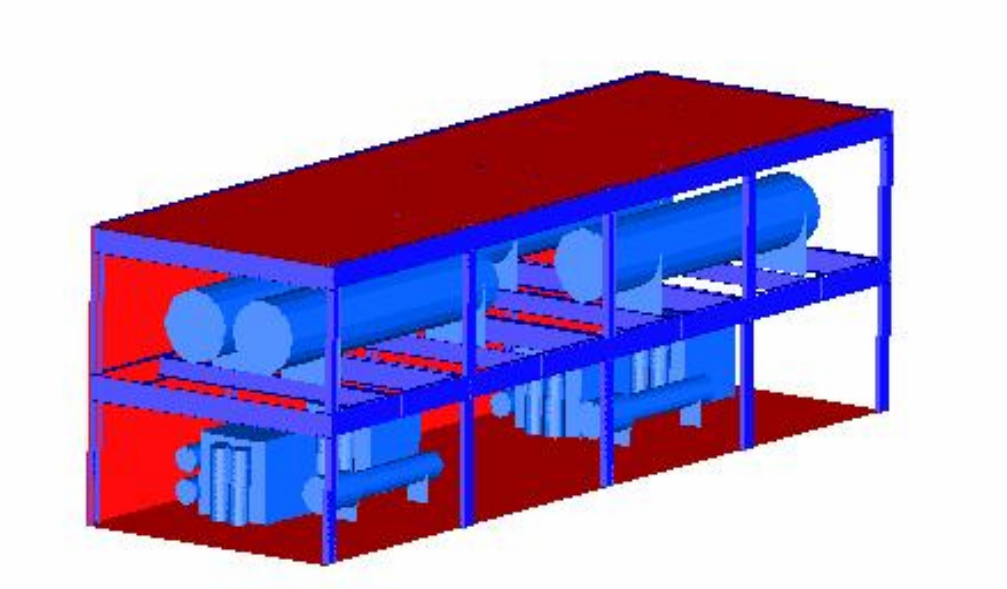

Figure 5.1.2: The geometry of the $50m^3$ M24-25 module.

Scenario definition: Most of the scenario input is described in appendix 8.
The scenario is divided into three different groups:

- Case 1: Propane, centre ignition and end walls open.
- Case 2: Methane, end ignition, louvered wall at ignition and open end opposite ignition
- Case 3: Methane, end ignition and ventilation only opposite ignition.

- WATER SPRAY:
  Three different types of water spray nozzles were used in these simulations:
  - High velocity nozzles: HV26
  - Sprinkler nozzles: CUP 10, CUP 5
  - Fog nozzles: P120

  The experiment includes totally 18 nozzles, with 9 different locations in x-direction at respectively 0.25m, 1.25m, 2.25m, 3.25m, 4m, 4.75m, 5.75m, 6.75m and 7.75m. At each of these points in x-directions two nozzles are located in y-direction at 0.625m and 1.875m. The two nozzles in y-direction that has the same x-direction is identified by they're 9 different x-locations, starting at number 1 at the end of ignition (north wall to the right), and is denoted as "water region". Figure 5.1.3 shows the locations of the different regions. The water spray from each nozzle is assumed to cover the y- and z-direction, and +/-1.25m (totally 2.5) in the x-direction from its location. Since the location of the nozzles will be in the centre of each water spray box, the scenario input will be as displayed in Table 5.1.3. Different regions of water spray are activated in the different simulations, and the water pressure from the nozzles is varied.

		Position			**Size**		
Water region	**Nozzle number**	$\mathbf{X_{min}}$	$\mathbf{Y_{min}}$	$\mathbf{Z_{min}}$	$\mathbf{X_{len}}$	$\mathbf{Y_{len}}$	$\mathbf{Z_{len}}$
9	1-2	-1	0 and 1.25	0	2.5	2.5	2.5
8	3-4	0	0 and 1.25	0	2.5	2.5	2.5
7	5-6	1	0 and 1.25	0	2.5	2.5	2.5
6	7-8	2	0 and 1.25	0	2.5	2.5	2.5
5	9-10	4	0 and 1.25	0	2.5	2.5	2.5
4	11-12	3.5	0 and 1.25	0	2.5	2.5	2.5
3	13-14	4.5	0 and 1.25	0	2.5	2.5	2.5
2	15-16	5.5	0 and 1.25	0	2.5	2.5	2.5
1	17-18	6.5	0 and 1.25	0	2.5	2.5	2.5

Table 5.1.3: Location of nozzles.

Nozzle numbers:

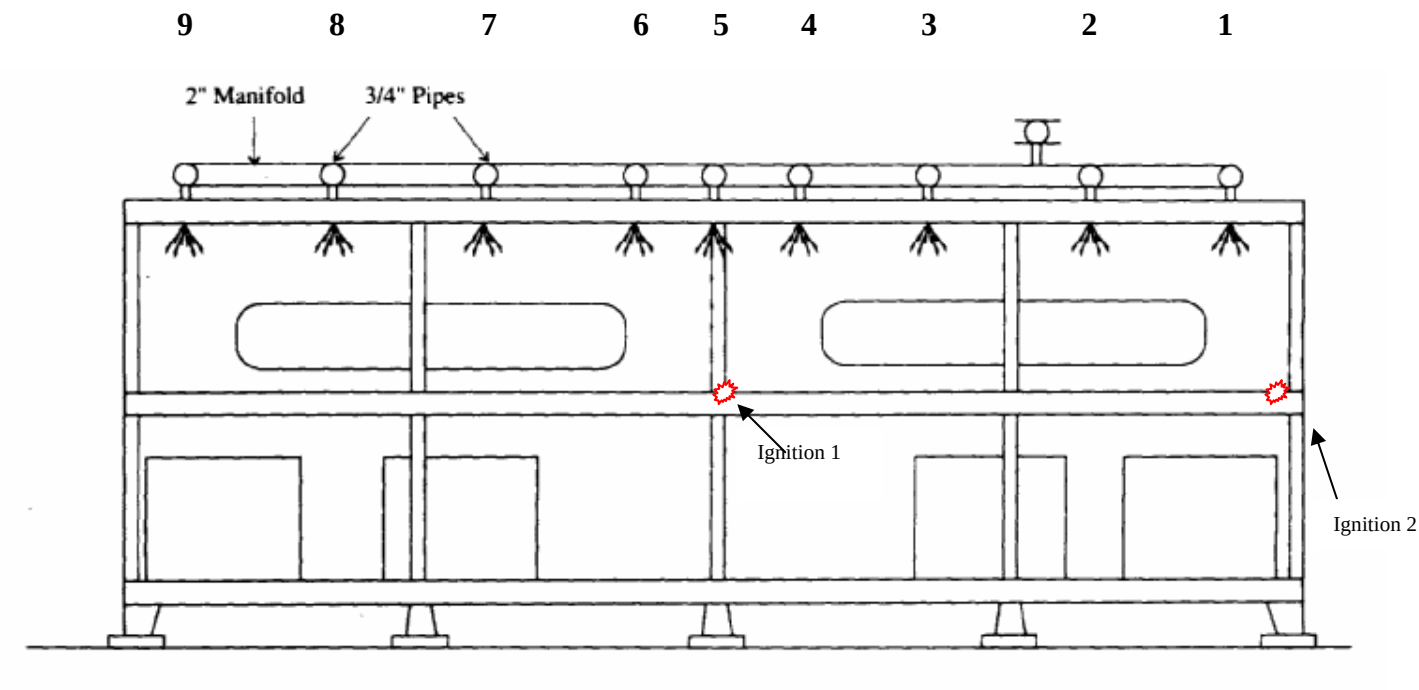

Figure 5.1.3: View of nozzle positions in the module.

The mean droplet diameter for the different water pressures is calculated by formula 4.2.4. The average droplet velocity for the CUP5, CUP10 and P120 nozzles are calculated by formula 4.2.6, but for the HV26 nozzle it is necessary to estimate a value because of a the high velocity. Table 5.1.3 gives X_{len} = 2.5m and Yl_{en} = 2.5m for regions containing 2 nozzles. In some of the simulations the regions overlap and are defined as one region with a larger number of nozzles, which results in different values for X_{len}. Y_{len} will always be 2.5m because there are always two nozzles in each region covering the whole y-direction. The water volume fraction, F1 and F2 are calculated respectively by formulas 4.2.5, 4.2.8 and 4.2.9. The characteristic parameters for the different nozzles and simulations are displayed in Table 5.1.4 and 5.1.5.

Nozzle	k-value	Sauter diameter (μm)	Average velocity
HV26	43	500-600	Assumed 4.5m/s
CUP5	17	600-700	Gravity driven
CUP10	57	600-700	Gravity driven
P120	6	500-600	Gravity driven

Table 5.1.4: Different parameters for the HV26, CUP5, CUP10 and P120 nozzles.

Sim nr	Nozzle	n	Region	X_{len}	P [bar]	D [μm]	Uz [m/s]	WVF [l/m^3]	F1	F2
2	HV26	4	4-6	4.0	3.5	658.9	4.50	0.12	7.51	0.38
3	CUP10	4	4-6	4.0	3.0	693.6	1.77	0.37	9.21	0.12
4	CUP10	2	3,7	2.5	3.0	693.6	1.77	0.29	7.37	0.07
5	CUP10	8	3-7	6.0	3.0	693.6	1.77	0.50	10.00	0.09
6	CUP10	2	2,8	2.5	3.0	693.6	1.77	0.29	7.37	0.07
7	CUP10	4	2-3 ,7-8	3.5	3.0	693.6	1.77	0.42	10.00	0.10
8	CUP10	2	1,9	2.5	3.0	693.6	1.77	0.29	7.37	0.07
9	CUP10	2,4	1,4-6,9	2.5,4	3.0	693.6	1.77	0.29,0.37	7.37,9.21	0.07,0.12
10	CUP10	4	1-2,8-9	3.5	3.0	693.6	1.77	0.42	10.00	0.10
12	HV26	8	6-9	5.5	3.0	693.6	4.50	0.16	10.00	0.27
13	HV26	8	3-7	6.0	3.0	693.6	4.50	0.15	9.27	0.29
14	HV26	8	2-8	7.0	3.0	693.6	4.50	0.13	7.94	0.34
15	HV26	8	1-4	5.5	3.0	693.6	4.50	0.16	10.00	0.27
16	HV26	4	6-7	3.5	3.5	658.9	4.50	0.14	8.58	0.33
17	HV26	4	2-3	3.5	3.5	658.9	4.50	0.14	8.58	0.33
18	P120	16	1-4,6-9	10	4.0	630.3	1.62	0.08	1.79	0.59
19	P120	4	7-8	3.5	7.6	509.0	1.33	0.09	1.76	0.65
20	P120	8	6-9	5.5	7.6	509.0	1.33	0.12	2.25	0.49
21	P120	8	3-7	6.0	7.6	509.0	1.33	0.11	2.06	0.54
22	P120	8	1-4	5.5	7.6	509.0	1.33	0.12	2.25	0.49
23	CUP5	4	6-7	3.5	7.0	523.1	1.36	0.25	4.78	0.23
24	CUP5	8	3-7	6.0	3.8	641.1	1.66	0.18	4.12	0.26
25	CUP5	8	2-7	8.0	3.8	641.1	1.66	0.13	3.09	0.35
26	CUP10	8	6-9	5.5	2.4	747.1	1.90	0.45	10.00	0.09
27	CUP10	8	3-7	6.0	2.4	747.1	1.90	0.41	10.00	0.10
28	CUP10	8	2,4,6,8	8.0	2.4	747.1	1.90	0.31	8.24	0.13
29	CUP10	4	2-3,7-8	3.5	2.4	747.1	1.90	0.35	9.42	0.11
30	CUP10	4	1-2,8-9	3.5	2.4	747.1	1.90	0.35	9.42	0.11
31	CUP10	4	1-4	5.5	2.4	747.1	1.90	0.45	10.00	0.09
32	CUP10	4	8-9	3.5	3.0	693.6	1.77	0.42	10.00	0.10
33	CUP10	4	7-8	3.5	3.0	693.6	1.77	0.42	10.00	0.10
34	CUP10	4	6-7	3.5	3.0	693.6	1.77	0.42	10.00	0.10
35	CUP10	4	4-6	4.0	3.0	693.6	1.77	0.37	9.21	0.12
36	CUP10	4	3-4	3.5	3.0	693.6	1.77	0.42	10.00	0.10
37	CUP10	4	2-3	3.5	3.0	693.6	1.77	0.42	10.00	0.10
38	CUP10	4	1-2	3.5	3.0	693.6	1.77	0.42	10.00	0.10
39	CUP10	8	3-7	6.0	3.5	658.9	1.69	0.56	10.00	0.08
41	CUP10	4	4-6	4.0	3.0	693.6	1.77	0.37	9.21	0.10
42	CUP10	8	1-4	5.5	3.8	641.1	1.66	0.19	4.50	0.25
43	CUP10	8	6-9	5.5	3.8	641.1	1.66	0.19	4.50	0.25
44	CUP5	4	7,8	3.5	3.0	693.6	1.77	0.42	10.00	0.10

Table 5.1.5: Characteristic values for the different simulations.

5.1.3 Full-scale geometry

British Gas performed the experiments with this full-scale geometry, which is a 3:2:1 scale copy of the 50m^3 M24-module [8]. This is again a 1:5 scale model of the M24-module on the Gullfaks-A platform in the North Sea. The module is filled with a stoichiometric mixture of 91.7% methane, 7% ethane and 1.3% propane in air.

Geometry
The geometry has the dimensions 25.6m x 8.0m x 8.0m. The sidewalls are closed, and there are ventilation openings at the two short ends. The geometry is shown in figure 5.1.4. One of the sidewalls is blanked so that the inside of the module is better displayed. The simulation configurations are listed in appendix 11.

Grid
The simulation volume of the grid was set to 46m × 30m × 20m, with 10.2 meters outside each end of the module in x-direction, 11 meter out on each side in y-direction and 12 meters upwards in z-direction. The size of one grid cells was set to 0.40 meters, which corresponds to 115 × 75 × 50 grid cells.

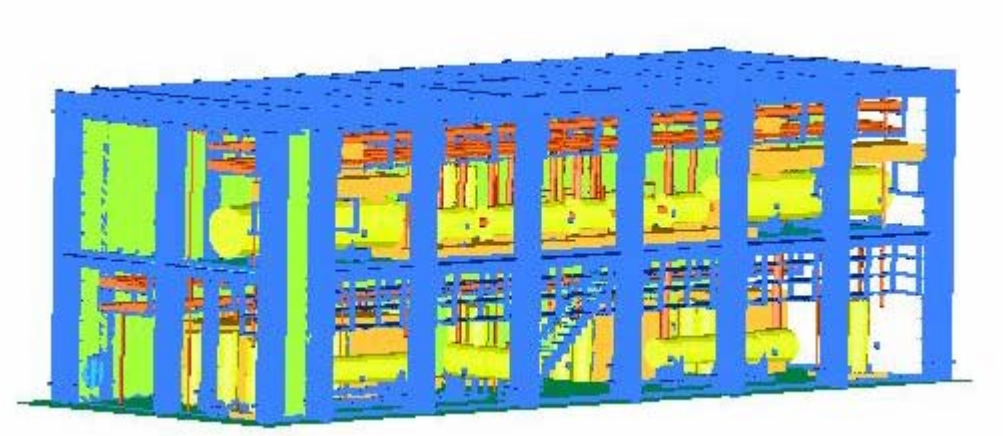

Figure 5.1.4: The geometry of the full-scale HIGH-A M24-module.

Scenario definition: Most of the scenario input is described in appendix 12.
The simulations are performed with 6 different scenarios, varying the point of ignition and the water spray system. The options are either centre or end ignition, and no water spray, MV57-nozzles or LDN-nozzles. The scenario input is in appendix 12.

- WATER SPRAY:
  Two different types of water spray were used in these simulations:
  - Medium velocity nozzles: MV57
  - Large droplet nozzles: LDN

The characteristic parameters for the two different nozzles are shown in Table 5.1.6. The k-factors from the manufacturer are originally 99.5 for the MV57-nozzles and 200 for the LDN-nozzles, but the values given in table 5.1.6 is estimated based on the experiments performed with the module [8]. The total flow rate for the nozzles is found by multiplying the water flow from one nozzle (Q) by the number of nozzles, and dividing by 60 to get the results in l/s. Q is found by formula 4.2.7 The flow rate is over 2 times higher with the LDN nozzle compared to the MV57 nozzle.

Nozzle	**Pressure [bar]**	**Number of nozzles**	**k-factor**	**Total flow rate [l/s]**
MV57	1.65	27	94.5	55
LDN	0.5	65	160	123

Table 5.1.6: Characteristic values for the MV57- and LDN-nozzles

The activated water spray is expected to cover the whole module in the simulations. In addition it is assumed that the water spray will cover two meters out on each side in the case of central ignition, and four meters out on the far side at end ignition. The average droplet size is calculated by formula 4.2.4.
If we have nozzles that get very small or very large droplet diameters, as the LDN-nozzles, it is normally not representative to use formula 4.2.4 when calculating the droplet diameter. With these nozzles the manufacturer value is normally used, but in this situation a different droplet diameter has little influence on the final result and the formula is therefore used [8]. The terminal velocity is found by formula 4.2.6, and the water volume fraction, F1 and F2 are calculated respectively by formulas 4.2.5, 4.2.8 and 4.2.9. The calculated values for the different nozzles are shown in Table 5.1.7:

Nozzle	**Number of nozzles**	**X_{len} [m]**	**Y_{len} [m]**	**D [μm]**	**Uz [m/s]**	**WVF [l/m^3]**	**F1**	**F2**
MV57	27	25.6	8.0	846	2.14	0.125	3.73	0.284
LDN	65	25.6	8.0	1260	3.11	0.192	5.98	0.124

Table 5.1.7: Calculated values for the different nozzles.

5.1.4 Kårstø

At 2003-11-12 a technical report was issued containing a detailed probabilistic explosion analysis of external explosions on the Kårstø process facilities, performed by DNV [1]. This report gives an analysis of two different areas at the Kårstø plant: Statpipe/Sleipner and Åsgard. This report states that due to the high explosion loads that is calculated, especially in the Åsgard area, it is recommended to consider mitigating measures. An effective "blow down" system would have a significant impact on the explosion risk at the Kårstø facility. Based on the performed simulations by DNV, water spray will be implemented in new FLACS-simulation to see which effect this will have on explosion pressure and gas dispersion. Representative simulation scenarios are used for each of the two areas. These scenarios are chosen based on the following facts:

- A smaller filling rate is more probable.
- A larger filling rate gives a higher ignition probability.
- A larger filling rate gives a higher explosion pressure.
- End ignition in the gas cloud gives a higher explosion pressure.
- Water spray has a better mitigating effect by end ignition compared to central ignition.

A water spray system consists of one or more water supplies and one or more sprinkler installations. This installation consists of one control valve set and a pipe system with attached sprinkler heads (nozzles). Because this system is placed outside, a dry system is required due to frost problems. This means that the pipes are normally filled with air or inert gas under pressure, downstream the dry alarm valve. The type of dry system that is most suitable in this case is a pre-action installation type B. This is like a normal dry system, where either an automatic fire/gas detection system or the sprinkler heads controls the alarm valve. In this case the system can be used for fighting both fires and gas explosions.

When designing a sprinkler system one first has to define the facilities risk class. Kårstø has a high-risk production, and therefore goes under the HHP-class [9]. This class covers industry activity where the product has a high combustion and fire load, which will cause rapid spreading or intense fire. This class has the following specifications:

- There shall always be a free space under the sprinkler deflector on at least 1.0m.
- The maximum area covered by each sprinkler shall not exceed 9.0m^2.
- The maximum distance between each sprinkler in x-and y-direction shall not exceed 3.7m.
- The minimum allowed pressure for a released sprinkler head is 0.5 bar.
- The minimum allowed pipe diameter is 25mm.

A) The Statpipe/Sleipner area

In the report by DNV [1] the following simplification is defined: Because of the large areas involved in the FLACS geometry model of Kårstø all simulations in the Statpipe/Sleipner area have been carried out in the train 200 (fire area FA17A and FA17B) sub area. This area is assessed to be the highest congested area and therefore exposed to the highest explosion loads. The other trains in the Statpipe/Sleipner area are assessed by engineering judgment relative to the results in the train 200 sub area.

Geometry

The geometry used by DNV was based on CAD import from MS Microstation, but the FLACS geometry imported from CAD was modified based on drawings and visits to the Kårstø process facility. The geometry of the Statpipe/Sleipner area is shown in Figure 5.1.5 and 5.1.6.

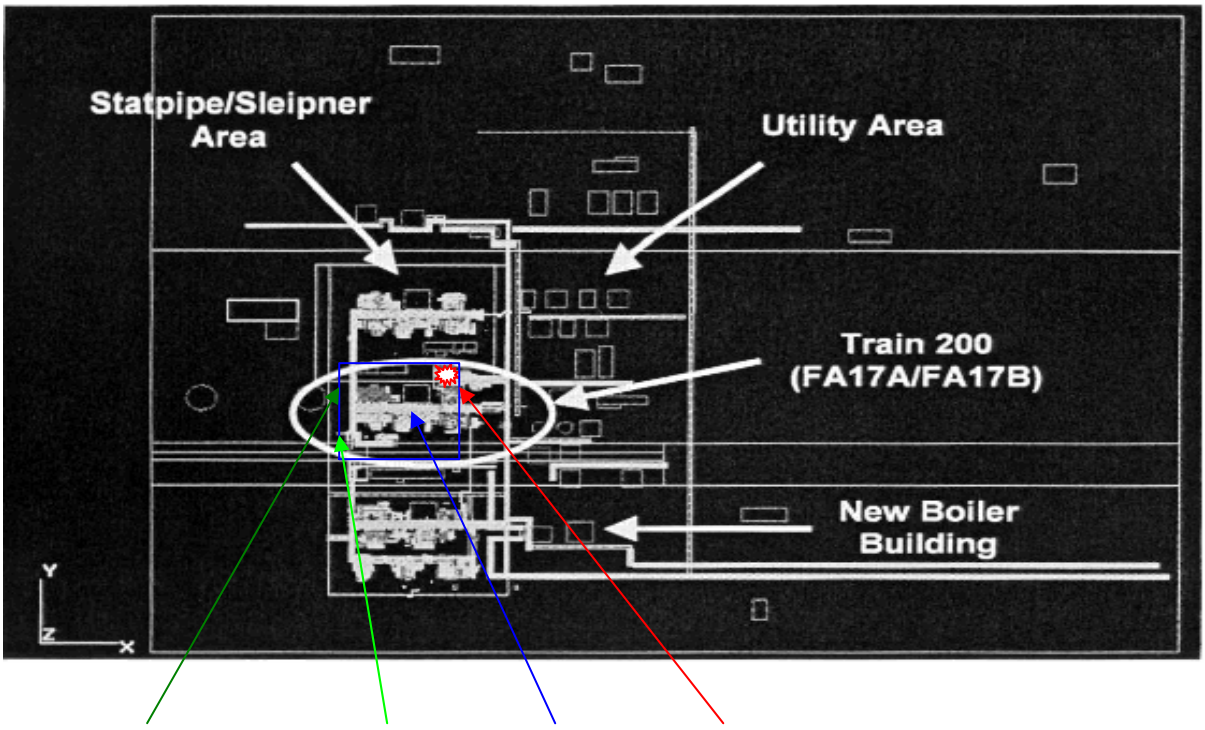

Figure 5.1.5: 2D Geometry model of the Statpipe/Sleipner area seen from above with north along the y-axis.

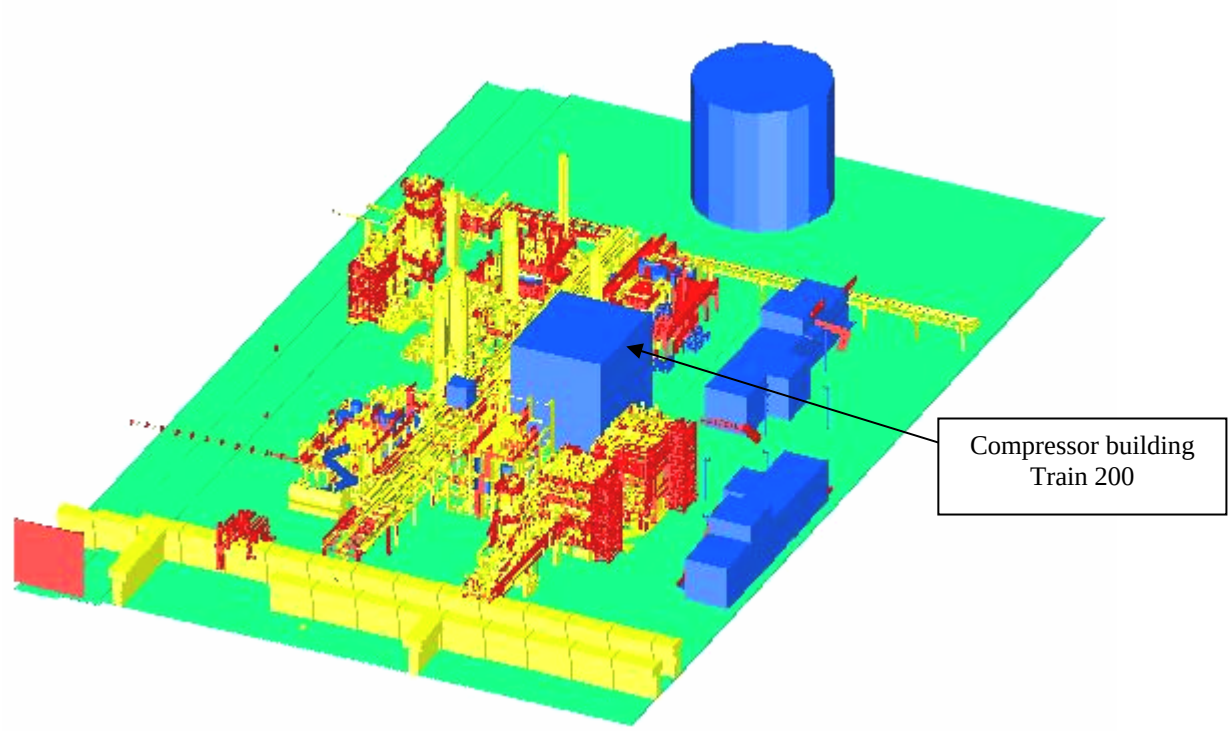

Figure 5.1.6: Close up view of Train 200 (FA17A/FA17B) seen from northeast.

Gas composition

The gas composition in the explosion simulations is shown in Table 5.1.8. The size of the gas cloud is varied between 100, 50, 30, 15, 10 and 5 % filling of train 200, and for each gas cloud size the cloud location, cloud shape and ignition location is varied. A total of 73 different explosion scenarios have been simulated by DNV [1]. Based on the facts listed in the last page a gas cloud positioned in the northwest with a filling of 30% is chosen.

Type of gas	Gas composition [%]
Methane	85.0
Ethane	6.7
Propane	8.0
CO_2	0.3

Table 5.1.8: Gas composition.

Grid

The simulation volume of the grid was set to 300m × 300m × 120m. The minimum control volume size is set to 1.5, and the grid is stretched with a factor of 1.2 in all directions outside the train 200 area. The final number of control volumes are 124 × 107 × 37.

Scenario: Most of the scenario input is described in appendix 15, and the location of the water spray is shown in appendix 17.

.

- WATER SPRAY:
  The following factors are varied in the simulations:
  - Type of nozzle
  - Nozzle region

  Three different types of water spray nozzles were used in these simulations:
  - Sprinkler nozzles: CUP 10
  - Large droplet nozzles: LDN
  - Medium velocity nozzles: MV57

  Nozzles are positioned at different locations in the different simulations:
  - Region 1: 100 nozzles near ignition
  - Region 2: 400 nozzles far from ignition
  - Region 3: 600 nozzles all over

	Position			**Size**		
Nozzle region	$\mathbf{X_{min}}$	$\mathbf{Y_{min}}$	$\mathbf{Z_{min}}$	$\mathbf{X_{len}}$	$\mathbf{Y_{len}}$	$\mathbf{Z_{len}}$
1	19867.8	5015	0	30	30	25
2	19775	4945	0	60	60	25
3	19780	4950	0	75	72	25

Table 5.1.9: Location of nozzle regions.

For one selected scenario performed by DNV, a variation of three different nozzle types at three different locations (regions) is implemented and simulated. The characteristic parameters for the different nozzles are given in Table 5.1.10, and the parameters for the 9 different scenario cases are given in Table 5.1.11.
The mean droplet diameter for the different water pressures is calculated by formula 4.2.4 for all of the nozzles except the LDN- nozzle, which have a given value from the manufacturer. For very small (P120) or very large droplets (LDN) the estimated Sauter diameter from formula 4.2.4 is normally not representative.
The average droplet velocity for all of the nozzles is calculated by formula 4.2.6, and the water volume fraction, F1 and F2 are calculated respectively by formulas 4.2.5, 4.2.8 and 4.2.9.

Nozzle	**k-value**	**Diameter [μm]**	**Average velocity [m/s]**
CUP10	57	Estimated Sauter diameter	Gravity driven
MV57	90.5	Estimated Sauter diameter	Gravity driven
LDN	200	From manufacturer: 2500	Gravity driven

Table 5.1.10: Characteristic parameters for the different nozzles.

Sim nr	Nozzle	N	Location	P [bar]	D [μm]	Uz [m/s]	WVF [l/m^3]	F1	F2
0	-	-	-	-	-	-	-	-	-
1	CUP10	100	Near ignition	3.0	693.6	1.77	0.10	2.56	0.42
2	CUP10	400	Far from ignition	3.0	693.6	1.77	0.10	2.56	0.42
3	CUP10	600	All	3.0	693.6	1.77	0.10	2.56	0.42
4	MV57	100	Near ignition	1.65	846	2.14	0.10	3.01	0.35
5	MV57	400	Far from ignition	1.65	846	2.14	0.10	3.01	0.35
6	MV57	600	All	1.65	846	2.14	0.10	3.01	0.35
7	LDN	100	Near ignition	0.5	2500	5.92	0.04	3.67	0.30
8	LDN	400	Far from ignition	0.5	2500	5.92	0.04	3.67	0.30
9	LDN	600	All	0.5	2500	5.92	0.04	3.67	0.30

Table 5.1.11: Characteristic values for the different simulations.

B) The Åsgard area

In the report by DNV [1] the following simplification is defined: Because of the large areas involved in the FLACS geometry model of Kårstø all simulations in the Åsgard area have been carried out in fire area FA102 and FA104. This area is assessed to be the highest congested area and therefore exposed to the highest explosion loads. The other fire areas in Åsgard are assessed by engineering judgment relative to the results in the FA102/FA104 area.

Geometry
The geometry used by DNV was based on CAD import from MS Microstation, but the FLACS geometry imported from CAD was modified based on drawings and visits to the Kårstø process facility. The geometry of the Åsgard area is shown in Figures 5.1.7 and 5.1.8. North is along the y-axis.

Gas composition
The gas composition in the explosion simulations is the same as in the Statpipe/Sleipner area, and is shown in Table 5.1.8. The size of the gas cloud is varied between 100, 50, 30, 15, 10 and 5 % filling of train 200, and for each gas cloud size the cloud location, cloud shape and ignition location is varied. A total of 72 different explosion scenarios have been simulated by DNV [1]. Based on the facts listed in page 38 a gas cloud positioned in the south, to the right, with a filling of 30% is chosen.

Grid
The simulation volume of the grid was set to 402m × 300m × 120m. The minimum control volume size is set to 1.5, and the grid is stretched with a factor of 1.2 in all directions outside fire area FA102/FA104. The final number of control volumes are 95 × 119 × 40.

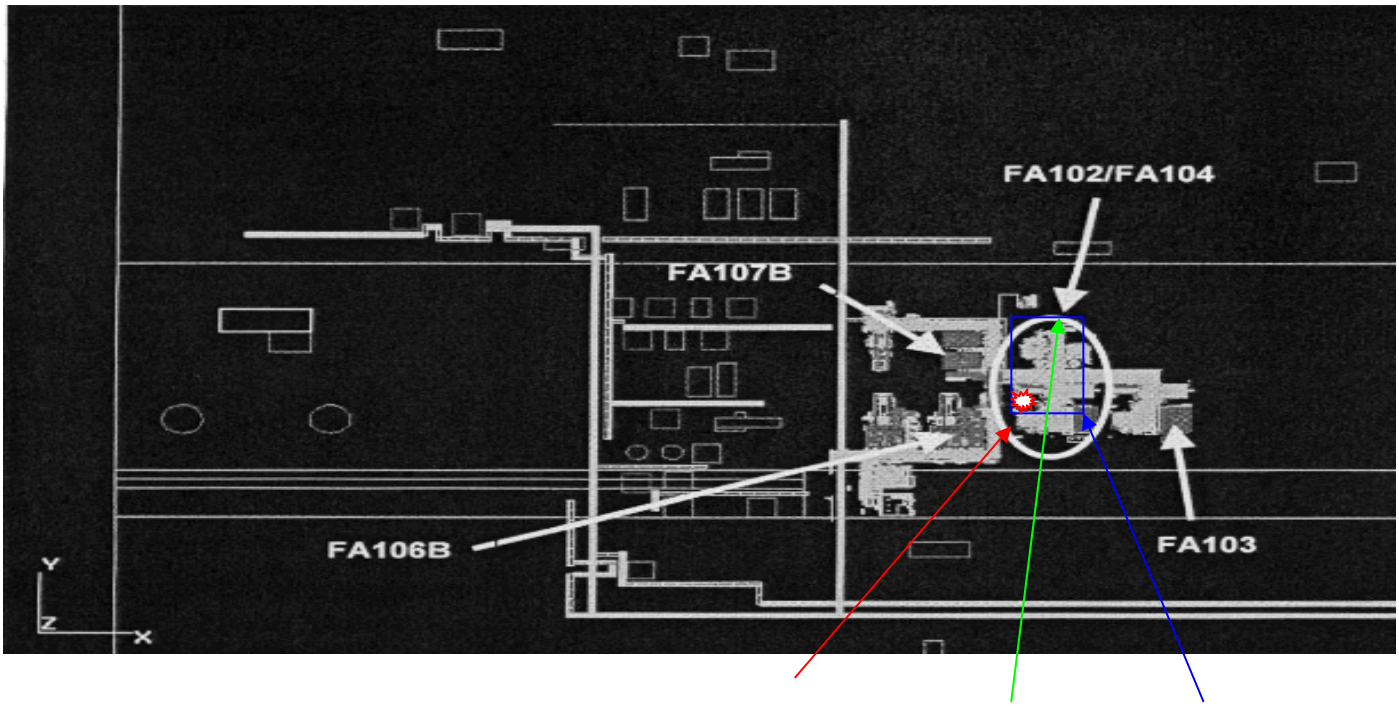

Figure 5.1.7: 2D Geometry model of the Åsgard area seen from above with north along the y-axis.

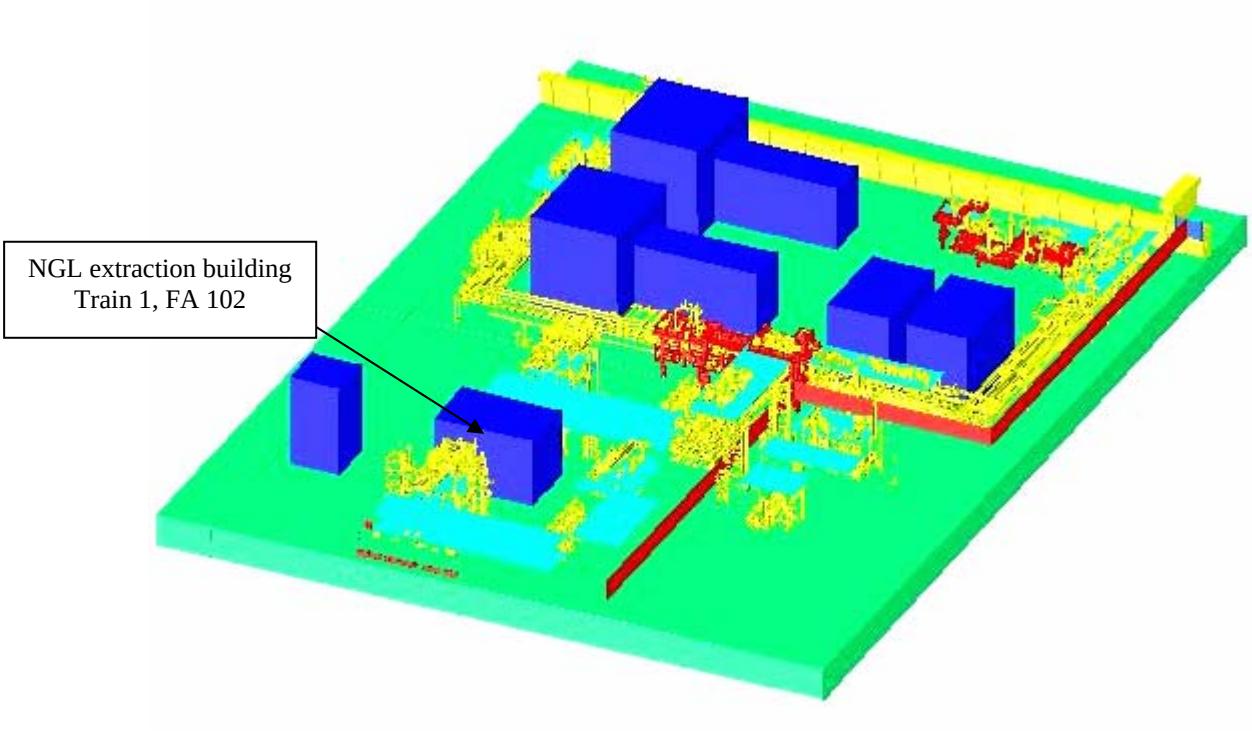

Figure 5.1.8: 3D close up view of fire area FA102/FA104 seen from northeast.

Scenario definition: Most of the scenario input is described in appendix 19, and the location of the water spray is shown in appendix 21.

- WATER SPRAY:
  The following factors are varied in the simulations:
  - Type of nozzle
  - Nozzle positions

  Three different types of water spray nozzles were used in these simulations:
  - Sprinkler nozzles: CUP 10
  - Large droplet nozzles: LDN
  - Medium velocity nozzles: MV57

  Nozzles are positioned at different locations in the different simulations:
  - Region 1: 100 nozzles near ignition
  - Region 2: 200 nozzles far from ignition
  - Region 3: 600 nozzles all over

	Position			**Size**		
Nozzle region	$\mathbf{X_{min}}$	$\mathbf{Y_{min}}$	$\mathbf{Z_{min}}$	$\mathbf{X_{len}}$	$\mathbf{Y_{len}}$	$\mathbf{Z_{len}}$
1	20221	5008.5	0	30	30	25
2	20230	5087	0	60	30	25
3	20230	5023	0	60	90	25

Table 5.1.12: Location of nozzles.

For one selected scenario performed by DNV, a variation of three different nozzle types at three different locations (regions) is implemented and simulated. The characteristic parameters for the different nozzles are already given in Table 5.1.10, and the parameters for the 9 different scenario cases are given in Table 5.1.13. The mean droplet diameter for the different water pressures is calculated by formula 4.2.4 for all of the nozzles except the LDN- nozzle, which have a given value from the manufacturer. For very small (P120) or very large droplets (LDN) the estimated Sauter diameter from formula 4.2.4 is normally not representative. The average droplet velocity for all but one of the nozzles is calculated by formula 4.2.6, but for the HV26 nozzle it is necessary to estimate a value because of the high velocity. The water volume fraction, F1 and F2 are calculated respectively by formulas 4.2.5, 4.2.8 and 4.2.9.

Sim nr	Nozzle	N	Location	P [bar]	D [μ]	Uz [m/s]	WVF [l/m3]	F1	F2
10	-	-	-	-	-	-	-	-	-
11	CUP10	100	Near ignition	3.0	693.6	1.77	0.10	2.56	0.42
12	CUP10	200	Far from ignition	3.0	693.6	1.77	0.10	2.56	0.42
13	CUP10	400	All	3.0	693.6	1.77	0.10	2.56	0.42
14	MV57	100	Near ignition	1.65	846	2.14	0.10	3.01	0.35
15	MV57	200	Far from ignition	1.65	846	2.14	0.10	3.01	0.35
16	MV57	400	All	1.65	846	2.14	0.10	3.01	0.35
17	LDN	100	Near ignition	0.5	2500	5.92	0.04	3.67	0.30
18	LDN	200	Far from ignition	0.5	2500	5.92	0.04	3.67	0.30
19	LDN	400	All	0.5	2500	5.92	0.04	3.67	0.30

Table 5.1.13: Characteristic values for the different simulations.

5.2 Modelling of water spray in FLACS 2.2.6

In 2003 an extension of the FLACS 2.2.5 model was made, now including oil mist modelling and two-phase flow [3]. This improved model is significantly extended due to the handling of liquid phase in the form of mist in addition to the gaseous phase. The mist involves a whole range of different droplet diameters that will vary in both space and time. To model this droplet size distribution a set of droplet classes is introduced, where each droplet class has a local representative value that varies in position and time. This model takes into account break-up of droplets, coalescence of droplets and evaporation of droplets. When this model was tested the boiling and evaporation of droplets didn't give a correct physical result. When the droplet speed was zero, the model transfers no heat to the droplets, which is not correct. To include the reduction in burning velocity due to the presence of water droplets, a reduction in flame temperature as a function of the mass of water divided by the mass of gas is made.

The adiabatic flame temperature can be calculated by the following formula:

$$T_f = T_0 + \frac{\Delta H_c}{\Sigma n_j * Cp_j} \qquad (5.2.1)$$

T_0 = Initial temperature [K]
T_f = Flame temperature [K]
n_j = The number of mole of species j [mole]
Cp_j = The specific heat capacity of species j [J/mole]
ΔH_c = Heat of combustion [J/K]

$\Delta H_c = \Delta H_f$, products - ΔH_f, reactants
ΔH_f = Heat of formation [J/K]

The calculations are based on an initial temperature of 293K, and the following reaction between methane and air:

$0.5CH_4 + O_2 + 3.76N_2 \rightarrow 0.5CO_2 + H_2O + 3.76N_2$

Liquid water is included in the reaction, representing the water spray droplets:

$0.5CH_4 + xH_2O(L) + O2 + 3.76N_2 \rightarrow (0.5\text{-}y)CO_2 + yCO + 3.76N_2 + OH + H_2 + zH_2O(g)$

The amount of liquid water represented by "x" is varied to obtain a relation between the reduction in flame temperature, $\Delta T = T_f - T_0$, and the mole of water per mole O_2. The calculations were confirmed with the chemical equilibrium calculator Grashof. The results are given in Table 5.2.1, Figure 5.2.1 and Figure 5.2.2. A trend line is calculated for the results in Figure 5.2.1 and 5.2.2, which gives the following equation for ΔT:

$f(x) = 402.97x \qquad (5.2.2)$

x = mole water per mole 0_2

Amount of water [mol] per mol O_2	Flame temperature [K]	$\Delta T = T_0 - T$
0	2232.4	0
0.1	2188.3	44.1
0.2	2144.6	87.8
0.3	2101.4	131.0
0.4	2058.7	173.7
0.5	2016.5	215.9
0.6	1974.8	257.6
0.7	1933.8	298.6
0.8	1893.4	339.0
0.9	1853.8	378.6
1.0	1814.9	417.5
1.1	1776.8	455.6
1.2	1739.6	492.8
1.3	1703.2	529.2
1.4	1667.7	564.7
1.5	1630.0	602.4
1.6	1599.2	633.2
2.0	1472.0	760.4

Table 5.2.1: The flame temperature and reduction in flame temperature as a function of mole water per mole O_2.

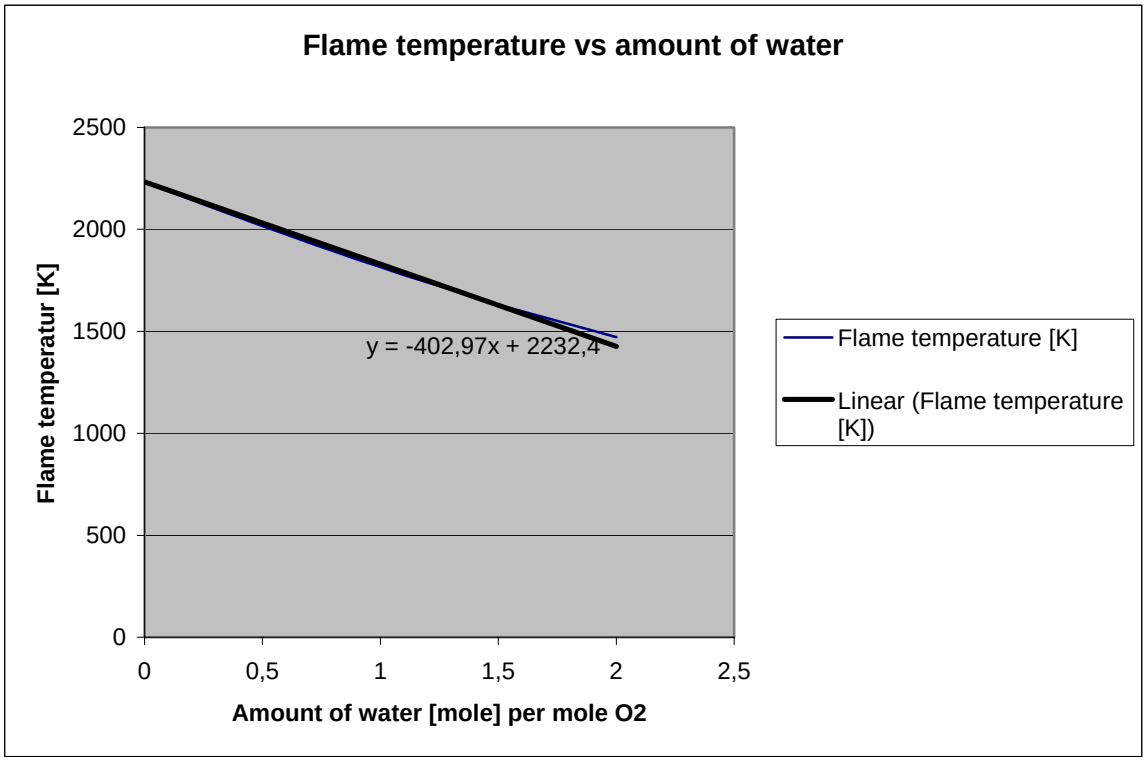

Figure 5.2.1: Flame temperature as a function of the amount of water per mole O_2

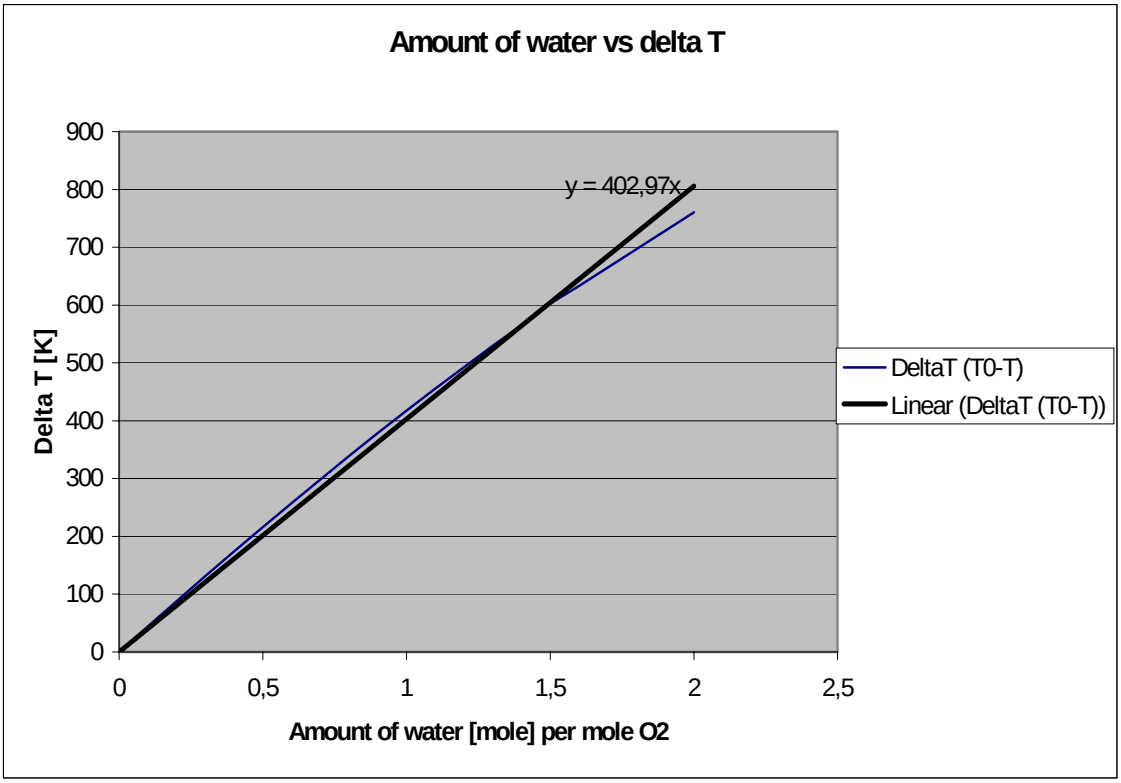

Figure 5.2.2: ΔT as a function of the amount of water per mole O_2.

To get the wanted relation between the reduction in flame temperature and mass of water divided by mass of gas, equation 5.2.2 has to be multiplied by a factor. This factor is found by doing the following conversion from (mole water/mole O_2) to (mass water/mass gas):

$$\frac{mole_{water}}{mole_{O_2}} \times \frac{Mm_{water}}{Mm_{O_2}} = \frac{mole_{water}}{mole_{O_2}} \times \frac{18g/mole}{32g/mole} \rightarrow$$

$$\frac{kg_{water}}{kg_{O_2}} \times \frac{kg_{O_2}}{kg_{gas}} = \frac{18}{32} \times \frac{(mole*Mm)O_2}{(mole/*Mm)O_2 + (mole*Mm)N_2 + (mole*Mm)CH_4} = \frac{18}{32} \times \frac{32}{145} = \frac{18}{145}$$

Equation 5.2.2 then becomes:

$$f(x) = 402.97x * \frac{18}{145} = 402.97x * 0.124 \rightarrow$$

$$\Delta T = 402.97x * 0.124 = 50x \qquad (5.2.3)$$

$$x = \frac{kg_{water}}{kg_{gas}}$$

The relation between the burning velocity and the decrease in flame temperature can be made based on formula 5.2.4, which is a relation between laminar burning velocity as a function of the flame temperature. This formula is taken from a dr.thesis written by Bjørn Arntzen [10]:

$$S_L = \frac{T_{products}}{1550} - 1 \qquad (5.2.4)$$

S_L" = k * S_L (5.2.5)

$$\rightarrow k = \frac{S_L''}{S_L} = \frac{\frac{T_p'' - 1550}{1550}}{\frac{T_p - 1550}{1550}} = \frac{T_p'' - 1550}{T_p - 1550} = 1 - \frac{T_p - T_p''}{T_p - 1550} = 1 - \frac{\Delta T}{T_p - 1550}$$

$$k = 1 - \frac{\Delta T}{T_p - 1550} \qquad (5.2.6)$$

S_L" = reduced burning velocity
T_p" = reduced flame temperature

We put Tp = 2232.4K and ΔT from equation 5.2.3 in equation 5.2.6, and get the following relation:

$$k = 1 - \frac{\Delta T}{T_p - 1550} = 1 - \frac{402.97x \times 0.124}{2232.4 - 1550} = 1 - \frac{50x}{682.4} = 1 - 0.07x \qquad (5.2.7)$$

$$S_L'' = S_L \times (1 - 0.07x) \qquad (5.2.8)$$

When there is no water present x = 0, and according to equation 5.2.7 the constant k = 1. This gives $S_L = S_L$" in equation 5.2.8, which is correct since there is no reduction in the burning velocity.

Equation 5.2.8 is implemented in the FLACS 2.2.6 code, and the model is now called FLACS 2.2.6*.

5.3 Explosion simulation with FLACS 2.2.6*

The following simulations will be performed by FLACS- version 2.2.6* (2004).

5.3.1 Explosion box

This simulation of the 180m^3 explosion box filled with stoichiometric natural gas/air mixture was based on a rapport of experiments performed with this geometry by British Gas [6]. The geometry, grid and scenario input is described in chapter 5.1.1. Deviations from the scenario input in chapter 5.1.1 will be listed below.

Scenario definition: Most of the scenario input is described in appendix 23.

Water spray:
Parameters used when modelling water spray release is for each nozzle the nozzle position, the release direction (vertically downward), the volume rate [l/min], the orifice area of the nozzle and the water temperature. The positions of the water spray nozzles are given under the scenario definition for "leaks", and the size of the initial droplet diameter [mm] are given under "sources". A so-called cl-file is made manually for each nozzle; cl010101.n001 would be the name of the cl-file for scenario 010101 and nozzle number 1. The first lines of a cl-file may look like the following:

J-Z: particle: region-water

TIME (s)	*AREA (m^2)*	*RATE (m^3/s)*	*VEL (m/s)*	*RTI (-)*	*TLS (m)*	*T(K)*
0.000E+01	*1.246E -04*	*3.103E -05*	*2.491E -01*	*0.05*	*0.00252*	*293.15*
0.050E+01	*1.246E -04*	*3.103E -03*	*2.491E+01*	*0.05*	*0.00252*	*293.15*
1.000E+01	*1.246E -04*	*3.103E -03*	*2.491E+01*	*0.05*	*0.00252*	*293.15*

It must be noted that the Relative turbulence intensity (RTI) and Turbulent length scale (TLS) is not active in this file. At start up the volume rate and flow velocity is given a value 1.0% of the value later on, this to get a smooth start up of the water spray. The parameters for the different scenarios are given in Table 5.3.1.

Nozzle	**Number nozzles**	**K-value**	**P [bar]**	**D [mm]**	**Total flow rate [l/min]**	**Flow rate/nozzle [l/min]**	**Orifice area [m^2]**	**Velocity [m/s]**
HV60	8	93	3.5	0.659	1392.0	174.0	$1.766*10^{-4}$	16.42
HV60	8	93	5.0	0.585	1664.0	208.0	$1.766*10^{-4}$	19.63
MV57	8	99.5	3.5	0.659	1489.2	186.2	$1.246*10^{-4}$	24.91

Table 5.3.1: Characteristic parameters for the different scenarios with HV60- and MV57-nozzles.

Water flow rate from one nozzle in l/min, Q, is found by equation 4.2.7. To get the value in m^3/s the flow rate is converted by:

$$Q\frac{l}{\min} = Q\frac{dm^3}{\min} \rightarrow Q\frac{dm^3}{\min} \times \frac{10^{-3}}{60s} = Q\frac{m^3}{s} \qquad (5.3.1)$$

Dividing Q from equation 5.3.1 on the orifice area gives the velocity of the water flowing trough the nozzle.

5.3.2 1:5 offshore module, M24-25

The experiments with the 1:5 offshore module was performed at the CMR large-scale gas explosion test site at Sotra outside Bergen [7]. The geometry used in the experiments is a $50m^3$ small-scale version combining the to modules M24 (compressor module) and M25 (separator module) at Gullfaks-A. The gases used in the experiments were slightly over-stoichiometric gas mixtures of methane (9.8%) or propane (4.2%) in air. The geometry, grid and scenario input is described in chapter 5.1.2. Deviations from the scenario input in chapter 5.1.2 and 5.3.1 will be listed below. The parameters for the different scenarios are given in Table 5.3.2.

- SOURCES: Under Diameter class the initial diameter is taken from table 5.3.2 for the different scenarios.

Nozzle	Number nozzles	K-value	P [bar]	D [mm]	Total flow rate [l/min]	Flow rate/nozzle [l/min]	Orifice area [m^2]	Velocity [m/s]
HV26	4	43	3.5	0.659	321.8	80.4	$1.1304*10^{-4}$	11.85
HV26	8	43	3.0	0.694	595.8	74.5	$1.1304*10^{-4}$	19.98
CUP5	4	17	7.0	0.523	179.9	45.0	$1.9625*10^{-5}$	38.20
CUP5	8	17	3.8	0.641	265.1	33.1	$1.9625*10^{-5}$	28.14
CUP10	4	57	2.4	0.747	353.2	88.3	$7.85*10^{-5}$	18.75
CUP10	4	57	3.0	0.694	394.9	98.7	$7.85*10^{-5}$	21.02
CUP10	6	57	3.0	0.694	592.4	98.7	$7.85*10^{-5}$	21.02
CUP10	8	57	2.4	0.747	706.4	88.3	$7.85*10^{-5}$	18.75
CUP10	8	57	3.0	0.694	789.6	98.7	$7.85*10^{-5}$	21.02
CUP10	8	57	3.5	0.659	853.1	106.6	$7.85*10^{-5}$	22.64
P120	4	6	7.6	0.509	66.2	16.5	$7.30*10^{-6}$	37.66
P120	8	6	7.6	0.509	132.3	16.5	$7.30*10^{-6}$	37.66
P120	16	6	4.0	0.630	192.0	12.0	$7.30*10^{-6}$	27.40

Table 5.3.2: Characteristic values for the different scenarios with CUP5, CUP10, MV57 and HV26 nozzles.

- LEAKS: 16 leaks are defined to represent the nozzles in the M24-25 module.
  Type: “Jet”
  Position:

Water region	Nozzle number	Position		
		X	Y	Z
9	1	0.25	0.625	2.5
9	2	0.25	1.875	2.5
8	3	1.25	0.625	2.5
8	4	1.25	1.875	2.5
7	5	2.25	0.625	2.5
7	6	2.25	1.875	2.5
6	7	3.25	0.625	2.5
6	8	3.25	1.875	2.5
4	9	4.75	0.625	2.5
4	10	4.75	1.875	2.5
3	11	5.75	0.625	2.5
3	12	5.75	1.875	2.5
2	13	6.75	0.625	2.5
2	14	6.75	1.875	2.5
1	15	7.75	0.625	2.5
1	16	7.75	1.875	2.5

Table 5.3.3: Position of nozzles in M24-25 module

5.3.3 Full scale module

British Gas performed the experiments with this full-scale geometry, which is a 3:2:1 scale copy of the 50m^3 M24-module [8]. This is again a 1:5 scale model of the M24-module on the Gullfaks-A platform in the North Sea. The module is filled with a stoichiometric mixture of 91.7% methane, 7% ethane and 1.3% propane in air. Deviations from the scenario input in chapter 5.1.2 and 5.3.1 will be listed below. The parameters for the different scenarios are given in Table 5.3.4.

- SOURCES: Under “diameter class” the initial diameter is taken from table 5.3.4 for the different scenarios. The K-value is based on the performed experiments and is therefore slightly different from the value from the manufacturer.

Nozzle	**Number nozzles**	**K-value**	**P [bar]**	**D [mm]**	**Total flow rate [l/min]**	**Flow rate/nozzle [l/min]**	**Orifice area [m^2]**	**Velocity [m/s]**
MV57	27	94.5	1.65	0.659	3277.5	121.39	$1.246*10^{-4}$	16.24

Table 5.3.4: Characteristic values for the different scenarios with MV57 and HV26 nozzles

- LEAKS, MV57: 27 leaks are defined to represent the nozzles in the full-scale module.
  Type: “Jet”
  Position:

Nozzle number	Position			Nozzle number	Position		
	X	Y	Z		X	Y	Z
1	3.1	2	8	15	15.0	6	8
2	5.6	2	8	16	17.3	6	8
3	8.1	2	8	17	20.0	6	8
4	10.6	2	8	18	3.1	8	8
5	13.1	2	8	19	5.6	8	8
6	15.6	2	8	20	8.1	8	8
7	18.1	2	8	21	10.6	8	8
8	20.6	2	8	22	13.1	8	8
9	23.1	2	8	23	15.6	8	8
10	2.5	6	8	24	18.1	8	8
11	5.0	6	8	25	20.6	8	8
12	7.5	6	8	26	23.1	8	8
13	10.0	6	8	27	3.1	8	8
14	12.5	6	8				

Table 5.3.5: Position of MV57-nozzles in the full-scale module.

5.4 Dispersion simulations with FLACS 2.2.6*

The following simulations will be performed by FLACS- version 2.2.6* (2004).

5.4.1 Kårstø

In this chapter the effect of water spray on gas dispersion at the Kårstø facility will be investigated. There will be performed four simulations, two in the Statpipe/Sleipner area and two in the Åsgard area. The scenarios are based on dispersion simulations without water spray performed by DNV [1]. These scenarios are to be interpreted as worst-case scenarios with formation of large flammable gas clouds, and the simulations will therefore be performed with very high leak rates. The largest flammable gas clouds occur when the relation between the flow of gas (Q_g) and the flow of air (Q_a) is close to 0.15. This can be expressed by the following expression:

$$R = \frac{Q_g}{Q_a} = 0.15 \qquad (5.4.1)$$

A) The Statpipe/Sleipner area

Two simulations will be performed in this area, one dry simulation and one simulation including water spray. The leak is positioned at the end (west) of the area. The nozzle used in the simulations is MV12. The scenarios for the four different simulations are shown in Table 5.4.1. The location of the two different leaks is shown in Figure 5.4.1. The grid and monitor points are the same as in the explosion scenarios in chapter 5.1.4.

Simulation	Water spray	Leak location	Leak jet direction	Leak rate [kg/s]	Wind direction	Wind speed [m/s]	R-value
1	-	West	East	878.6	East	3.2	0.15
2	MV12	West	East	878.6	East	3.2	0.15

Table 5.4.1: Scenario configurations for the Statpipe/Sleipner area.

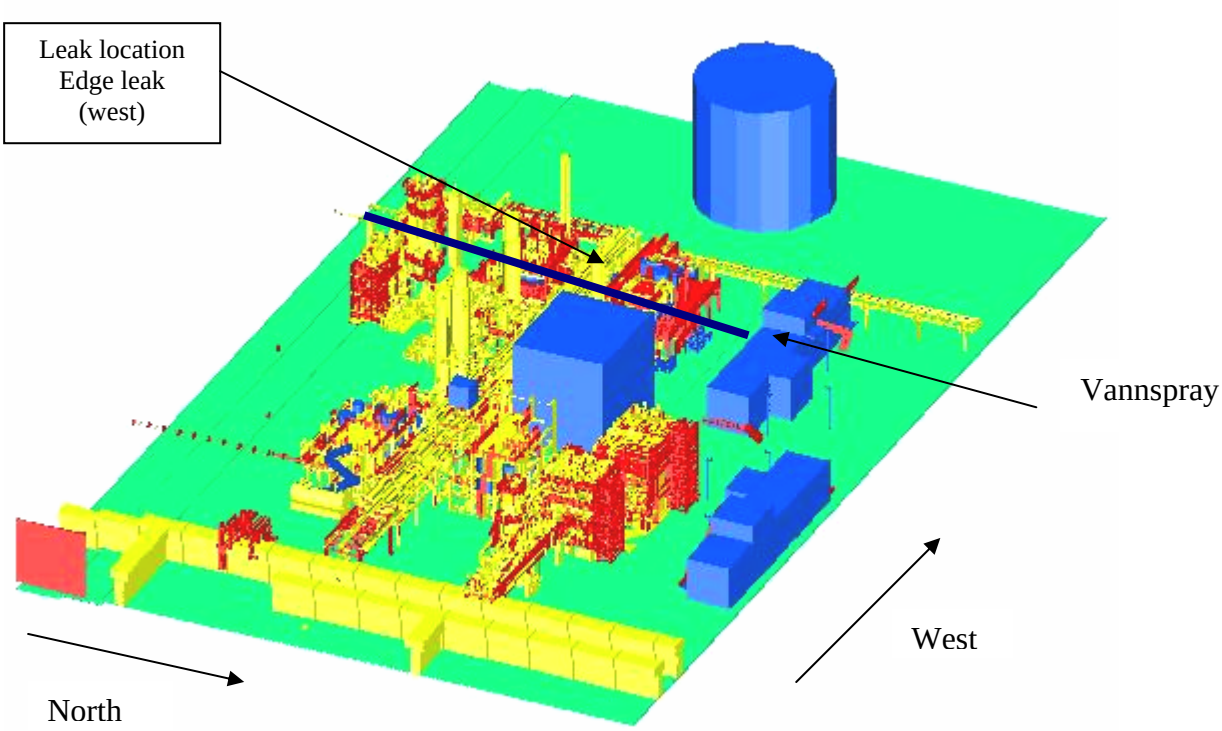

Figure 5.4.1: Location of centre and edge (west) leaks at the Statpipe/Sleipner area seen from the northeast.

Scenario definition: Most of the scenario input is listed in appendix 24.

- WATER SPRAY:
  The position of the water spray is defined under "LEAKS". A cl-file is made manually for each water spray nozzle, including orifice area, flow rate, velocity and temperature. The flow rate from one nozzle, Q, in l/min is found by equation 4.2.7 to be 33.33l/min. The volume rate m^3/s from one nozzle is found by using equation 5.3.1, which gives $Q = 5.55*10^{-4}$ m^3/s. The orifice diameter for the MV12-nozzle is 0.0054 m, which gives an orifice area of $2.2902*10^{-5}$. The velocity of the water flowing from the nozzle can now easily be calculated by dividing the volume rate on the orifice area, which gives a value of 24, 234 m/s. The characteristic parameters for the nozzle are displayed in Table 5.4.2. At the start the flow rate and the velocity are given a value 1 % of the calculated value to get a smooth start-up.

Nozzle type	**K-factor**	**Pressure [bar]**	**Droplet diameter [mm]**	**Number of nozzles**	**Total Flow rate [m^3/s]**	**Flow rate/ Nozzle [m^3/s]**	**Orifice area [m^2]**	**Velocity [m/s]**
MV12	18	3.43	0.7	20	$1.11*10^{-2}$	$5.55*10^{-4}$	$2.2902*10^{-5}$	24.234

Table 5.4.2: Different parameters for the MV12 nozzles.

6. Results

This chapter contains a presentation of the primary results from the simulations, and gives a comment to important primary findings. A thorough analysis and discussion of the results will be performed in the next chapter.

6.1 Simulation results with FLACS 2.2.5

Simulations were performed for different geometries and different scenarios with the existing FLACS model, version 2.2.5 (2001).

6.1.1 Simulations with explosion box

The simulations were performed with two different ventilation openings of 1.5m×1.5m (Kv=9) and 4.5m×4.5m (Kv=1), and five different congestions of 0, 20, 40, 56 and 80 pipes. There were performed simulations without water spray and with two different water spray nozzles, HV60 and MV57. Configurations for the different simulations are shown in appendix 2, and maximum overpressure data at the different monitors for the simulations is shown in appendix 3.

Simulation 1, 2, 3 and 4:
In these simulations we have a small vent opening and no congestion. Table 6.1.1 shows the maximum overpressure and when this occurs for the different simulations. These results show that the maximum overpressure becomes larger and the pressure build-up is enhanced with the use of water spray. The pressure peak occurs significantly earlier with the use of water spray. A plot combining the pressure from monitor 1 in these four simulations is shown at the top in appendix 5 page 114. At a water pressure of 3.5 bar the use of MV57-nozzles gives a slightly larger pressure and occurs earlier than with the use of HV60 nozzles, but the deviations are minimal. When the water pressure is increased to 5 bars for the HV60-nozzle, the pressure peak comes earlier and has a higher over pressure value. This is due to the increase in turbulence when operating at higher water pressure. These results seem to be coherent with the fact that a small vent opening and no obstructions are unable to cause the rapid acceleration needed for the water droplets to break up and have a mitigating effect. The use of water spray will in these conditions lead to enhanced pressure build-up and larger overpressure because of the dominating turbulence caused by the water droplets.

Simulation nr	Maximum overpressure (bar)	Time (ms)
1 (no water)	0.47	1100
2 (HV60) P=3.5	1.85	387
3 (HV60) P=5	2.03	345
4 (MV57) P=3.5	1.91	367

Table 6.1.1: Maximum overpressure and time for simulation 1, 2, 3 and 4.

Simulation 5, 6 and 7:
In this case a congestion of 20 pipes was implemented in the explosion box. The results are displayed in Table 6.1.2. As the three simulations performed without pipes the pressure is increased when water spray is present, and the pressure peak is significantly earlier. There is a small deviation in the maximum overpressure for the HV60 and MV57 nozzle, and the HV60 nozzle gives the highest value. A plot combining the pressure from monitor 1 in these three simulations is shown at the bottom in appendix 5 page114. As a result of the increased congestion in the box, the maximum overpressure is higher and appears earlier than with no congestion. This is a result of the increased burning- and flow velocity caused by the turbulence created by the flow past the piping. The rate between maximum overpressure with and without water spray has decreased from 4.3 to 1.5 when the congestion is increased from 0 to 20 pipes.

Simulation number	Maximum overpressure (bar)	Time (ms)
5 (no water)	2.26	774
6 (HV60)	3.31	299
7 (MV57)	3.20	295

Table 6.1.2: Maximum overpressure and time for simulation 5, 6 and 7.

Simulation 8, 9 and 10:
In these simulations a congestion of 40 pipes is present in the explosion box. Table 6.1.3 shows the results. The maximum overpressures have increased and the time of arrival is earlier due to turbulence caused by the higher congestion. The deviation between the nozzles is also larger, where the HV60 nozzle gives a higher explosion pressure. The rate between overpressure with and without water spray has now decreased to a value of 1.2. A plot of the three simulations is displayed at the top in appendix 5 page 115.

Simulation number	Maximum overpressure (bar)	Time (ms)
8 (no water)	3.54	684
9 (HV60)	4.38	256
10 (MV57)	4.01	279

Table 6.1.3: Maximum overpressure and time for simulation 8, 9 and 10.

Simulation 11, 12 and 13:
In this case the congestion was increased to 80 pipes. The results are shown I Table 6.1.4, and show that the pressure actually is lower with the use of water spray. This can be a result of the increased turbulence cause by the high congestion, which after a while will dominate the turbulence caused by the water spray. The time of arrival is still earlier when there is water spray present, and there is little deviation between the results from the two nozzle types. A plot combining the pressure from monitor 1 in these three simulations is shown at the bottom in appendix 4 page 115.

Simulation number	Maximum overpressure (bar)	Time (ms)
11 (no water)	5.49	569
12 (HV60)	4.65	267
13 (MV57)	4.24	263

Table 6.1.4: Maximum overpressure and time for simulation 11, 12 and 13.

Simulation 14, 15 and 16:
Here we have a vent opening that covers the whole left wall of the box and no congestion. The results are shown in Table 6.1.5. As the plot of the overpressure at the top in appendix 5 page 116 shows, the overpressures created in these simulations are minimal and negligible in the case of no water spray. This is due to the large ventilation opening providing good venting of the gas, and because there is no piping to cause turbulence. The overpressure will increase and the time of arrival will be earlier in the presences of water spray, because of the turbulence created by the droplets. The pressure-time curves for the two different nozzles are almost identical, but with a pressure-peak slightly earlier with the MV57 nozzle.

Simulation number	Maximum overpressure (bar)	Time (ms)
14 (no water)	0.005	721
15 (HV60)	0.08	287
16(MV57)	0.08	269

Table 6.1.5: Maximum overpressure and time for simulation 14, 15 and 16.

Simulation 17, 18 and 19:
In this case the congestion of 20 pipes and a large vent opening results in a more turbulent flow that will give a sufficiently high flow velocity, which will dominate over the turbulence caused by the water droplets. The results are seen in Table 6.1.6. As we can se from the pressure-time plot at the bottom in appendix 5 page 116 the positive effect of the water spray is now beginning to show. With the HV60 nozzle the overpressure is slightly larger and with the MV57 nozzle the overpressure is reduced. The time of arrival for the pressure peak is earlier with the use of water spray.

Simulation number	Maximum overpressure (bar)	Time (ms)
17 (no water)	0.35	679
18 (HV60)	0.40	252
19(MV57)	0.25	227

Table 6.1.6: Maximum overpressure and time for simulation 17, 18 and 19.

Simulation 20, 21 and 22:
In these simulations the congestion is increased to 56 pipes, and therefore the maximum overpressures have increased and the time of arrival is earlier due to turbulence caused by the higher congestion. The positive effect of water spray is here clearer than the congestion with 20 pipes. The HV60 nozzle gives a bit smaller reduction in the maximum overpressure than the MV57 nozzle, but the time of arrival is relatively similar. The results are displayed in Table 6.1.7, and a plot of the simulations is shown at the top in appendix 5 page 117.

Simulation number	Maximum overpressure (bar)	Time (ms)
20 (no water)	1.42	593
21 (HV60)	0.98	239
22(MV57)	0.52	227

Table 6.1.7: Maximum overpressure and time for simulation 20, 21 and 22.

Simulation 23, 24 and 25:
When increasing the congestion to 80 pipes the positive effect of the water spray is clearly detected. Table 6.1.8 shows the maximum overpressure results. The pressure-time plot at the bottom in appendix 5 page 117 gives a clear picture of the effect of water spray. The pressure peak is reduced by a factor of 1.7 with the use of the HV60 nozzle and with a factor of 3.2 with the use of the MV57 nozzle. The deviation between the two nozzles can be explained by the fact that the HV60 nozzle has a much higher velocity leaving the nozzle and therefore creates more turbulence in the water spray. The turbulence from the water spray will then become more dominant with the HV60 nozzle than with the MV57 nozzle. The time of arrival for the pressure peak is earlier when water spray is present, but there is little deviation in the time between the two different nozzles.

Simulation number	Maximum overpressure (bar)	Time (ms)
23 (no water)	2.31	553
24 (HV60)	1.39	233
25(MV57)	0.73	220

Table 6.1.8: Maximum overpressure and time for simulation 23, 24 and 25.

6.1.2 Simulations with M24-25 module

The simulations were performed with three different main scenarios. Within these three cases the nozzle type and activated water spray regions were varied. Configurations for the different simulations are shown in appendix 6, and maximum overpressure data at the different monitors for the simulations is shown in appendix 7.

Case 1: Propane, centre ignition, open ends
The maximum pressure and time of arrival results from some of the simulations is shown in Table 6.1.9. If we compare the pressure results from simulation 1 with no water spray with the results from simulation 2 and 3 with water spray activated near the ignition, we see that the maximum overpressure becomes significantly higher. The results also show that the time of arrival is much earlier in the simulations containing water spray. The increased pressure and the earlier time of arrival of the pressure peak are caused by an enhancement of the initial turbulence, due to the turbulence created by the water spray in the early stage of the explosion This is shown in the pressure-time curve at the top of page 123 in appendix 10.

There is little deviation between the HV26 and CUP10 nozzles, but it would be expected that the HV26 nozzle would give higher pressure and an earlier pressure peak due to the higher velocity when leaving the nozzle, creating strong turbulence near the ignition.

When the water spray is activated in regions further and further away from the ignition and closer to the openings, the pressure becomes lower and the pressure peak comes later. In simulation 6, 7, 8 and 10 the pressure is lower than the pressure obtained in the dry test, which means that the mitigating effect of the water spray is dominant when it is activated in the accelerating phase of the explosion. This is illustrated in the pressure-time curve at the bottom of page 123 in appendix 10. The illustrated effect is seen in the scenarios with both 4 and 8 nozzles, but it was a bit clearer in the case of 4 nozzles. This can be explained with the fact that in the case of 8 nozzles a very large part of the module is covered with the water spray, but in the case of 4 nozzles the dry and wet zone is approximately equal and is more specified in position. The pressure time curve for the simulations with 8 nozzles is illustrated at the top of page 124 in appendix 10.

Simulation number	Nozzle	Number of nozzles	Water spray region	Maximum overpressure (bar)	Time (ms)
1	-	-	-	0.39	321
2	HV26	4	4,6	0.93	141
3	CUP10	4	4,6	0.94	126
4	CUP10	4	3,7	0.52	249
5	CUP10	8	3,4,6,7	0.61	122
6	CUP10	4	2,8	0.21	301
7	CUP10	8	2,3,7,8	0.27	218
8	CUP10	4	1,9	0.20	313
9	CUP10	8	1,4,6,9	0.50	118
10	CUP10	8	1,2,8,9	0,25	298

Table 6.1.9: Maximum overpressure and time for the simulations in case 1.

Case 2: Methane, north end ignition, louvered wall at ignition
At first we look at the simulations done with the CUP10 nozzles, since they appear in more simulations than the other types of nozzles. The simulation results from this scenario with end ignition show the same tendencies as case 1 with central ignition. The maximum overpressure is reduced and becomes lower than in the case of no water spray when the water spray is activated at the accelerating and turbulent phase of the explosion, i.e. in this case at the opening in the south. When the water spray is activated near the ignition the turbulence from the water droplets will increase the pressure and give a higher maximum overpressure than in the test without water spray. This is illustrated in the pressure-time curve at the bottom in page 124 in appendix 10 and in Table 6.1.10, where simulation 11 shows the dry test, 38 the water spray near ignition and 32 the water spray at the opening. The pressure peak will also arrive significantly earlier, by a factor of 3, when the water spray is activated near the ignition than when it is activated near the opening. Also in this case the effect is much clearer in the case of 4 nozzles than in the case of 8 nozzles.

This trend of pressure-dependence on the location of the activated nozzles is seen for all the different nozzles types, but in comparison to the CUP10 nozzle they doesn't achieve a maximum pressure lower than in the case of no water spray, and have therefore no positive effect on the explosion. The P120 nozzles increase the pressure when they are activated near the ignition due to the initial turbulence, but have little or slightly negative effect when activated near the opening in the south end. In simulation 18 there are activated 16 nozzles covering the whole module, and we observe a little increase in the explosion pressure compared to the dry test. The HV26 nozzle does also have no or a slightly negative effect on the explosion pressure, and the pressure becomes higher when nozzles near ignition is activated than when it is activated near the opening. The CUP 5 nozzle has a similar effect as the CUP10 nozzle when activated near the opening, but produces higher pressures when activated near ignition. A comparison between the effects the different nozzles have on the explosion is shown in Figure 6.1.1.

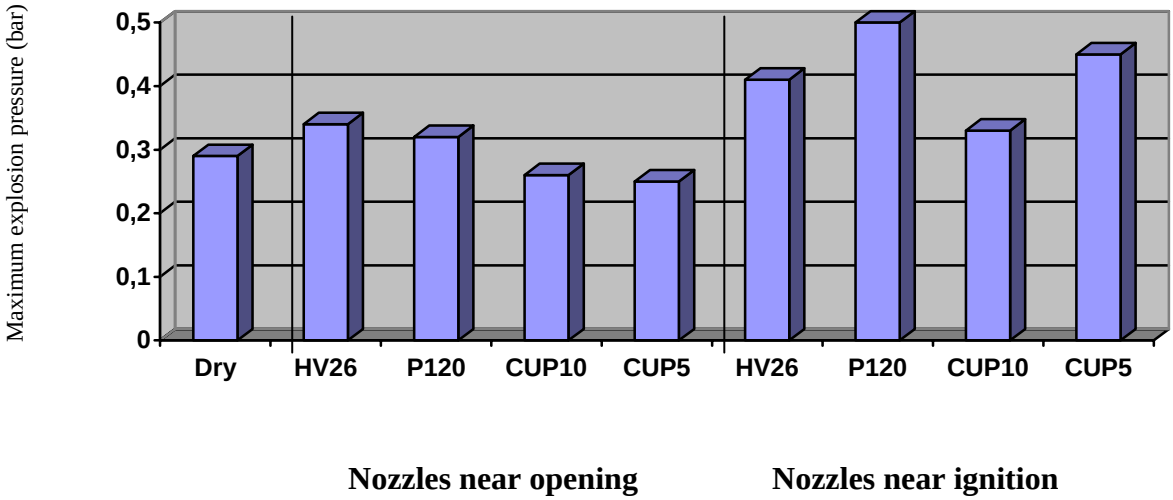

Figure 6.1.1: A comparison of results from identical simulations with no water spray and water spray activated near vent opening (6,7,8,9) and near ignition (1,2,3,4) but with different types of nozzles.

Simulation number	Nozzle	Number of nozzles	Water spray region	Maximum overpressure [bar]	Time [ms]
11	-	-	-	0.29	166
12	HV26	8	6,7,8,9	0.34	556
13	HV26	8	3,4,6,7	0.45	363
14	HV26	8	2,4,6,8	0.47	374
15	HV26	8	1,2,3,4	0.41	168
16	HV26	4	6,7	0.45	566
17	HV26	4	2,3	0.48	187
18	P120	16	1-4,6-9	0.34	388
19	P120	4	6,7	0.39	581
20	P120	8	6,7,8,9	0.32	576
21	P120	8	3,4,6,7	0.41	490
22	P120	8	1,2,3,4	0.50	362
23	CUP5	4	6,7	0.38	574
24	CUP5	8	3,4,6,7	0.33	430
25	CUP5	8	2,4,6,7	0.29	314
26	CUP10	8	6,7,8,9	0.26	551
27	CUP10	8	3,4,6,7	0.36	354
28	CUP10	8	2,4,6,8	0.25	179
29	CUP10	8	2,3,7,8	0.19	571
30	CUP10	8	1,2,8,9	0.17	574
31	CUP10	8	1,2,3,4	0.33	175
32	CUP10	4	8,9	0.17	576
33	CUP10	4	7,8	0.19	570
34	CUP10	4	6,7	0.35	568
35	CUP10	4	4,6	0.42	491
36	CUP10	4	3,4	0.48	359
37	CUP10	4	2,3	0.41	174
38	CUP10	4	1,2	0.46	178
39	CUP10	8	3,4,6,7	0.36	354
42	CUP5	8	1,2,3,4	0.45	270
43	CUP5	8	6,7,8,9	0.25	566
45	P120	4	8,9	0.36	581
46	HV26	4	8,9	0.26	581
47	CUP5	4	8,9	0.21	578

Table 6.1.10: Maximum pressure and time of arrival for the different simulations

Case 3: Methane, end ignition, closed wall at ignition.
Only three simulations were performed with a closed end in the north wall, i.e. at ignition, one without water spray, one with water spray at the centre (4,6) and one with water spray near the opening (7,8). As shown in Table 6.1.11 the explosion simulations obtained a high maximum pressure in this scenario, also with the use of water spray, but the pressure was significantly reduced in comparison to the dry test. The reason why the pressures became much higher with a closed wall at ignition is that the explosion was not ventilated in the ignition area, but had to propagate through the whole module to the opening in the south. This propagating past the obstacles in the module creates a strong turbulence field and enhances the burning, resulting in higher pressures. Figure 6.1.2 shows a comparison between to simulations with (7,8) and without water spray, having a closed wall or a louvered wall at ignition. There is a clear difference in the size of the maximum explosion pressure; the maximum explosion pressure is 5 times higher in the case of a closed wall at ignition than in the case of a louvered wall.

Simulation number	Maximum overpressure (bar)	Time (ms)
40 (no water)	1.56	362
41 (CUP10: 4,6)	1.09	358
44 (CUP10: 7,8)	0.77	354

Table 6.1.11: Maximum explosion pressure and time of arrival for the different simulations.

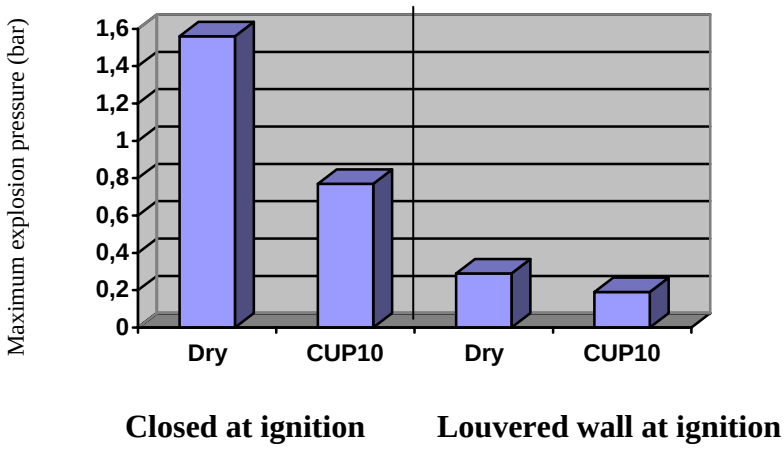

Figure 6.1.2: A comparison between a dry and a wet simulation (7,8) performed with a closed wall or a louvered wall at ignition.

6.1.3 Simulations with full-scale module

The simulations were performed with six different main scenarios, where the nozzle type and ignition point were varied. Configurations for the different simulations are shown in appendix 9, and maximum overpressure data at the different monitors for the simulations is shown in appendix 10.

Simulations 1, 2, 3 and 4:
These simulations were performed with centre ignition. The first simulation was performed without any water spray, and a pressure of 1.12 bar was achieved. Simulation 2 was performed with water spray from MV57-nozzles covering the whole module, and we see that the maximum pressure is reduced by 35%. A new simulation with the MV57-nozzles was performed, but this time the water spray was extended 2 meters out on each end of the module. As we can se from Table 6.1.12, there is almost no difference between the two simulations 2 and 3. At last a simulation including LDN-nozzles was performed with water spray extended outside the module. As mentioned earlier in chapter 5.1.3, the total flow rate of the LDN nozzle is over twice as high as with the MV57 nozzle. This is seen in the pressure result from simulation 4 including the LDN-nozzles, where the pressure is lower than with the MV57-nozzle. The LDN-nozzle reduced the pressure by 50%. The pressure peak comes earlier in the simulations where water spray is activated, and the LDN nozzle has the earliest pressure-peak. Simulation 1,3 and 4 is illustrated in the pressure-time curve on the top of page 130 in appendix 14.

Simulation number	Nozzle	Maximum pressure [bar]	Time of arrival [ms]
1	-	1.12	737
2	MV57	0.73	446
3	MV57 ext	0.76	446
4	LDN ext	0.57	383

Table 6.1.12: Maximum explosion pressure and time of arrival for the different simulations with centre ignition.

Simulations 5, 6, 7 and 8:
These simulations were performed with end ignition. The results are displayed in Table 6.1.13. In simulation 5, without water spray, a higher pressure is achieved in comparison to simulation 1 with centre ignition. The MV57- and LDN-nozzles reduces the maximum pressure with respectively 78% and 83%. This shows a significant reduction in the maximum overpressure, and a stronger mitigating effect compared to the case of centre ignition. The LDN-nozzles does also in this case have a better mitigating effect than the MV57 nozzle, and an earlier pressure peak. A simulation was also performed with water spray only covering the module, and if we compare simulation 7 and 8 there is no deviation in the maximum pressure. The pressure peak is earlier in the simulations with water spray compared to the dry test. Simulation 5, 6 and 7 is illustrated in the pressure-time curve at the bottom of page 130 in appendix 14.

Simulation number	Nozzle	Maximum pressure [bar]	Time of arrival [ms]
5	-	1.97	1250
6	MV57 ext	0.44	647
7	LDN ext	0.33	575
8	LDN	0.33	561

Table 6.1.13: Maximum explosion pressure and time of arrival for the different simulations with end ignition.

6.1.4 Simulations with the Kårstø model

Explosion simulations were performed in two areas at the Kårstø plant: Statpipe/Sleipner and Åsgard. A number of simulations containing water spray were performed at each of these areas, varying the location of the water spray and the type of water spray nozzles.

A) Statpipe/Sleipner area

A representative scenario was chosen to investigate how the activation of water spray at gas detection would influence an explosion. The type of water spray nozzle and location of the activated water spray was varied to se if this could make a variation in the results. A total of 10 simulations were performed, and the results are displayed in Table 6.1.14. Monitors 1, 2 and 11, which are marked in Figure 5.1.8, gave the highest pressures. The maximum overpressure data for the different monitors are displayed in appendix 12.

The first simulation (nr 0) was without water spray. This gave an explosion pressure of 1.49 bar in monitor 1.

Simulations 1, 2 and 3 are performed with CUP10 nozzles at different locations:
Simulation 1: With water spray activated near ignition the maximum explosion pressure is the same as in the dry simulation, but the time of arrival is earlier with water spray.
Simulation 2: With the water spray located far from the ignition the maximum pressure now appears in monitor 11, with a pressure of 0.62 bar. The maximum explosion pressure is reduced by 58%, from 1.49 bar to 0.62 bar. The maximum pressure in monitor 1 is reduced by 95%, from 1.49 bar to 0.08 bar.
Simulation 3: With a large area covered by water spray the maximum explosion pressure is reduced by 90 % compared to the pressure obtained in the dry simulation, from 1.49 bar to 0.14 bar. The pressure in monitor 1, which had the highest value in simulation 0 and 1, has now a value of 0.08 bar as in simulation 2. Simulation 3 with water spray covering almost the whole gas cloud area gives the best mitigating effect, hence the largest reduction in maximum explosion pressure. Only the simulation with water spray near ignition has a pressure peak significantly earlier than the dry simulation. A scalar-time plot can be seen at the top of page 136 in appendix 18.

Simulations 4, 5 and 6 are performed with MV57 nozzles at different locations:
Simulation 4: In this simulation the water spray is activated near ignition, which gives no change in the maximum explosion pressure compared to the dry simulation. However, the time of arrival is earlier than in the dry simulation and the simulation with the CUP10 nozzle at the same location.
Simulation 5: The maximum explosion pressure and time of arrival is almost identical to the results in simulation 2 with the CUP10 nozzle at the same location.
Simulation 6: The explosion pressure is slightly more reduced (93%), compared to simulation 3 with the CUP10 nozzle, and the time of arrival is at the same time. A scalar-time plot can be seen at the bottom of page 136 in appendix 18.

Simulations 7, 8 and 9 are performed with LDN nozzles at different locations:
Simulation 7: The explosion pressure is the same as in the dry test and the simulations with CUP10 and MV57 at the same location, but the time of arrival is somewhat earlier.
Simulation 8: The explosion pressure is reduced by 66%, which is a lager reduction compared to the CUP10 and MV57 nozzle. The time of arrival has not been much effected compared to the dry simulation.
Simulation 9: The explosion pressure is reduced by 95% and has an almost insignificant value. The time of arrival comes later than in the dry simulation. A scalar-time plot can be seen at the top of page 137 in appendix 18.

Simulation number	Nozzle	Location	Maximum pressure (bar)	Time of arrival (s)	Monitor point
0	-	-	1.49	2.81	1
1	CUP10	Near ignition	1.49	2.24	1
2	CUP10	Far from ignition	0.62	2.73	11
3	CUP10	All	0.15	2.82	2
4	MV57	Near ignition	1.49	2.18	1
5	MV57	Far from ignition	0.60	2.75	11
6	MV57	All	0.11	2.83	2
7	LDN	Near ignition	1.49	2.10	1
8	LDN	Far from ignition	0.50	2.79	11
9	LDN	All	0.07	2.95	2

Table 6.1.14: Maximum explosion pressure and time of arrival for the different simulations at the Statpipe/Sleipner area.

B) Åsgard area

As with the Statpipe/Sleipner area a representative scenario was chosen to investigate how the activation of water spray at gas detection would influence an explosion. The type of water spray nozzle and location of the activated water spray was varied to se if this could make a variation in the results. A total of 10 simulations were performed, and the results are displayed in Table 6.1.15. Monitors 7, 11 and 23, which is marked in Figure 5.1.11, gave the highest pressure. The maximum overpressure data for the different monitors are displayed in appendix 15.

The first simulation (nr 10) was without water spray. This gave an explosion pressure of 1.03 bar in monitor 23.

Simulation 11, 12 and 13 are performed with CUP10 nozzles at different locations:
Simulation 11: With water spray located near ignition the maximum explosion pressure was actually increased by 14 %, and the pressure peak appears almost 5 seconds earlier.
Simulation 12: The explosion pressure is reduced by 39%, and the time of arrival is little effected compared to the dry simulation.
Simulation 13: The explosion pressure is reduced by 80%, but he time of arrival comes significantly earlier, almost 10 seconds compared to the simulation without water spray. A scalar-time plot can be seen at the top of page 143 in appendix 22.

Simulation 14, 15 and 16 are performed with MV57 nozzles at different locations:
Simulation 14: The explosion pressure is increased by 21% compared to the pressure in the dry simulation, which is a larger increase compared to the simulation with the CUP10 nozzle. The time of arrival comes almost 8 seconds earlier.
Simulation 15: The time of arrival and the explosion pressure is identical to simulation 12 with the CUP10 nozzle.
Simulation 16: The explosion pressure is reduced by 83%, which is more than the reduction obtained with the CUP10 nozzle, but the time of arrival comes over 10 second earlier than the dry simulation. A scalar-time plot can be seen at the bottom of page 143 in appendix 22.

Simulation 17, 18 and 19 are performed with LDN nozzles at different locations:
Simulation 17: The explosion pressure is actually increased by 36% compared to the simulation without water spray, and the time of arrival comes much earlier.
Simulation 18: The results are identical to simulation 12 and 15 with CUP10 and MV57 nozzles.
Simulation 19: The explosion pressure is reduced by almost 90%, which is more than the reduction with the CUP10 and MV57 nozzle at the same location, but the time of arrival comes much earlier. A scalar-time plot can be seen at the top of page 144 in appendix 22.

Simulation number	Nozzle	Location	Maximum pressure (bar)	Time of arrival (s)	Monitor point
10	-	-	1.03	13.96	23
11	CUP10	Near ignition	1.17	9.16	23
12	CUP10	Far from ignition	0.63	13.88	7
13	CUP10	All	0.21	4.26	11
14	MV57	Near ignition	1.31	6.17	23
15	MV57	Far from ignition	0.63	13.88	7
16	MV57	All	0.17	3.68	11
17	LDN	Near ignition	1.61	4.31	23
18	LDN	Far from ignition	0.63	13.88	7
19	LDN	All	0.11	3.23	11

Table 6.1.15: Maximum explosion pressure and time of arrival for the different simulations at the Åsgard area.

6.2 Simulation results with FLACS 2.2.6*

Simulations were performed for different geometries and different scenarios with the new FLACS model, version 2.2.6* (2004).

6.2.1 Simulations with explosion box

Results without setDROP

At first the simulations were performed without the setup-file called setDROP to se how the results would be without evaporation of droplets. The simulations were performed with two different ventilation openings of 1.5m×1.5m (Kv=9) and 4.5m×4.5m (Kv=1), and three different congestions of 0, 20 and 80 pipes. There were performed simulations with two different water spray nozzles, HV60 and MV57. Configurations for the different simulations are shown in appendix 2, and maximum overpressure data at the different monitors for the simulations is shown in appendix 3.

Simulation 1, 2, 3 and 4:
In these simulations we have a small vent opening and no congestion. Table 6.2.1 shows the maximum overpressure and when this occurs for the different simulations. These results show that the maximum overpressure becomes larger and the pressure build-up is enhanced with the use of water spray. The pressure peak occurs significantly earlier with the use of water spray. At water pressure of 3.5 bar the use of MV57 nozzles gives a slightly larger pressure and occurs earlier than with the use of HV60 nozzles, but the deviations are minimal. When the water pressure is increased to 5 bars for the HV60 nozzle, the pressure peak comes earlier and has a higher over pressure value. This is due to the increase in turbulence when operating at higher water pressure. These results seems to be coherent with the fact that a small vent opening and no obstructions is unable to cause the rapid acceleration needed for the water droplets to break up and have a mitigating effect. The use of water spray will in these conditions lead to enhanced pressure build-up and larger overpressure because of the dominating turbulence caused by the water droplets.

Simulation nr	Maximum overpressure (bar)	Time (ms)
1 (no water)	0.47	1100
2 (HV60) P=3.5	1.80	640
3 (HV60) P=5	1.90	611
4 (MV57)	1.87	611

Table 6.2.1: Maximum overpressure and time for simulation 1, 2, 3 and 4.

Simulation 5, 6 and 7:
In these simulations a congestion of 20 pipes was implemented in the explosion box. The results are displayed in Table 6.2.2. As the three simulations performed without pipes the pressure is increased when water spray is present, and the pressure peak comes slightly earlier. There is a small deviation of 0.06 bar in the maximum overpressure for the HV60 and MV57 nozzle, and the MV57 nozzle gives the highest value. As a result of the increased congestion in the box the maximum overpressure is higher and appears earlier than with no

congestion. This is due to the increased burning- and flow velocity caused by the turbulence created by the flow past the piping. The rate between maximum overpressure with and without water spray has decreased from 4.0 to 1.3 when the congestion is increased from 0 to 20 pipes.

Simulation number	Maximum overpressure (bar)	Time (ms)
5 (no water)	2.26	774
6 (HV60)	2.85	636
7 (MV57)	2.91	584

Table 6.2.2: Maximum overpressure and time for simulation 5, 6 and 7.

Simulation 8, 9 and 10:
In these simulations a congestion of 40 pipes is present in the explosion box. Table 6.2.3 shows the results. The maximum overpressures have increased and the time of arrival is earlier due to turbulence caused by the higher congestion. The deviation between the nozzles is also larger, where the MV57 nozzle gives a higher value of the explosion pressure. The rate between overpressure with and without water spray has now decreased to a value of 1.1.

Simulation number	Maximum overpressure (bar)	Time (ms)
8 (no water)	3.54	684
9 (HV60)	3.92	556
10 (MV57)	4.03	515

Table 6.2.3: Maximum overpressure and time for simulation 8, 9 and 10.

Simulation 11, 12 and 13:
In these simulations the congestion was increased to 80 pipes. The results are shown I table 6.2.4, and show that the pressure is higher with the use of water spray. The rate between the overpressure with and without water spray is 1.3.The time of arrival is still earlier when there is water spray present, and there is little deviation between the results from the two nozzle types.

Simulation number	Maximum overpressure (bar)	Time (ms)
11 (no water)	5.49	569
12 (HV60)	7.14	433
13 (MV57)	7.26	400

Table 6.2.4: Maximum overpressure and time for simulation 11, 12 and 13.

Simulation 14, 15 and 16:
Here we have a vent opening that covers the whole left wall of the box and no congestion. The results are shown in Table 6.2.5. The overpressures created in these simulations are minimal and negligible in the case of no water spray because of the large vent opening providing good venting of the gas and because there is no piping to cause turbulence. The overpressure will increase and the time of arrival will be earlier in the presences of water spray, because of the turbulence created by the droplets. The pressure-time curves for the two different nozzles are almost identical, but with a pressure-peak slightly earlier with the MV57 nozzle.

Simulation number	Maximum overpressure (bar)	Time (ms)
14 (no water)	0.005	721
15 (HV60)	0.07	504
16(MV57)	0.08	500

Table 6.2.5: Maximum overpressure and time for simulation 14, 15 and 16.

Simulation 17, 18 and 19:
In this case the box has a congestion of 20 pipes and a large vent opening. The results are seen in Table 6.2.6. The maximum explosion pressure is somewhat higher when water spray is activated, but there is little deviation between the pressure results from the MV57 and HV60 nozzles. The time of arrival for the pressure peak is earlier with the use of water spray.

Simulation number	Maximum overpressure (bar)	Time (ms)
17 (no water)	0.35	679
18 (HV60)	0.48	561
19(MV57)	0.50	510

Table 6.2.6: Maximum overpressure and time for simulation 17, 18 and 19.

Simulation 20, 21 and 22:
In these simulations the congestion is increased to 56 pipes, and therefore the maximum overpressures have increased and the time of arrival is earlier due to turbulence caused by the higher congestion. The explosion pressure is reduced by 0.8 bar with the use of HV60-nozzles, but with the MV57-nozzles the pressure is increased by 0.11 bar. The results are displayed in Table 6.2.7.

Simulation number	Maximum overpressure (bar)	Time (ms)
20 (no water)	1.42	593
21 (HV60)	0.62	615
22(MV57)	1.53	469

Table 6.2.7: Maximum overpressure and time for simulation 20, 21 and 22.

Simulation 23, 24 and 25:
When increasing the congestion to 80 pipes the maximum overpressure is higher and the time of arrival is earlier due to the increased amount of obstructions. Table 6.2.8 shows the maximum overpressure results. The maximum explosion pressure is increased by 0.19 bar, and there value for the MV57- and HV60 nozzle is almost identical. The pressure peak comes earlier with water spray present, and it comes slightly earlier with the MV57-nozzle compared to the HV60-nozzle.

Simulation number	Maximum overpressure (bar)	Time (ms)
23 (no water)	2.31	553
24 (HV60)	2.50	427
25(MV57)	2.49	396

Table 6.2.8: Maximum overpressure and time for simulation 23, 24 and 25.

Results with setDROP

The simulations are then performed with setDROP, where the evaporation is set to maximum for all the defined droplet sizes. This file also ensures that the break-up and evaporation of droplets is “switched “ on.

Simulation 1, 2, 3 and 4:
In these simulations we have a small vent opening and no congestion. Table 6.2.9 shows the maximum overpressure and when this occurs for the different simulations. These results show that the maximum overpressure becomes significantly larger when water spray is present. The pressure peak occurs t earlier with the use of water spray. At water pressure of 3.5 bar the use of MV57 nozzles gives a larger pressure than with the use of HV60 nozzles, but the deviations in time of arrival are minimal. When the water pressure is increased to 5 bars for the HV60 nozzle the pressure is significantly increased and the pressure peak comes slightly later. This is due to the increase in turbulence when operating at higher water pressure. These results seems to be coherent with the fact that a small vent opening and no obstructions is unable to cause the rapid acceleration needed for the water droplets to break up and have a mitigating effect. The use of water spray will in these conditions lead to enhanced pressure build-up and larger overpressure because of the dominating turbulence caused by the water droplets.

Simulation nr	Maximum overpressure (bar)	Time (ms)
1 (no water)	0.47	1100
2 (HV60) P=3.5	12.2	891
3 (HV60) P=5	28.4	906
4 (MV57) P=3.5	28.9	893

Table 6.2.9: Maximum overpressure and time for simulation 1, 2, 3 and 4.

Simulation 5, 6 and 7:
In these simulations a congestion of 20 pipes was implemented in the explosion box. The results are displayed in Table 6.2.10. As the three simulations performed without pipes the pressure is increased when water spray is present, and the pressure peak comes slightly earlier. The pressure from the MV57-nozzle has an almost 10 bar higher value than the HV60- nozzle, and the time of arrival is about 200 ms earlier with the MV57-nozzle.
As a result of the increased congestion in the box the maximum overpressure is higher and appears earlier than with no congestion. This is due to the increased burning- and flow velocity caused by the turbulence created by the flow past the piping.

Simulation number	Maximum overpressure (bar)	Time (ms)
5 (no water)	2.26	774
6 (HV60)	22.9	862
7 (MV57)	32.6	651

Table 6.2.10: Maximum overpressure and time for simulation 5, 6 and 7.

Simulation 8, 9 and 10:
In these simulations a congestion of 40 pipes is present in the explosion box. Table 6.2.11 shows the results. The maximum overpressures have increased and the time of arrival is earlier due to turbulence caused by the higher congestion. The deviation between the nozzles is also larger, but now the HV60-nozzle gives a higher value of the explosion pressure. The pressure peak is also earlier with the HV60-nozzle, which would be expected since this nozzle has a higher exiting velocity and thereby creates more initial turbulence. The

Simulation number	Maximum overpressure (bar)	Time (ms)
8 (no water)	3.54	684
9 (HV60)	33.9	621
10 (MV57)	21.6	651

Table 6.2.11: Maximum overpressure and time for simulation 8, 9 and 10.

Simulation 11, 12 and 13:
In these simulations the congestion was increased to 80 pipes. The results are shown I Table 6.2.12, and show that the pressure is significantly higher with the use of water spray.

Simulation number	Maximum overpressure (bar)	Time (ms)
11 (no water)	5.49	569
12 (HV60)	32.9	479
13 (MV57)	42.6	490

Table 6.2.12: Maximum overpressure and time for simulation 11, 12 and 13.

Simulation 14, 15 and 16:
Here we have a vent opening that covers the whole left wall of the box and no congestion. The results are shown in Table 6.2.13. The overpressures created in these simulations are minimal and negligible in the case of no water spray because of the large vent opening providing good venting of the gas and because there is no piping to cause turbulence. The overpressure is significantly increased and the time of arrival is earlier in for the MV57-nozzle at the presences of water spray, because of the turbulence created by the droplets. The HV60-nozzle creates a much larger pressure than the MV57-nozzle.

Simulation number	Maximum overpressure (bar)	Time (ms)
14 (no water)	0.005	721
15 (HV60)	13.6	891
16(MV57)	3.9	476

Table 6.2.13: Maximum overpressure and time for simulation 14, 15 and 16.

Simulation 17, 18 and 19:
In this case the box has a congestion of 20 pipes and a large vent opening. The results are seen in Table 6.2.14. The maximum explosion pressure is somewhat higher when water spray is activated, and the explosion pressure is increased in the simulations where water spray is included. The rate of increase in explosion pressure is lower than in the case of no pipes. The combination between a large ventilation opening and obstruction causes a turbulent flow field with higher flow velocity, and this may then fulfil the critical droplet break-up velocity. The MV57-nozzle creates a much larger pressure than the HV60-nozzle.

Simulation number	Maximum overpressure (bar)	Time (ms)
17 (no water)	0.35	679
18 (HV60)	0.68	598
19(MV57)	3.19	543

Table 6.2.14: Maximum overpressure and time for simulation 17, 18 and 19.

Simulation 20, 21 and 22:
In these simulations the congestion is increased to 56 pipes, and therefore the maximum overpressures have increased and the time of arrival is earlier due to turbulence caused by the higher congestion. The explosion pressure is increased with water spray activated, but the rate of increase is lower than with 20 pipes. The results are displayed in Table 6.2.15

Simulation number	Maximum overpressure (bar)	Time (ms)
20 (no water)	1.42	593
21 (HV60)	9.65	534
22(MV57)	12.7	527

Table 6.2.15: Maximum overpressure and time for simulation 20, 21 and 22.

Simulation 23, 24 and 25:
When increasing the congestion to 80 pipes the maximum overpressure is higher and the time of arrival is earlier due to the increased amount of obstructions. Table 6.2.16 shows the maximum overpressure results. The explosion pressure is increased when water spray is present, and the HV60-nozzle gives a larger increase than the MV57-nozzle. The rate of increase in explosion pressure is now lower due to the increase in obstructions.

Simulation number	Maximum overpressure (bar)	Time (ms)
23 (no water)	2.31	553
24 (HV60)	8.71	467
25(MV57)	4.33	460

Table 6.2.16: Maximum overpressure and time for simulation 23, 24 and 25.

6.2.2 Simulations with M24-25 module

The simulations were performed with three different main scenarios. Within these three cases the nozzle type and activated water spray regions were varied. The setup-file is included in all the simulations with maximum evaporation.

Case 1: Propane, centre ignition, open ends
The maximum pressure and time of arrival results from some of the simulations is shown in Table 6.2.17. If we compare the pressure results from simulation 1 with no water spray with the result from simulation 3 with water spray activated near the ignition, we see that the maximum overpressure becomes significantly higher, but the time of arrival comes later than in the simulations containing water spray. The increased pressure is caused by an enhancement of the initial turbulence, due to the turbulence created by the water spray in the early stage of the

With water spray activated near the ignition the pressure becomes higher than in the simulation without water spray, due to the initial turbulence from the water spray. The time of arrival is earlier than in the simulation with water spray activated far from ignition.

Simulation number	Nozzle	Water spray region	Maximum overpressure (bar)	Time (ms)
1	-	-	0.39	321
3	CUP10	4,6	0.55	234
8	CUP10	1,9	0.22	407

Table 6.2.17: Maximum overpressure and time for the simulations in case 1.

Case 2: Methane, north end ignition, louvered wall at ignition
With the CUP5-nozzle the maximum pressure is slightly larger and the time of arrival earlier when activated near ignition compared to at the ventilation opening. The CUP-nozzles gives the largest pressure.

Simulation number	Nozzle	Water spray region	Maximum overpressure (bar)	Time (ms)
11	-	-	0.29	166
12	HV26	6,7,8,9	0.45	780
20	P120	6,7,8,9	0.56	786
26	CUP10	6,7,8,9	0,67	791
42	CUP5	1,2,3,4	0.86	958
43	CUP5	6,7,8,9	0.87	822

Table 6.2.18: Maximum pressure and time of arrival for the different simulations

Case 3: Methane, end ignition, closed wall at ignition.
Only three simulations were performed with a closed end in the north wall at ignition, one without water spray, one with water spray at the centre (4,6) and one with water spray near the opening (7,8). As shown in Table 6.2.19 the explosion simulations obtained a high maximum pressure in this scenario. With water spray activated at the centre the explosion pressure was reduced, and the time of arrival a bit later. This propagating past the obstacles in the module creates a strong turbulence field and enhances the burning resulting in higher pressures. When the water spray is activated near the opening the explosion pressure actually becomes higher than in the case of no water spray. The droplets will not achieve the same velocity as with water spray activated near ignition**,** because they doesn't flow past as many obstacles creating turbulent flow. The break-up will be limited and thereby the extraction of energy due to evaporation of droplets.

Simulation number	Maximum overpressure (bar)	Time (ms)
40 (no water)	1.56	362
41 (CUP10: 4,6)	1.38	368
44 (CUP10: 7,8)	2.03	395

Table 6.2.19: Maximum explosion pressure and time of arrival for the different simulations.

6.3 Dispersion results with FLACS 2.2.6*

The dispersion simulations were performed with FLACS 2.2.6*

6.3.1 Simulations with Kårstø

Dispersion simulations were performed with end leakage at the Statpipe/Sleipner area. Water spray was activated to see the effect this would have on the gas dispersion.

The Statpipe/Sleipner area

The leakage was located at the end (west) of the area. The time line in seconds is shown in Figure 6.3.1. The leakage is started after 3 second in order to let the wind build up to the maximum value. The leakage is left on for 37 seconds i.e. until 40 seconds, and is then shut of. The simulation is stopped at 60 seconds, so from 40 to 60 seconds the gas cloud can disperse and form an even larger gas cloud. The water spray is activated after 10 seconds and is left on until the simulation is stopped.

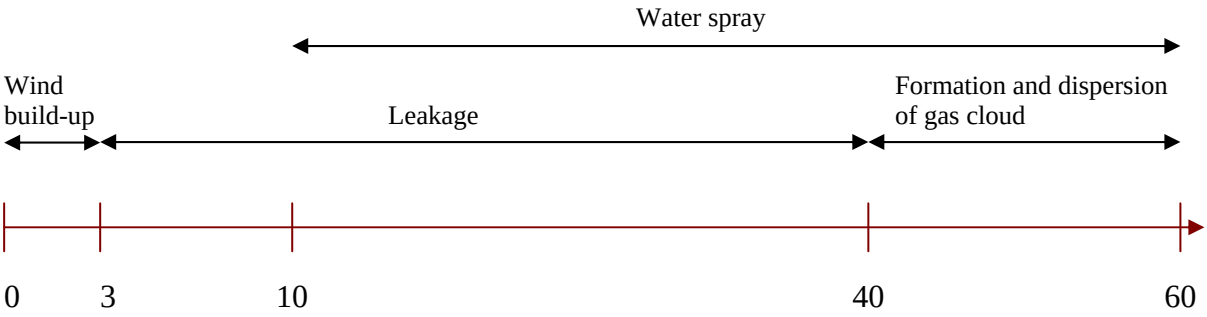

Figure 6.3.1: A time line in seconds showing the dispersion scenarios.

Simulation without water spray
The simulation was performed with a leak located at the edge (west) of the area and without water spray. Figure 6.3.2 shows a scalar-time plot of the fuel fraction. A small peak comes straight after the gas leak starts. The leakage is turned of after 40 seconds, and the maximum peak comes at about 50 seconds, when the gas has dispersed for 10 seconds. Figure 6.3.3 is a 2D plot of the gas dispersion, showing the size and position of the gas cloud after 60 seconds.

Simulations with water spray
Water spray was activated after 10 seconds, and a scalar-time plot of this scenario can be seen in Figure 6.3.4.

Simulation without water spray

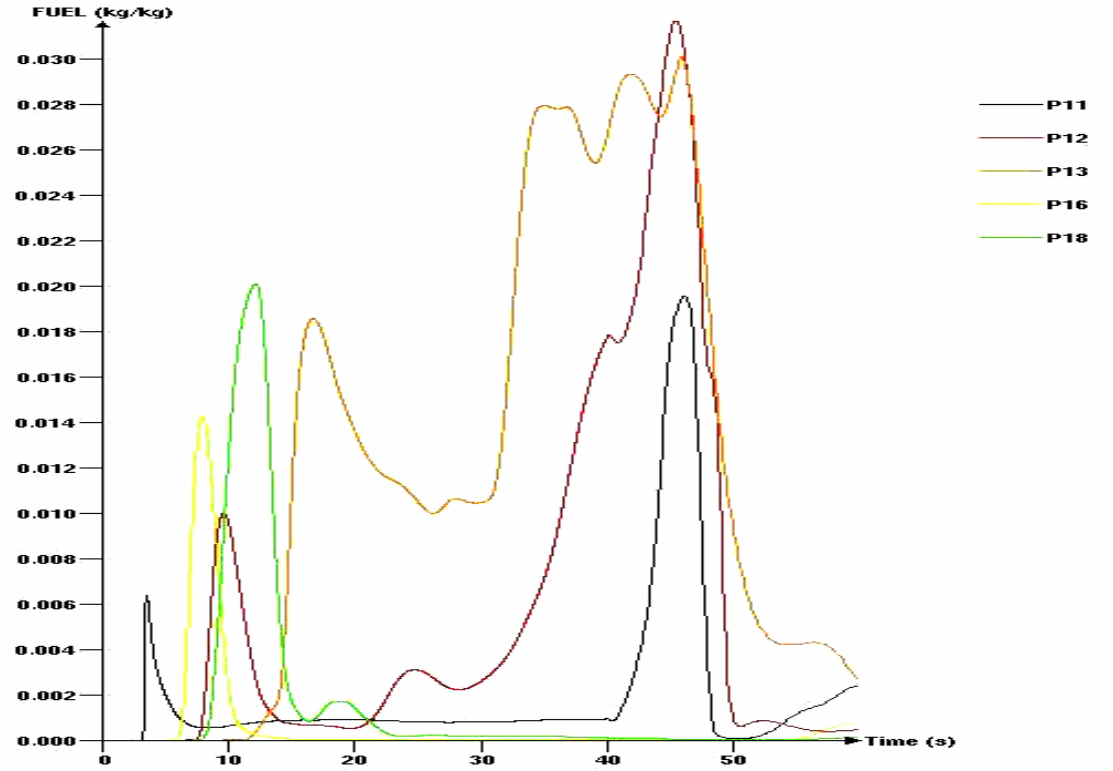

Figure 6.3.2: Scalar-time plot of fuel fraction.

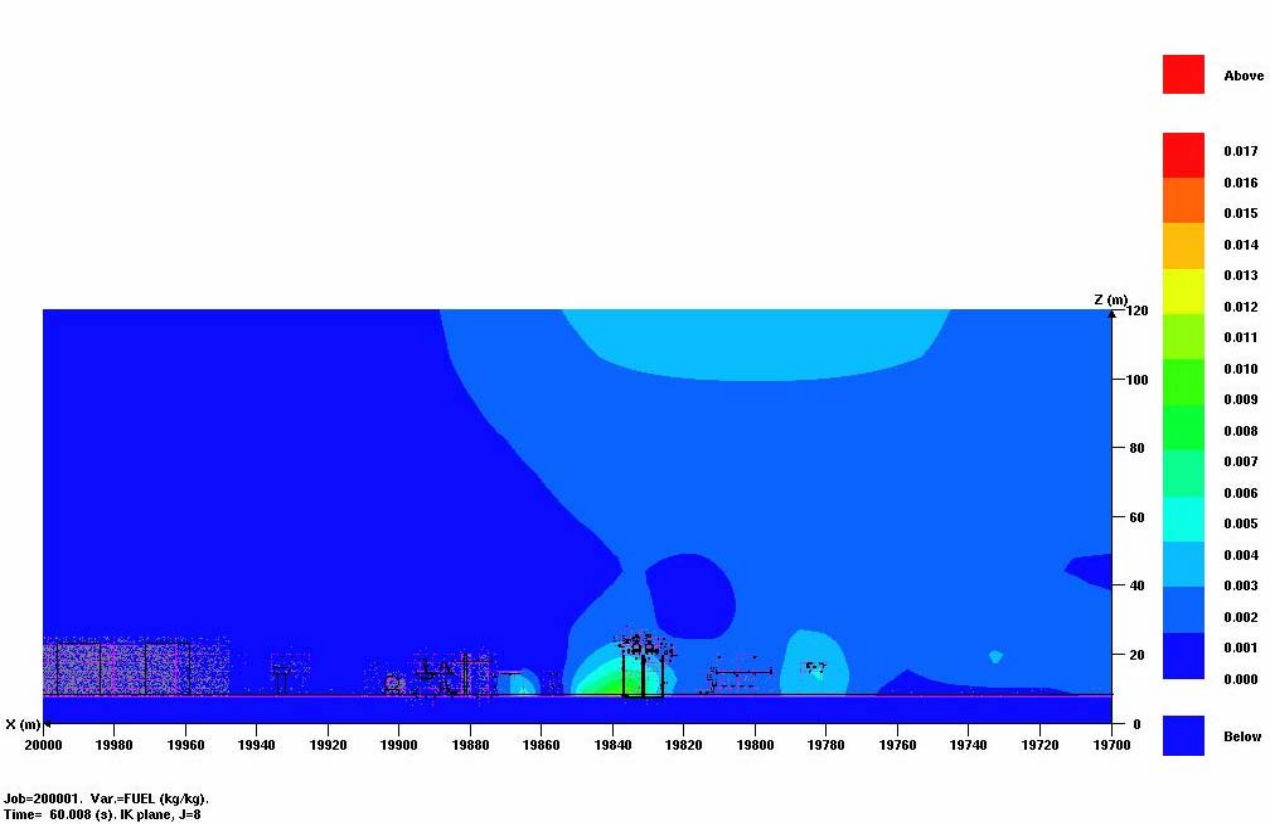

Figure 6.3.3: 2D plot of gas dispersion (fuel) after 60 seconds in the Statpipe/Sleipner area.

Simulations with water spray

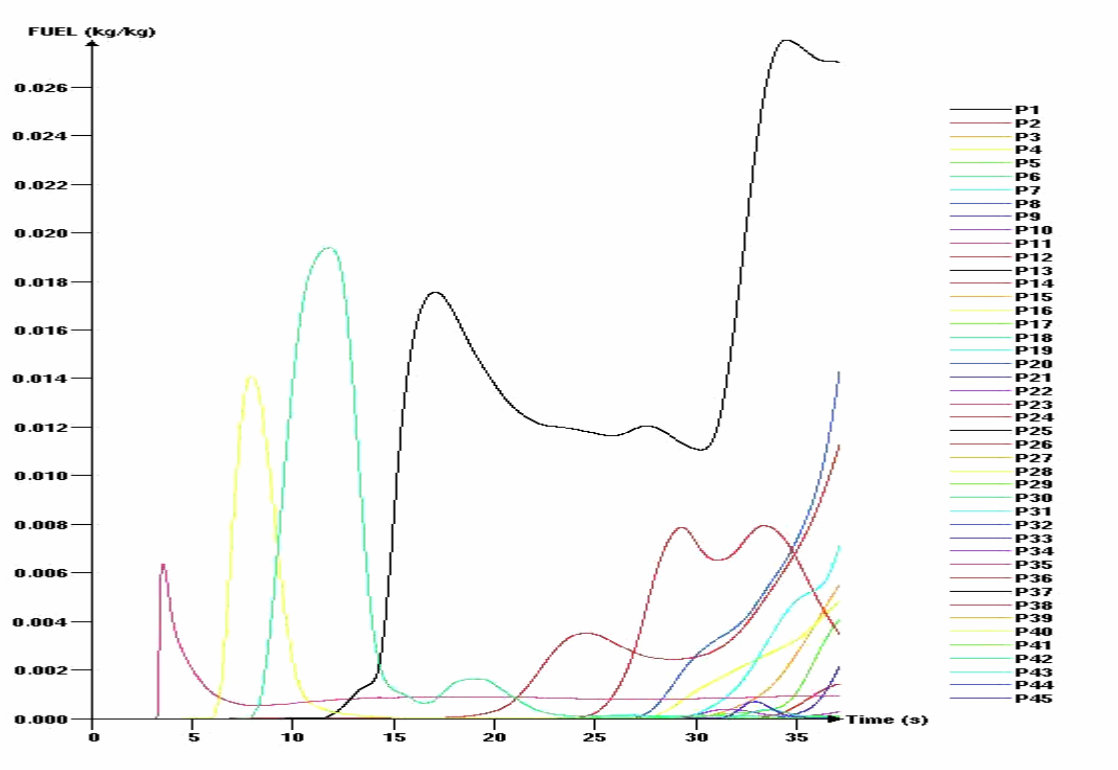

6.3.4: Scalar-time plot of fuel fraction.

7. Discussion

7.1 Comparison between experiments and simulations performed FLACS 2.2.5

This chapter will contain a comparison between the simulations performed with FLACS version 2.2.5 (2001) and results from experiments performed by British gas and CMR for different specific geometries.

7.1.1 Explosion box

The general results from the simulations are coherent with the main conclusions in the report with experiments performed with the explosion box [6].

In the case of high confinement, i.e. a small ventilation opening, the water spray had generally no mitigating effect and could in some cases give a higher pressure peak due to the turbulence created by the water droplets. The water droplets from the water spray nozzle have to be broken up in order to extract energy, and this requires high gas acceleration in front of the flame. In the case of a small ventilation area the flow is restricted and will not reach a sufficient velocity to cause droplet break-up. A 2D plot of a simulation with a small ventilation opening is shown in Figure 7.1.1 in the next page. The ventilation of burned products is restricted and high pressures are obtained. The rate of maximum overpressure between simulations with and without water spray did however decrease when the number of pipes was increased, and in the case of 80 pipes the pressure is actually slightly reduced when using water spray. The reduction is illustrated in Table 7.1.1 The explanation for this reduction can be that the turbulence caused by obstacles increases when the number of pipes increases, and therefore becomes more and more dominating over the water spray induced turbulence. This reduction effect was also seen in the experiments, but they only included maximum 40 pipes and it is therefore not determined whether the pressure would be lower in the case of 80 pipes and the presences of water spray in an experiment.

Number of pipes	**0**	**20**	**40**	**80**
Pressure rate	4.3	1.5	1.2	0.9

Table 7.1.1: Pressure rate between simulations with and without water spray for different congestions with small vent opening.

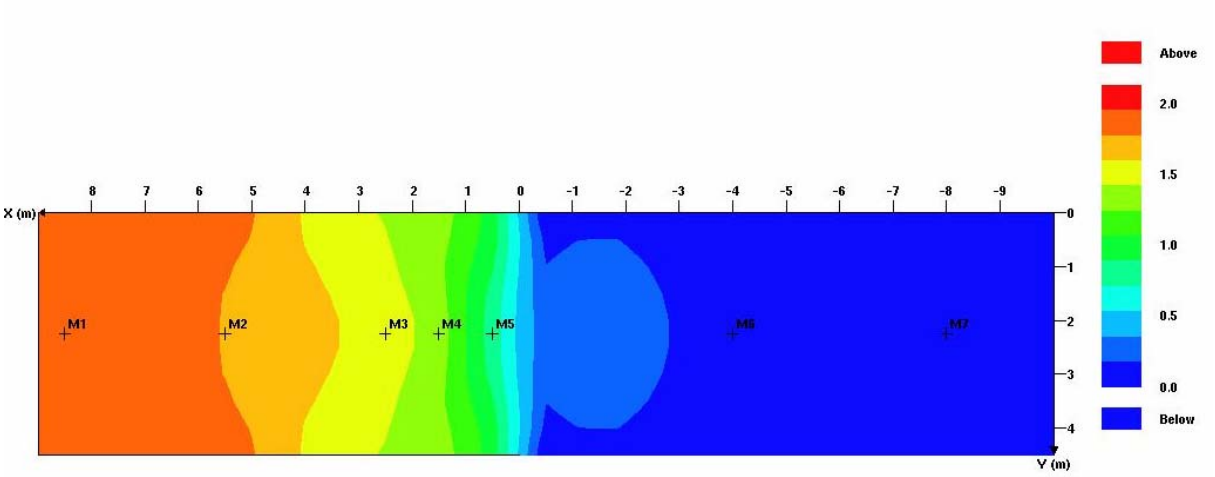

Figure 7.1.1: 2D plot of pressure [bar] in a simulation with a small ventilation opening.

When the ventilation opening was increased to cover the whole left side of the box and the pipe-congestion was high, the water spay had an effective mitigating effect reducing the peak overpressure significantly. This is a result of an effective ventilation of the burned gas and turbulence caused by the pipe congestion, resulting in break-up of droplets and extraction of heat. The explosion is mitigated as a result of these factors.

The type of water nozzle didn't give much deviation in the results from the high-congested simulations, but with the increased ventilation opening the differences became clearer. In this case the MV57 (medium velocity) nozzle was more effective than the HV60 (high velocity) nozzle, which can be seen in the pressure-time plot in appendix 7 and 8. The reason why the HV60 nozzle is less effective than the MV57 can be that the HV60 nozzle has a higher vertical velocity, and thereby creates more turbulence in the water droplet spray.

A quantitative comparison is made between the simulation results and result from experiments for some of the different geometries:

In the case of a small ventilation opening and variable congestion the results from experiments and simulations are coherent and only small deviations are seen. The model seems to give a good representation of the experiments. In Figure 7.1.2 one can clearly see the negative effect of water spray, where the overpressure is considerably increased at the presence of water spray. This effect is coherent with the fact that due to the small ventilation opening the turbulence caused by the water spray will dominate the situation and create higher pressures and earlier pressure peaks. When the congestion is increased the rate between the overpressure with and without water spray is reduced, this because the obstacle created turbulence will become more and more dominating in condition to the turbulence created by the water spray. This can be seen in Figures 7.1.3 and 7.1.4. In the experiments this rate is 4.7 1.36 and 1.28 for the congestion of 0, 20 and 40 pipes respectively. Compared to this rate from the simulations shown in Table 7.1.2 we see that the values are relatively coherent.

In the case of a large ventilation opening the simulations has a tendency to under predicate the overpressures. Figure 7.1.5 shows the case with 56 pipes, and here the simulations with both MV57 and HV60 nozzles are under predicated. The simulation without water spray is well

represented. In the case of 80 pipes, Figure 7.1.6, both the dry simulation and the simulation with the HV60 nozzle gives a pressure value that is to weak, and the MV57 nozzle gives an over predication. These deviations can be explained by the fact that the simulation with a large ventilation opening gives a more difficult and complex scenario. The products and water spray will in this case be transported outside the explosion box in a much larger scale than with the small ventilation opening. This can be difficult to define with the current model. Another moment to mention is that the experiments performed by British Gas are from 1992, and can contain uncertain factors. The time of arrival seems to be good represented by the model.

Box with small vent opening and no pipes (Kv=9, n=0)

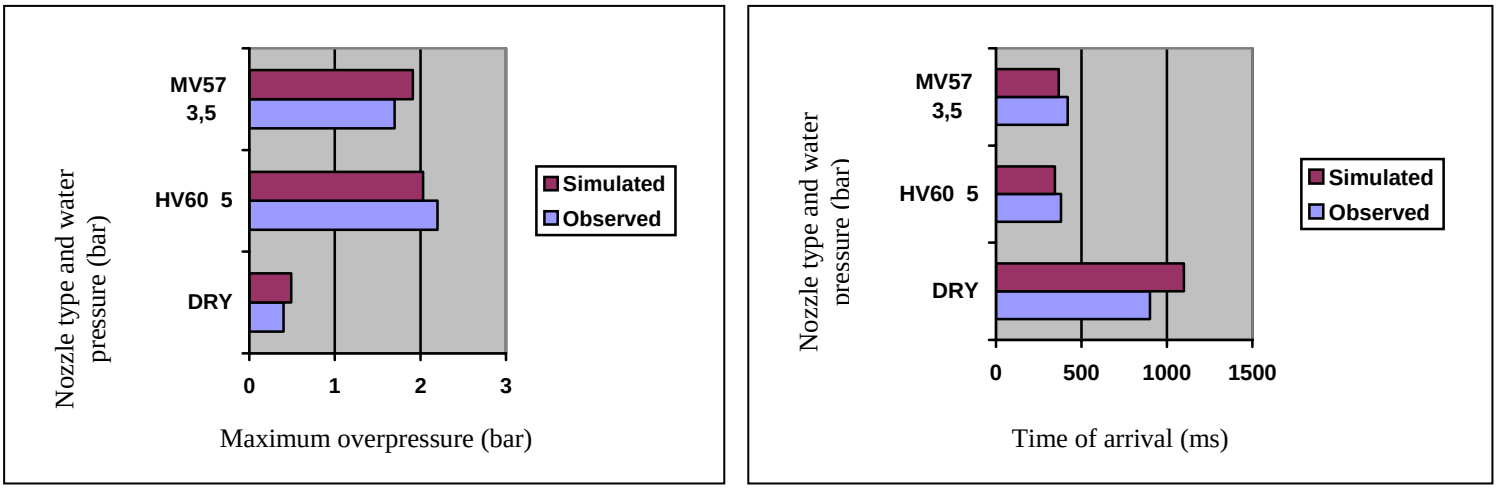

Figure 7.1.2: A comparison between results from experiments with British Gas 180m^3 box and simulations with small vent opening and no congestion, pressure (left) and time of arrival (right).

Box with small vent opening and 20 pipes (Kv=9, n=20)

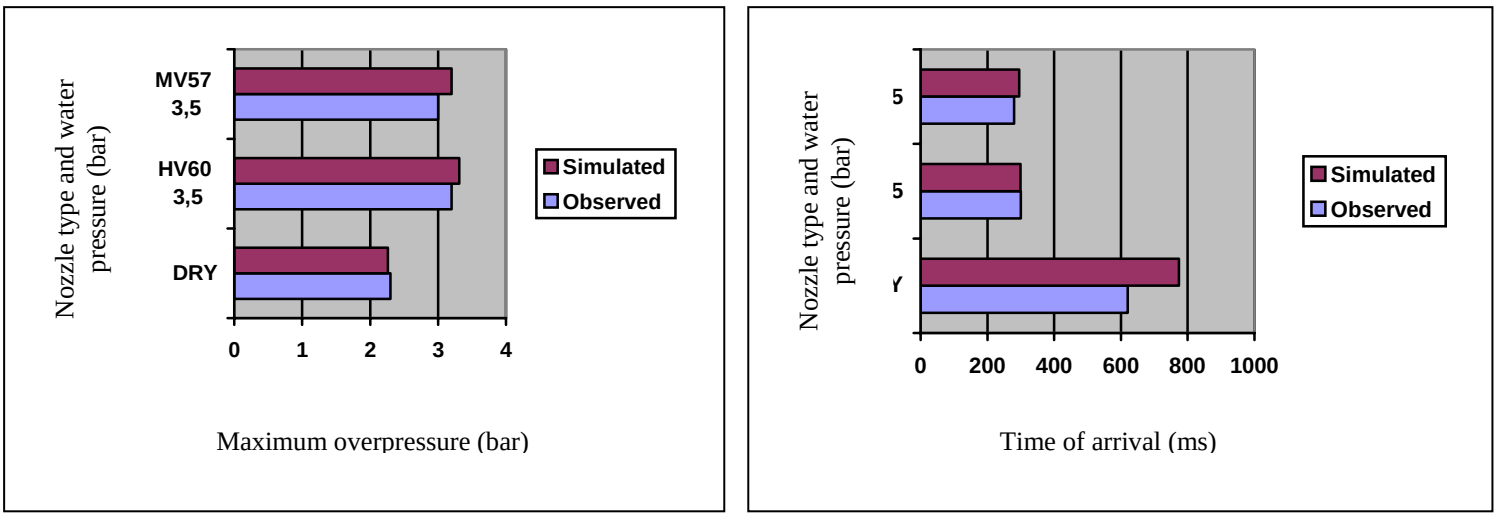

Figure 7.1.3: A comparison between results from experiments with British Gas 180m^3 box and simulations with small vent opening and 20 pipes, pressure (left) and time of arrival (right).

Box with small vent opening and 40 pipes (Kv=9, n=40)

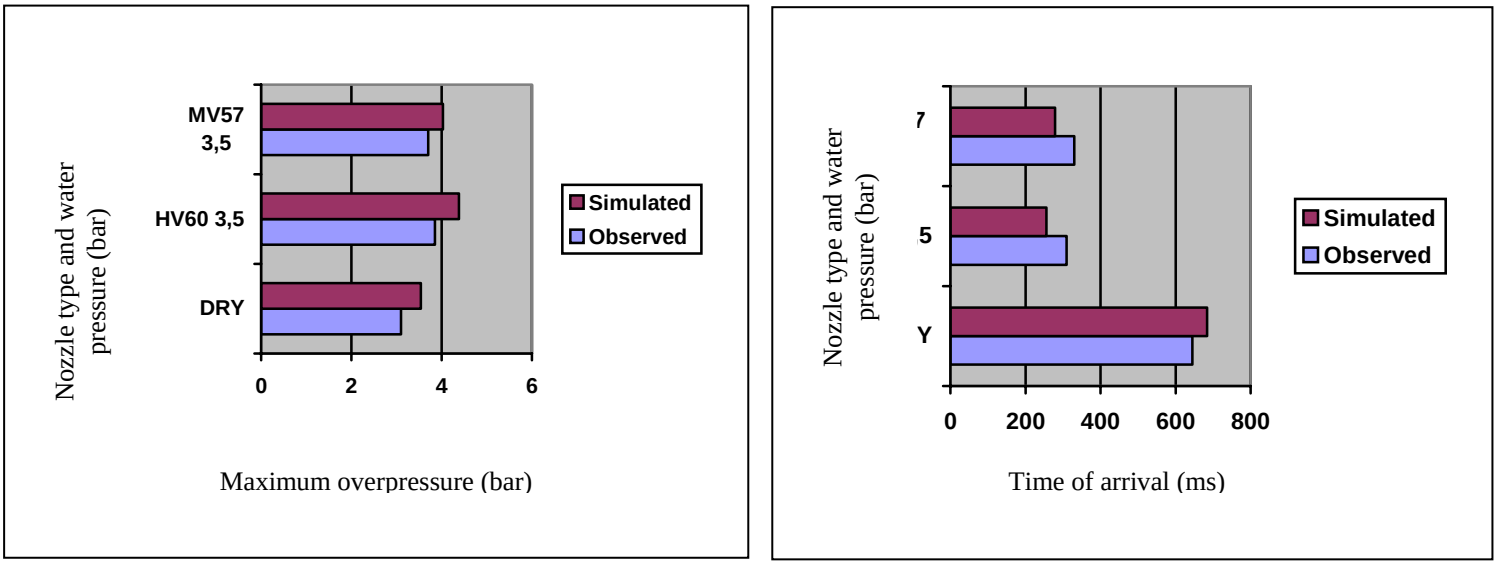

Figure 7.1.4: A comparison between results from experiments with British Gas 180m^3 box and simulations with small vent opening and 40 pipes, pressure (left) and time of arrival (right).

Box with large vent opening and 56 pipes (Kv=1, n=56)

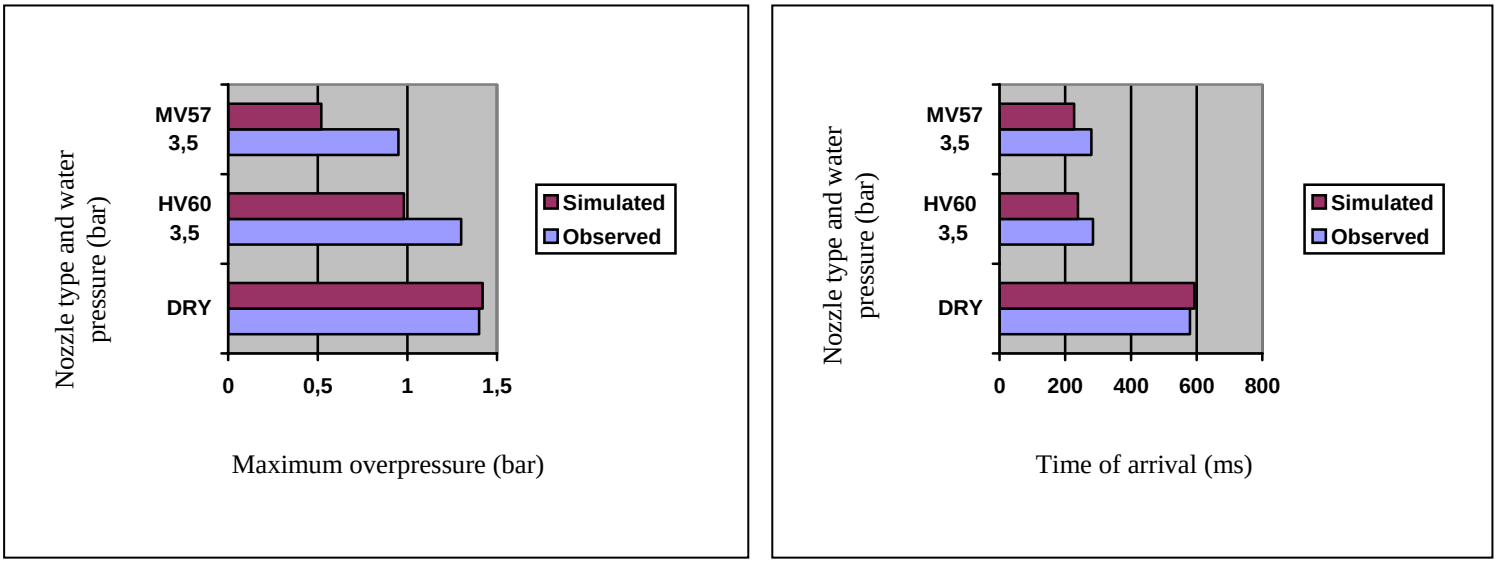

Figure 7.1.5: A comparison between results from experiments with British Gas 180m^3 box and simulations with small vent opening and 56 pipes, pressure (left) and time of arrival (right).

Box with large vent opening and 80 pipes (Kv=1, n=80)

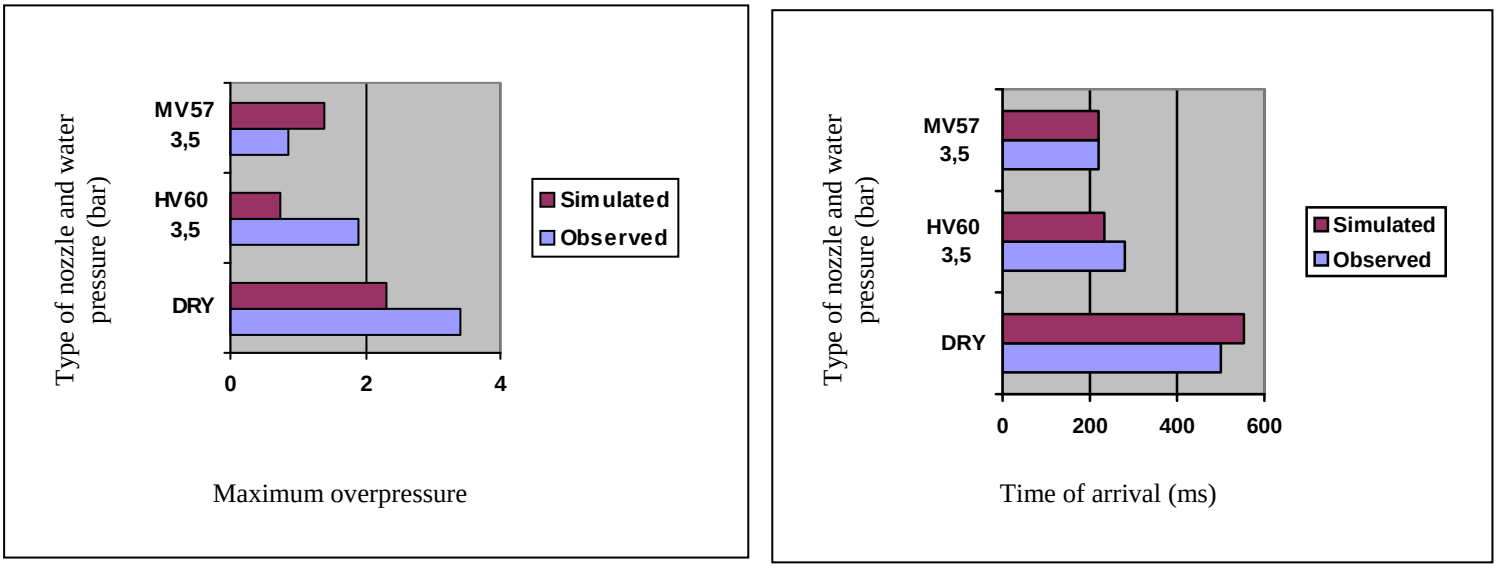

Figure 7.1.6: A comparison between results from experiments with British Gas 180m^3 box and simulations with large vent opening and 80 pipes, pressure (left) and time of arrival (right).

7.1.2 M24-25 module

The performed simulations show that water deluge systems have a significant influence on how a gas explosion develops, and can result in large deviations in maximum explosion pressure.

The water spray has a clearly negative influence on the explosion when it is activated near the ignition point. In this case the pressure can be increased by a factor of over 2 between the simulation without and with water spray. This effect is coherent with the fact that the water spray will create turbulence at the ignition when activated, and will give a large increase of the initial turbulence in the explosion, hence leading to enhanced burning and higher pressures.

When the water spray is activated further and further away from the ignition and closer to the ventilation opening it is seen see that the water spray will have an increasing positive effect, and in some cases give maximum explosion pressures lower than in the simulations with no water spray. The largest simulated reduction is by a factor of 2. The burning will propagate slower in the absence of the initial water spray turbulence and will then not achieve as high pressures. Close to the ventilation openings the burning rate and flame speed will be at its largest, due to the turbulence caused by the flow past the obstructions in the module. When the water spray is activated at this point it will dampen the explosion and give a lower maximum pressure. The turbulence from the water spray will not be dominant and the water spray will have a positive effect on the explosion pressures when it is activated at the accelerating phase of the explosion. This positive and negative effect from the water spray is

illustrated in the pressure-time curve at the bottom of page 124 in appendix 10. The pressure peak is lower and arrives much later when the water spray is activated near the opening.

When comparing the different nozzles used in the simulations the high velocity nozzle (HV26), fog nozzle (P120) and the sprinkler nozzle (CUP5) create a large initial turbulence when activated near the ignition in comparison to the CUP10 nozzle. Wilkins and Van Wingerden have in their report come to the conclusion that the highest flame speed, and therefore pressure increases, can be expected from the P120 nozzle followed by the HV26 nozzles and then the CUP10 nozzle [11]. This is coherent with the results from the simulations displayed in Table 7.1.2 in the next page.

When the nozzles are activated in regions close to the opening the CUP-nozzles seem to have the best mitigating effect. The HV26- and P120 nozzles gives a slightly higher pressure than in the dry simulation with 8 nozzles, but the CUP5 and CUP10 nozzles reduces the pressure to a slightly lower value than in the dry simulation. In the case of 4 nozzles P120 gives a slightly higher value, HV26 a slightly lower value and CUP5 and CUP10 a lower value. This is also illustrated in Figure 6.1.1.

Nozzle	**Pressure increase (8 nozzles)**	**Pressure decrease (8 nozzles)**	**Pressure decrease (4 nozzles)**
P120	0.21	-0.03	-0.07
CUP5	0.16	0.04	0.08
HV26	0.12	-0.05	0.03
CUP10	0.04	0.03	0.12

Table 7.1.2: Comparison of pressure increase and decrease with the use of different nozzles when activated near ignition (1,2,3,4) and near opening (6,7,8,9 and 8,9). End ignition and louvered wall at ignition.

In one of the simulations with the P120 nozzle all of the 16 nozzles were activated covering the whole module. The resulting pressure became slightly higher than in the case of no water spray. This is coherent with the findings above that the fog-nozzle has an increasing effect on the pressure when activated at ignition and almost no effect when activated at the accelerating phase of the explosion.

In three of the simulations the louvered wall at the ignition was changed to a closed wall. This resulted in much larger pressures both with and without water spray in comparison to the simulations with the louvered wall. The reason for this pressure increase is because the explosion is not vented in the initial stage as with the louvered wall. Instead the explosion propagates through the whole module to the other opening, creating a turbulent flow field when it passes the obstacles in the module. This results in a higher burning rate, increased flame speed and then a higher explosion pressure. Ventilation in the early stages of an explosion has a good effect in reducing the maximum explosion pressure. If the wall at ignition had been totally open the pressure would be even lower.

A quantitative comparison is made between the simulation results and result from experiments for some of the different scenarios:

Case 1:
In chapter 6.1.2 the simulation results was commented and it was then registered that the HV26 and CUP10 nozzles gave a similar result, which was not expected. From Figure 7.1.6 we see a comparison between the results from the experiments and the simulations, and this show that in the experiments the HV26 nozzle creates a much larger pressure than the CUP10 nozzle. In the simulations it is assumed that the two different nozzles distribute the water in the same way, but in reality the CUP10 nozzle transports the water further away than the HV26 nozzle. If this is taken account for the pressure result from the CUP10 nozzle would be lower and the results would be improved and more correct in comparison to a real situation. This points out the limitation about this model, that the water droplets aren't transported with the flow and that a uniform droplet distribution is assumed.

There is a deviation between the results from the experiments and the results from the simulation in the test without water spray. Four tests were performed with no water spray and the results had a variation of +/- 16% [7]. The simulated result is about 20% lower than a typical experiment.
There are some deviations between the results from the experiments and the results from the simulations, but they have the same tendencies when the location of the activated water spray is varied. Both the experiments and the simulations show that the explosion pressure increases as the water spray is activated near the ignition and that the pressure decreases more and more the further away from the ignition the water spray is activated. This effect the location of the water spray has on the explosion pressure is well represented in the simulations. The deviations between the results from the experiments and the simulations are significantly larger in the scenarios where the water spray is activated in one region in each end of the module. This again leads back to the limitation in the model where the droplets aren't transported with the flow, as they would have been in a real situation.

Case 2:
The same tendencies that explosion pressure is dependent on the location of the nozzles are also seen in this situation with methane, ignition at the end and louvered wall at ignition. See Figure 7.1.7. A reduction in maximum pressure is seen as the water spray is activated further away from the ignition, and this seems to be clearer in the case of 4 nozzles than with 8 nozzles. In the case of using 4 nozzles the dry and wet regions will be more specified and therefore the influence in activating different regions will be clearer.

Some deviations are seen between the simulations and the experiments in most of the cases, and this is mainly due to the lack of droplet transport in the model. A possible reason for the deviation can also lie in the uncertainty in the performing of the experiments. In the dry test in case 2 there were performed 7 identical shots, because there were such significant variation between the results. A possible explanation for this is the ignition source [7]. This variation may then also be possible when repeating experiments with water spray.

As in the experiments it was observed that the CUP-nozzles had the best mitigating effect on the explosion pressure, and that the HV26 and P120 nozzle created large overpressures when activated near ignition. The simulations seem to under predicate the explosion pressure for all of the HV26, P120 and CUP10 nozzles when it is activated near ignition, but the expected effect of using the different nozzles is coherent with that seen in the experiments. When the

water spray is activated nearer the opening the simulations tend to over predicate the results. This can again be explained with the fact that the droplets aren't transported down the module with the flow. If the water spray region is extended further down towards the opening the pressures becomes lower and more accurate compared to the experiments.

Case 3:
In this case a solid wall replaced the louvered wall at the ignition. See the results in Figure 7.1.8. The explosion pressure became much larger in this case compared to case 2 with the louvered wall, but it was somewhat under predicated by the FLACS simulation. This can be a result of the repeatability problem, where the results from the dry test performed gave a large variation in the results. When water spray is activated at the centre of the module the pressure is significantly reduced compared to the dry test. This reduction is smaller in the simulation, and the result is over predicated compared to the experiment. This is probably a result of the models lack of droplet transport. If the water spray is extended 2 m down towards the vent opening, the pressure is reduced to 0.60 bar and becomes coherent with the result of 0.62 bar from the experiment. This is illustrated in the pressure-time curve at the top of page 125 in appendix 10.

Case 1: Propane, centre ignition and open ends.

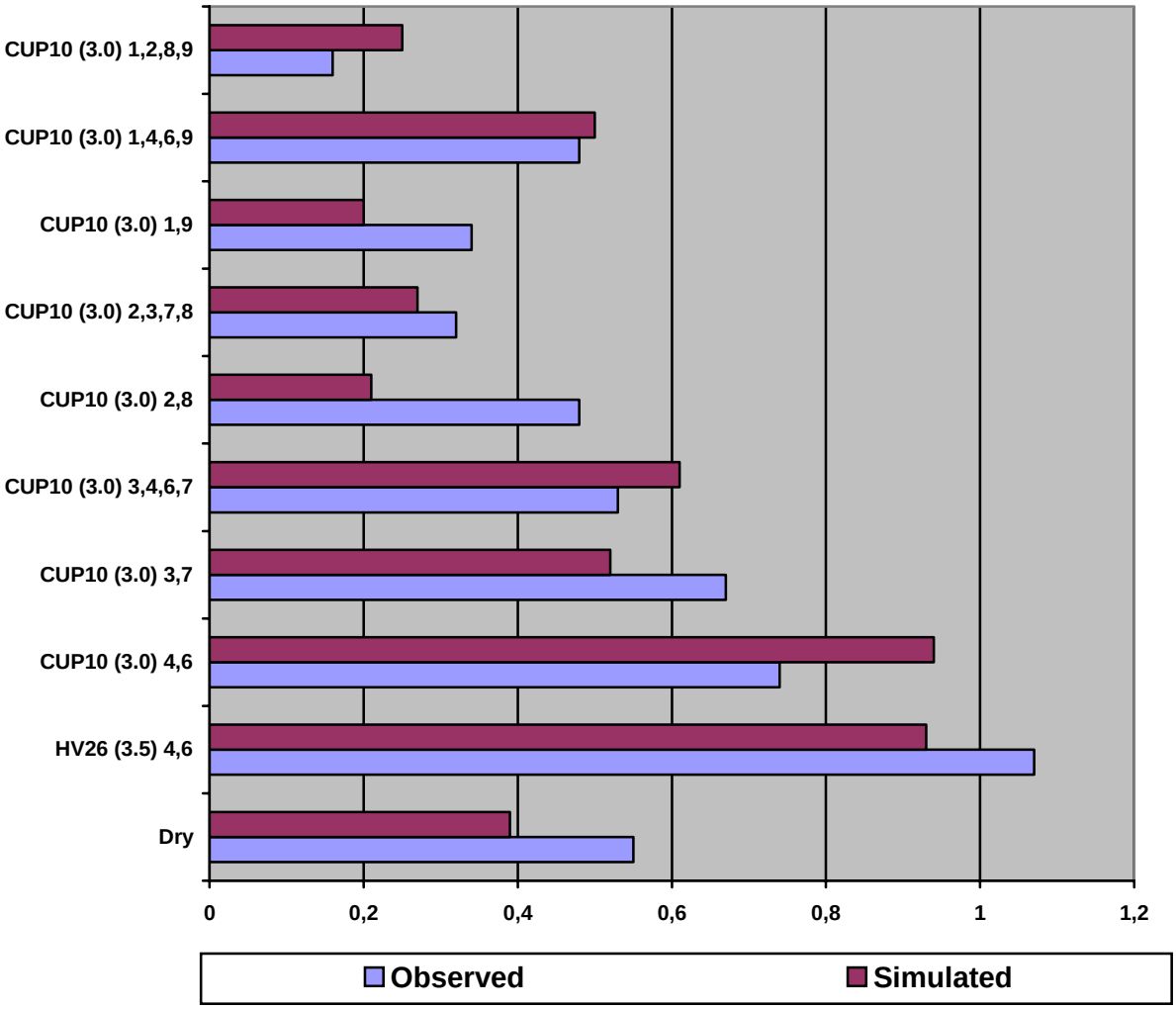

Figure 7.1.6: Experiments with propane in M24-25 module versus simulations with CUP10 and HV26 nozzles.

Case 2: Methane, end ignition, louvered wall at ignition and open opposite ignition.

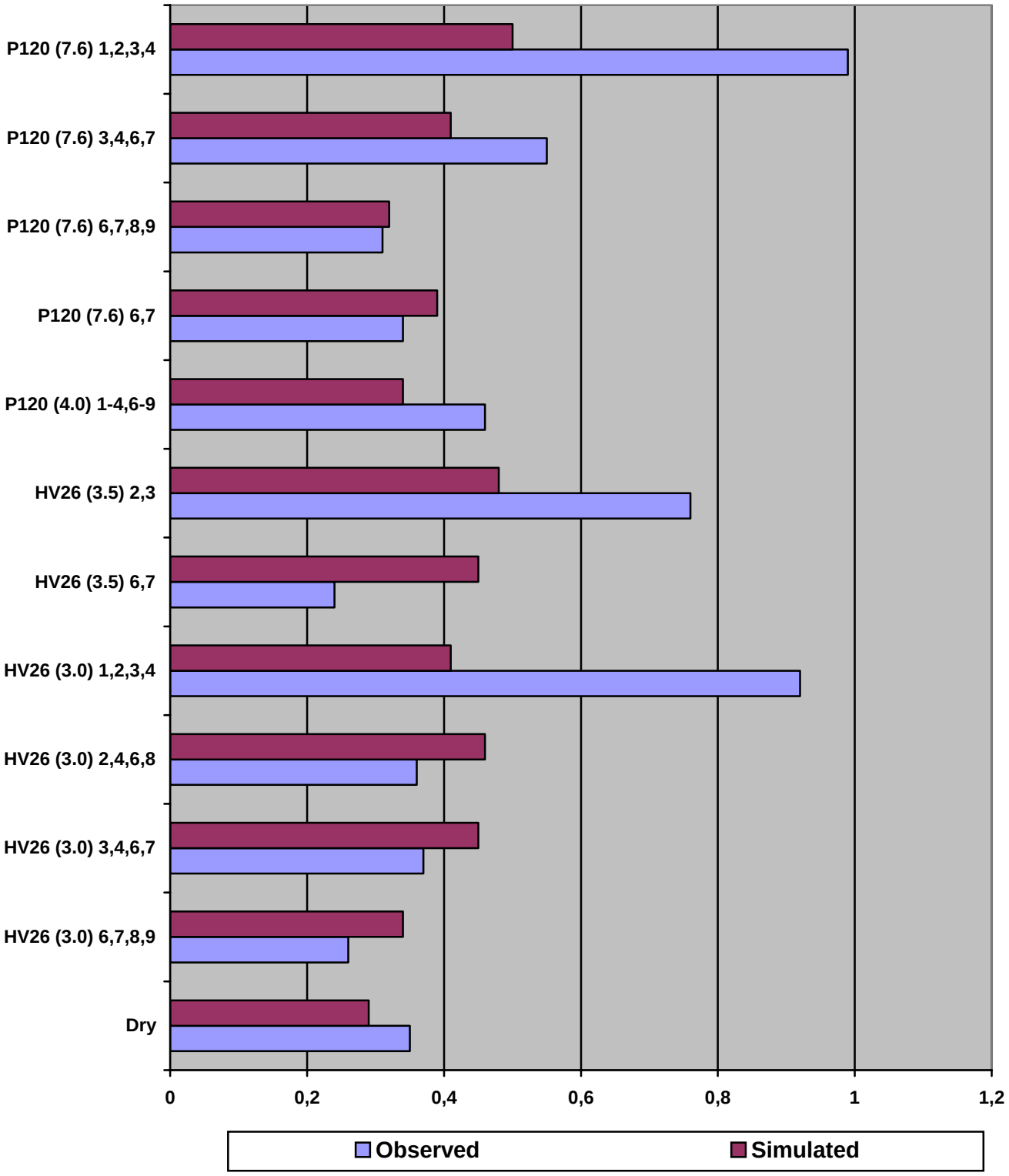

Figure 7.1.7: Experiments with methane in M24-25 module versus simulations with HV26 and P120 nozzles.

Case 2: Methane, end ignition, louvered wall at ignition and open opposite ignition.

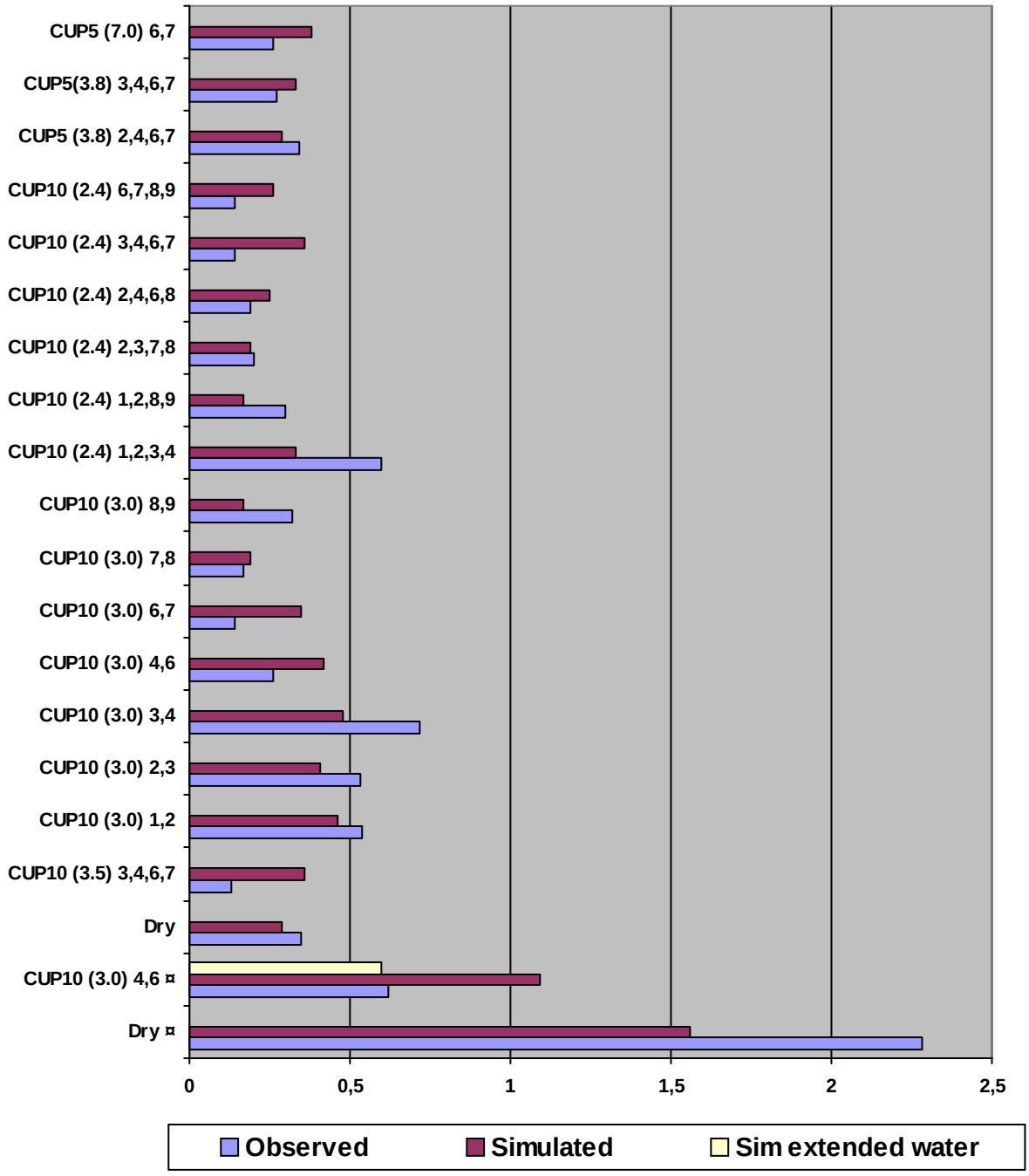

¤ Case 3: closed wall at ignition

Figure 7.1.8: Experiments with methane in M24-25 module versus simulations with CUP10 and CUP5 nozzles.

7.1.3 Full-scale module

In all the simulations the water spray has a positive mitigating effect on the explosion pressure. The pressure is reduced due to the cooling of the flame and the diluting of the flammable gas. As seen before the pressure peak comes earlier when water spray is used, as a consequence of the initial turbulence caused by the water droplets.

The LDN nozzle has a better mitigating effect than the MV57 nozzle, which is expected because the LDN nozzle has a flow rate over two times higher than he MV57 nozzle. The pressure peak comes slightly earlier with the use of the LDN nozzle compared to the MV57 nozzle. This can also be explained with the difference in the flow rate, where the larger flow rate from the LDN nozzle will create more initial turbulence and hence an earlier time of arrival for the pressure peak.

If we compare the explosion pressures from the two dry tests with centre- and end ignition, we see that the pressure is higher in the case of end ignition. This is expected, as the flame will propagate through a longer distance creating more turbulence and a higher explosion pressure. The water spray has a larger mitigating effect in the case of end ignition, and the pressure peaks comes later compared to centre ignition. The larger propagating distance allowing the flow created turbulence to become more dominant over the water spray turbulence, and the more effective droplet break-up due to the strong gas flow can explain this.

Two simulations were performed where the water spray was not extended but covered only the module. The purpose was to check weather this would influence the results. The simulation results show that there is no variation between the maximum pressure and the time of arrival for the two different water spray scenarios.

A quantitative comparison is made between the simulation results and result from experiments for the different scenarios:

Centre ignition:
Figure 7.1.9 shows a comparison between the results from the experiments and the simulations. In the simulations with no water spray the explosion pressure is under predicted and the time of arrival is over predicated compared to the experiments. This difference can be traced back to the uncertainty in the experiments, and different values when repeating the experiment. In the simulations with water spray the time of arrival is represented rather well but with some over predication, but the mitigating effect of the water spray on the explosion pressure is over predicated. In general the simulations represent the experiments quite well, with the same tendencies: Water spray mitigates the explosion pressure in all the simulations, the LDN nozzle has a better mitigating effect than the MV57 nozzle, the time of arrival is earlier with the use of water spray and the time of arrival is earlier with the LDN nozzle than with the MV57 nozzle. This is shown in the pressure-time curve at the top of page 130 in appendix 14.

End ignition:
Figure 7.1.10 shows a comparison between the results from the experiments and the simulations. In the dry test the explosion pressure is under predicated and the time of arrival is over predicated, as in the case of centre ignition. It is noted that the maximum pressure is

higher in the dry test with end ignition compared to centre ignition, due to the longer propagating distance creating more turbulence and therefore higher pressures. The explosion pressure and time of arrival from the simulation with water spray has good coherence with the results from the experiments. As in the case of centre ignition the water spray has a mitigating effect, with the LDN nozzle as the most effective. The reduction factor due to water spray is larger in this case compared to centre ignition, as a result of the more dominating flow turbulence caused by the larger propagating distance. The time of arrival is earlier in the case of centre ignition because of the greater effect from the initial turbulence, due to the flow propagating a shorter distance compared to end ignition. The results from the simulations are shown in the pressure-time curve at the bottom of page 130 in appendix 14.

Simulations with centre ignition:

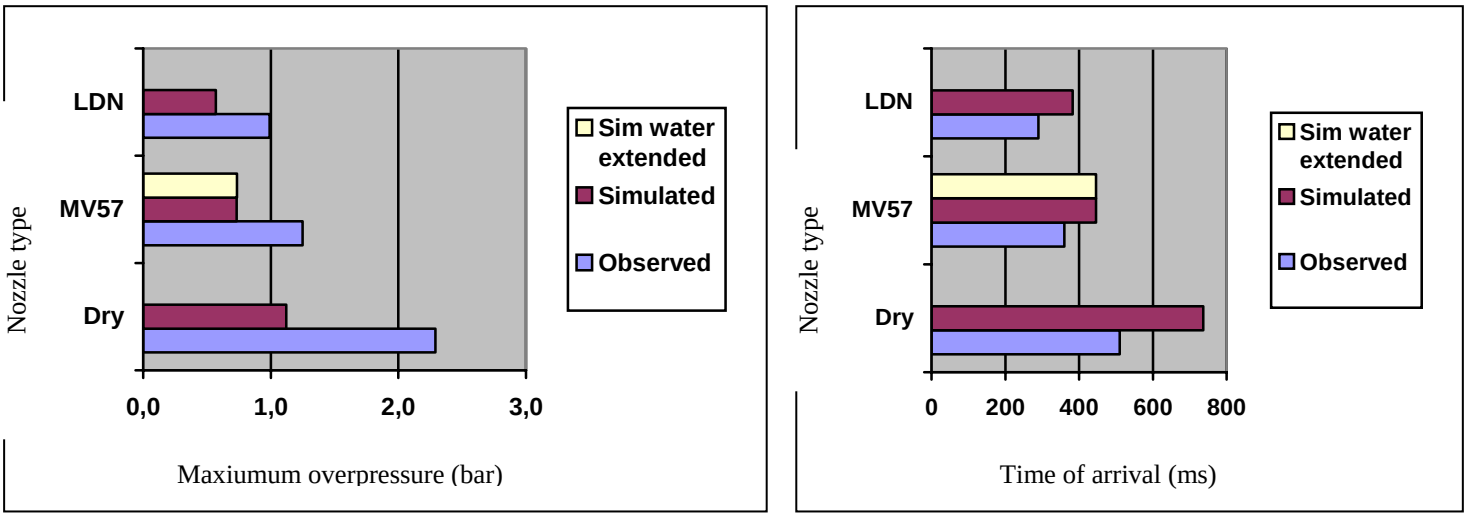

Figure 7.1.9: A comparison between simulations and results from experiments with M24 full-scale geometry with centre ignition, pressure (left) and time of arrival (right).

Simulations with end ignition:

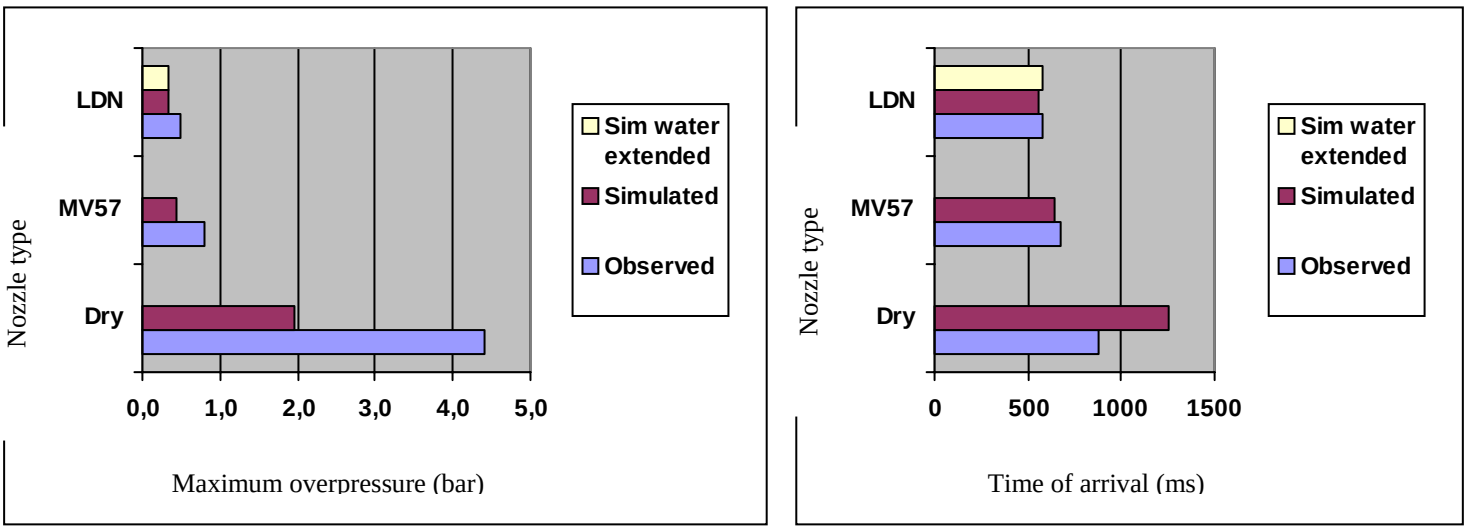

Figure 7.1.10: A comparison between simulations and results from experiments with M24 full-scale geometry with end ignition, pressure (left) and time of arrival (right).

7.2 Comparison of results from experiments and simulations performed with FLACS 2.2.6*

7.2.1 Explosion box

Results without setDROP

In the case of high confinement, i.e. a small ventilation opening, the water spray had no mitigating effect and gave a higher pressure-peak due to the turbulence created by the water droplets. The water droplets from the water spray nozzle have to be broken up in order to extract energy, and this requires high gas acceleration in front of the flame. In the case of small ventilation area the flow is restricted and will not reach a sufficient velocity to cause droplet break-up. The rate of maximum overpressure between simulations with and without water spray did however decrease when the number of pipes was increased, but in the case of 80 pipes the pressure rate is the same as with 20 pipes. The reduction is illustrated in Table 7.2.1. The explanation for this reduction can be that the turbulence caused by obstacles increases when the number of pipes increases, and therefore becomes more and more dominating over the water spray induced turbulence. This reduction effect was also seen in the experiments, but they only included maximum 40 pipes. There was little deviation between the results with the MV57- and HV60-nozzle.

Number of pipes	**0**	**20**	**40**	**80**
Pressure rate	4.0	1.3	1.1	1.3

Table 7.2.1: Pressure rate between simulations with and without water spray for different congestions with small vent opening.

When the ventilation opening was increased to cover the whole left side of the box, the explosion pressure was lower compared to the case with a small ventilation opening. This is a result of an effective ventilation of the burned gas. There was again little deviation between the MV57- and HV60-nozzle, except for the case with 56 pipes. At this scenario the HV60-nozzle reduces the maximum explosion pressure by 0.8 bar compared to the dry test, but the MV57-nozzle increases the pressure by 0.1 bar.

A quantitative comparison is made between the simulation results and result from experiments for some of the different geometries:

In the case of a small ventilation opening and variable congestion the maximum explosion pressure results from experiments and simulations are coherent and only small deviations are seen. The model seems to give a good representation of the experiments. In Figure 7.2.1 one can clearly see the negative effect of water spray, where the overpressure is considerably increased at the presence of water spray. This effect is coherent with the fact that due to the small ventilation opening the turbulence caused by the water spray will dominate the situation and create higher pressures and earlier pressure peaks. When the congestion is increased the

rate between the overpressure with and without water spray is reduced, this because the obstacle created turbulence will become more and more dominating in condition to the turbulence created by the water spray. This can be seen in figures 7.2.2 and 7.2.3. In the experiments this rate is 4.7 1.36 and 1.28 for the congestion of 0, 20 and 40 pipes respectively. Compared to this rate from the simulations shown in Table 7.2.1 we see that the values are relatively coherent. If we look at the time of arrival this comes much later than in the experiments. A reason for this can be that the initial turbulence by the water spray is not represented well enough, due to the fact that the RTI and TLS parameters in the created cl-files are inactive. Another limitation concerning the cl-files is that the water spray exits the nozzles in a thin jet instead of a broad cone, which would be the case in a real situation.

In the case of a large ventilation opening the simulations has a tendency to under predicate the overpressures Figure 7.2.5 shows the case with 80 pipes, and here the simulations with both MV57 and HV60 nozzles are under predicated. In Figure 7.2.4 the MV57-nozzle is under predicated and the HV60-nozzle is over predicated. These deviations can be explained by the fact that the simulation with a large ventilation opening gives a more difficult and complex scenario. The products and water spray will in this case be transported outside the explosion box in a much larger scale than with the small ventilation opening. Another moment to mention is that the experiments performed by British Gas are from 1992, and can contain uncertain factors.

Box with small vent opening and no pipes (Kv=9, n=0)

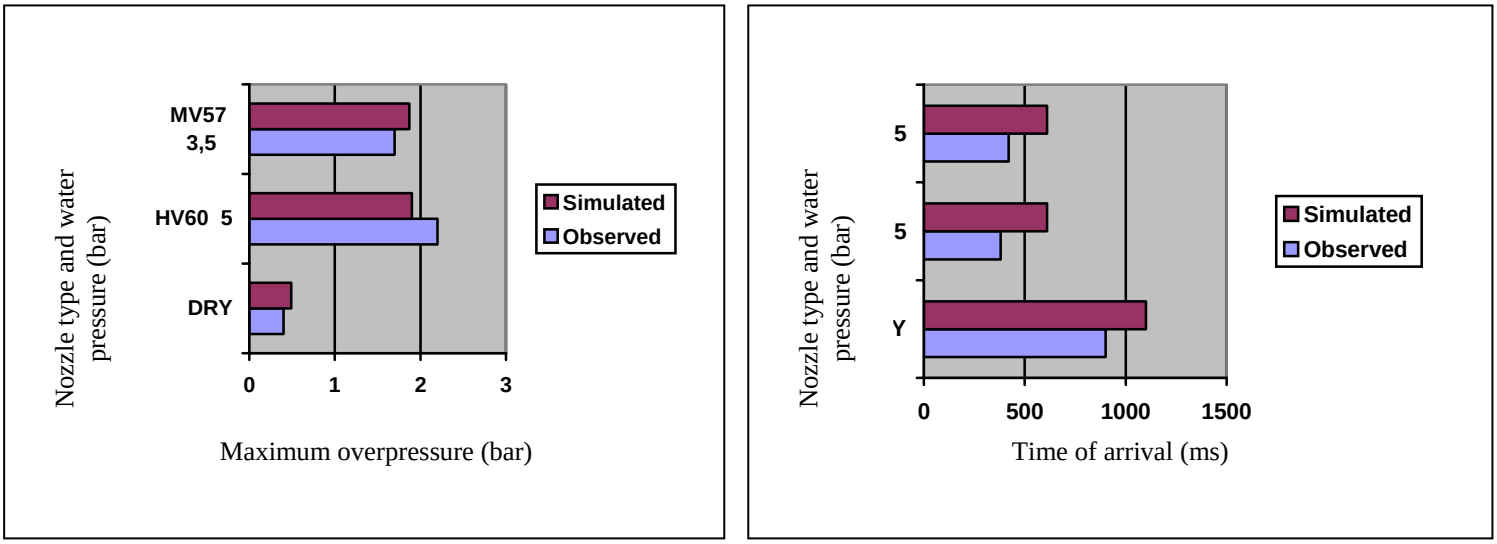

Figure 7.2.1: A comparison between results from experiments with British Gas 180m^3 box and simulations with small vent opening and no congestion, pressure (left) and time of arrival (right).

Box with small vent opening and 20 pipes (Kv=9, n=20)

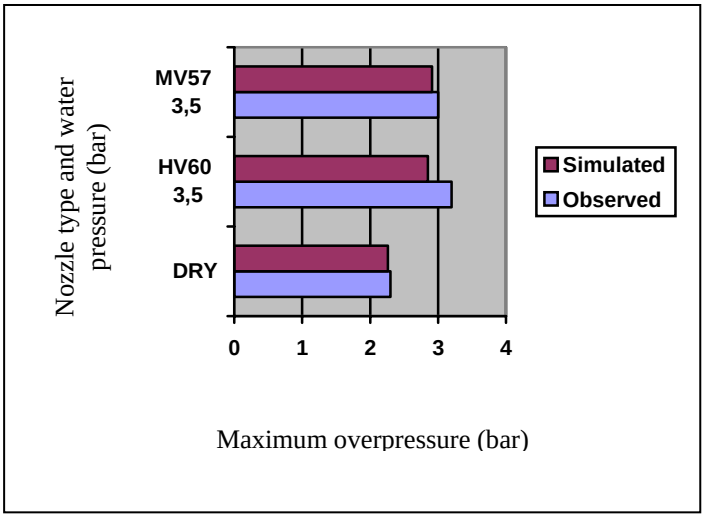

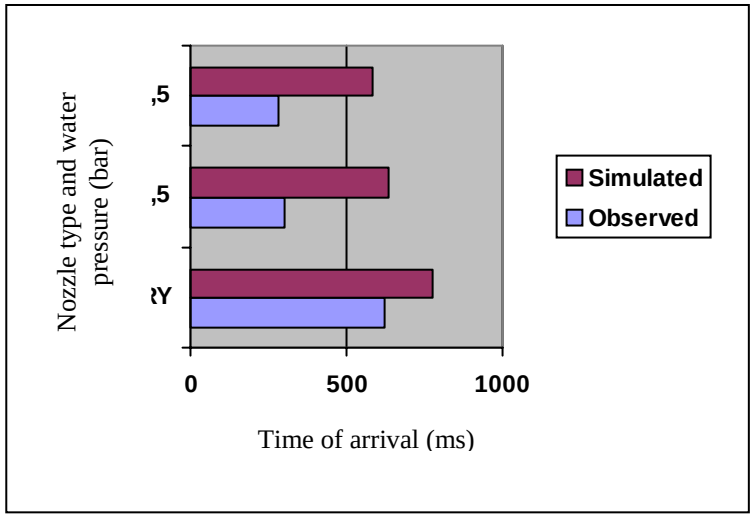

Figure 7.2.2: A comparison between results from experiments with British Gas 180m^3 box and simulations with small vent opening and 20 pipes, pressure (left) and time of arrival (right).

Box with small vent opening and 40 pipes (Kv=9, n=40)

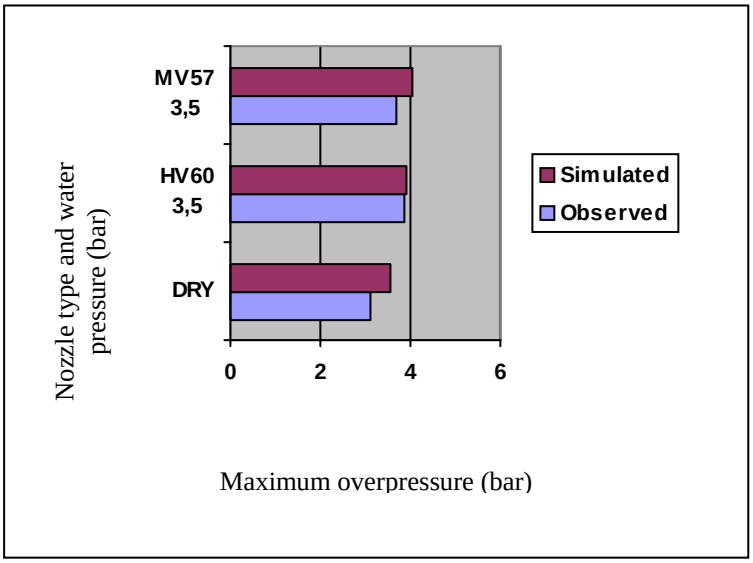

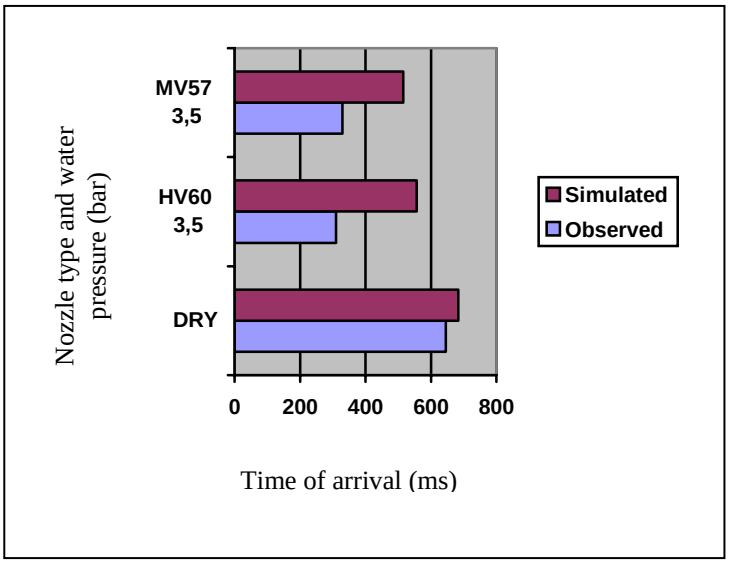

Figure 7.2.3: A comparison between results from experiments with British Gas 180m^3 box and simulations with small vent opening and 40 pipes, pressure (left) and time of arrival (right).

Box with large vent opening and 56 pipes (Kv=1, n=56)

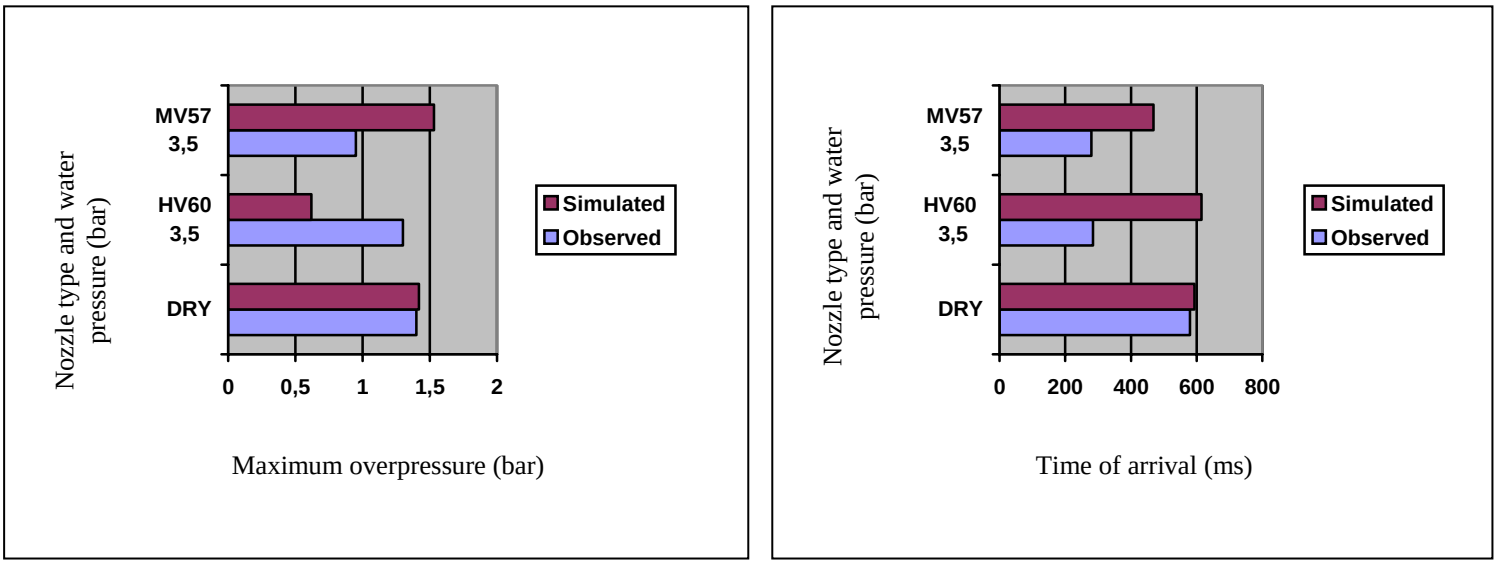

Figure 7.2.4: A comparison between results from experiments with British Gas 180m^3 box and simulations with small vent opening and 56 pipes, pressure (left) and time of arrival (right).

Box with large vent opening and 80 pipes (Kv=1, n=80)

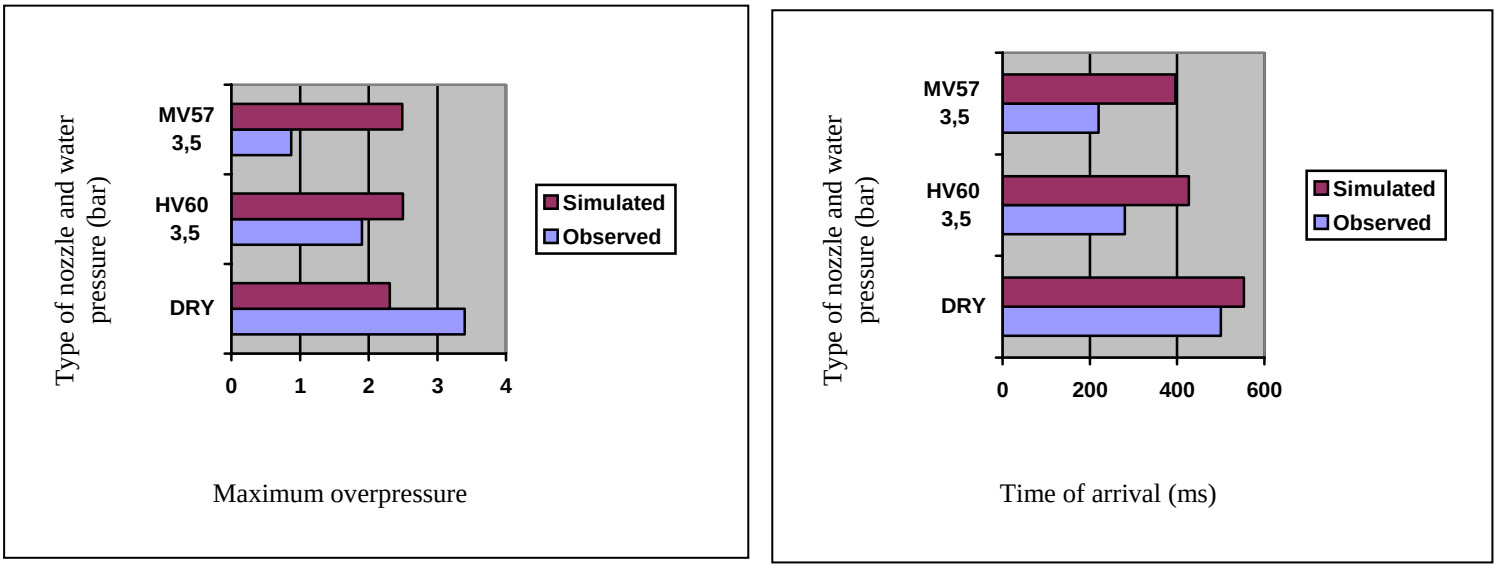

Figure 7.2.5: A comparison between results from experiments with British Gas 180m^3 box and simulations with large vent opening and 80 pipes, pressure (left) and time of arrival (right).

Results with setDROP

In the case of high confinement, i.e. a small ventilation opening, the water spray had no mitigating effect and gave a significantly higher pressure-peak due to the turbulence created by the water droplets. In order for the evaporation to be effective and thereby extract energy from the explosion, the water droplets had to be broken up. Due to the small ventilation opening the flow is restricted and doesn't reach the critical droplet break-up velocity. As a result of this the water spray has a severe negative effect on the explosion pressure. Although the pressure is larger with the use of water spray in all the scenarios with a small ventilation opening, the rate of maximum overpressure between simulations with and without water spray did however decrease as the amount of pipes in the explosion box increased. The reduction is illustrated in Table 7.2.2. There was some deviation between the results with the MV57- and HV60-nozzle.

Number of pipes	**0**	**20**	**40**	**80**
Pressure rate	61.5	14.4	9.57	7.76

Table 7.2.2: Pressure rate between simulations with and without water spray for different congestions with small vent opening.

When the ventilation opening was increased to cover the whole left side of the box, the explosion pressure was lower compared to the case with a small ventilation opening. This is a result of an effective ventilation of the burned gas. The water spray does not have a mitigating effect on the explosion pressure, but the increase in pressure decreases as the number of obstruction increases. There was a larger deviation between the two nozzles compared to the case with a small ventilation opening, but the nozzles switches on having the best mitigating effect.

A quantitative comparison is made between the simulation results and result from experiments for some of the different geometries:

In the case of a small ventilation opening and variable congestion the maximum explosion pressure results from experiments and simulations are over predicted. The same tendencies as in the experiments are seen, but the maximum explosion pressure is significantly higher and the time of arrival later than in the experiments. In Figure 7.1.6 one can clearly see the negative effect of water spray, where the overpressure is considerably increased at the presence of water spray. This effect is coherent with the fact that due to the small ventilation opening the turbulence caused by the water spray will dominate the situation and create higher pressures and earlier pressure peaks. When the congestion is increased the rate between the overpressure with and without water spray is reduced, this because the obstacle created turbulence will become more and more dominating in condition to the turbulence created by the water spray. This can be seen in Figures 7.1.7 and 7.1.8. In the experiments this rate is 4.7 1.36 and 1.28 for the congestion of 0, 20 and 40 pipes respectively. Although these values deviate from the values in Table 7.2.2, the same tendencies are seen. If we look at the time of arrival this comes much later than in the experiments. A reason for this can be that the initial turbulence by the water spray is not represented well enough, due to the fact that the RTI and TLS parameters in the created cl-files are inactive. Another limitation concerning the cl-files is that the water spray exits the nozzles in a thin jet instead of a broad cone, which would be the case in a real situation.

In the case of a large ventilation opening the simulations has a tendency to over predicate the overpressures and the time of arrival. Figure 7.1.10 shows the case with 80 pipes. The maximum pressure obtained with the HV60-nozzle has a larger deviation from the experiments than the maximum explosion pressure with the MV57-nozzle. The experiments are not represented well.

Box with small vent opening and no pipes (Kv=9, n=0)

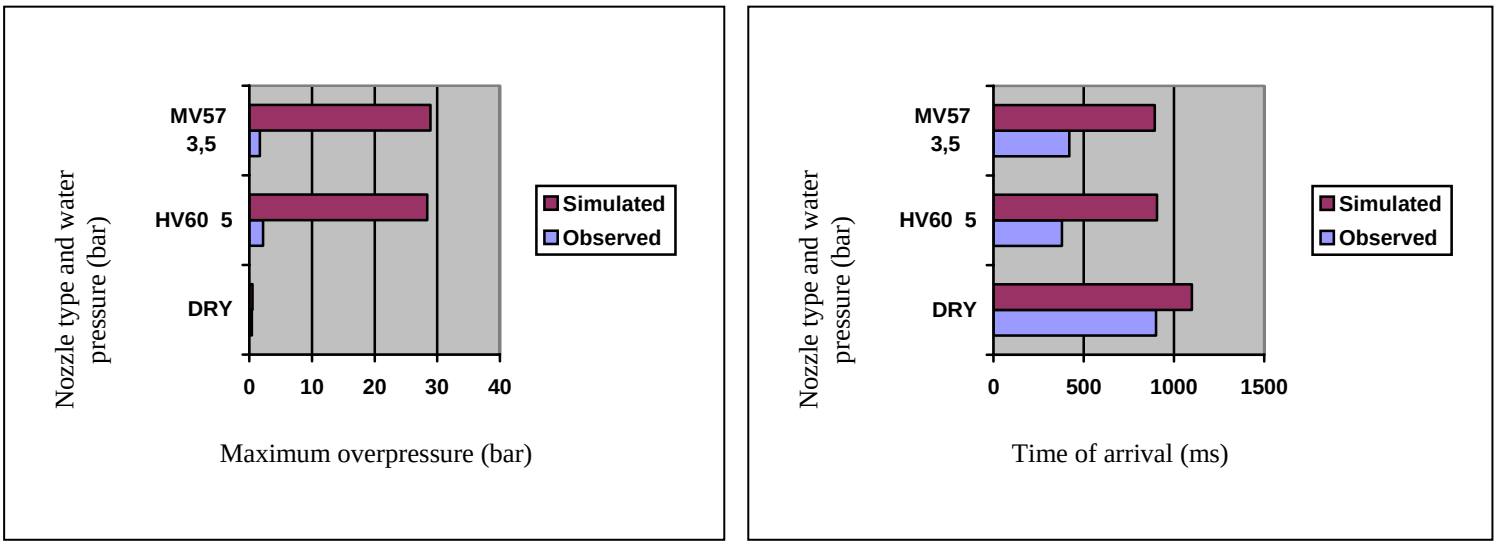

Figure 7.2.6: A comparison between results from experiments with British Gas 180m^3 box and simulations with small vent opening and no congestion, pressure (left) and time of arrival (right).

Box with small vent opening and 20 pipes (Kv=9, n=20)

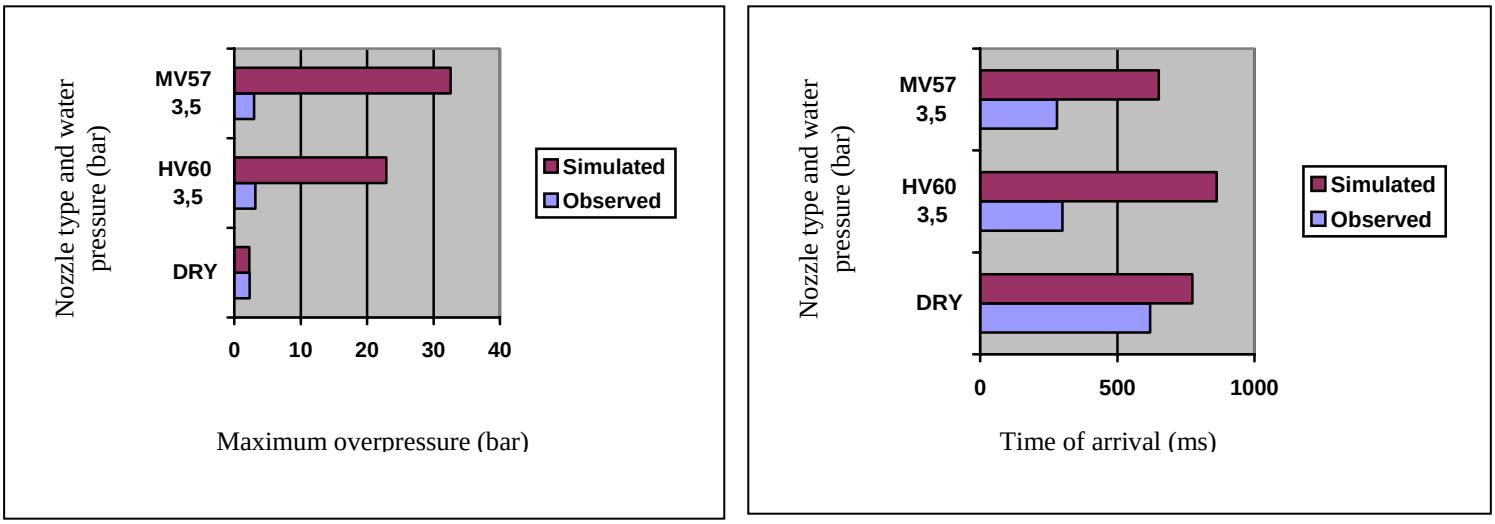

Figure 7.2.7: A comparison between results from experiments with British Gas 180m^3 box and simulations with small vent opening and 20 pipes, pressure (left) and time of arrival (right).

Box with small vent opening and 40 pipes (Kv=9, n=40)

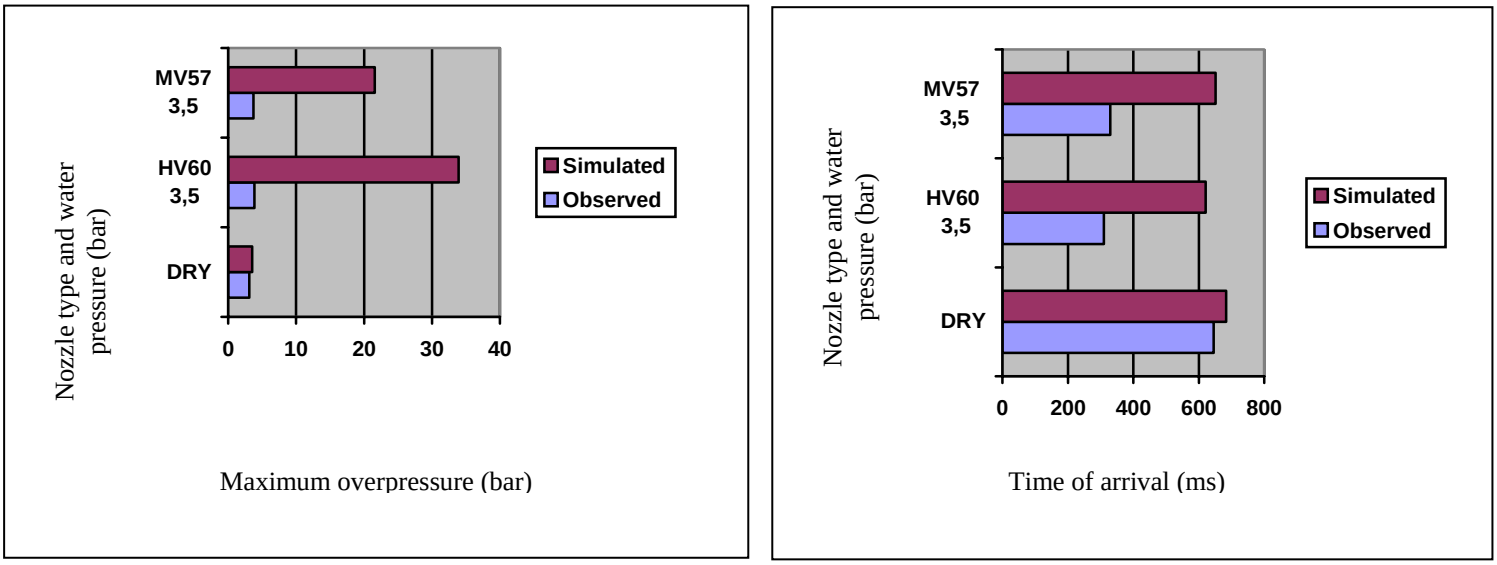

Figure 7.2.8: A comparison between results from experiments with British Gas 180m^3 box and simulations with small vent opening and 40 pipes, pressure (left) and time of arrival (right).

Box with large vent opening and 56 pipes (Kv=1, n=56)

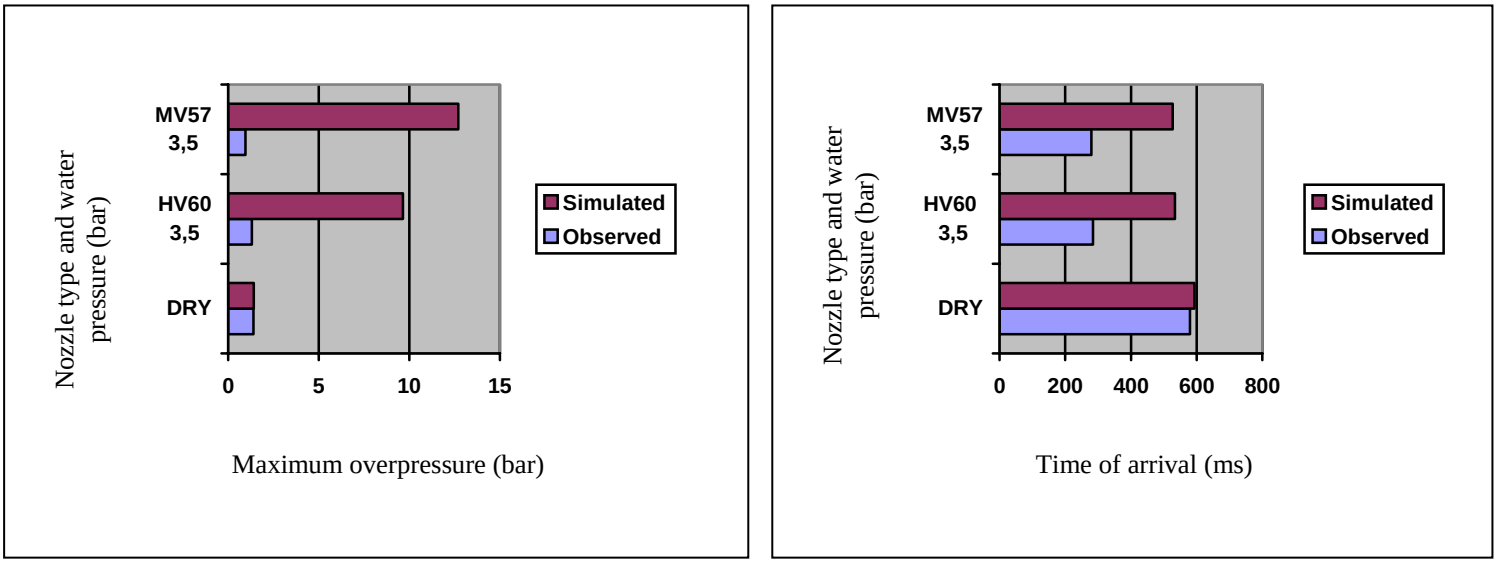

Figure 7.2.9: A comparison between results from experiments with British Gas 180m^3 box and simulations with small vent opening and 56 pipes, pressure (left) and time of arrival (right).

Box with large vent opening and 80 pipes (Kv=1, n=80)

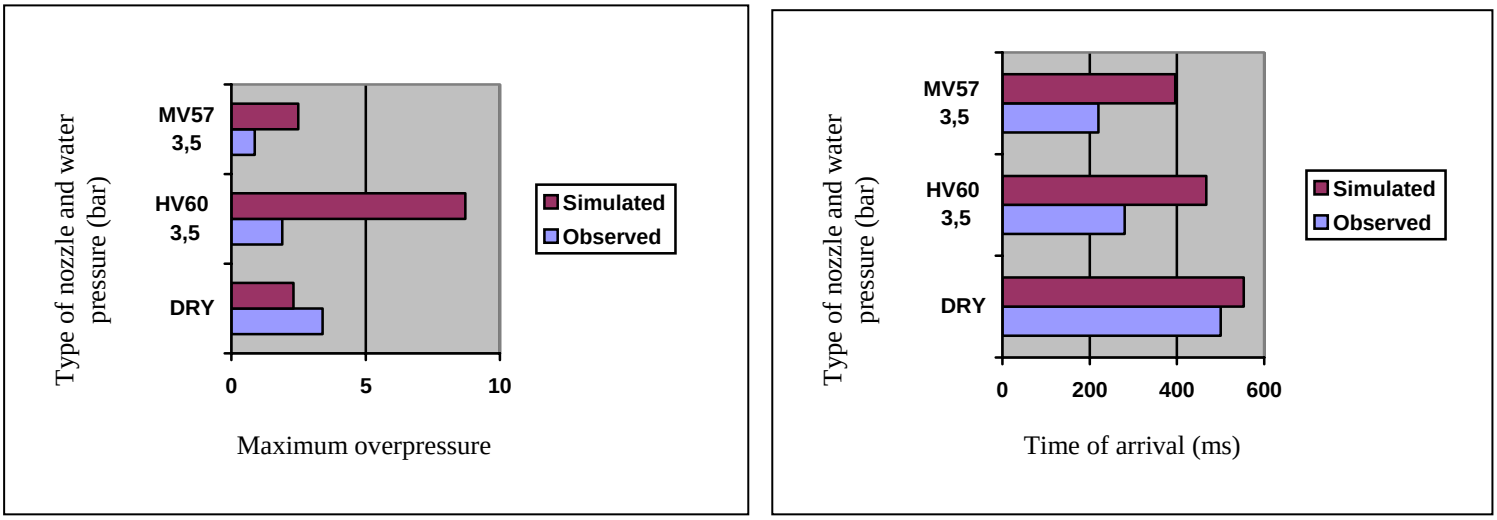

Figure 7.2.10: A comparison between results from experiments with British Gas 180m^3 box and simulations with large vent opening and 80 pipes, pressure (left) and time of arrival (right).

7.2.2 1:5 offshore module, M24-25

All of the simulations were performed with the setDROP-file.

Case 1: Propane, centre ignition and open ends.
The results are shown in Figure 7.2.11. When water spray activated far from ignition, at each end of the module (1,9), the maximum explosion pressure is somewhat lower than in the experiments. With water spray activated near the ignition at the centre of the module (4,6), the simulated explosion pressure is also a bit lower compared to the experiments. The same tendencies are seen in both experiments and simulations.

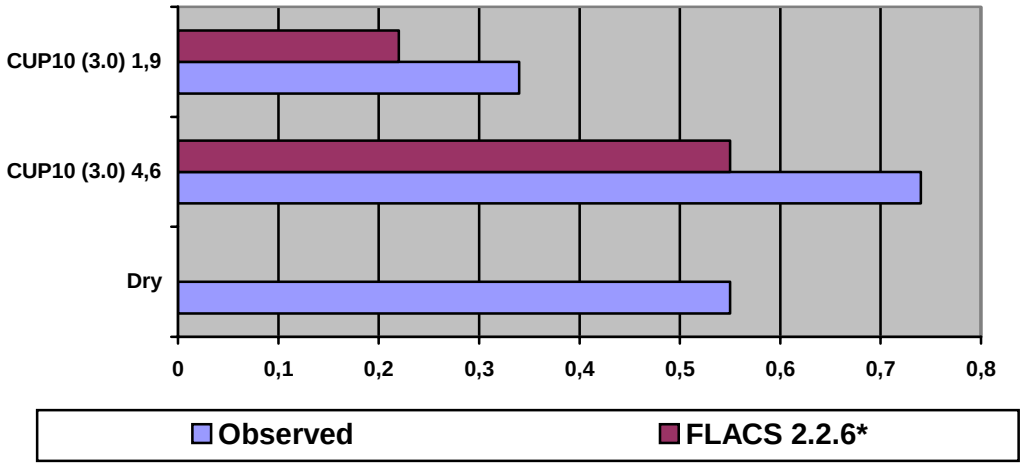

Figure 7.2.11: Experiments with propane in M24-25 module versus simulations by FLACS 2.2.5 and FLACS 2.2.6 with CUP10 nozzles.*

Case 2: Methane, end ignition, louvered wall at ignition and open opposite ignition.

The maximum explosion pressure seems to be over predicated with the use of FLACS 2.2.6* when water spray is activated. According to the experiments the CUP-nozzles should give the lowest pressure, but this is not the case in the simulations.

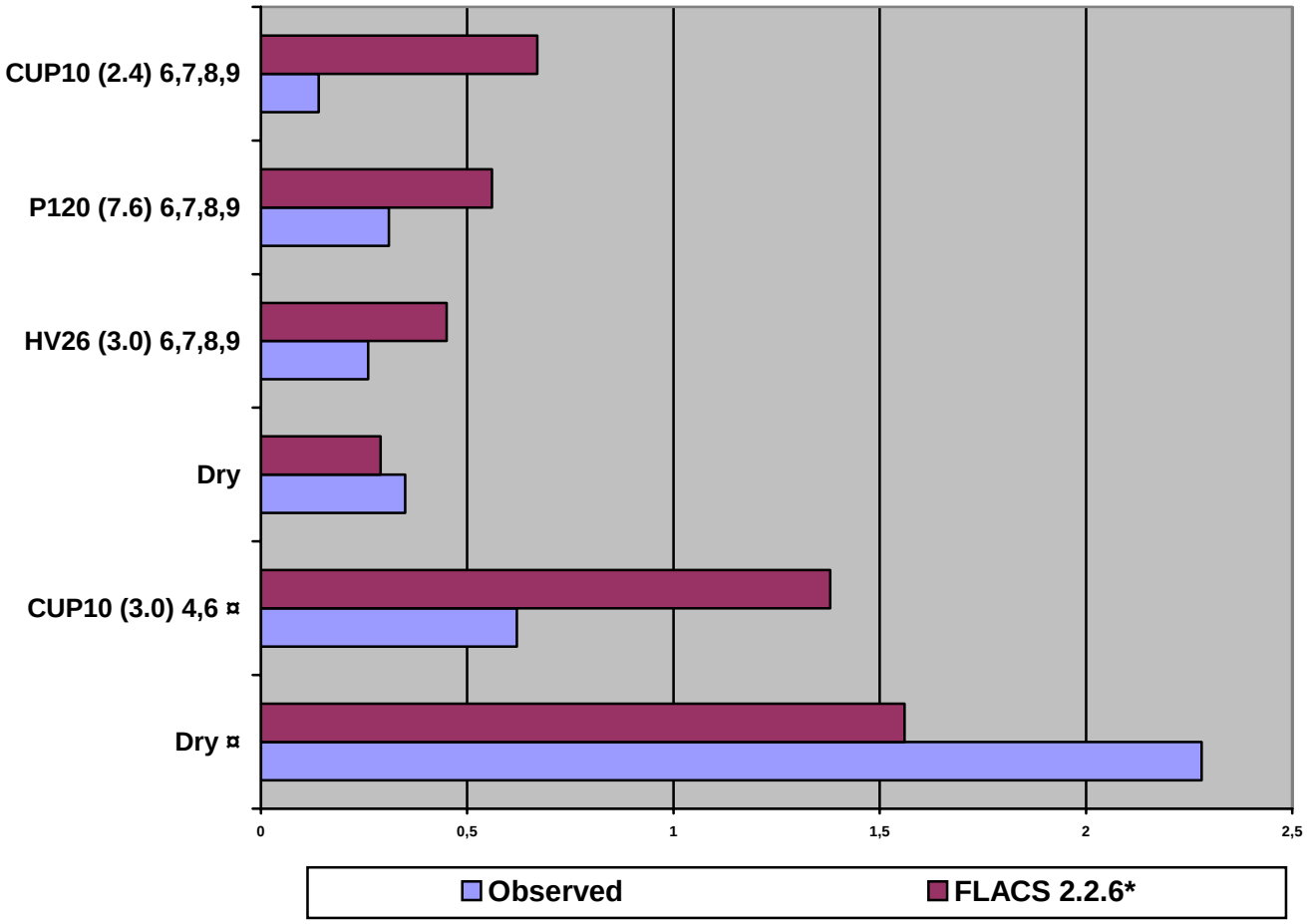

Figure 7.2.12: Experiments with methane in M24-25 module versus simulations by FLACS 2.2.5 and FLACS 2.2.6 with HV26, CUP10 and P120 nozzles.*

¤ Case 3: closed wall at ignition

7.3 Comparison between FLACS 2.2.5 and FLACS 2.2.6*

A comparison is made between the simulation results from FLACS 2.2.5 and FLACS 2.2.6* for the explosion box, M24-25 module and full-scale module to determine their strengths and weaknesses.

7.3.1 Explosion box

A comparison between the results from experiments and simulations performed with both FLACS 2.2.5 and FLACS 2.2.6* without setDROP is illustrated in Figures 7.3.1 to 7.3.5.

FLACS 2.2.5
In the case of a small ventilation opening this model gives a good representation of the real situation, both the maximum explosion pressure and time of arrival is coherent with the results from the experiments

In the case of a large ventilation opening the maximum overpressure is under predicated. With this large ventilation opening the scenario becomes more complex, and the water spray will in a much larger scale be transported towards and outside the opening. The model doesn't take into account the transport of droplets with the fluid flow.

FLACS 2.2.6*
Without setDROP
In the case of a small ventilation opening this model gives a good representation of the explosion pressure, but the time of arrival comes later than in the experiments. The deviations in the time of arrival can be because the RTI and TLS are not active in the cl-file, and therefore the initial turbulence from the water spray that normally creates the earlier pressure peaks is not represented well enough. The rate between maximum explosion pressure with and without water spray decreases as the number of obstacles increases with very similar values as in the experiments, and the tendencies from the experiments are well represented.

With a large ventilation opening the explosion pressure and time of arrival is somewhat over predicated.

With setDROP
In the case of a small ventilation opening this model gives a large over predication in the explosion pressure and the time of arrival. Reasons for this can be that the criteria for droplet break-up is not fulfilled due to the small ventilation opening, and the evaporation is therefore not effective. The same tendency that the rate between the maximum pressure with and without water spray is decreasing as the number of obstacles are increasing is seen, although the rate is much higher due to the over predication.

With a large ventilation opening both the explosion pressure and the time of arrival is also over predicated, but the deviation is not so large in some of the scenarios.

A general reason for deviations between the simulation results and the results from the experiments can be that the cl-file generates the water spray exiting the nozzles as a narrow jet, which is not coherent with the normally broad cone seen in a real situation. This is clearly seen in Figure 7.3.6, which illustrates the velocity of the water spray.

Box with small vent opening and no pipes (Kv=9, n=0)

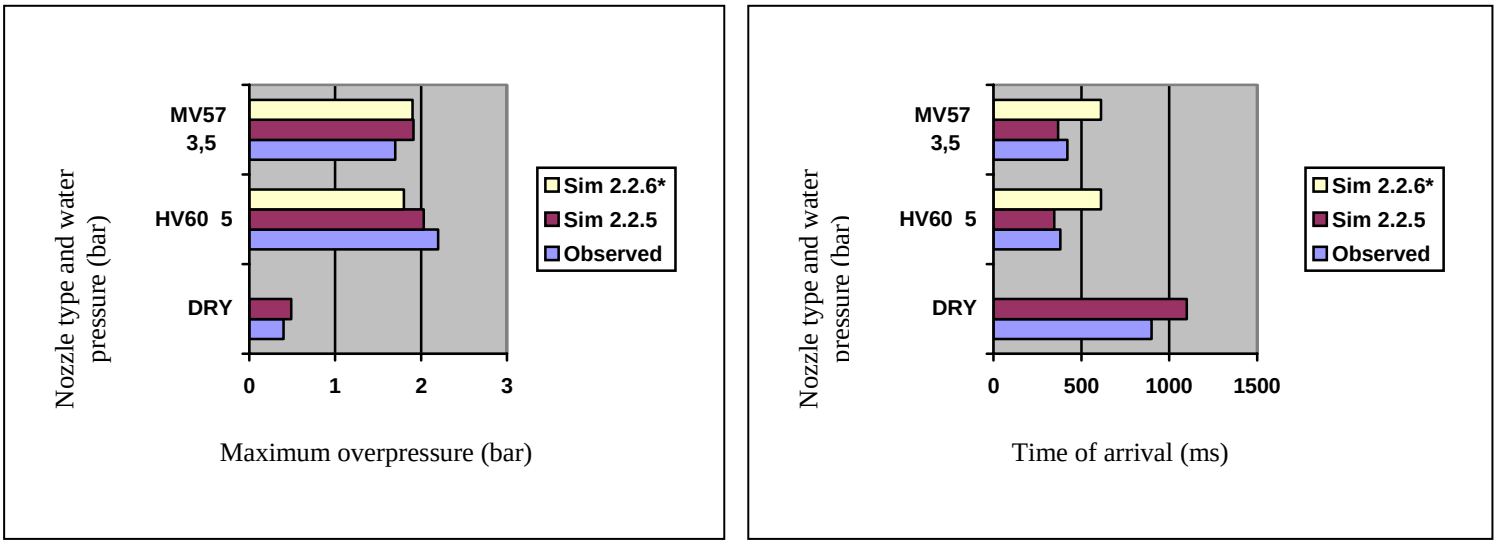

Figure 7.3.1: A comparison between results from experiments with British Gas 180m^3 box and simulations performed by FLACS 2.2.5 and FLACS 2.2.6 (without setDROP) with small vent opening and no congestion, pressure (left) and time of arrival (right).*

Box with small vent opening and 20 pipes (Kv=9, n=20)

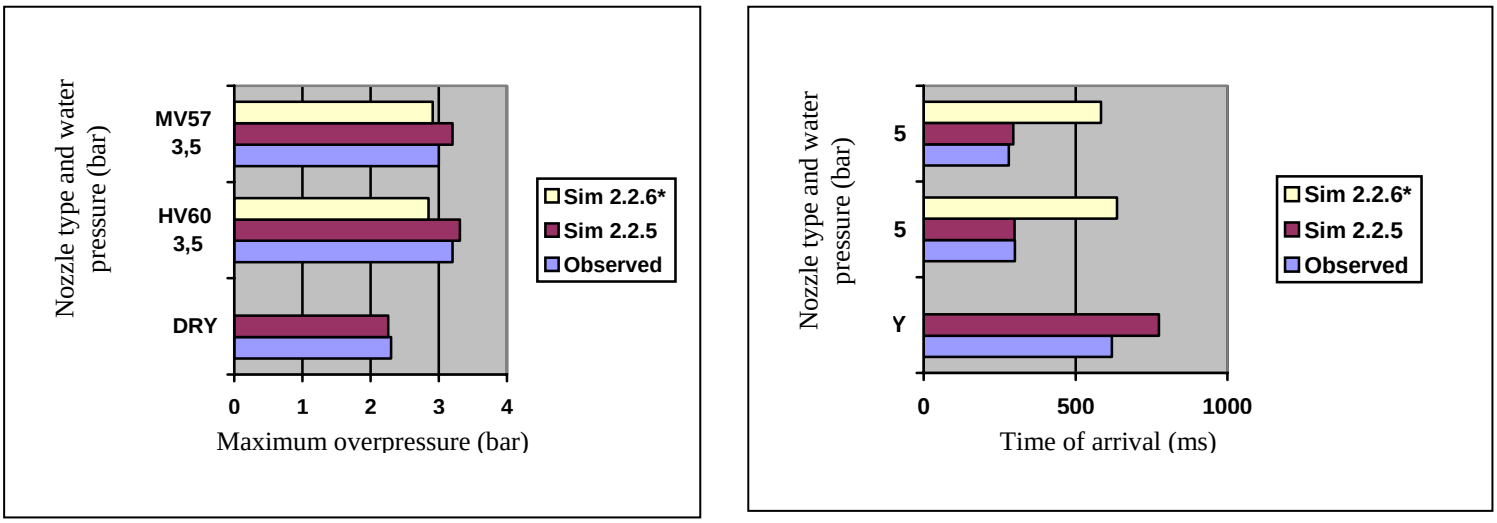

Figure 7.3.2: A comparison between results from experiments with British Gas 180m^3 box and simulations performed by FLACS 2.2.5 and FLACS 2.2.6 (without setDROP) with small vent opening and 20 pipes, pressure (left) and time of arrival (right).*

Box with small vent opening and 40 pipes (Kv=9, n=40)

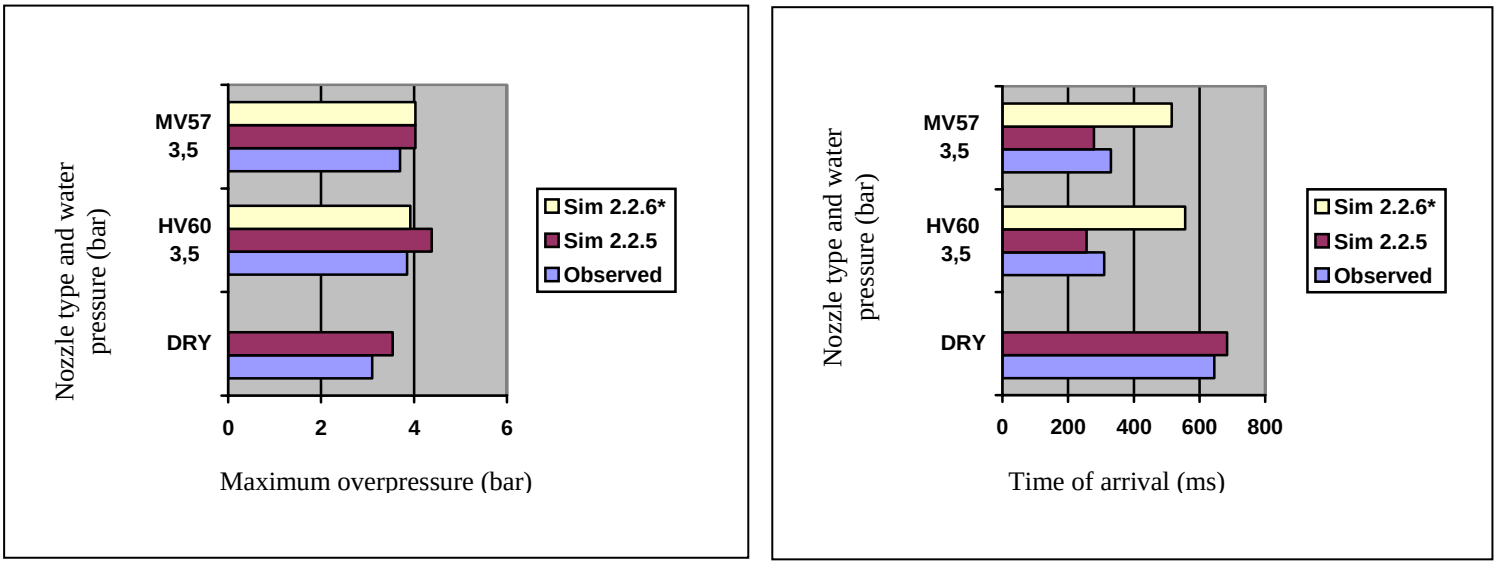

Figure 7.3.3: A comparison between results from experiments with British Gas 180m^3 box and simulations performed by FLACS 2.2.5 and FLACS 2.2.6 (without setDROP) with small vent opening and 40 pipes, pressure (left) and time of arrival (right).*

Box with large vent opening and 56 pipes (Kv=1, n=56)

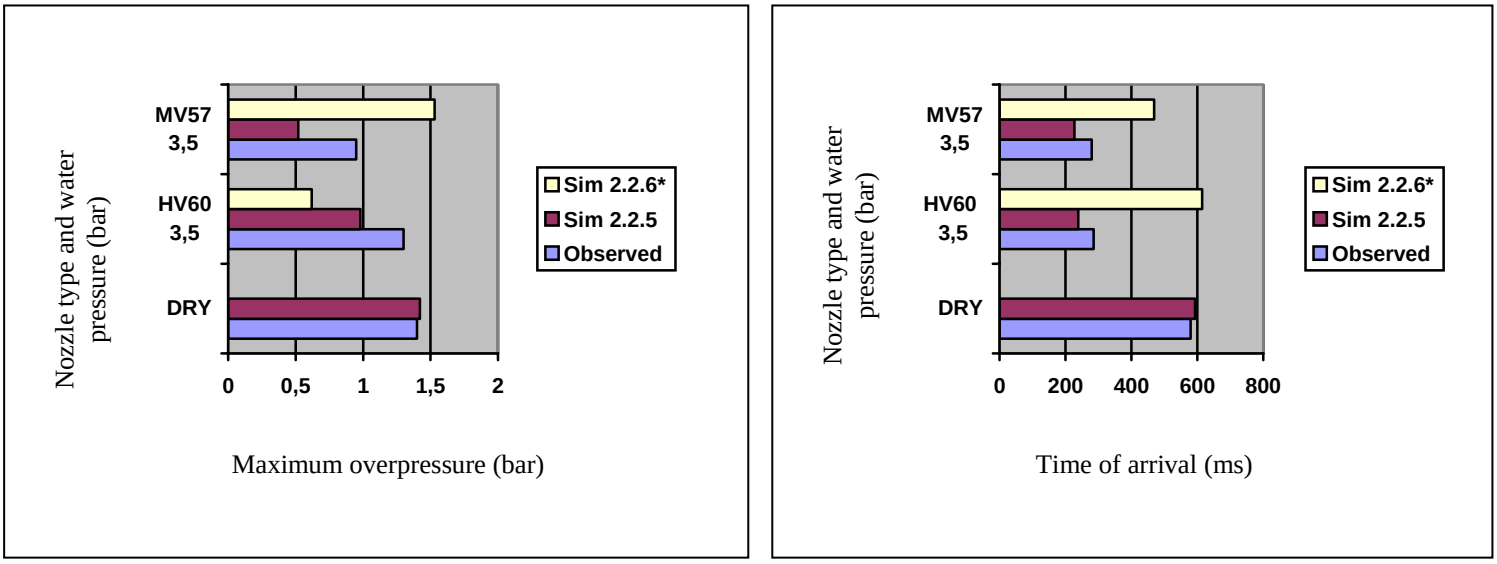

Figure 7.3.4: A comparison between results from experiments with British Gas 180m^3 box and simulations performed by FLACS 2.2.5 and FLACS 2.2.6 (without setDROP)with small vent opening and 56 pipes, pressure (left) and time of arrival (right).*

Box with large vent opening and 80 pipes (Kv=1, n=80)

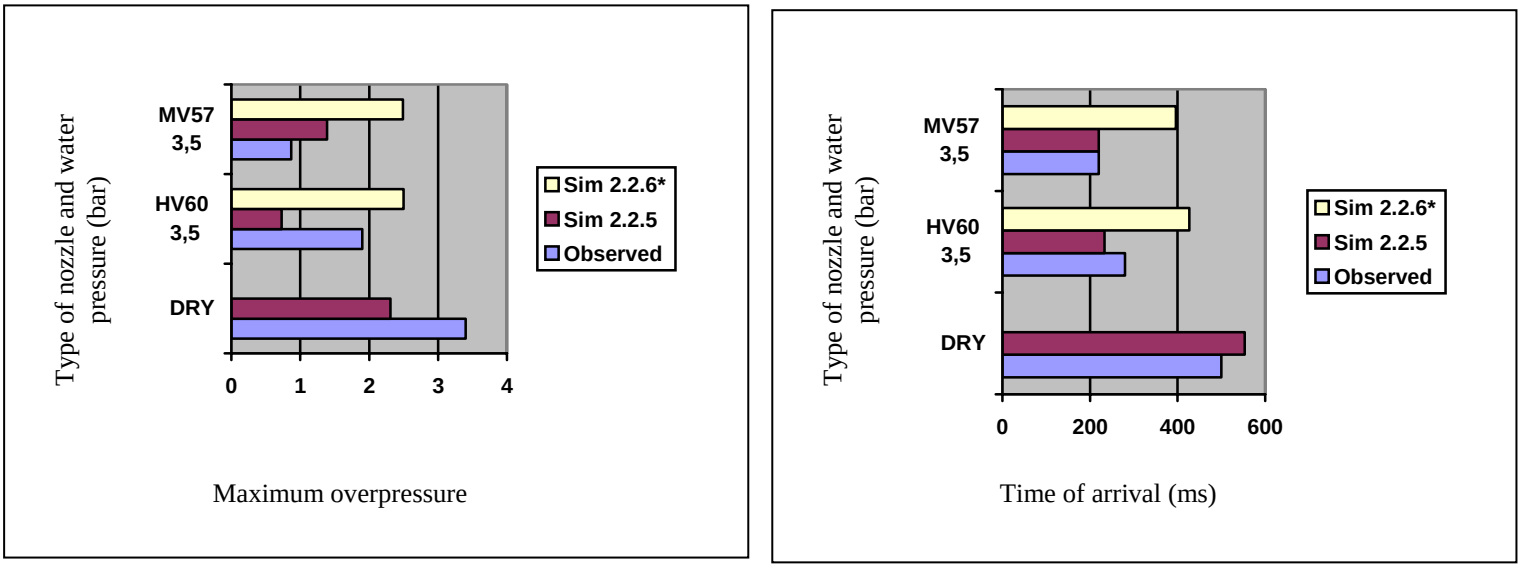

Figure 7.3.5: A comparison between results from experiments with British Gas 180m^3 box and simulations performed by FLACS 2.2.5 and FLACS 2.2.6 (without setDROP) with large vent opening and 80 pipes, pressure (left) and time of arrival (right).*

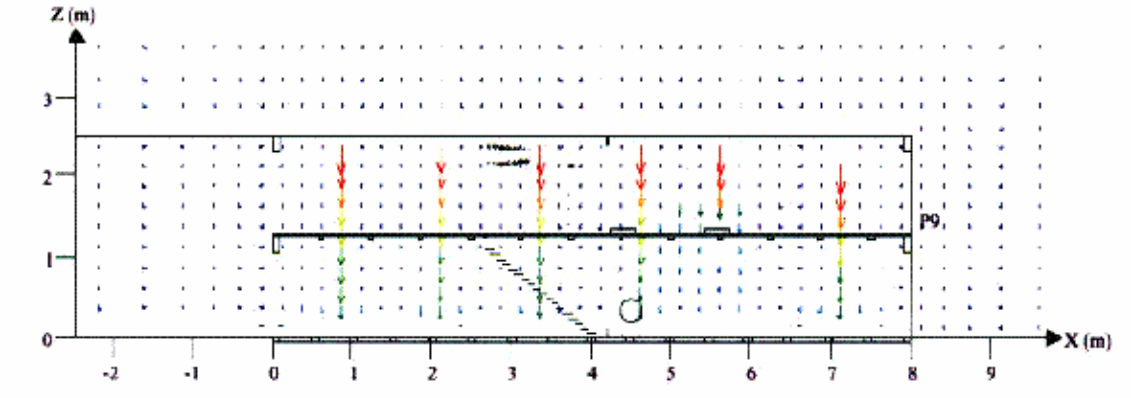

Figure 7.3.6: The velocity of the water spray exiting the nozzles.

7.3.2 1:5 offshore module, M24-25

A comparison between the results from experiments and simulations performed with both FLACS 2.2.5 and FLACS 2.2.6* is illustrated in Figures 7.3.7 to 7.3.9.

FLACS 2.2.5
The effect of activating water spray at different locations shows the same tendencies in both the simulations and experiments. The water spray has a better and better effect the further away from the ignition it is activated. Some deviations are seen between the results from the experiments and the simulations, especially in the situations where the water spray is activated in one region in each end of the module and droplet transport will play a significant role. If the water spray is extended outside the defined area, in the flow direction, the results is more or less coherent with the experiments. This deviation can again be related to the fact that the droplets aren't transported with the flow in the FLACS 2.2.5 version.

FLACS 2.2.6*
Case 1: With water spray activated far from ignition, at each end of the module, the maximum explosion pressure is somewhat lower than in the experiments, but higher than in the simulation performed with FLACS 2.2.5, and thereby closer to the value obtained by the experiments. With water spray activated far from ignition the obtained pressure is a bit lower than in the simulations, and much lower than the results from simulations with FLACS 2.2.5. This lower value can be due to the transport of droplets with the flow.
Case 2: The explosion pressure results from the simulations are somewhat over predicated, especially when the water spray is located near the openings. This can be because the flow will not propagate trough the module and past the obstructions creating a turbulent flow. As a result of this the velocity will not reach the criteria for droplet break-up, and extraction of energy due to evaporation will not take place.
Case 3: The explosion pressure is much higher compared to the pressure obtained in the experiments. FLACS 2.2.5 gives a better representation of the scenario.

Case 1: Propane, centre ignition and open ends.

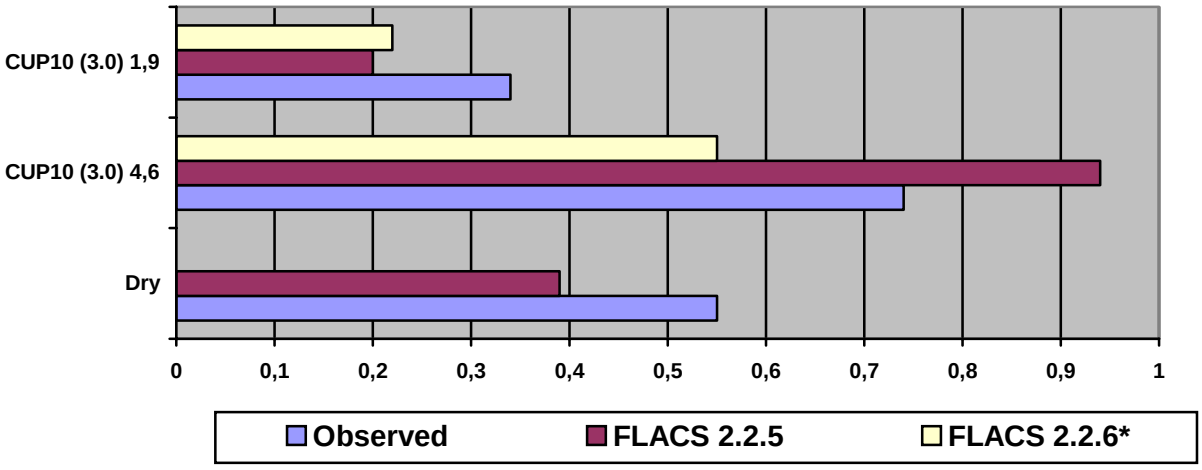

Figure 7.3.7: Experiments with propane in M24-25 module versus simulations by FLACS 2.2.5 and FLACS 2.2.6 with CUP10 nozzles.*

Case 2: Methane, end ignition, louvered wall at ignition and open opposite ignition.

FLACS 2.2.6* seems to over predicate the explosion results. The water spray is activated at the opening and will thereby not propagate throughout the module. The required flow velocity for droplet break-up may then not be fulfilled, and the extraction of energy due to evaporation will not occur.

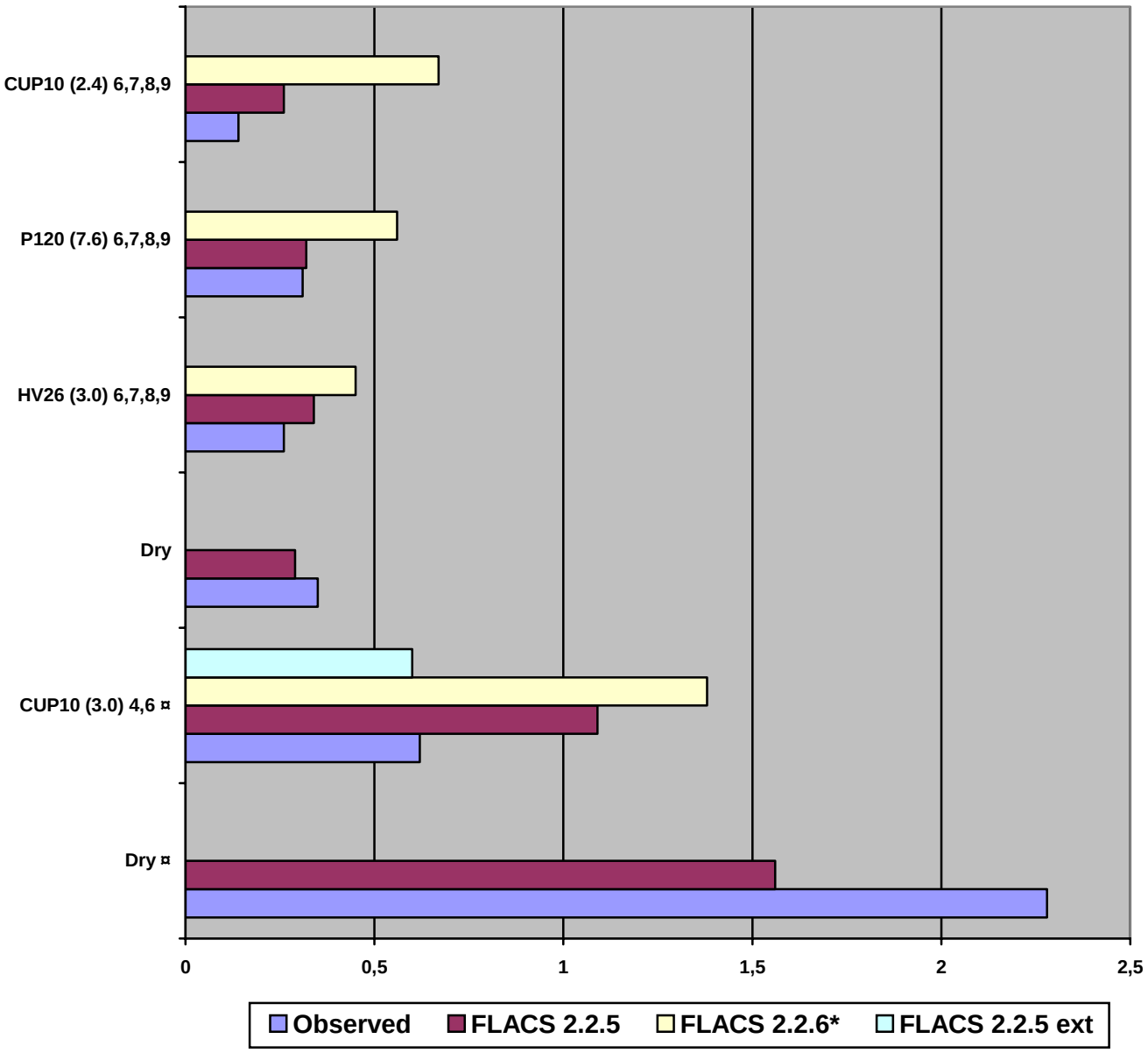

Figure 7.3.8: Experiments with methane in M24-25 module versus simulations by FLACS 2.2.5 and FLACS 2.2.6 with HV26, CUP10 and P120 nozzles.*

¤ *Case 3: closed wall at ignition*

7.4 Kårstø

This chapter contains a discussion of the effect of water spray on gas explosions and gas dispersion at two different areas at the Kårstø plant.

7.4.1 The effect of water spray on gas explosions

The water spray was activated at three different locations to see in which case the water spray would have an optimal positive effect, and thereby find the most favourable placing. In addition three different nozzles were tested to see which of them would give the best mitigating effect.

A) The Statpipe/Sleipner area

Nine different simulations with water spray are performed. The three different locations of water spray are shown in appendix 13. The maximum explosion pressure and time of arrival for the different simulations are displayed in Figure 7.4.1

CUP10-nozzle:
The first three simulations containing water spray were performed with a CUP10 nozzle. In the first simulation the water spray was located at the ignition, which gave no influence on the maximum explosion pressure, but an earlier time of arrival. This behaviour was expected based on the simulations performed earlier with different geometries. The pressure peak comes earlier due to the enhanced initial turbulence created by the water spray. This is not a good placing of the water spray. The next simulation was performed with the water spray placed at the northwest corner of the gas cloud, away from the ignition point. This reduced the maximum explosion pressure by 58%. The pressure peak in simulations 0 and 1 were located at monitor point 1, but in simulation 2 the pressure at this point is reduced by 95 % compared to the dry scenario. The reason for this is that the water spray blocks the explosion, which results in an almost insignificant pressure in monitor 1. The maximum pressure in simulation 2 is located at monitor point 11, which is reduced by 17 % compared to the dry simulation. In simulation 3, with water spray activated over a large area, the maximum explosion pressure was reduced by 90 % compared to the dry simulation, and thereby gives the best mitigating result. The pressure in monitor 1 and 11 is reduced to a minimum due to the water spray blockading the propagation of the explosion. A maximum pressure of 0.15 bar now occurs in monitor 2. A pressure-time plot showing the pressure in monitor 1, 2 and 11 for the different simulation is shown at the top of page 147 in appendix 14.

MV57-nozzle:
The activation of MV57-nozzles at ignition gives no change in the maximum explosion pressure compared to the dry simulation, but the time of arrival is slightly earlier than both the dry simulation and the simulation with CUP10-nozzles at the same location. The reason why the MV57-nozzle gives a slightly earlier pressure peak than the CUP10 nozzle is probably because the water exits at a higher velocity in the MV57-nozzle creating more initial turbulence, and thereby an earlier pressure peak. With water spray activated far from the ignition the explosion pressure is reduced by 60%, which is a slightly larger reduction than with the CUP10 nozzle, but the time of arrival is the same as with the CUP10 nozzle. When the water spray is activated all over the gas cloud area the explosion pressure is reduced to a value of 0.11 bar, which is a better reduction than the CUP10 nozzle. The time of arrival for

the MV57 and CUP10 nozzle is the same, and has increased somewhat compared to the scenario with water spray located far from the ignition. A pressure-time plot showing the pressure in monitor 1, 2 and 11 for the different simulation is shown at the bottom of page 147 in appendix 14.

LDN-nozzle:
The maximum explosion pressure is not affected when the water spray is activated near the ignition, as we also saw with MV57- and CUP10-nozzles at the same location. The time of arrival is somewhat earlier compared to the other two nozzles, which can be explained by the larger flow rate using the LDN-nozzle that will probably create more initial turbulence. With water spray located far from ignition the LDN nozzle gives a larger reduction than the other nozzles, and thereby the best mitigating effect. The time of arrival is almost unaffected compared to the dry test, which was not the case with the other two nozzles. When the water spray is located all over the gas cloud area the pressure is reduced to 0.07 bar, which is a almost insignificant value. The time of arrival actually comes later than in the dry test, which shows that the initial turbulence doesn't have any effect like in the case of water spray only at the ignition. A pressure-time plot showing the pressure in monitor 1, 2 and 11 for the different simulation is shown at the top of page 148 in appendix 14.

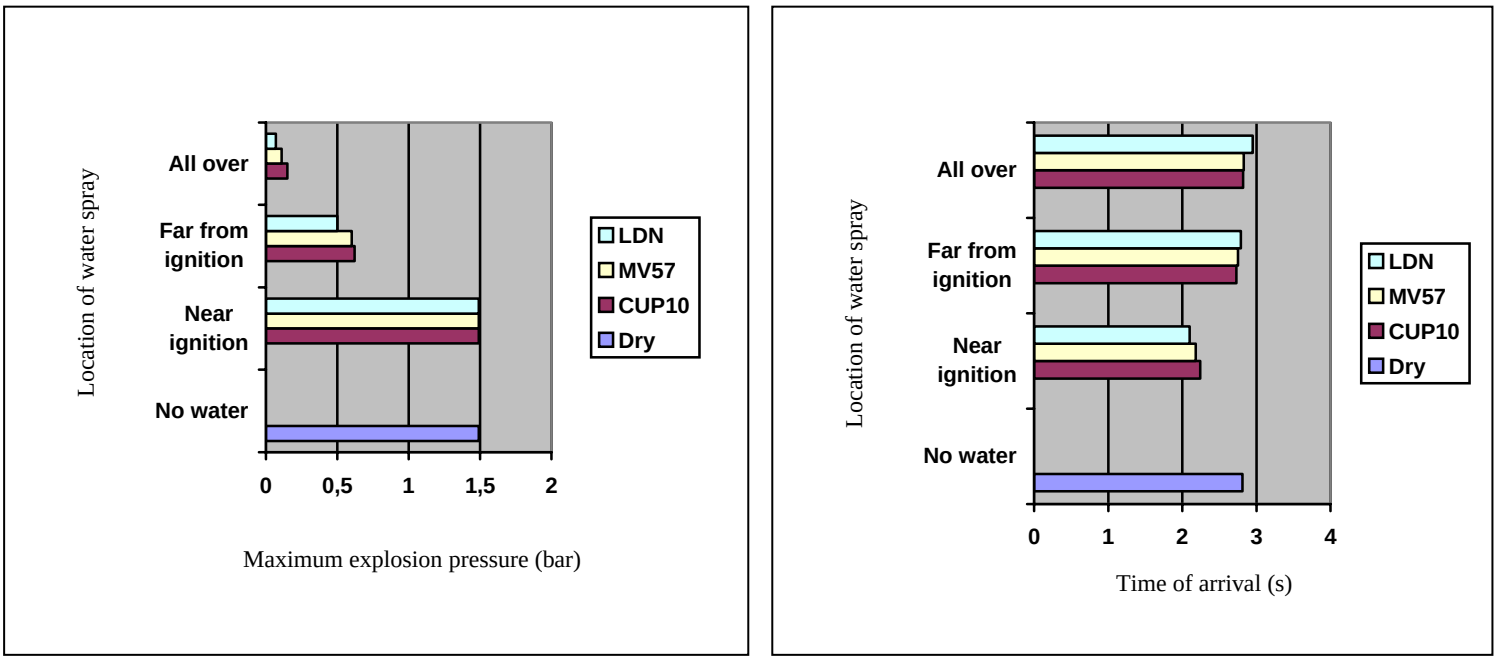

Figure 7.4.1: Maximum explosion pressure and time of arrival for the different location of water spray at the Statpipe/Sleipner area.

B) The Åsgard area

Nine different simulations with water spray are performed. The three different locations of water spray are shown in appendix 16. The maximum explosion pressure and time of arrival for the different simulations are displayed in Figure 7.4.2.

CUP10-nozzle:
With water spray activated at ignition (simulation 11), the maximum explosion pressure was increased by 0.14 bar and the time of arrival for the pressure peak was almost 5 seconds earlier. The initial turbulence from the water spray caused an enhanced burning rate, which resulted in an increase in the explosion pressure and an earlier pressure peak. This is not a good placing of the water spray. When the water spray is located far from the ignition (simulation 12), the explosion pressure is reduced by almost 40% and the time of arrival is not affected compared to the dry test. The pressure peak in simulations 10 (dry) and 11 were located at monitor point 23. In simulation 12, the pressure at this point is reduced by 65 % compared to the dry scenario. The reason for this is that the water spray blocks the explosion, which results in a much lower pressure in monitor 23. The maximum pressure in simulation 12 is located at monitor point 7. The pressure is reduced by 80 % when the water spray is located all over the gas cloud area (simulation 13), but is must be noted that the time of arrival is almost 10 seconds earlier compared to the dry test. The maximum pressure now appears in monitor 11, which is reduced by 46 % compared to the dry test. A pressure-time plot showing the pressure in monitor 7, 11 and 23 for the different simulation is shown at the top of page 151 in appendix 17.

MV57-nozzle:
The explosion pressure is increased by 0.27 bar with water spray located near ignition, and the time of arrival comes 8 second earlier. This location will enhance the explosion and create a larger maximum explosion pressure, due to the increased initial turbulence caused by the water spray. With water spray located far from ignition the same results as with the CUP10-nozzle is archived, both explosion pressure and time of arrival. When water spray is activated all over the gas cloud area the pressure is reduced by 83.5 % to 0.17 bar, which is a slightly larger reduction than the CUP10-nozzle, but the time of arrival is over 10 second earlier. A pressure-time plot showing the pressure in monitor 7, 11 and 23 for the different simulation is shown at the bottom of page 151 in appendix 17.

LDN-nozzle:
This nozzle increases the explosion pressure with almost 0.60 bar, and gives a pressure peak 10 seconds earlier. This is definitely not a good placing of the water spray. With water spray far from ignition the results are the same as with the CUP10- and MV57-nozzle. The explosion pressure is reduced by 40 % and the water spray does not affect the time of arrival. When the water spray is located all over the gas cloud area the explosion pressure is reduced by 89 % to almost insignificantly 0.11 bar, and thereby gives the best mitigating effect compared to the other two nozzles. The time of arrival comes over 10 seconds earlier. A pressure-time plot showing the pressure in monitor 7, 11 and 23 for the different simulation is shown at the top of page 152 in appendix 17.

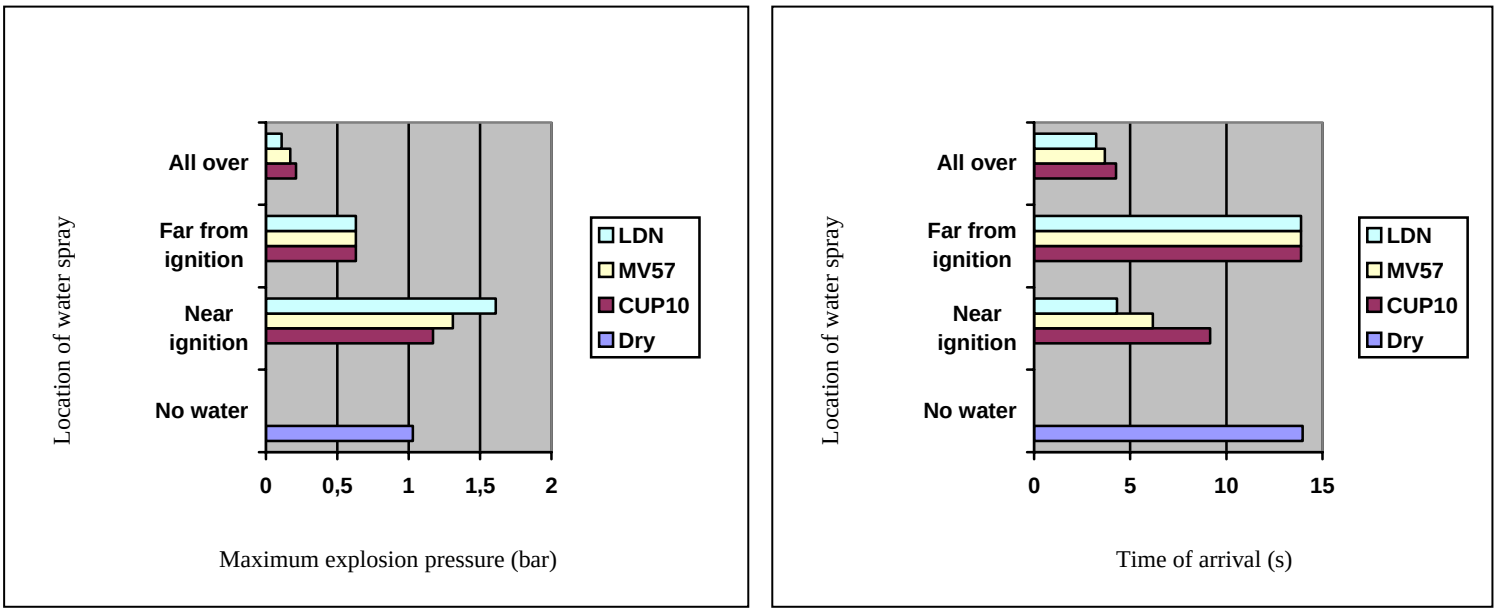

Figure 7.4.2: Maximum explosion pressure and time of arrival for the different location of water spray at Åsgard area.

7.4.2 The effect of water spray on gas dispersion

The formation of a large flammable gas cloud and the spreading of gas to other areas would result in a stronger explosion and more serious consequences. Simulations were performed to investigate the effect of water spray on gas dispersion at the Kårstø facility. A scalar-time plot and 2D plot of the fuel fraction was displayed in chapter 6.3.1. This show that the water spray on one side will have a negative effect on the gas dispersion, because the activation of water spray will cause turbulence and then increased mixing of gas and air. The water spray will have a positive effect by limiting the spreading of the gas to other areas.

8. Conclusions

The following conclusions are determined based on the discussion of the results:

- Water spray will have the best mitigating effect in the case of sufficient ventilation openings and obstructions.

- In the case of high confinement, i.e. a small ventilation opening, the water spray had generally no mitigating effect and could in some cases give a higher and earlier pressure peak due to the turbulence created by the water droplets.

- The water droplets from the water spray nozzle have to be broken up in order to extract energy, and this requires high gas acceleration in front of the flame. In the case of a small ventilation area the flow is restricted and will not reach a sufficient velocity to cause droplet break-up.

- When the number of obstructions is increased in a geometry with high confinement, the increase in explosion pressure due to water spray decreases. The explanation for this reduction can be that the flow created turbulence caused by the obstacles increases, and therefore becomes more and more dominating over the water spray induced turbulence.

- The water spray has a clearly negative influence on the explosion when it is activated near the ignition point. This effect is coherent with the fact that the water spray will create turbulence at the ignition when activated, and will give a large increase of the initial turbulence in the explosion, hence leading to enhanced burning and higher pressures.

- The turbulence from the water spray will not be dominant and the water spray will have a positive effect on the explosion pressures when it is activated at the accelerating phase of the explosion, i.e. near ventilation openings.

- Ventilation in the early stages of an explosion has a good effect in reducing the maximum explosion pressure.

- When comparing the different nozzles used in the simulations with the M24-25 module, the high velocity nozzle (HV26), fog nozzle (P120) and the sprinkler nozzle (CUP5) creates a large initial turbulence when activated near the ignition in comparison to the CUP10 nozzle.

- When the nozzles are activated in regions close to the opening the CUP-nozzles seem to have the best mitigating effect.

- When comparing the different nozzles used in the simulations with the full-scale module the LDN nozzle has a better mitigating effect than the MV57 nozzle, which is expected because the LDN nozzle has a flow rate over two times higher than he MV57 nozzle.

- If we compare the explosion pressures from two dry tests with centre- and end ignition, we see that the pressure is higher in the case of end ignition. This is expected, as the flame will propagate through a longer distance creating more turbulence and a higher explosion pressure.

- The water spray has a larger mitigating effect in the case of end ignition, and the pressure peaks comes later compared to centre ignition. The larger propagating distance allowing the flow created turbulence to become more dominant over the water spray induced turbulence, and the more effective droplet break-up due to the strong gas flow can explain this.

- FLACS 2.2.5 does in most cases give simulation results coherent with a real situation. In scenarios where the water spray normally would be transported with the flow FLACS 2.2.5 has a tendency to under predicate the explosion results.

- When water spray is activated at the ignition in the explosion simulations with the Kårstø geometry, the pressure peak comes earlier and the pressure is in most cases increased due to the initial turbulence caused by the water droplets.

- When the water spray is activated far from ignition or over a large area at the Kårstø geometry, the water spray has a significant mitigating effect.

- In the simulations with the Kårstø geometry the LDN-nozzle has a better mitigating effect compared to the CUP10- and MV57-nozzle.

- The formation of a large flammable gas cloud and the spreading of gas to other areas would result in a stronger explosion and more serious consequences. Simulations were performed to investigate the effect of water spray on gas dispersion at the Kårstø facility. The water spray will have a negative effect on the gas dispersion because the activation of water spray will cause turbulence and then increased mixing of gas and air. The water spray will have a positive effect by limiting the spreading of the gas to other areas.

- FLACS 2.2.6*, explosion box without the setup-file gives a good representation of the explosion pressure, but does in most cases over predicate the time of arrival. The tendencies are although the same as in the experiments. FLACS 2.2.6* with the setup-file over predicates both the explosion pressure and the time of arrival. The deviations are probably because the flow doesn’t reach high enough values to fulfil the critical droplet velocity, and the evaporation and extraction of energy is thereby not effective.

- FLACS 2.2.6*, M24-25 module. With this geometry the simulation results are more coherent with the experiments. This is because the flow will propagate over a larger distance, and thereby the droplet break-up criteria will be fulfilled and energy can be extracted by evaporation.

- A general source to deviation between results with FLACS 2.2.6* and experiments is that the water spray is also exiting the nozzle as a narrow jet instead of a broad cone, as it would do in real life, and the lack of initial water spray turbulence gives a over predication in the time of arrival.

- Further work is recommended to create a better modelling for the release of water spray, in order for it to exit as a broad cone instead of a narrow jet, and a modelling of initial turbulence from the water spray.

- It is also recommended that the input of water spray will be made less time demanding than creating a cl-file for each nozzle.

9. References

1. Joar Dalheim, Kjersti Ottestad, Nils Fredriksen and Thor Foyn, *"STATOIL-KÅRSTØ: DETAILED PROBABILISTIC EXPLOSION ANALYSIS"*, 2003-11-12.

2. Dag Bjerketvedt, Jan Roar Bakke, Kees van Wingerden, *"Gas Explosion Handbook"*, September 1993.

3. Bjørn Arntzen, Sanjay K. Khattri, Hans-Fredrik Nordhaug, Hans-Christen Salvesen, Idar E. Storvik, *"Oil mist modeling"*, GexCon 2003.

4. Brian Wilkins, Anders Wiik, Olav Roald Hansen, *"Experimental Investigation of the influence of Waterspray on Gas Dispersion, Phase 2 of LICOREFLA project"*, Technical report, GexCon, 2003.

5. Hans-Christen Salvesen, *"Simulation of water spray and gas dispersion using CFD code FLACS"*, July 2003.

6. C.A Catlin, D.M Johnson and G.A. Shale, *"An experimental study of the influence of water sprays on gas cloud explosions"*, June 1992.

7. Kees Van Wingerden, G.H Pedersen, B.A. Wilkins and J. Bakken, *"Experimental Investigation of the Effect of Water Deluge on Turbulent Gas Explosions in a 1:5 Offshore Module"*, December 1994.

8. Olav Roald Hansen, *"Improvement of the water spray model in FLACS"*, March 1997.

9. Den europeiske forsikringskomitè, *"Sprinklersystemer, planlegging og installasjon"*, 1995-09 (NO).

10. Bjørn Arntzen, "Modelling of turbulence and combustion for simulation of gas explosions in complex geometries, " Dr.ing. thesis, NTNU, Trondheim, 1998.

11. B.A. Wilkins and Kees Van Wingerden, *"The influence of Waterspray on Quasi-Laminar Combustion"*, CMR 1994.

10. Appendix

Appendix 1: Side view of obstacle configurations in explosion box

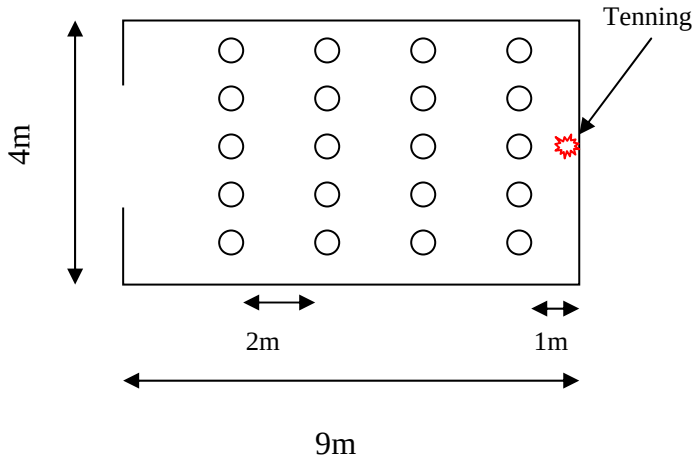

Pipe number	X	Y	Z
1-2	2 and 6	0	0.7
3-4	2 and 6	0	1.58
5-6	2 and 6	0	2.46
7-8	2 and 6	0	3.34
9-10	2 and 6	0	4.22
11-12	4 and 8	0	0.1
13-14	4 and 8	0	0.98
15-16	4 and 8	0	1.86
17-18	4 and 8	0	2.74
19-20	4 and 8	0	3.62

Box with 20 pipes

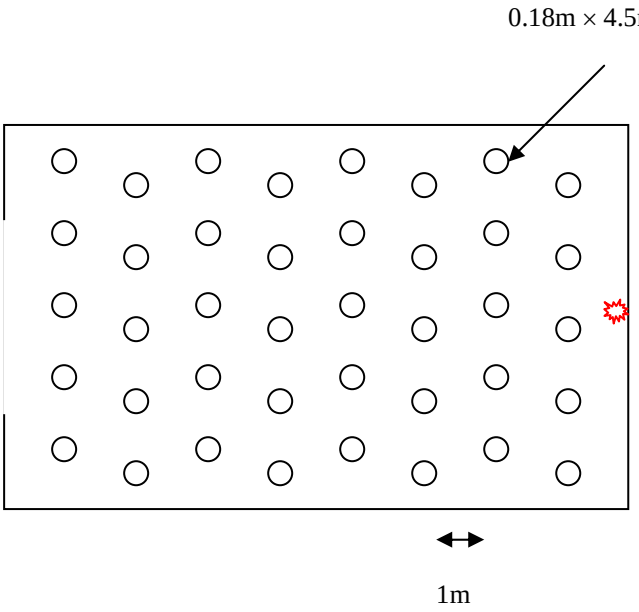

Pipe number	X	Y	Z
1-5	1	0	0.3 1.28 2.26 3.24 4.22
6-10	2	0	0.1 1.08 2.06 3.04 4.02
11-15	3	0	0.3 1.28 2.26 3.24 4.22
16-20	4	0	0.1 1.08 2.06 3.04 4.02
21-25	5	0	0.3 1.28 2.26 3.24 4.22
26-30	6	0	0.1 1.08 2.06 3.04 4.02
31-35	7	0	0.3 1.28 2.26 3.24 4.22
36-40	8	0	0.1 1.08 2.06 3.04 4.02

Box with 40 pipes

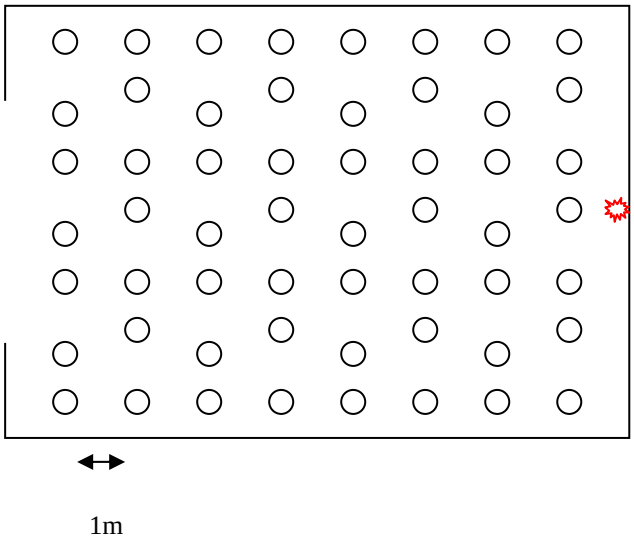

Pipe number	X	Y	Z
1-7	1	0	0.12 0.5 1.48 1.86 2.84 3.22 4.2
8-14	2	0	0.12 1.1 1.48 2.46 2.84 3.82 4.2
15-21	3	0	0.12 0.5 1.48 1.86 2.84 3.22 4.2
22-28	4	0	0.12 1.1 1.48 2.46 2.84 3.82 4.2
29-35	5	0	0.12 0.5 1.48 1.86 2.84 3.22 4.2
36-42	6	0	0.12 1.1 1.48 2.46 2.84 3.82 4.2
43-49	7	0	0.12 0.5 1.48 1.86 2.84 3.22 4.2
50-56	8	0	0.12 1.1 1.48 2.46 2.84 3.82 4.2

Box with 56 pipes

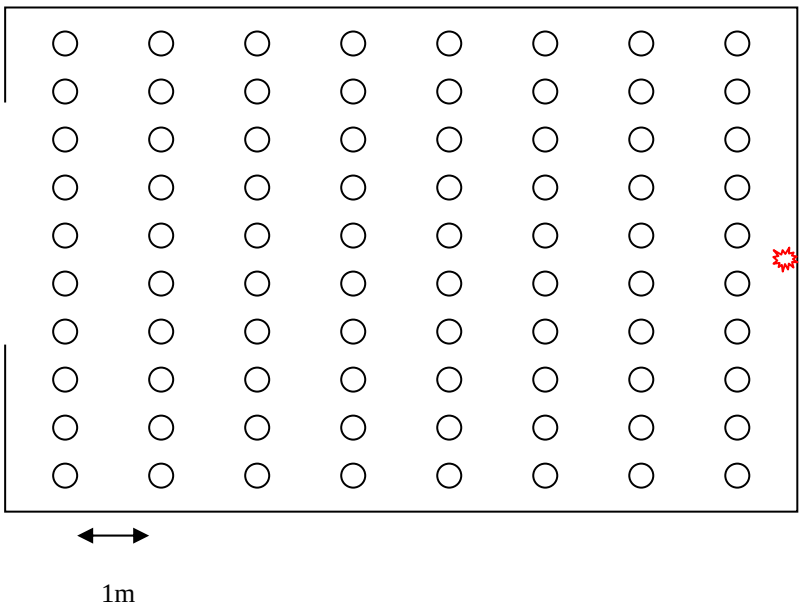

Pipe number	X	Y	Z
1-8	1-8	0	0.045
9-16	1-8	0	0.515
17-24	1-8	0	0.985
25-32	1-8	0	1.455
33-40	1-8	0	1.925
41-48	1-8	0	2.395
49-56	1-8	0	2.865
57-64	1-8	0	3.335
65-72	1-8	0	3.805
73-80	1-8	0	4.275

Box with 80 pipes

Appendix 2: Simulation configurations for explosion box:

Simulation nr	Scenario	Kv-value	Number of pipes	Nozzle type	Water pressure (bar)
1	010000	9	0	-	-
2	010001	9	0	HV60	3.5
3	010006	9	0	HV60	5.0
4	010002	9	0	MV57	3.5
5	010100	9	20	-	-
6	010101	9	20	HV60	3.5
7	010102	9	20	MV57	3.5
8	010007	9	40	-	-
9	010008	9	40	HV60	3.5
10	010009	9	40	MV57	3.5
11	010106	9	80	-	-
12	010107	9	80	HV60	3.5
13	010108	9	80	MV57	3.5
14	010003	1	0	-	-
15	010004	1	0	HV60	3.5
16	010005	1	0	MV57	3.5
17	010103	1	20	-	-
18	010104	1	20	HV60	3.5
19	010105	1	20	MV57	3.5
20	010010	1	56	-	-
21	010011	1	56	HV60	3.5
22	010012	1	56	MV57	3.5
23	010109	1	80	-	-
24	010110	1	80	HV60	3.5
25	010111	1	80	MV57	3.5

Appendix 3: Scenario definition for explosion box:

Scenario definition
The scenario has following subdirectories:

- MONITOR POINTS: The location in x-, y- and z-direction of monitors to record different wanted parameters. In this case 9 monitors are located as following:

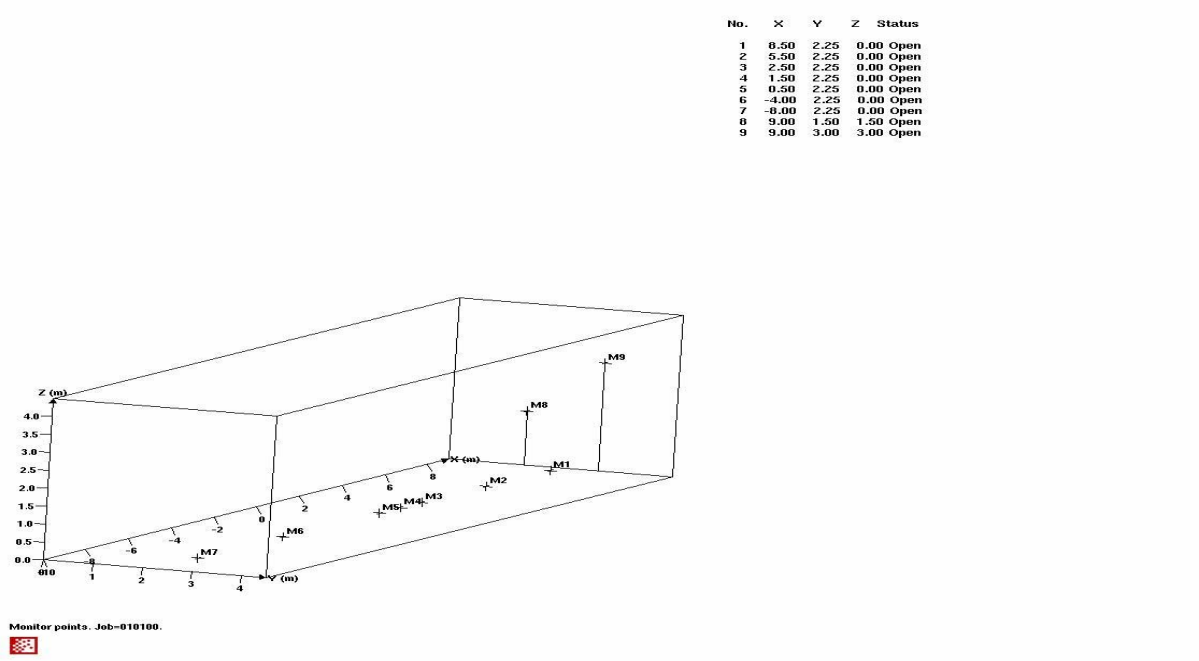

Figure 3.1: Location of monitor points.

- SINGLE FIELD SCALAR TIME OUTPUT: Chose the parameter(s) you want to measure, in this case pressure (P).

- SINGLE FIELD 3D OUTPUT: Chose the parameter(s) you want to display in the 3D output, in this case pressure (P).

- SIMULATION AND OUTPUT CONTROL:
  Tmax: The maximum time interval FLACS will simulate.
  Tmax = 999999
  Last: The maximum number of time steps allowed for the simulation.
  Last = 999999
  CFLC: Courant-Friedrich-Levy number based on sound velocity.
  CFLC = 5.0
  CFLV: Courant-Friedrich-Levy number based on fluid flow velocity.
  CFLV = 0.5
  Scale: A factor used if scaling of the dimensions is wanted, no scaling = 1.
  Scale= 1
  Modd: Determines the amount of data stored for scalar-time plots.

Modd = 1
NPLOT: Determines the amount of data stored for field plots.
NPLOT = 5
DTPLOT: This is the time interval for field output.
DTPLOT = 999999
Grid = ”Cartesian”
Wallf: Control switch specifying wall-functions
Wallf: = 1
Heat switch (not used) = 0

- BOUNDARY CONDITIONS: “Euler”.

- INITIAL CONDITIONS:
  Up direction: A vector determining the direction to be taken as upwards.
  Up direction: 0 0 1
  Gravity = 9.8m/s^2
  Temperature (initial) = 20°C
  Characteristic velocity: Changes the reference velocity of the initial turbulence field.
  Characteristic velocity = 0
  Relative turbulence intensity: Changes the relative turbulence intensity of the initial turbulence field.
  Relative turbulence intensity = 0
  Turbulent length scale: Changes the value of the length scale of the initial turbulence.
  Turbulent length scale = 0

- GAS COMPOSITION AND VOLUME:
  Position of fuel region: The location of the minimum point of the box
  Position of fuel region = 0 0 0
  Dimension of fuel region: The dimensions of the box
  Dimension of fuel region = 9m 4.5m 4.5m
  Volume fraction: The volume fraction of the different gas components.
  Volume fraction: Methane = 95 Ethane = 5
  Equivalence ratios: Concentrations of gas inside (ER0) and outside (ER9) the gas cloud.
  Equivalence ratios (stoichiometric): ER0 = 1,0 ER9 = 0,0

- IGNITION:
  Position of ignition region = 9m 2.25m 2.25m
  Dimension of ignition region = 0 0 0
  Time of ignition = 0
  Radmax = 0

Appendix 4: Max overpressure data from explosion box

Monitor number									
Simulation number	**1**	**2**	**3**	**4**	**5**	**6**	**7**	**8**	**9**
1	0.47	0.47	0.47	0.47	0.47	-	-	0.47	0.47
2	1.85	1.84	1.83	1.82	1.82	-	-	1.85	1.85
3	2.03	2.02	1.99	1.98	1.98	-	-	2.03	2.03
4	1.91	1.90	1.88	1.88	1.88	-	-	1.91	1.91
5	2.26	2.25	2.24	2.23	2.23	-0.01	-0.01	2.26	2.26
6	3.30	3.29	3.27	3.26	3.26	-	-	3.30	3.31
7	3.18	3.16	3.17	3.18	3.20	-	-	3.18	3.17
8	3.44	3.48	3.52	3.54	3.54	-0.01	-0.01	3.44	3.44
9	4.38	4.31	4.24	4.21	4.19	-0.01	-	4.38	4.38
10	4.01	3.98	3.93	3.93	3.94	-0.01	-	4.02	4.03
11	5.49	4.95	4.01	3.79	3.74	-	-	5.47	5.43
12	4.62	4.43	4.12	4.04	4.01	-0.05	-	4.63	4.65
13	4.23	4.11	4.01	3.98	3.96	-	-	4.23	4.24
14	-	-	-	-	-	-	-	-	-
15	0.08	0.08	0.06	0.04	0.02	-	-	0.08	0.08
16	0.08	0.07	0.05	0.04	0.02	-	-	0.08	0.08
17	0.35	0.31	0.18	0.11	0.06	0.02	-	0.35	0.35
18	0.40	0.38	0.32	0.26	0.17	-	-	0.40	0.40
19	0.25	0.23	0.17	0.11	0.06	-	-	0.25	0.25
20	1.42	1.20	0.60	0.40	-0.10	0.03	-	1.40	1.40
21	0.98	0.91	0.82	0.71	0.22	0.02	-	0.97	0.96
22	0.52	0.49	0.37	0.30	-	-	-	0.52	0.51
23	2.30	1.84	1.00	0.61	-0.05	0.07	-	2.31	2.31
24	1.39	1.26	1.04	0.81	0.20	0.06	-	1.39	1.39
25	0.73	0.72	0.61	0.44	0.03	-	-	0.72	0.72

- = Over pressure lower than 0,01

Appendix 5: Simulation plots from explosion box

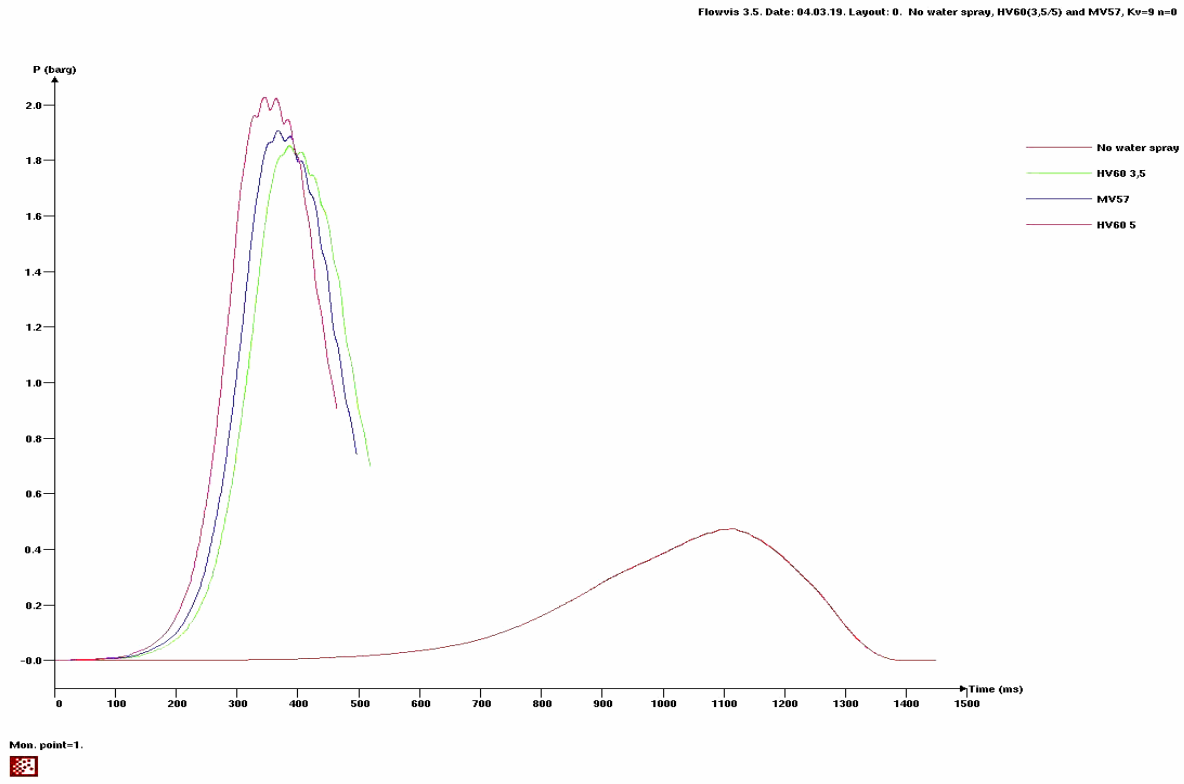

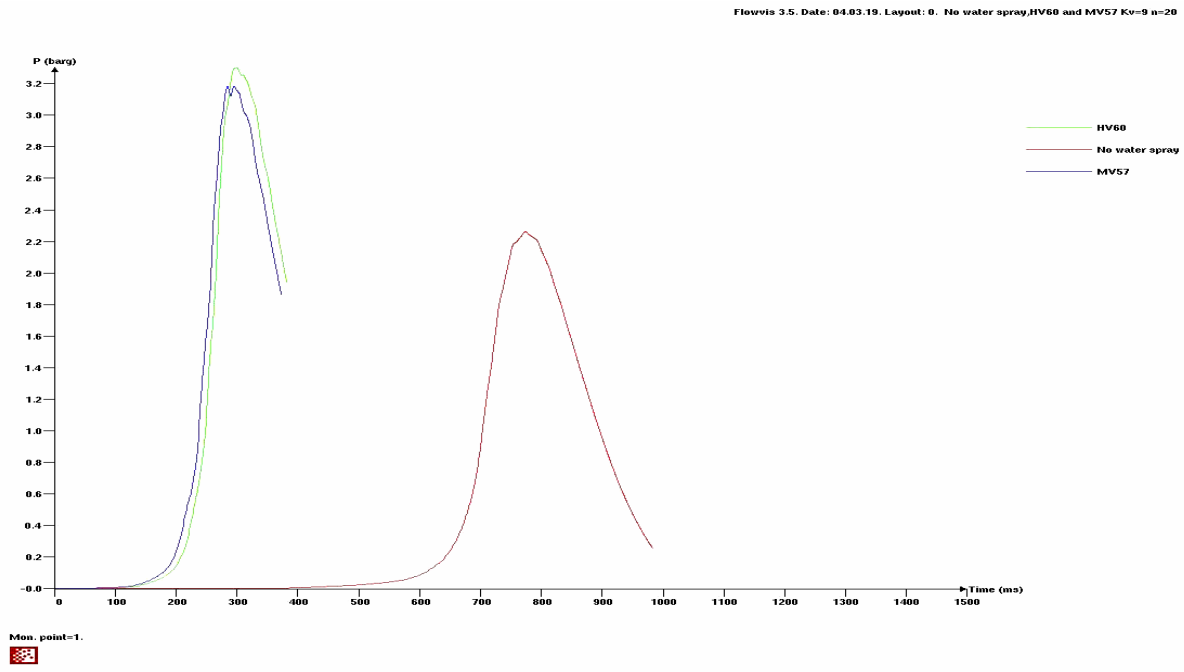

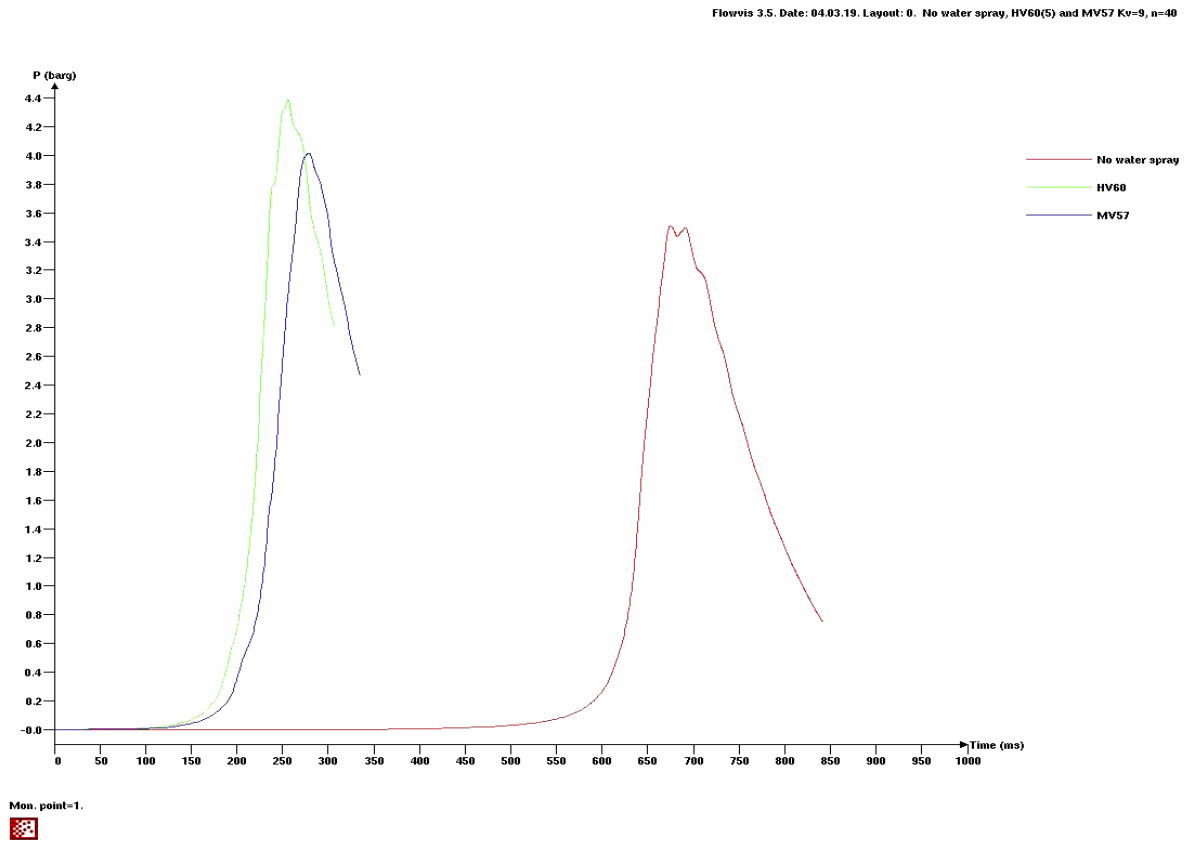
Flowvis 3.5. Date: 04.03.19. Layout: 0. No water spray, HV60(5) and MV57 Kv=9, n=40
P (barg)
4.4
4.2
4.0
3.8
3.6
3.4
3.2
3.0
2.8
2.6
2.4
2.2
2.0
1.8
1.6
1.4
1.2
1.0
0.8
0.6
0.4
0.2
-0.0
0
50
100
150
200
250
300
350
400
450
500
550
600
650
700
750
800
850
900
950
1000
Time (ms)
No water spray
HV60
MV57
Mon. point=1.

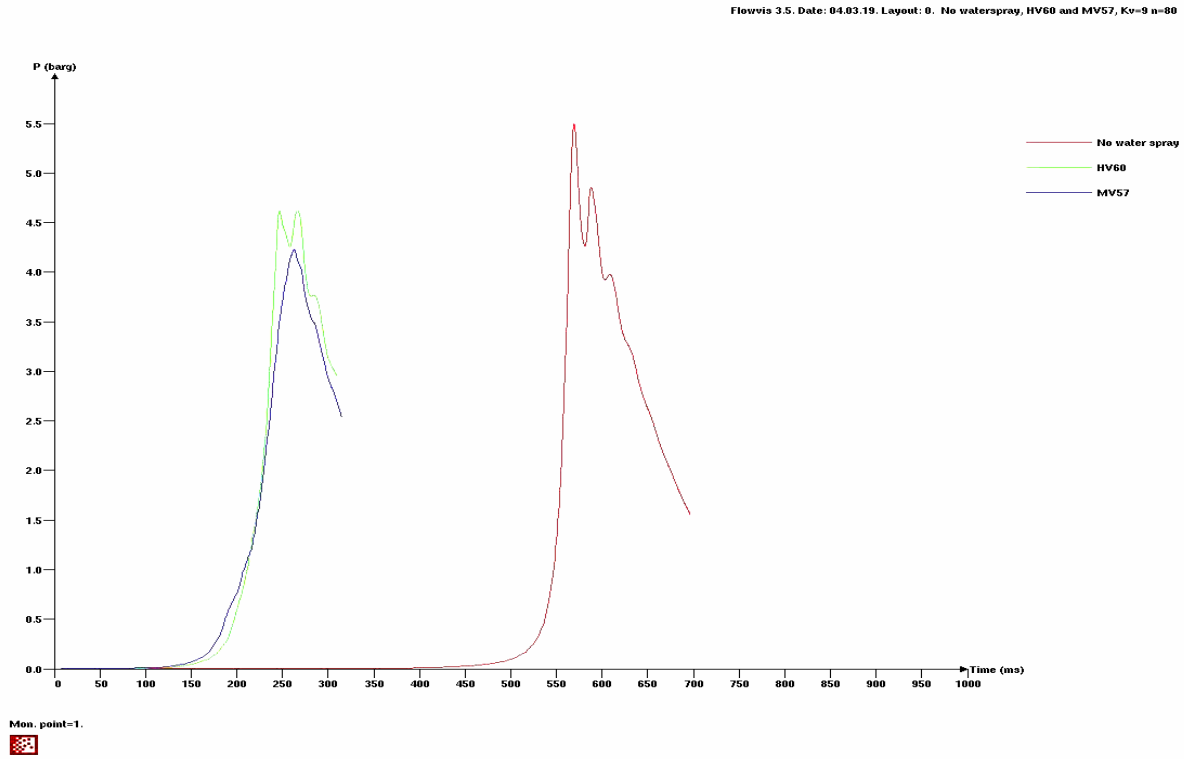
Flowvis 3.5. Date: 04.03.19. Layout: 0. No waterspray, HV60 and MV57, Kv=9 n=80
P (barg)
5.5
5.0
4.5
4.0
3.5
3.0
2.5
2.0
1.5
1.0
0.5
0.0
0
50
100
150
200
250
300
350
400
450
500
550
600
650
700
750
800
850
900
950
1000
Time (ms)
No water spray
HV60
MV57
Mon. point=1.

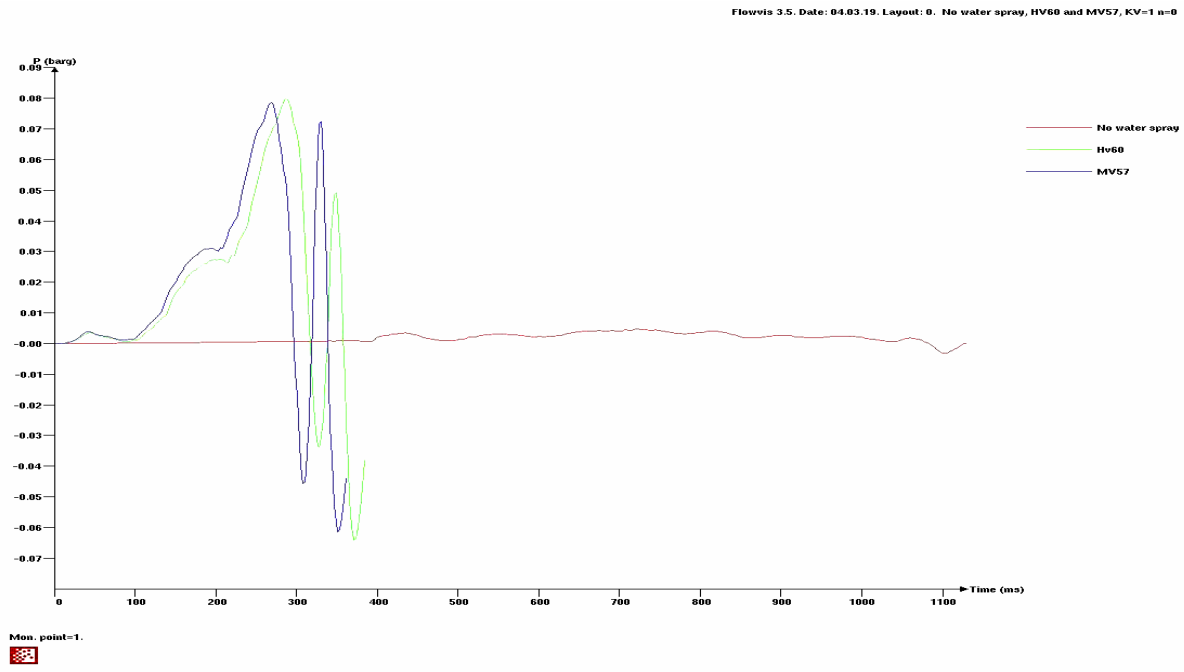
Flowvis 3.5. Date: 04.03.19. Layout: 0. No water spray, HV60 and MV57, KV=1 n=0
P (barg)
0.09
0.08
0.07
0.06
0.05
0.04
0.03
0.02
0.01
-0.00
-0.01
-0.02
-0.03
-0.04
-0.05
-0.06
-0.07
0
100
200
300
400
500
600
700
800
900
1000
1100
Time (ms)
No water spray
Hv60
MV57
Mon. point=1.

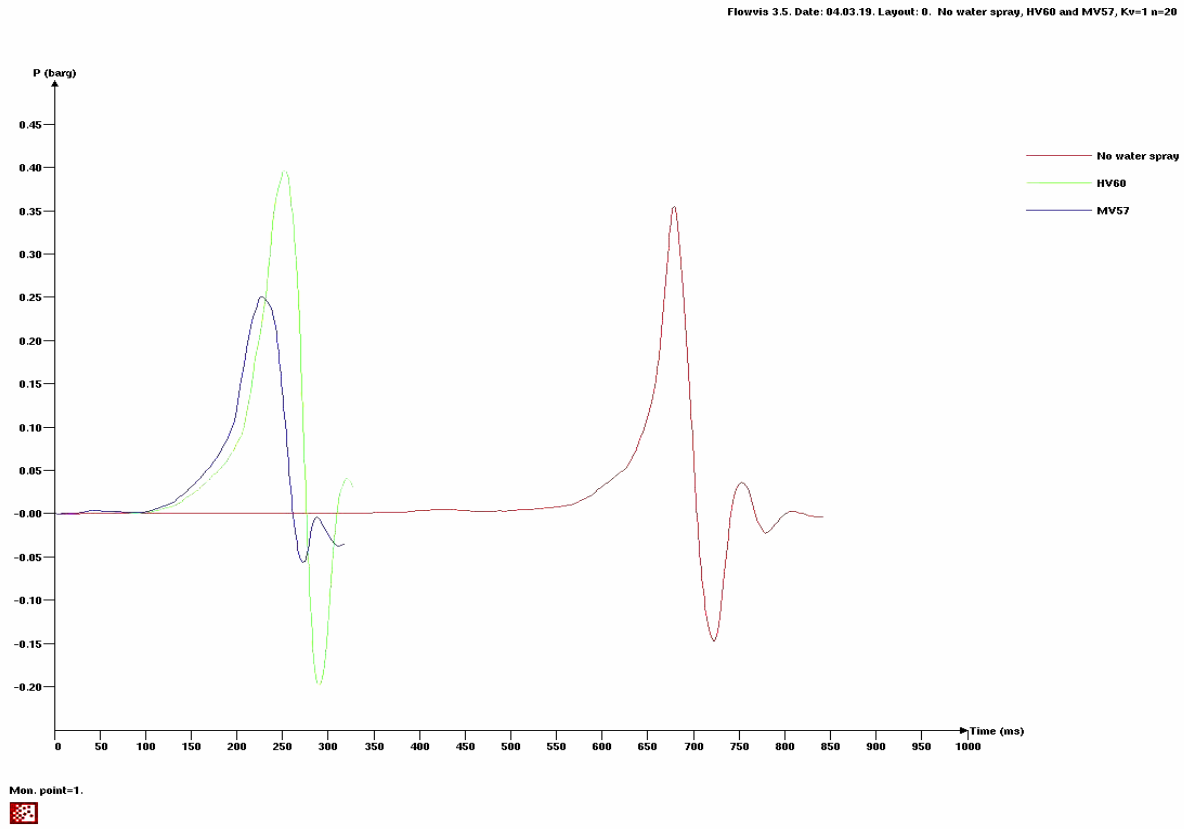
Flowvis 3.5. Date: 04.03.19. Layout: 0. No water spray, HV60 and MV57, Kv=1 n=20
P (barg)
0.45
0.40
0.35
0.30
0.25
0.20
0.15
0.10
0.05
-0.00
-0.05
-0.10
-0.15
-0.20
0
50
100
150
200
250
300
350
400
450
500
550
600
650
700
750
800
850
900
950
1000
Time (ms)
No water spray
HV60
MV57
Mon. point=1.

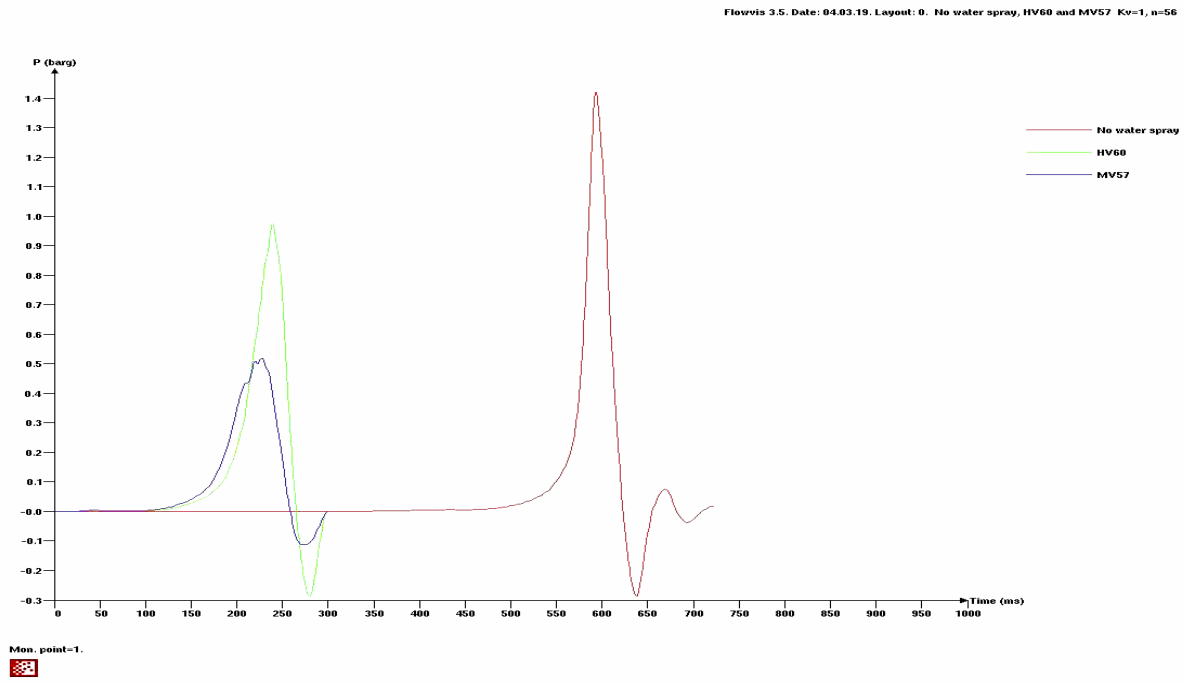
Flowvis 3.5. Date: 04.03.19. Layout: 0. No water spray, HV60 and MV57 Kv=1, n=56
P (barg)
1.4
1.3
1.2
1.1
1.0
0.9
0.8
0.7
0.6
0.5
0.4
0.3
0.2
0.1
-0.0
-0.1
-0.2
-0.3
0
50
100
150
200
250
300
350
400
450
500
550
600
650
700
750
800
850
900
950
1000
Time (ms)
No water spray
HV60
MV57
Mon. point=1.

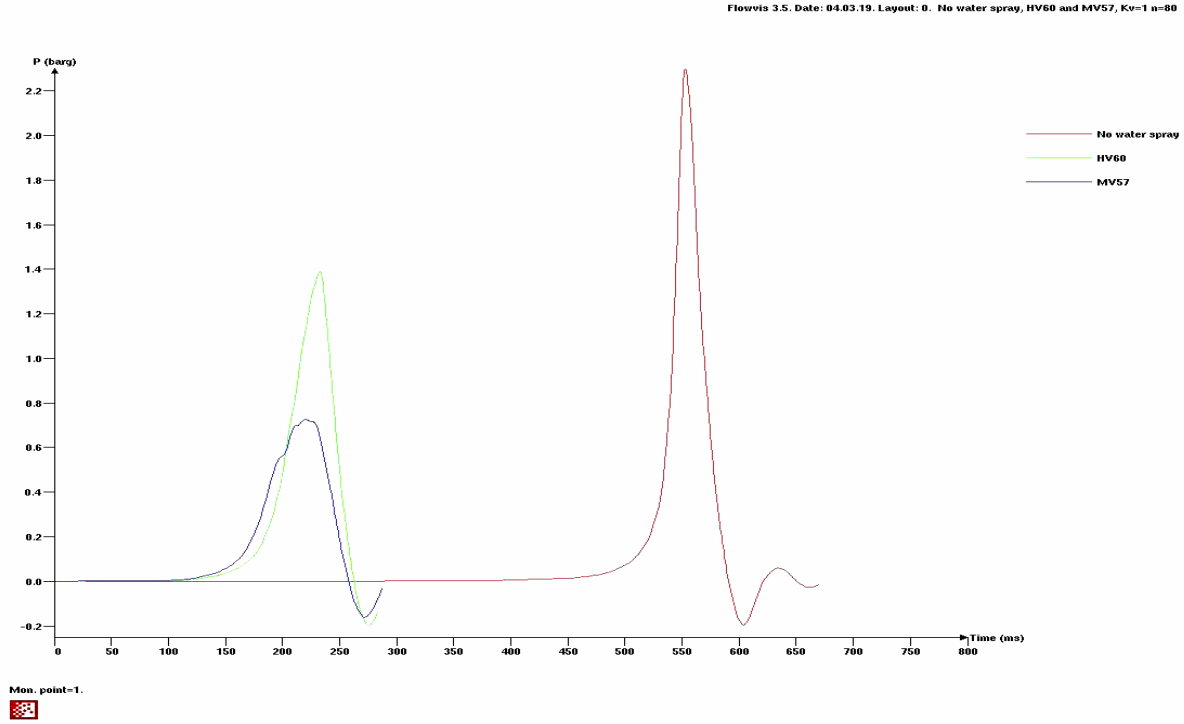
Flowvis 3.5. Date: 04.03.19. Layout: 0. No water spray, HV60 and MV57, Kv=1 n=80
P (barg)
2.2
2.0
1.8
1.6
1.4
1.2
1.0
0.8
0.6
0.4
0.2
0.0
-0.2
0
50
100
150
200
250
300
350
400
450
500
550
600
650
700
750
800
Time (ms)
No water spray
HV60
MV57
Mon. point=1.

Appendix 6: Obstacle configurations in M24-25 module

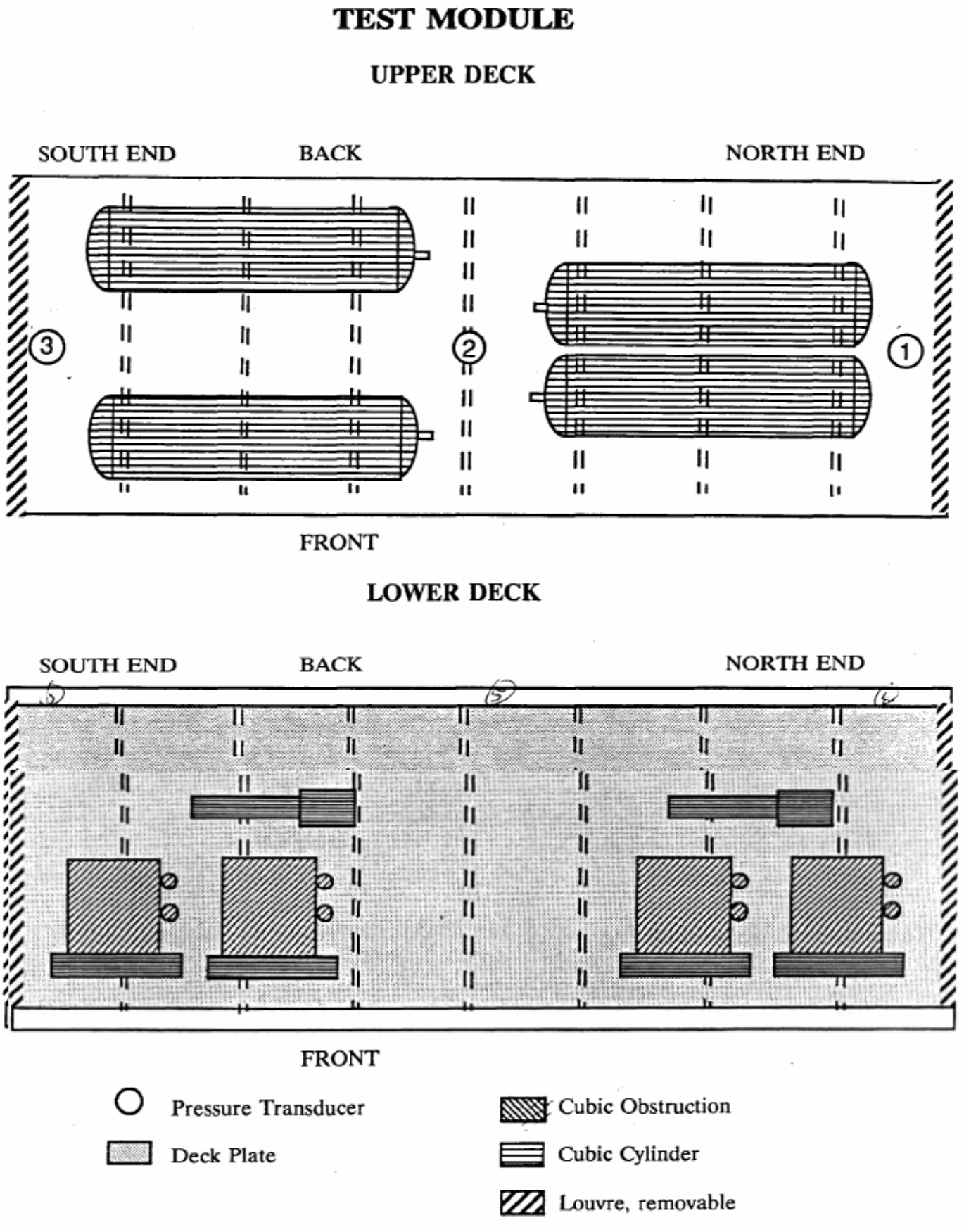

Appendix 7: Simulation configurations for M24-25 module

Simulation nr	Scenario	Type of gas	Location of ignition	Type of end wall		Nozzle type	Nozzle region	Water pressure [bar]
				At ignition	Opposite ignition			
1	300001	Propane	Centre	Open	Open	-	-	-
2	300002	Propane	Centre	Open	Open	HV26	4,6	3.5
3	300003	Propane	Centre	Open	Open	CUP10	4,6	3.0
4	300004	Propane	Centre	Open	Open	CUP10	3,7	3.0
5	300005	Propane	Centre	Open	Open	CUP10	3,4,6,7	3.0
6	300006	Propane	Centre	Open	Open	CUP10	2,8	3.0
7	300007	Propane	Centre	Open	Open	CUP10	2,3,7,8	3.0
8	300008	Propane	Centre	Open	Open	CUP10	1,9	3.0
9	300009	Propane	Centre	Open	Open	CUP10	1,4,6,9	3.0
10	300010	Propane	Centre	Open	Open	CUP10	1,2,8,9	3.0
11	300011	Methane	End	Louvered	Open	-	-	-
12	300012	Methane	End	Louvered	Open	HV26	6,7,8,9	3.0
13	300013	Methane	End	Louvered	Open	HV26	3,4,6,7	3.0
14	300014	Methane	End	Louvered	Open	HV26	2,4,6,8	3.0
15	300015	Methane	End	Louvered	Open	HV26	1,2,3,4	3.0
16	300016	Methane	End	Louvered	Open	HV26	6,7	3.5
17	300017	Methane	End	Louvered	Open	HV26	2,3	3.5
18	300018	Methane	End	Louvered	Open	P120	1-4, 6-9	4.0
19	300019	Methane	End	Louvered	Open	P120	6,7	7.6
20	300020	Methane	End	Louvered	Open	P120	6,7,8,9	7.6
21	300021	Methane	End	Louvered	Open	P120	3,4,6,7	7.6
22	300022	Methane	End	Louvered	Open	P120	1,2,3,4	7.6
23	300023	Methane	End	Louvered	Open	CUP5	6,7	7.0
24	300024	Methane	End	Louvered	Open	CUP5	3,4,6,7	3.8
25	300025	Methane	End	Louvered	Open	CUP5	2,4,6,7	3.8
26	300026	Methane	End	Louvered	Open	CUP10	6,7,8,9	2.4
27	300027	Methane	End	Louvered	Open	CUP10	3,4,6,7	2.4
28	300028	Methane	End	Louvered	Open	CUP10	2,4,6,8	2.4
29	300029	Methane	End	Louvered	Open	CUP10	2,3,7,8	2.4
30	300030	Methane	End	Louvered	Open	CUP10	1,2,8,9	2.4
31	300031	Methane	End	Louvered	Open	CUP10	1,2,3,4	2.4
32	300032	Methane	End	Louvered	Open	CUP10	8,9	3.0
33	300033	Methane	End	Louvered	Open	CUP10	7,8	3.0
34	300034	Methane	End	Louvered	Open	CUP10	6,7	3.0
35	300035	Methane	End	Louvered	Open	CUP10	4,6	3.0
36	300036	Methane	End	Louvered	Open	CUP10	3,4	3.0
37	300037	Methane	End	Louvered	Open	CUP10	2,3	3.0
38	300038	Methane	End	Louvered	Open	CUP10	1,2	3.0
39	300039	Methane	End	Louvered	Open	CUP10	3,4,6,7	3.5
40	300040	Methane	End	Closed	Open	-	-	-
41	300041	Methane	End	Closed	Open	CUP10	4,6	3.0
42	300042	Methane	End	Louvered	Open	CUP5	1,2,3,4	3.8
43	300043	Methane	End	Louvered	Open	CUP5	6,7,8,9	3.8
44	300044	Methane	End	Closed	Open	CUP10	7,8	3.0
45	300045	Methane	End	Louvered	Open	P120	8,9	7.6
46	300047	Methane	End	Louvered	Open	HV26	8,9	3.0
47	300049	Methane	End	Louvered	Open	CUP5	8,9	3.8
48	300051	Methane	End	Closed	Open	CUP10	4,6extended	3.0

Appendix 8: Scenario definition for M24-25 module

- MONITOR POINTS: 6 monitor points to record the pressure was located at the following positions:

No.	X	Y	Z	Status
1	7.00	1.00	2.00	Open
2	3.80	0.75	2.00	Open
3	0.50	1.00	2.00	Open
4	7.00	2.00	0.50	Open
5	3.80	2.00	0.50	Open
6	0.50	2.00	0.50	Open

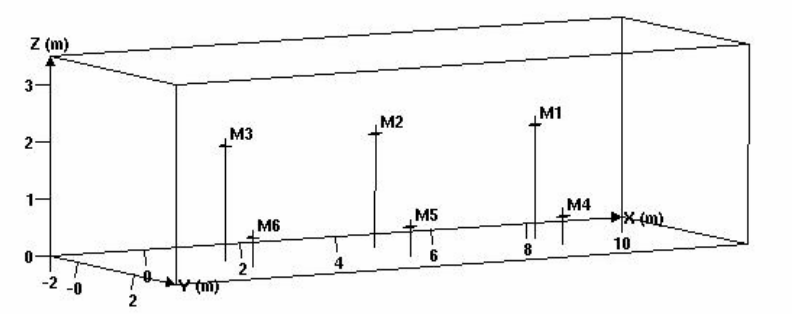

Figure 8.1: Location of monitor points.

- SINGLE FIELD SCALAR TIME OUTPUT: Chose the parameter(s) you want to measure, in this case pressure (P).

- SINGLE FIRLED 3D OUTPUT: Chose the parameter(s) you want to display in the 3D output, in this case pressure (P).

- SIMULATION AND OUTPUT CONTROL:
  Tmax: The maximum time interval FLACS will simulate.
  Tmax = 999999
  Last: The maximum number of time steps allowed for the simulation.
  Last = 999999
  CFLC: Courant-Friedrich-Levy number based on sound velocity.
  CFLC = 5.0
  CFLV: Courant-Friedrich-Levy number based on fluid flow velocity.
  CFLV = 0.5
  Scale: A factor used if scaling of the dimensions is wanted, no scaling = 1
  Scale= 1
  Modd: Determines the amount of data stored for scalar-time plots.
  Modd = 1
  NPLOT: Determines the amount of data stored for field plots.
  NPLOT = 5
  PTPLOT: This is the time interval for field output.
  PTPLOT = 999999
  Grid = ”Cartesian”

Wallf: Control switch specifying wall-functions
Wallf: = 1
Heat switch (not used) = 0

- BOUNDARY CONDITIONS: "Euler".

- INITIAL CONDITIONS:
  Up direction: A vector determining the direction to be taken as upwards.
  Up direction: 0 0 1
  Gravity = 9.8m/s^2
  Temperature (initial) = 20°C
  Characteristic velocity: Changes the reference velocity of the initial turbulence field.
  Characteristic velocity = 0
  Relative turbulence intensity: Changes the relative turbulence intensity of the initial turbulence field.
  Relative turbulence intensity = 0
  Turbulent length scale: Changes the value of the length scale of the initial turbulence.
  Turbulent length scale = 0

- GAS COMPOSITION AND VOLUME:
  Position of fuel region: The location of the minimum point of the box
  Position of fuel region = 0 0 0
  Dimension of fuel region: The dimensions of the box
  Dimension of fuel region = 8m 2.5m 2.5m
  Volume fraction: The volume fraction of the different gas components.
  Volume fraction: Methane = 1 or Propane = 1
  Equivalence ratios: Concentrations of gas inside (ER0) and outside (ER9) the gas cloud.
  Equivalence ratios (stoichiometric): ER0 = 1,03 ER9 = 0,0

- IGNITION:
  Position of ignition region:
  End ignition = 7.8m 1.25m 1.25m
  Centre ignition= 4m 1.25m 1.25m
  Dimension of ignition region = 0 0 0
  Time of ignition = 0
  Radmax = 0

- LOUVRE PANELS:
  Name = North wall
  Position= 8.0m 0m 0m
  Size= 0m 2.5m 2.5m
  Normal vector slats positive = 1 0 1
  Normal vector slats negative = 1 0 1
  $Drag_{acc}$ = 1.0
  $Drag_{bend}$ = 0.14 1/rad
  $Drag_{fric}$ = 9.0
  Area porosity = 0.5

Appendix 9: Max overpressure data from M24-25 module

	Monitor number					
Simulation number	**1**	**2**	**3**	**4**	**5**	**6**
1	0.29	0.38	0.22	0.34	0.39	0.22
2	0.75	0.91	0.64	0.81	0.93	0.62
3	0.77	0.92	0.64	0.86	0.94	0.62
4	0.47	0.39	0.34	0.52	0.38	0.32
5	0.55	0.55	0.38	0.61	0.59	0.35
6	0.16	0.21	0.14	0.17	0.21	0.14
7	0.20	0.27	0.17	0.19	0.27	0.17
8	0.11	0.19	0.10	0.14	0.20	0.11
9	0.31	0.50	0.22	0.33	0.50	0.26
10	0.14	0.24	0.12	0.16	0.24	0.13
11	0.19	0.28	0.10	0.23	0.29	0.10
12	0.25	0.33	0.17	0.30	0.34	0.20
13	0.30	0.43	0.29	0.36	0.45	0.34
14	0.32	0.45	0.20	0.38	0.46	0.18
15	0.25	0.37	0.33	0.30	0.39	0.41
16	0.33	0.45	0.37	0.41	0.44	0.37
17	0.32	0.48	0.42	0.40	0.46	0.46
18	0.23	0.33	0.21	0.28	0.34	0.23
19	0.28	0.37	0.26	0.34	0.39	0.25
20	0.24	0.32	0.20	0.29	0.32	0.19
21	0.29	0.41	0.31	0.35	0.41	0.33
22	0.35	0.48	0.39	0.42	0.50	0.40
23	0.29	0.38	0.31	0.35	0.38	0.31
24	0.23	0.31	0.27	0.28	0.33	0.29
25	0.20	0.28	0.15	0.24	0.29	0.16
26	0.20	0.25	0.11	0.24	0.26	0.10
27	0.25	0.36	0.23	0.32	0.36	0.27
28	0.16	0.24	0.10	0.20	0.25	0.12
29	0.12	0.19	0.13	0.15	0.18	0.12
30	0.12	0.17	0.08	0.14	0.17	0.07
31	0.21	0.30	0.27	0.25	0.29	0.33
32	0.12	.17	0.07	0.14	0.17	0.07
33	0.13	0.18	0.12	0.15	0.19	0.12
34	0.27	0.35	0.29	0.33	0.35	0.29
35	0.31	0.42	0.38	0.37	0.42	0.39
36	0.32	0.46	0.39	0.39	0.48	0.46
37	0.28	0.41	0.35	0.34	0.40	0.40
38	0.31	0.46	0.39	0.38	0.44	0.43
39	0.25	0.35	0.24	0.31	0.35	0.28
40	1.31	1.39	1.01	1.56	1.38	0.99
41	0.91	0.99	0.69	1.09	1.01	1.63
42	0.31	0.45	0.38	0.38	0.45	0.41
43	0.17	0.24	0.12	0.20	0.25	0.13
44	0.65	0.66	0.30	0.77	0.66	0.33
45	0.26	0.34	0.22	0.32	0.36	0.21
46	0.18	0.25	0.14	0.23	0.26	0.14
47	0.15	0.21	0.12	0.19	0.21	0.11
48	0.47	0.53	0.24	0.57	0.54	0.27

Appendix 10: Simulation plots from M24-25 module

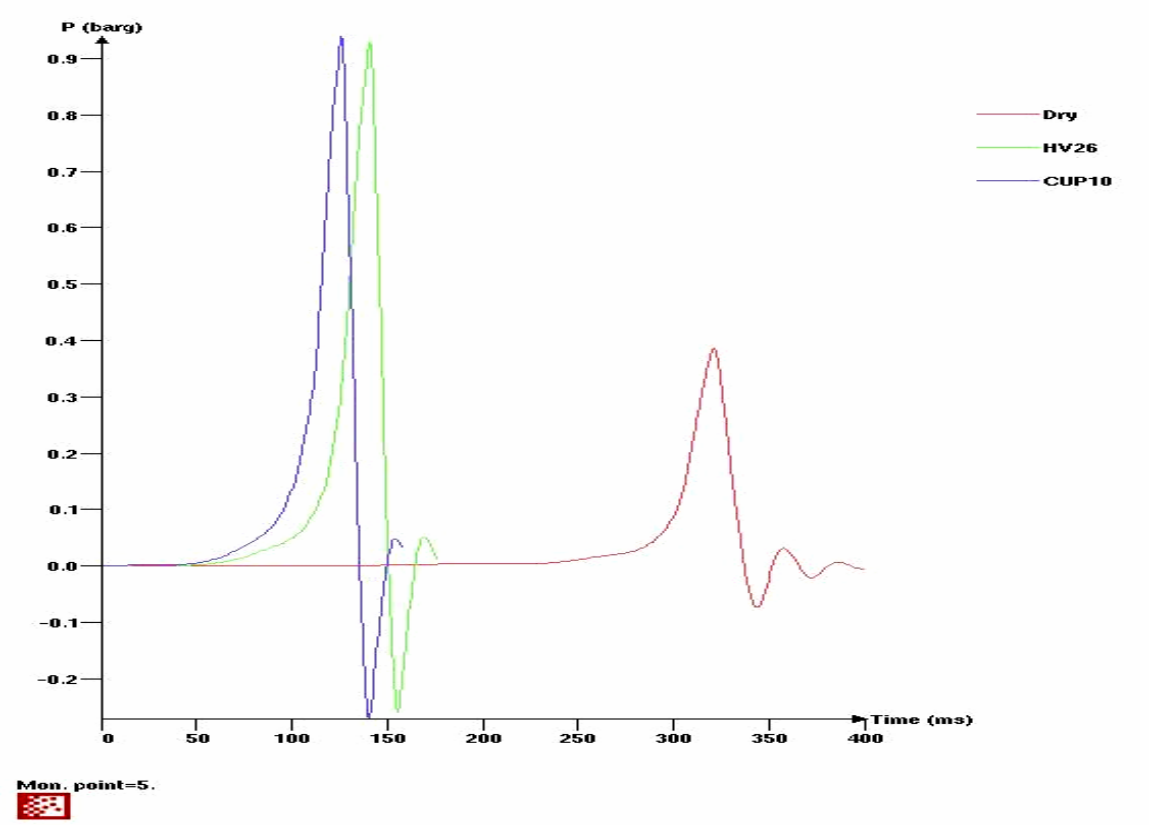

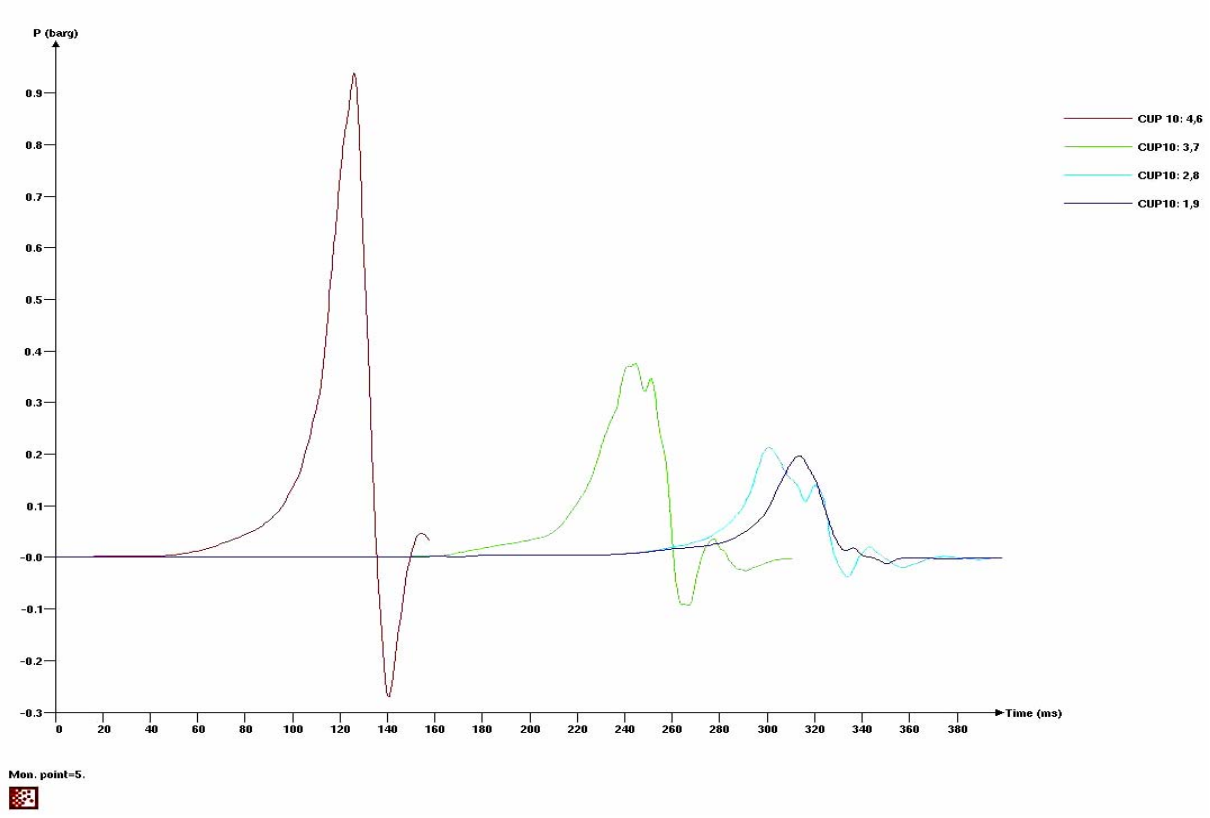

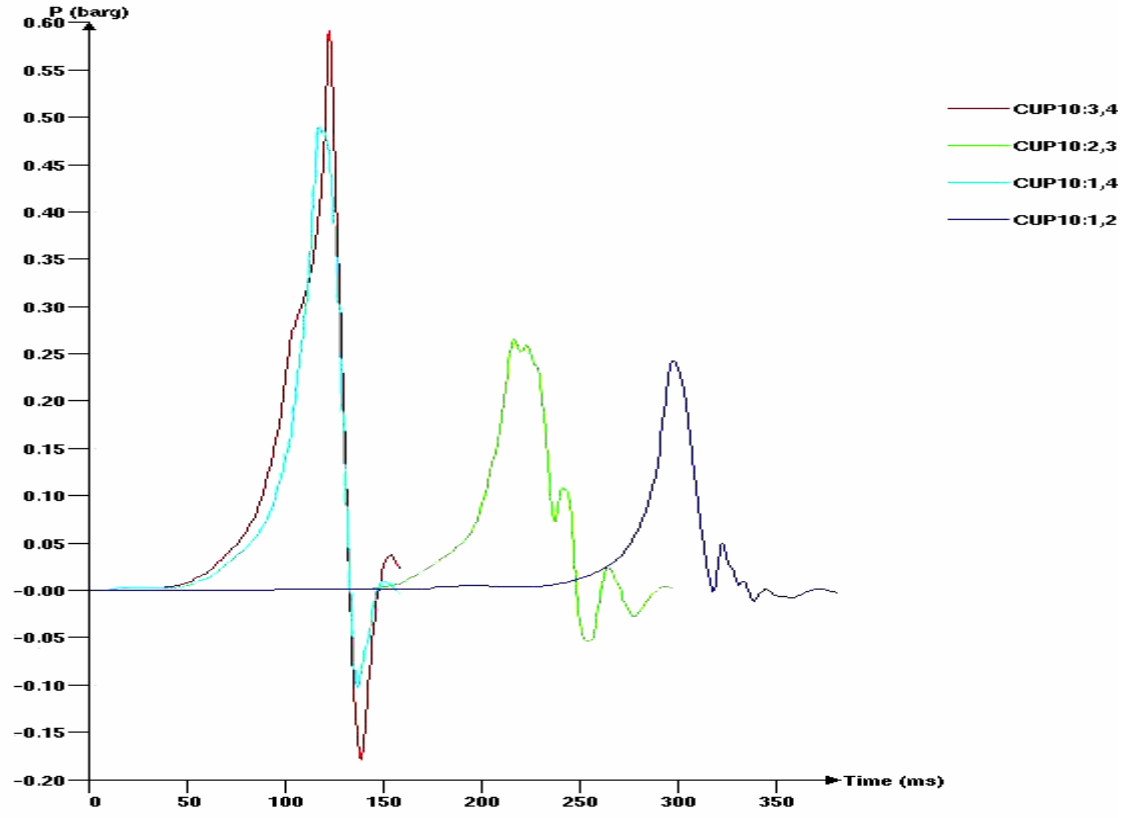
P (barg)
0.60
0.55
0.50
0.45
0.40
0.35
0.30
0.25
0.20
0.15
0.10
0.05
-0.00
-0.05
-0.10
-0.15
-0.20
0
50
100
150
200
250
300
350
Time (ms)
CUP10:3,4
CUP10:2,3
CUP10:1,4
CUP10:1,2

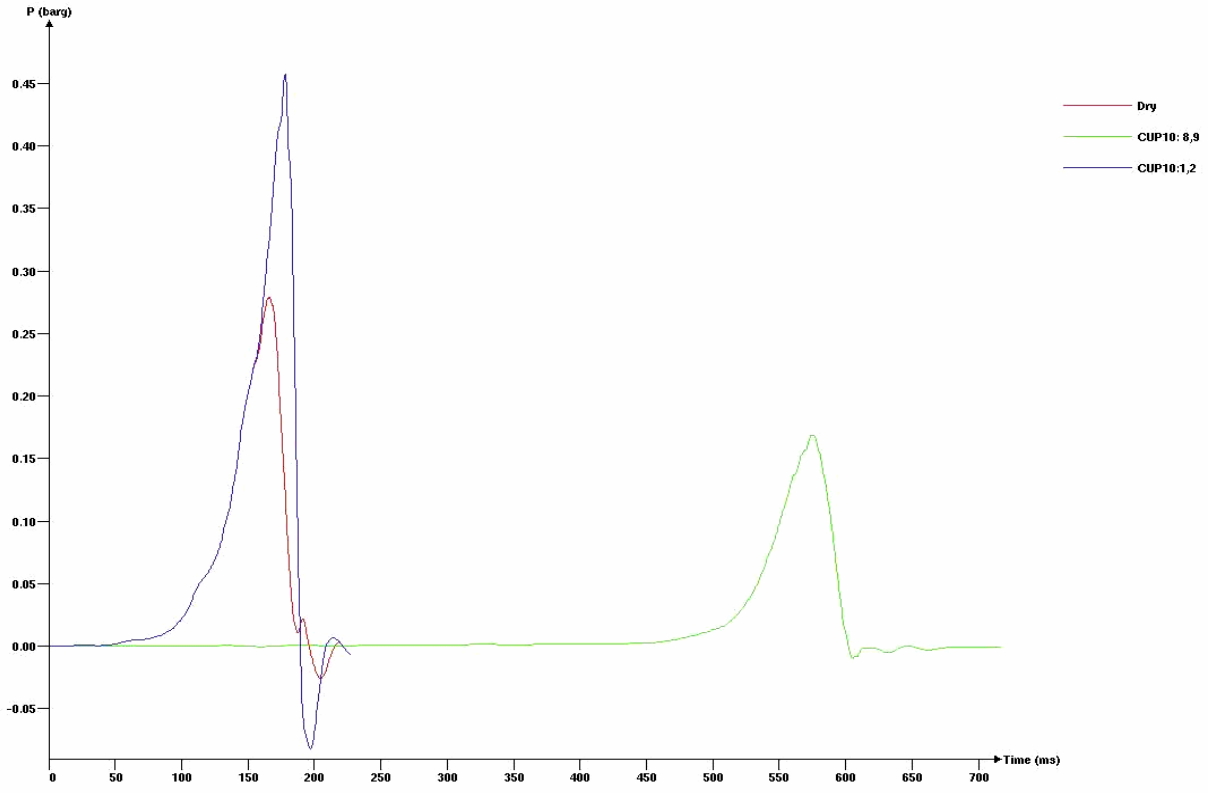
P (barg)
0.45
0.40
0.35
0.30
0.25
0.20
0.15
0.10
0.05
0.00
-0.05
0
50
100
150
200
250
300
350
400
450
500
550
600
650
700
Time (ms)
Dry
CUP10: 8,9
CUP10:1,2

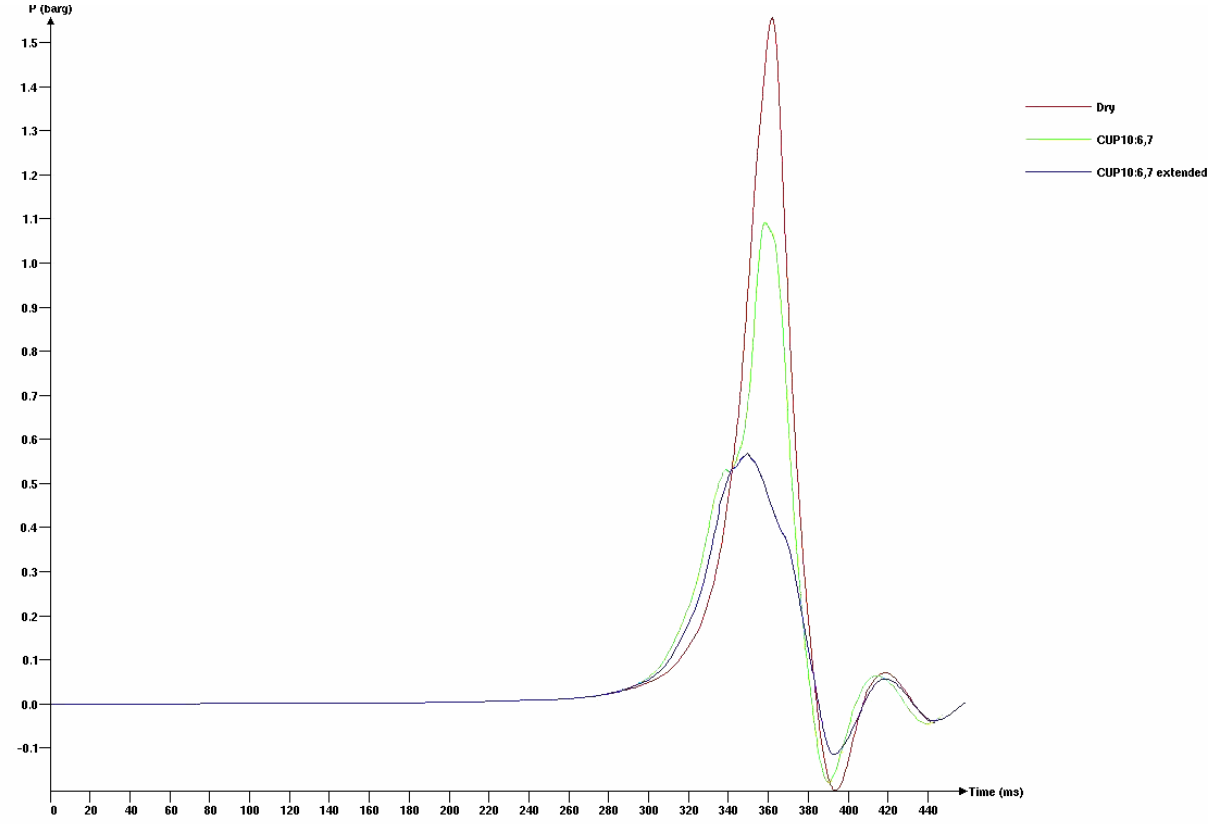
P (barg)
1.5
1.4
1.3
1.2
1.1
1.0
0.9
0.8
0.7
0.6
0.5
0.4
0.3
0.2
0.1
0.0
-0.1
0
20
40
60
80
100
120
140
160
180
200
220
240
260
280
300
320
340
360
380
400
420
440
Time (ms)
Dry
CUP10:6,7
CUP10:6,7 extended

Mon. point=4.

Appendix 11: Simulation configurations for full-scale module

Simulation nr	Scenario	Location of ignition	Nozzle type	Water pressure [bar]
1	100001	Centre	-	-
2	100002	Centre	MV57	1.65
3	100003	Centre	MV57 extended	1.65
4	100004	Centre	LDN extended	0.5
5	100005	End	-	-
6	100006	End	MV57 extended	1.65
7	100007	End	LDN extended	0.5
8	100008	End	LDN	0.5

Appendix 12: Scenario definition for full-scale module

- MONITOR POINTS: 20 monitor points recording the pressure is located at the following positions:

No.	X	Y	Z	Status
1	2.33	2.50	2.50	Open
2	2.33	4.50	4.50	Open
3	4.66	2.50	2.50	Open
4	4.66	6.50	6.50	Open
5	6.99	2.50	2.50	Open
6	6.99	4.50	4.50	Open
7	9.32	2.50	2.50	Open
8	9.32	6.50	6.50	Open
9	11.65	1.50	1.50	Open
10	11.65	4.50	4.50	Open
11	13.98	2.50	2.50	Open
12	13.98	6.50	6.50	Open
13	16.31	2.50	2.50	Open
14	16.31	4.50	4.50	Open
15	18.64	2.50	2.50	Open
16	18.64	6.50	6.50	Open
17	20.97	2.50	2.50	Open
18	20.97	4.50	4.50	Open
19	23.30	2.50	2.50	Open
20	23.30	6.50	6.50	Open

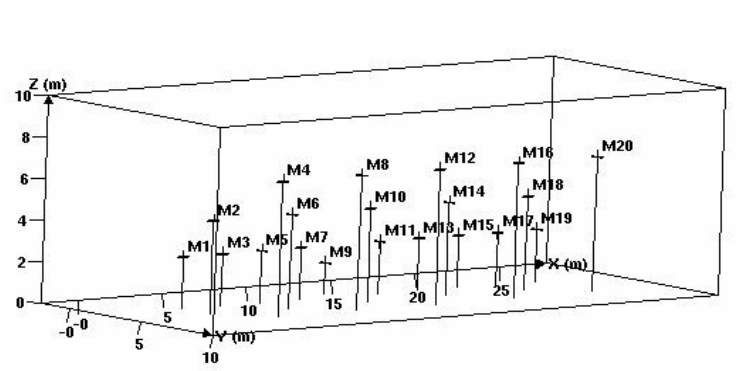

Figure 12.1: Location of monitor points

- SINGLE FIELD SCALAR TIME OUTPUT: Chose the parameter(s) you want to measure, in this case pressure (P).

- SINGLE FIELD 3D OUTPUT: Chose the parameter(s) you want to display in the 3D output, in this case pressure (P).

- SIMULATION AND OUTPUT CONTROL:
  Tmax: The maximum time interval FLACS will simulate.
  Tmax = 999999
  Last: The maximum number of time steps allowed for the simulation.
  Last = 999999
  CFLC: Courant-Friedrich-Levy number based on sound velocity.
  CFLC = 5.0
  CFLV: Courant-Friedrich-Levy number based on fluid flow velocity.
  CFLV = 0.5
  Scale: A factor used if scaling of the dimensions is wanted, no scaling = 1

Scale= 1
Modd: Determines the amount of data stored for scalar-time plots.
Modd = 1
NPLOT: Determines the amount of data stored for field plots.
NPLOT = 5
PTPLOT: This is the time interval for field output.
PTPLOT = 999999
Grid = ”Cartesian”
Wallf: Control switch specifying wall-functions
Wallf: = 1
Heat switch (not used) = 0

- BOUNDARY CONDITIONS: “Euler”.

- INITIAL CONDITIONS:
  Up direction: A vector determining the direction to be taken as upwards.
  Up direction: 0 0 1
  Gravity = 9.8m/s^2
  Temperature (initial) = 20°C
  Characteristic velocity: Changes the reference velocity of the initial turbulence field.
  Characteristic velocity = 0
  Relative turbulence intensity: Changes the relative turbulence intensity of the initial turbulence field.
  Relative turbulence intensity = 0
  Turbulent length scale: Changes the value of the length scale of the initial turbulence.
  Turbulent length scale = 0

- GAS COMPOSITION AND VOLUME:
  Position of fuel region: The location of the minimum point of the box
  Position of fuel region = 0 0 0
  Dimension of fuel region: The dimensions of the box
  Dimension of fuel region = 25.6m 8.0m 8.0m
  Volume fraction: The volume fraction of the different gas components.
  Volume fraction: Methane = 0.917 Ethane = 0.07 Propane = 0.013
  Equivalence ratios: Concentrations of gas inside (ER0) and outside (ER9) the gas cloud.
  Equivalence ratios (stoichiometric): ER0 = 1 ER9 = 0

- IGNITION:
  Position of ignition region:
  End ignition = 0.52m 4.29m 4.26m
  Centre ignition= 12.76m 4.00m 4.23m
  Dimension of ignition region = 0 0 0
  Time of ignition = 0
  Radmax = 0

Appendix 13: Max overpressure data from full-scale module

Sim nr / Monitor nr	1	2	3	4	5	6	7	8
1	0.82	0.60	0.59	0.40	0.40	0.13	0.10	0.10
2	0.94	0.60	0.58	0.43	0.46	0.15	0.12	0.12
3	1.00	0.69	0.69	0.54	0.75	0.27	0.21	0.21
4	1.07	0.73	0.74	0.51	0.66	0.23	0.18	0.18
5	1.06	0.70	0.70	0.55	0.85	0.30	0.24	0.24
6	1.07	0.71	0.71	0.55	0.91	0.32	0.26	0.26
7	1.10	0.69	0.69	0.55	1.05	0.35	0.29	0.29
8	1.07	0.70	0.70	0.57	0.93	0.33	0.27	0.27
9	1.12	0.69	0.69	0.54	1.07	0.37	0.30	0.30
10	1.09	0.69	0.69	0.54	0.96	0.35	0.29	0.29
11	1.10	0.69	0.69	0.54	1.03	0.38	0.31	0.31
12	1.03	0.67	0.67	0.54	0.98	0.37	0.33	0.33
13	1.02	0.65	0.65	0.50	1.08	0.40	0.31	0.31
14	1.01	0.66	0.66	0.52	1.05	0.41	0.32	0.32
15	0.98	0.63	0.63	0.48	1.22	0.42	0.28	0.28
16	0.94	0.64	0.64	0.51	1.24	0.44	0.31	0.31
17	0.74	0.46	0.46	0.35	1.25	0.33	0.11	0.17
18	0.88	0.53	0.54	0.39	1.36	0.36	0.14	0.15
19	0.65	0.42	0.42	0.29	1.24	0.29	0.06	0.20
20	0.92	0.50	0.50	0.34	1.97	0.34	0.10	0.17

Appendix 14: Simulation plots from full-scale model

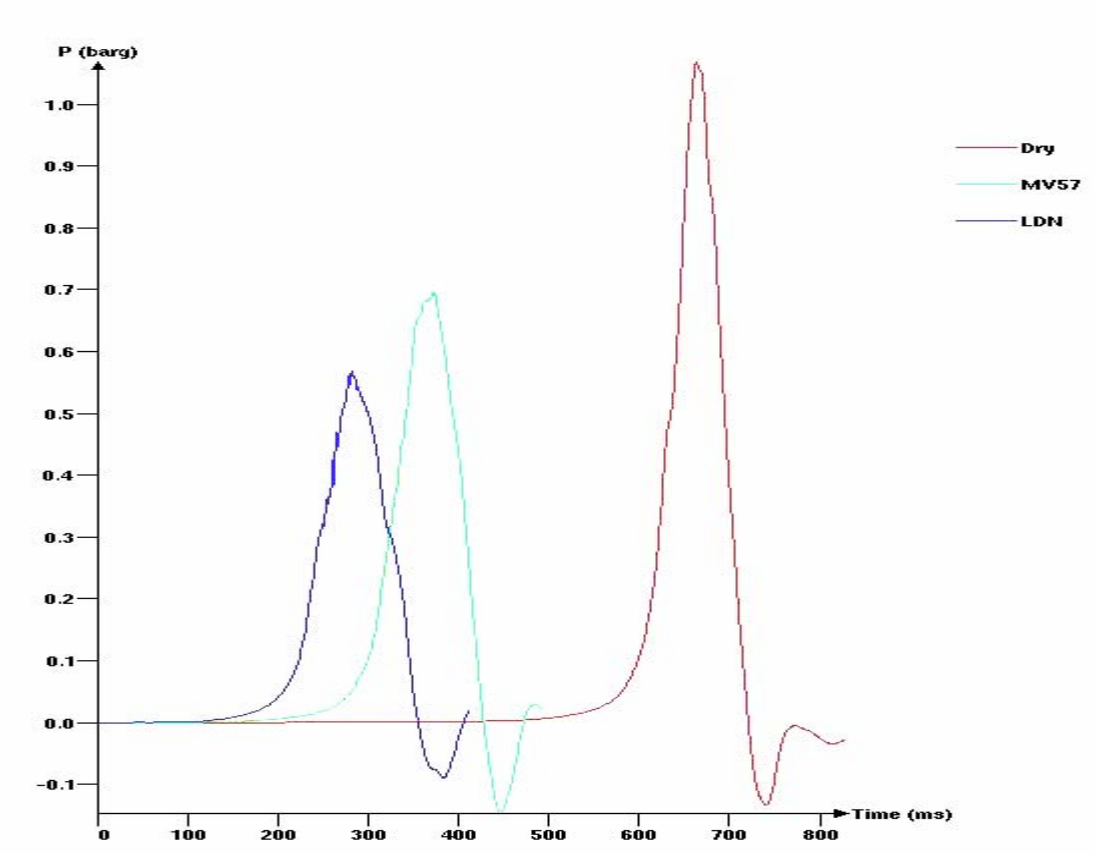

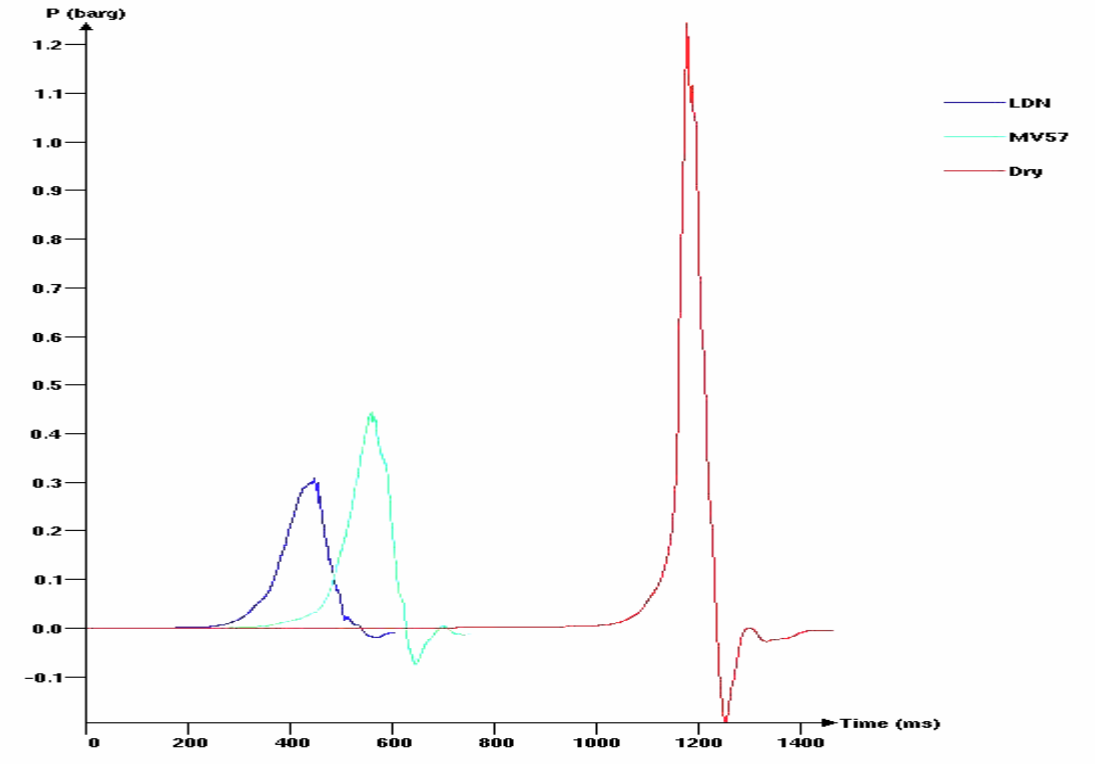

Appendix 15: Scenario definition for Kårstø, Statpipe/Sleipener.

Scenario definition
The scenario has following subdirectories:

- MONITOR POINTS: The location in x-, y- and z-direction of monitors to record different wanted parameters. In the scenario defined by DNV, monitor 13 and 33 was not operative because they had status as “solid”. These monitor points were therefore slightly moved so that they were able to monitor the pressure. In this case the overpressure is monitored at 45 different monitor points:

No.	X	Y	Z	Status	No.	X	Y	Z	Status	No.	X	Y	Z	Status
1	19775.00	4945.00	10.00	Open	16	19775.00	5055.00	10.00	Open	31	19775.00	5018.00	23.00	Open
2	19814.00	4945.00	10.00	Open	17	19814.00	5055.00	10.00	Open	32	19814.00	5018.00	23.00	Open
3	19853.00	4945.00	10.00	Open	18	19853.00	5055.00	10.00	Open	33	19860.00	5018.00	23.00	Open
4	19892.00	4945.00	10.00	Open	19	19892.00	5055.00	10.00	Open	34	19892.00	5018.00	23.00	Open
5	19932.00	4945.00	10.00	Open	20	19932.00	5055.00	10.00	Open	35	19932.00	5018.00	23.00	Open
6	19775.00	4982.00	10.00	Open	21	19775.00	4945.00	23.00	Open	36	19775.00	5055.00	23.00	Open
7	19814.00	4982.00	10.00	Open	22	19814.00	4945.00	23.00	Open	37	19814.00	5055.00	23.00	Open
8	19853.00	4982.00	10.00	Open	23	19853.00	4945.00	23.00	Open	38	19853.00	5055.00	23.00	Open
9	19892.00	4982.00	10.00	Open	24	19892.00	4945.00	23.00	Open	39	19892.00	5055.00	23.00	Open
10	19932.00	4982.00	10.00	Open	25	19932.00	4945.00	23.00	Open	40	19932.00	5055.00	23.00	Open
11	19775.00	5018.00	10.00	Open	26	19775.00	4982.00	23.00	Open	41	19760.00	4982.00	10.00	Open
12	19814.00	5018.00	10.00	Open	27	19814.00	4982.00	23.00	Open	42	19720.00	4982.00	10.00	Open
13	19860.00	5018.00	10.00	Open	28	19853.00	4982.00	23.00	Open	43	19680.00	4982.00	10.00	Open
14	19892.00	5018.00	10.00	Open	29	19892.00	4982.00	23.00	Open	44	19640.00	4982.00	10.00	Open
15	19932.00	5018.00	10.00	Open	30	19932.00	4982.00	23.00	Open	45	19600.00	4982.00	10.00	Open

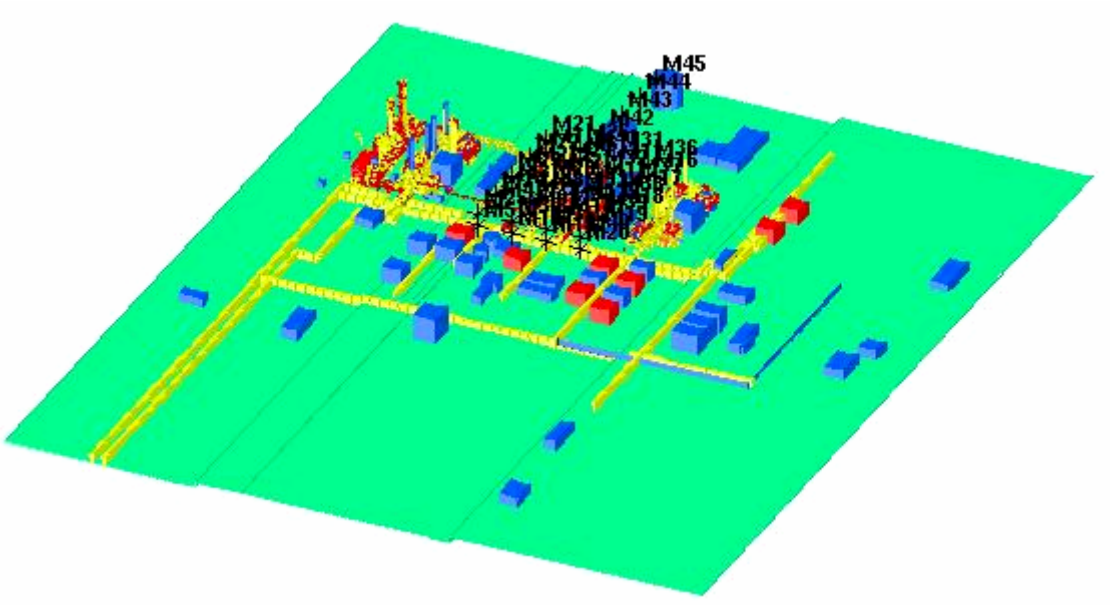

Figure 5.1.10: Location of monitor points in Statpipe/Sleipner.

- SINGLE FIELD SCALAR TIME OUTPUT: Chose the parameter(s) you want to measure in this case local pressure (P), pressure impulse (PIMP), panel average pressure (PP) and drag loads (DRAG).

- SINGLE FIELD 3D OUTPUT: Chose the parameter(s) you want to display in the 3D output, in this case pressure (P), pressure impulse (PIMP), panel average pressure (PP) and drag loads (DRAG).

- SIMULATION AND OUTPUT CONTROL:
  Tmax: The maximum time interval FLACS will simulate.
  Tmax = 999999
  Last: The maximum number of time steps allowed for the simulation.
  Last = 999999
  CFLC: Courant-Friedrich-Levy number based on sound velocity.
  CFLC = 5.0
  CFLV: Courant-Friedrich-Levy number based on fluid flow velocity.
  CFLV = 0.5
  Scale: A factor used if scaling of the dimensions is wanted, no scaling = 1
  Scale= 1
  Modd: Determines the amount of data stored for scalar-time plots.
  Modd = 1
  NPLOT: Determines the amount of data stored for field plots.
  NPLOT = 5
  PTPLOT: This is the time interval for field output.
  PTPLOT = 999999
  Grid = ”Cartesian”
  Wallf: Control switch specifying wall-functions
  Wallf: = 1
  Heat switch (not used) = 0

- BOUNDARY CONDITIONS: “Euler”.

- INITIAL CONDITIONS:
  Up direction: A vector determining the direction to be taken as upwards.
  Up direction: 0 0 1
  Gravity = 9.8m/s^2
  Temperature (initial) = 10°C
  Characteristic velocity: Changes the reference velocity of the initial turbulence field.
  Characteristic velocity = 0
  Relative turbulence intensity: Changes the relative turbulence intensity of the initial turbulence field.
  Relative turbulence intensity = 0
  Turbulent length scale: Changes the value of the length scale of the initial turbulence.
  Turbulent length scale = 0

- PRESSURE RELIEF PANELS:
  A total of 151 panels are defined. The first 148 panels are defined as “Inactive” which means that this is a passive panel that does not affect the numerical

simulations in any way. The purpose of these panels is to monitor variables (P) related to the area the panel occupies. The final three panels are defined as "pop out"-panels, and have the following specifications:
Opening pressure differences = -0.25 0.1
Initial and final porosity: 0 = closed, 1 = open
Initial and final porosity = 0 0.8
Weight (kg) = 6
Drag coefficient = 1
Maximum travel distance = 0
Sub sizes = 10 5

- GAS COMPOSITION AND VOLUME:
  The gas cloud is positioned at the southwest.
  Fill fraction, V_f/V: 0.30
  Cloud mass, E: 9100.2 kg
  Gas cloud position (x, y, z): 19775.0 4945.0 8.2
  Size of gas cloud (dx, dy, dz): 117.8 88.0 12.9
  Volume fraction: The volume fraction of the different gas components.
  Volume fraction: Methane = 0.85, Ethane 0.067, Propane = 0.08 and CO_2 = 0.003
  Equivalence ratios: Concentrations of gas inside (ER0) and outside (ER9) the gas cloud.
  Equivalence ratios (stoichiometric): ER0 = 1,0 ER9 = 0,0

- IGNITION:
  The ignition is positioned at the northeast corner of the cloud, centre z position.
  Ignition location (x, y, z): 19882.8 5030.0 14.7
  Dimension of ignition region = 0 0 0
  Time of ignition = 0
  Radmax = 0

Appendix 16: Max overpressure data from Kårstø, Statpipe/Sleipener.

Sim nr / Monitor nr	0	1	2	3	4	5	6	7	8	9
1	1.49	1.49	0.08	0.08	1.49	0.07	0.06	1.49	0.04	0.03
2	0.85	0.83	0.19	0.15	0.82	0.15	0.11	0.81	0.09	0.07
3	0.25	0.25	0.08	0.07	0.27	0.08	0.06	0.27	0.06	0.04
4	0.19	0.20	0.07	0.05	0.21	0.07	0.04	0.21	0.04	0.01
5	0.08	0.08	0.03	0.02	0.08	0.03	0.02	0.08	0.02	0.00
6	1.08	1.09	0.17	0.10	1.09	0.16	0.08	1.08	0.14	0.06
7	0.31	0.31	0.10	0.08	0.31	0.09	0.07	0.30	0.07	0.05
8	0.14	0.13	0.08	0.06	0.13	0.08	0.05	0.13	0.08	0.04
9	0.09	0.09	0.07	0.07	0.09	0.07	0.07	0.10	0.07	0.06
10	0.10	0.11	0.05	0.03	0.11	0.04	0.02	0.11	0.03	0.01
11	0.75	0.76	0.62	0.09	0.76	0.60	0.08	0.76	0.50	0.06
12	0.27	0.28	0.27	0.10	0.28	0.27	0.09	0.28	0.23	0.06
13	0.08	0.08	0.03	0.03	0.08	0.03	0.04	0.08	0.03	0.04
14	0.08	0.08	0.03	0.03	0.08	0.03	0.03	0.08	0.03	0.03
15	0.09	0.08	0.04	0.02	0.08	0.04	0.02	0.08	0.03	0.01
16	0.21	0.22	0.17	0.03	0.21	0.17	0.03	0.22	0.14	0.02
17	0.10	0.11	0.05	0.03	0.11	0.05	0.02	0.11	0.04	0.02
18	0.10	0.10	0.05	0.03	0.11	0.04	0.02	0.10	0.03	0.02
19	0.08	0.08	0.03	0.03	0.08	0.03	0.02	0.08	0.02	0.02
20	0.06	0.07	0.03	0.02	0.07	0.03	0.02	0.06	0.03	0.01
21	1.23	1.23	0.10	0.09	1.22	0.08	0.06	1.23	0.05	0.03
22	0.65	0.66	0.17	0.13	0.07	0.13	0.10	0.68	0.09	0.06
23	0.29	0.29	0.10	0.05	0.29	0.08	0.04	0.29	0.04	0.03
24	0.14	0.14	0.06	0.04	0.14	0.06	0.03	0.14	0.04	0.02
25	0.08	0.09	0.04	0.02	0.09	0.03	0.02	0.09	0.02	0.01
26	0.70	0.70	0.16	0.09	0.70	0.15	0.08	0.70	0.13	0.05
27	0.28	0.28	0.09	0.07	0.28	0.08	0.06	0.28	0.07	0.04
28	0.13	0.12	0.05	0.05	0.12	0.05	0.05	0.12	0.05	0.04
29	0.10	0.10	0.04	0.04	0.10	0.04	0.04	0.11	0.03	0.03
30	0.09	0.10	0.04	0.02	0.10	0.04	0.02	0.10	0.03	0.01
31	0.56	0.56	0.45	0.07	0.56	0.44	0.06	0.56	0.37	0.04
32	0.17	0.18	0.18	0.07	0.18	0.18	0.06	0.18	0.16	0.03
33	0.07	0.07	0.03	0.03	0.07	0.03	0.03	0.07	0.03	0.03
34	0.08	0.08	0.03	0.03	0.08	0.03	0.03	0.08	0.03	0.03
35	0.08	0.08	0.04	0.02	0.08	0.04	0.02	0.08	0.03	0.01
36	0.20	0.21	0.17	0.03	0.21	0.16	0.03	0.21	0.13	0.02
37	0.13	0.13	0.08	0.03	0.13	0.07	0.02	0.13	0.06	0.02
38	0.10	0.10	0.05	0.03	0.10	0.05	0.02	0.10	0.03	0.02
39	0.07	0.08	0.03	0.03	0.08	0.03	0.02	0.08	0.02	0.01
40	0.06	0.07	0.03	0.02	0.06	0.03	0.02	0.07	0.03	0.01
41	0.99	1.01	0.18	0.07	1.00	0.17	0.06	1.00	0.14	0.04
42	0.13	0.13	0.06	0.02	0.13	0.06	0.02	0.13	0.05	0.01
43	0.01	0.02	0.00	0.00	0.02	0.00	0.00	0.01	0.00	0.00
44	0.01	0.02	0.00	0.00	0.02	0.00	0.00	0.01	0.00	0.00
45	0.01	0.02	0.00	0.00	0.02	0.00	0.00	0.01	0.00	0.00

Appendix 17: Location of water spray, Statpipe/Sleipner

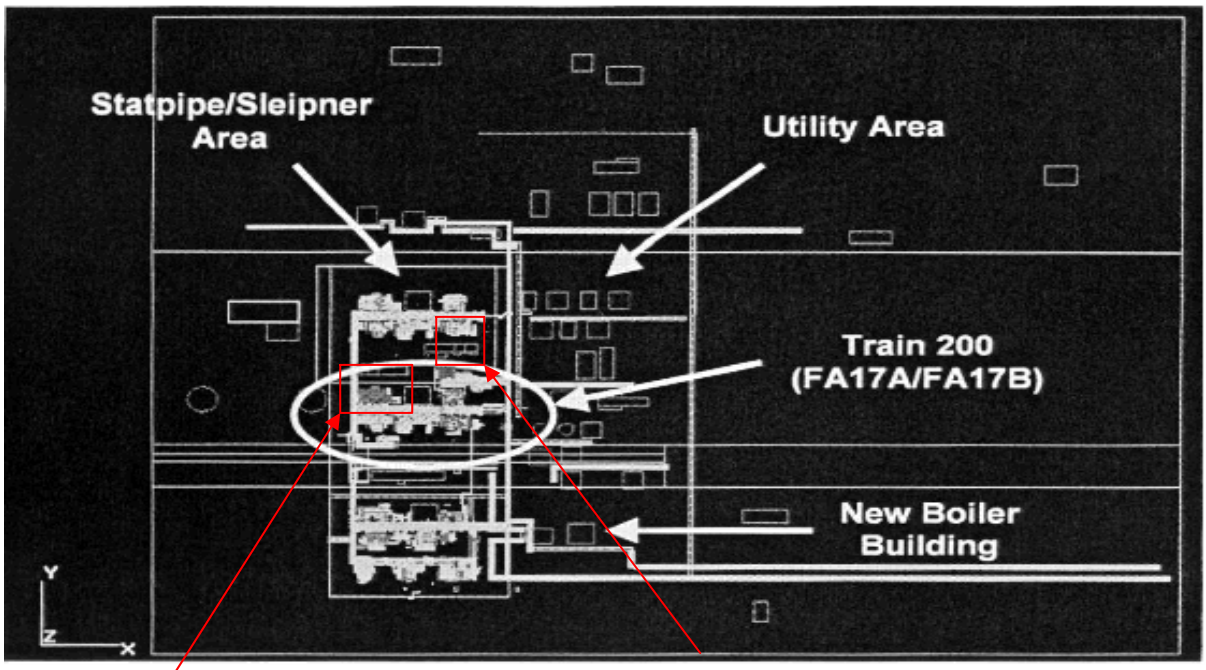

Case 2 Case 1

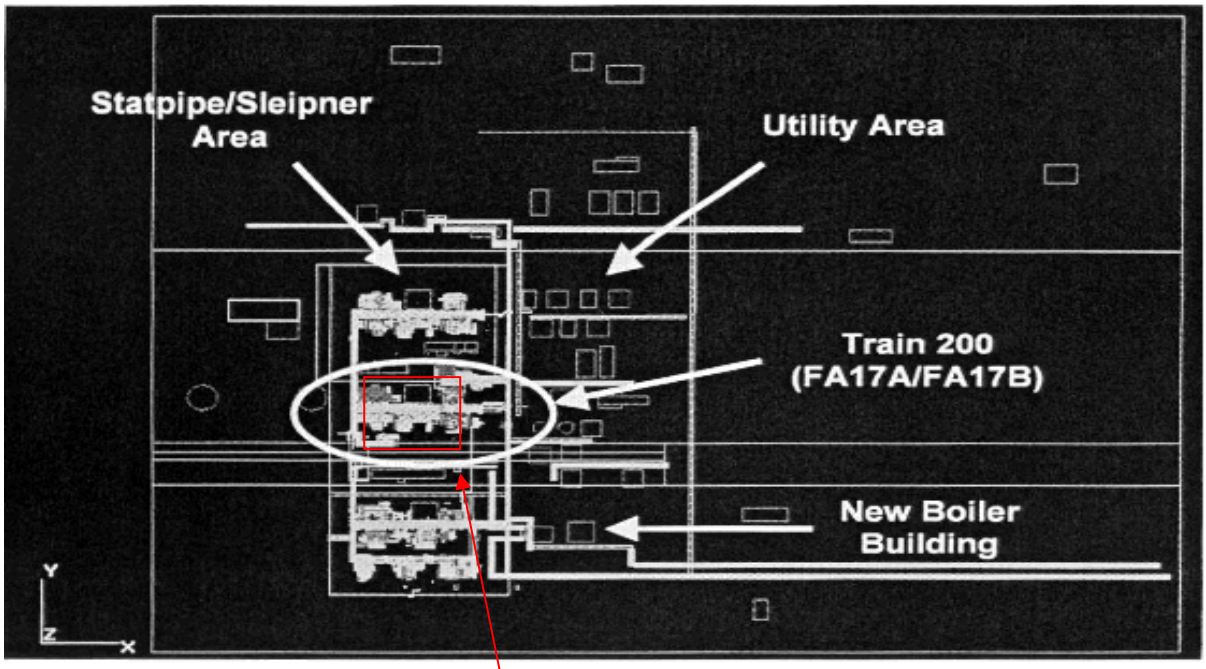

Case 3

Appendix 18: Simulation plots from Kårstø, Statpipe/Sleipner

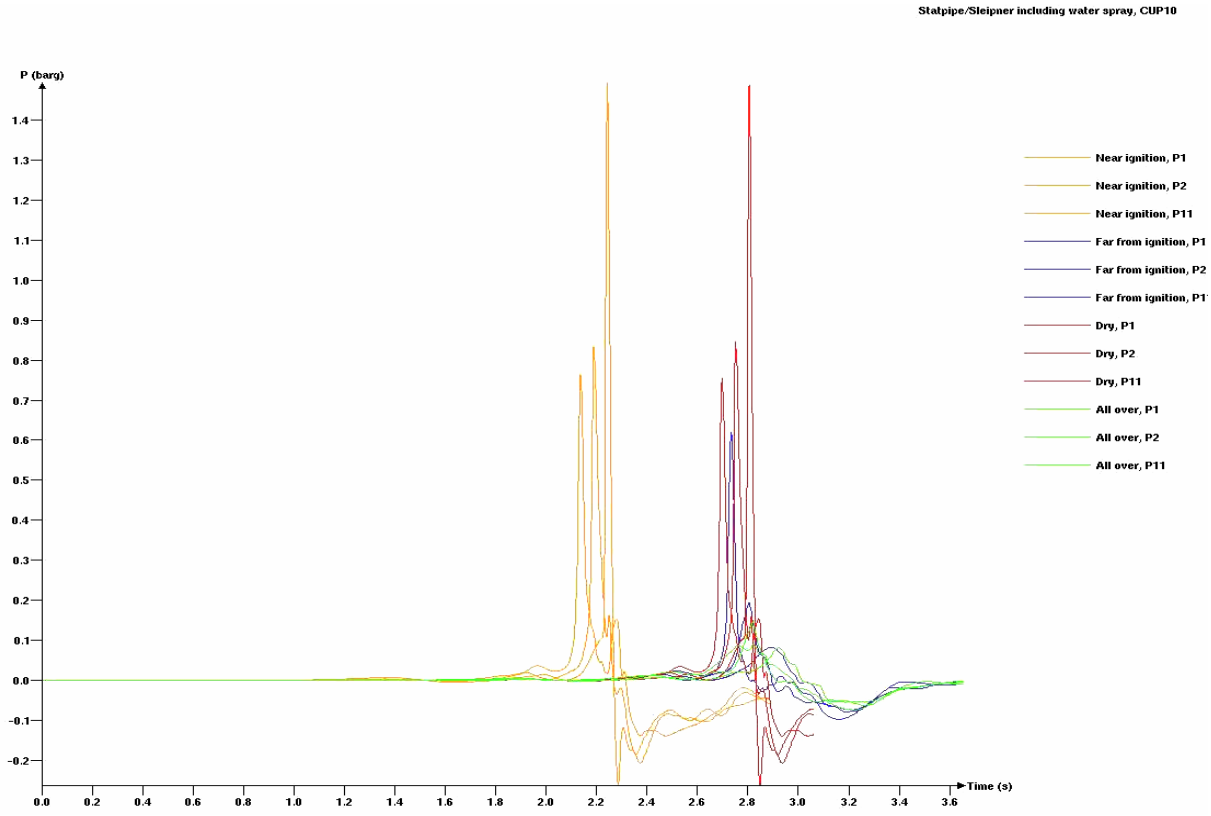

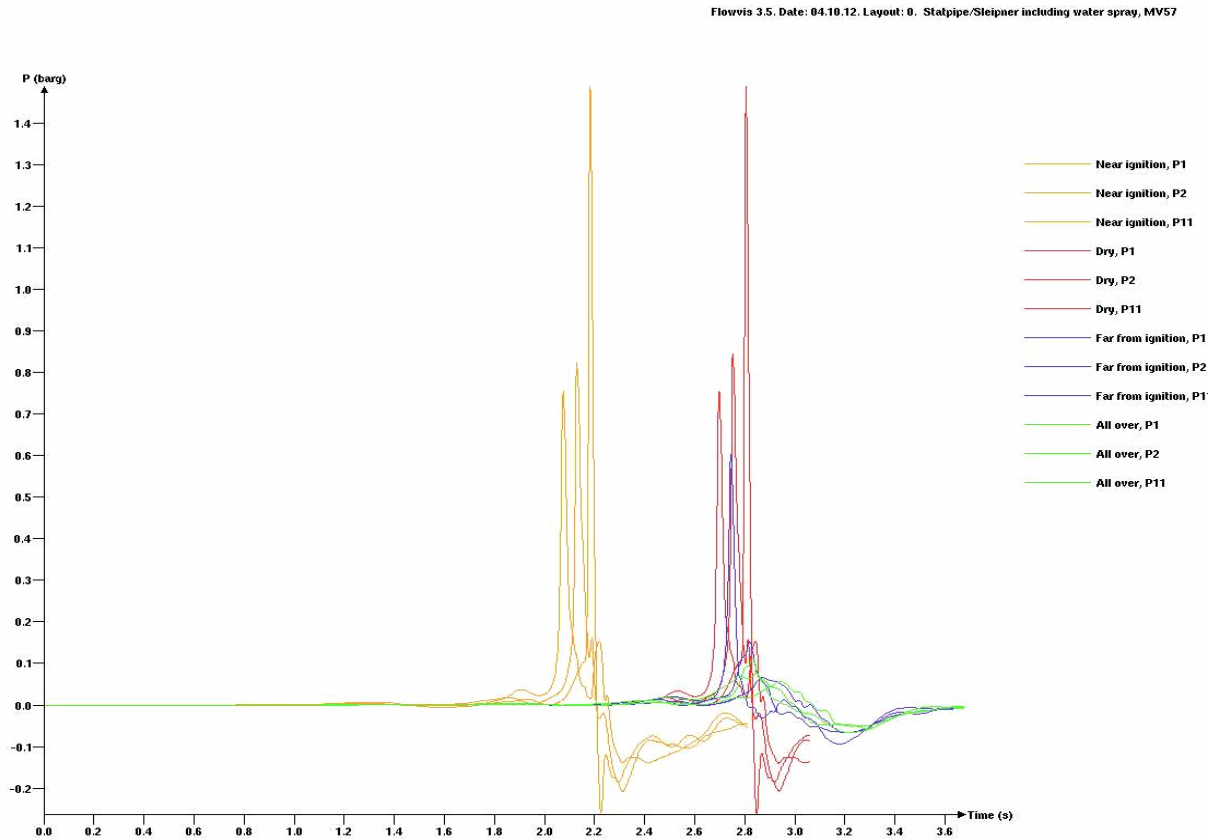

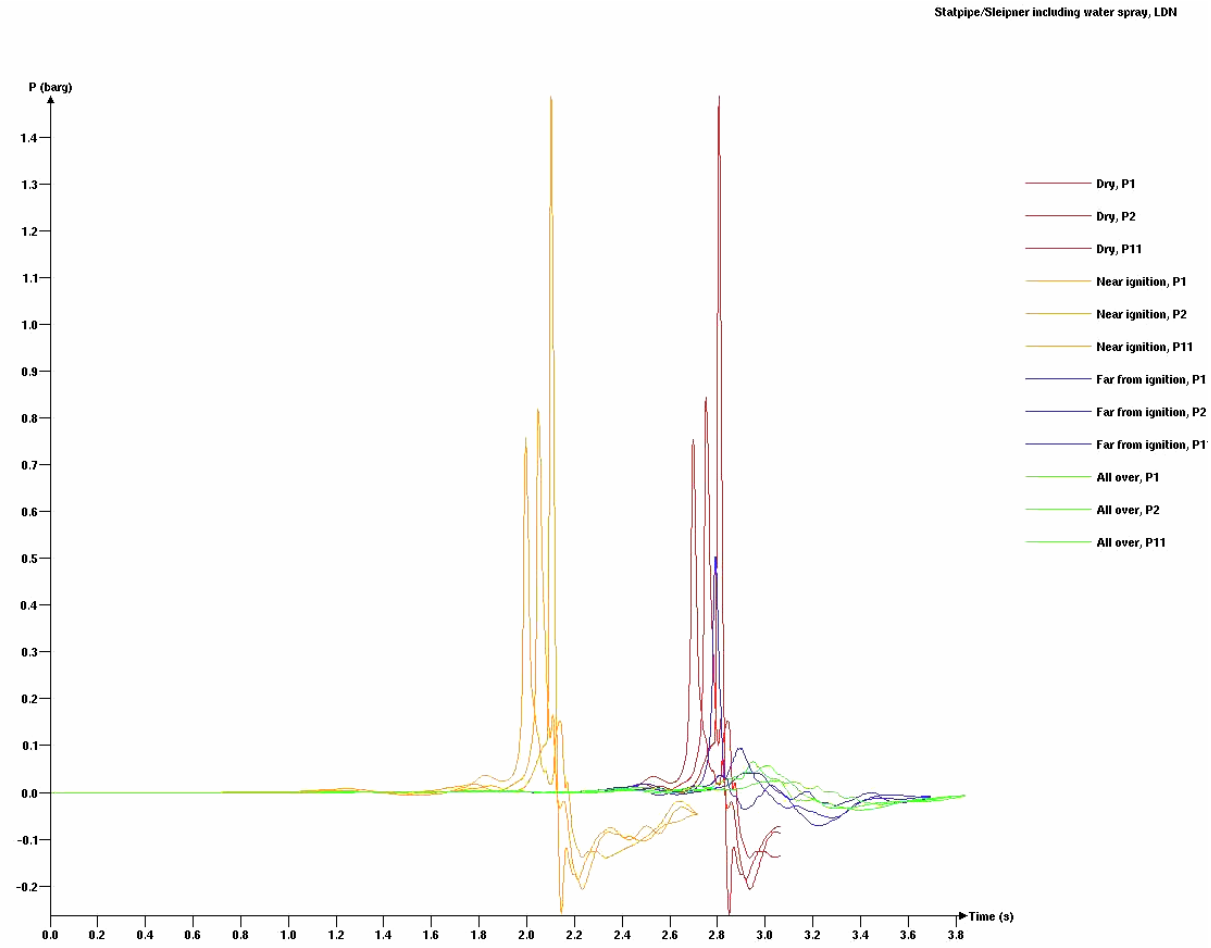
Statpipe/Sleipner including water spray, LDN
P (barg)
1.4
1.3
1.2
1.1
1.0
0.9
0.8
0.7
0.6
0.5
0.4
0.3
0.2
0.1
0.0
-0.1
-0.2
0.0
0.2
0.4
0.6
0.8
1.0
1.2
1.4
1.6
1.8
2.0
2.2
2.4
2.6
2.8
3.0
3.2
3.4
3.6
3.8
Time (s)
Dry, P1
Dry, P2
Dry, P11
Near ignition, P1
Near ignition, P2
Near ignition, P11
Far from ignition, P1
Far from ignition, P2
Far from ignition, P1
All over, P1
All over, P2
All over, P11

Appendix 19: Scenario definition for Kårstø, Åsgard.

- MONITOR POINTS: The location in x-, y- and z-direction of monitors to record different wanted parameters. In this case the overpressure and drag force is monitored at 28 different monitor points:

No.	X	Y	Z	Status	No.	X	Y	Z	Status	No.	X	Y	Z	Status
1	20235.00	4994.00	15.00	Open	11	20275.00	5043.00	15.00	Open					
2	20255.00	4994.00	15.00	Open	12	20298.00	5043.00	15.00	Open					
3	20275.00	4994.00	15.00	Open	13	20235.00	5073.00	15.00	Open	21	20235.00	5107.00	15.00	Open
4	20298.00	4994.00	15.00	Open	14	20255.00	5073.00	15.00	Open	22	20255.00	5107.00	15.00	Open
5	20235.00	5013.00	15.00	Open	15	20275.00	5073.00	15.00	Open	23	20275.00	5107.00	15.00	Open
6	20255.00	5013.00	15.00	Open	16	20298.00	5073.00	15.00	Open	24	20298.00	5107.00	15.00	Open
7	20275.00	5013.00	15.00	Open	17	20235.00	5103.00	15.00	Open	35	20030.00	5115.00	15.00	Open
8	20298.00	5013.00	15.00	Open	18	20255.00	5103.00	15.00	Open	36	20060.00	5115.00	15.00	Open
9	20235.00	5043.00	15.00	Open	19	20275.00	5103.00	15.00	Open	37	20090.00	5115.00	15.00	Open
10	20255.00	5043.00	15.00	Open	20	20298.00	5103.00	15.00	Open	38	20120.00	5115.00	15.00	Open

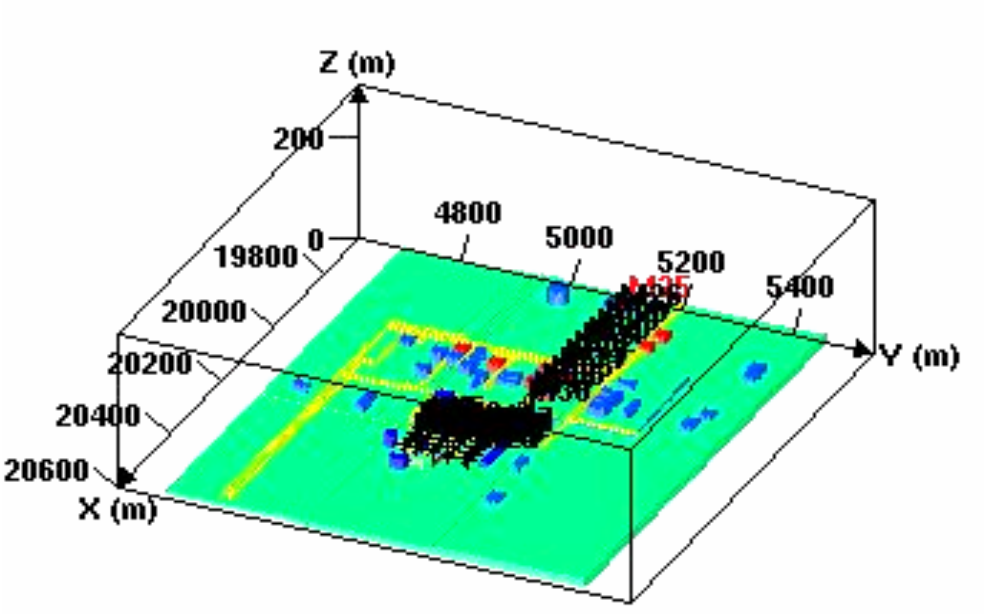

Figure 5.1.13: Location of monitor points in Åsgard.

- SINGLE FIELD SCALAR TIME OUTPUT: Chose the parameter(s) you want to measure in this case pressure (P), panel average pressure (PP) and drag loads (DRAG).

- SINGLE FIELD 3D OUTPUT: Chose the parameter(s) you want to display in the 3D output, in this case pressure (P), panel average pressure (PP) and drag loads (DRAG).

- SIMULATION AND OUTPUT CONTROL:
  Tmax: The maximum time interval FLACS will simulate.

Tmax = 999999
Last: The maximum number of time steps allowed for the simulation.
Last = 999999
CFLC: Courant-Friedrich-Levy number based on sound velocity.
CFLC = 5.0
CFLV: Courant-Friedrich-Levy number based on fluid flow velocity.
CFLV = 0.5
Scale: A factor used if scaling of the dimensions is wanted, no scaling = 1
Scale= 1
Modd: Determines the amount of data stored for scalar-time plots.
Modd = 1
NPLOT: Determines the amount of data stored for field plots.
NPLOT = 5
PTPLOT: This is the time interval for field output.
PTPLOT = 999999
Grid = ”Cartesian”
Wallf: Control switch specifying wall-functions
Wallf: = 1
Heat switch (not used) = 0

- BOUNDARY CONDITIONS: “Euler”.

- INITIAL CONDITIONS:
  Up direction: A vector determining the direction to be taken as upwards.
  Up direction: 0 0 1
  Gravity = 9.8m/s^2
  Temperature (initial) = 10°C
  Characteristic velocity: Changes the reference velocity of the initial turbulence field.
  Characteristic velocity = 0
  Relative turbulence intensity: Changes the relative turbulence intensity of the initial turbulence field.
  Relative turbulence intensity = 0
  Turbulent length scale: Changes the value of the length scale of the initial turbulence.
  Turbulent length scale = 0

- PRESSURE RELIEF PANELS:
  A total of 129 panels are defined. The first 118 and the last 8 panels are defined as “Inactive” which means that this is a passive panel that does not affect the numerical simulations in any way. The purpose of these panels is to monitor variables (P) related to the area the panel occupies. Panel number 119, 120 and 121 are defined as “pop out”-panels, and has the following specifications:
  Opening pressure differences = -0.25 0.1
  Initial and final porosity: 0 =closed, 1 = open
  Initial and final porosity = 0 0.8
  Weight (kg) = 6
  Drag coefficient = 1
  Maximum travel distance = 0
  Sub sizes = 10 5

- GAS COMPOSITION AND VOLUME:
  The gas cloud is positioned in the centre of FA102/FA104.
  Fill fraction, V_f/V: 0.30
  Cloud mass, E: 3203.7 kg
  Gas cloud position (x, y, z): 20235.0 5022.3 9.0
  Size of gas cloud (dx, dy, dz): 50.4 84.8 11.0
  Volume fraction: The volume fraction of the different gas components.
  Volume fraction: Methane = 0.85, Ethane 0.067, Propane = 0.08 and CO_2 = 0.003
  Equivalence ratios: Concentrations of gas inside (ER0) and outside (ER9) the gas cloud.
  Equivalence ratios (stoichiometric): ER0 = 1.0 ER9 = 0.0

- IGNITION:
  The ignition is positioned at the southwest corner of the cloud, centre z position.
  Ignition location (x, y, z): 20236.0 5023.3 14.5
  Dimension of ignition region = 0 0 0
  Time of ignition = 0
  Radmax = 0

Appendix 20: Max overpressure data from Kårstø, Åsgard.

Sim nr / Monitor nr	10	11	12	13	14	15	16	17	18	19
1	0.10	0.08	0.10	0.03	0.08	0.10	0.03	0.09	0.01	0.02
2	0.15	0.09	0.14	0.04	0.11	0.15	0.03	0.10	0.15	0.02
3	0.18	0.08	0.17	0.04	0.13	0.17	0.03	0.14	0.17	0.02
4	0.13	0.11	0.12	0.04	0.12	0.12	0.03	0.13	0.12	0.01
5	0.12	0.11	0.12	0.04	0.11	0.12	0.04	0.13	0.12	0.03
6	0.22	0.15	0.22	0.06	0.17	0.22	0.06	0.14	0.22	0.04
7	0.63	0.20	0.63	0.14	0.44	0.63	0.11	0.49	0.63	0.06
8	0.17	0.17	0.17	0.05	0.19	0.17	0.04	0.20	0.17	0.02
9	0.19	0.16	0.19	0.05	0.16	0.19	0.05	0.17	0.19	0.03
10	0.19	0.14	0.19	0.07	0.15	0.19	0.06	0.14	0.19	0.04
11	0.39	0.29	0.39	0.21	0.31	0.39	0.17	0.39	0.39	0.11
12	0.47	0.43	0.50	0.12	0.58	0.47	0.09	0.64	0.47	0.05
13	0.24	0.23	0.21	0.07	0.24	0.21	0.01	0.27	0.21	0.05
14	0.29	0.29	0.28	0.12	0.30	0.28	0.11	0.33	0.28	0.06
15	0.54	0.50	0.54	0.16	0.51	0.54	0.13	0.62	0.54	0.08
16	0.43	0.38	0.43	0.10	0.45	0.43	0.08	0.52	0.43	0.04
17	0.44	0.42	0.24	0.07	0.47	0.24	0.05	0.63	0.23	0.03
18	0.91	0.78	0.33	0.11	0.91	0.32	0.09	1.35	0.31	0.03
19	0.91	0.95	0.08	0.09	1.07	0.37	0.08	1.36	0.36	0.03
20	0.56	0.62	0.33	0.06	0.74	0.33	0.05	0.76	0.32	0.03
21	0.44	0.42	0.23	0.06	0.47	0.22	0.05	0.63	0.21	0.03
22	0.71	0.80	0.27	0.09	0.92	0.26	0.07	1.30	0.25	0.03
23	1.03	1.17	0.36	0.08	1.31	0.35	0.07	1.61	0.34	0.03
24	0.56	0.61	0.32	0.06	0.72	0.31	0.05	0.75	0.30	0.03
35	0.01	0.01	0.01	0.00	0.01	0.01	0.00	0.01	0.01	0.00
36	0.02	0.02	0.02	0.00	0.02	0.02	0.00	0.03	0.01	0.00
37	0.03	0.03	0.02	0.01	0.03	0.02	0.01	0.04	0.02	0.00
38	0.05	0.06	0.04	0.01	0.06	0.04	0.01	0.06	0.04	0.00

Appendix 21: Location of water spray, Åsgard.

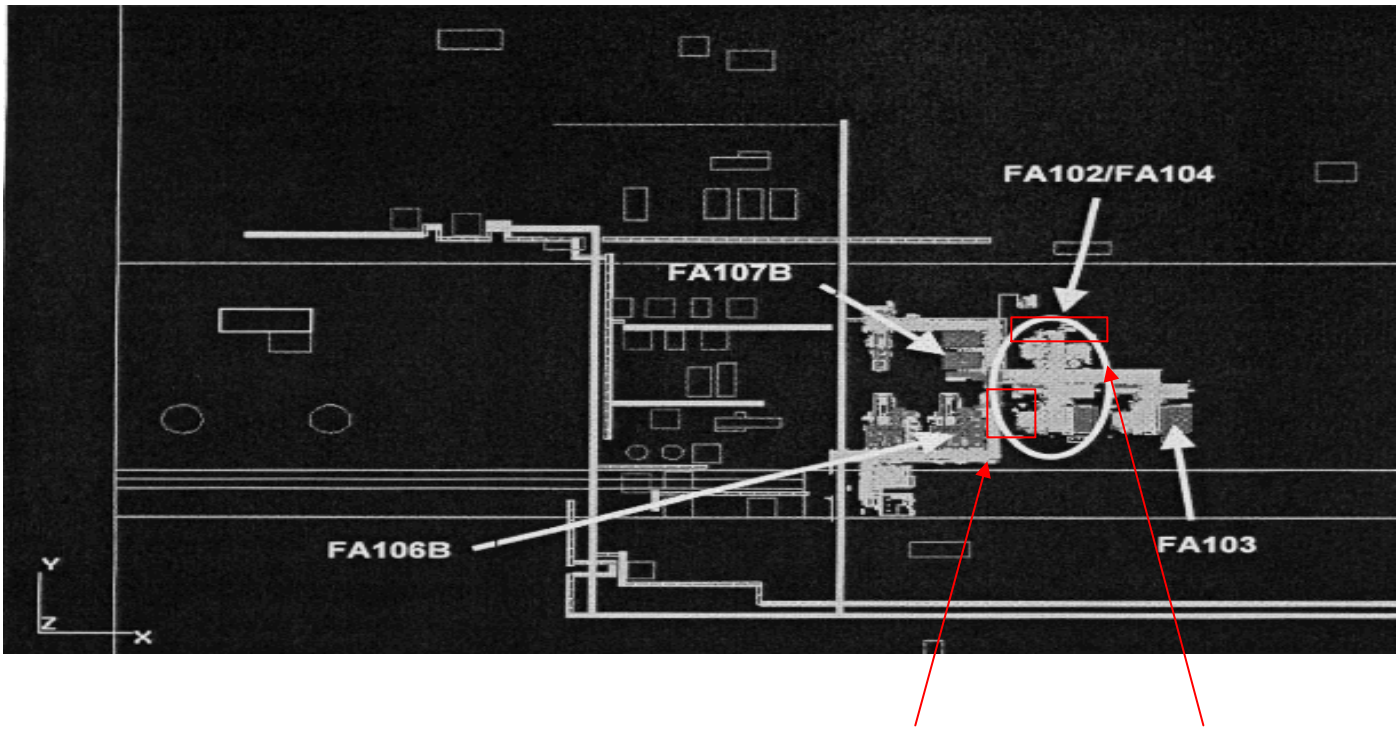

Case 1 Case 2

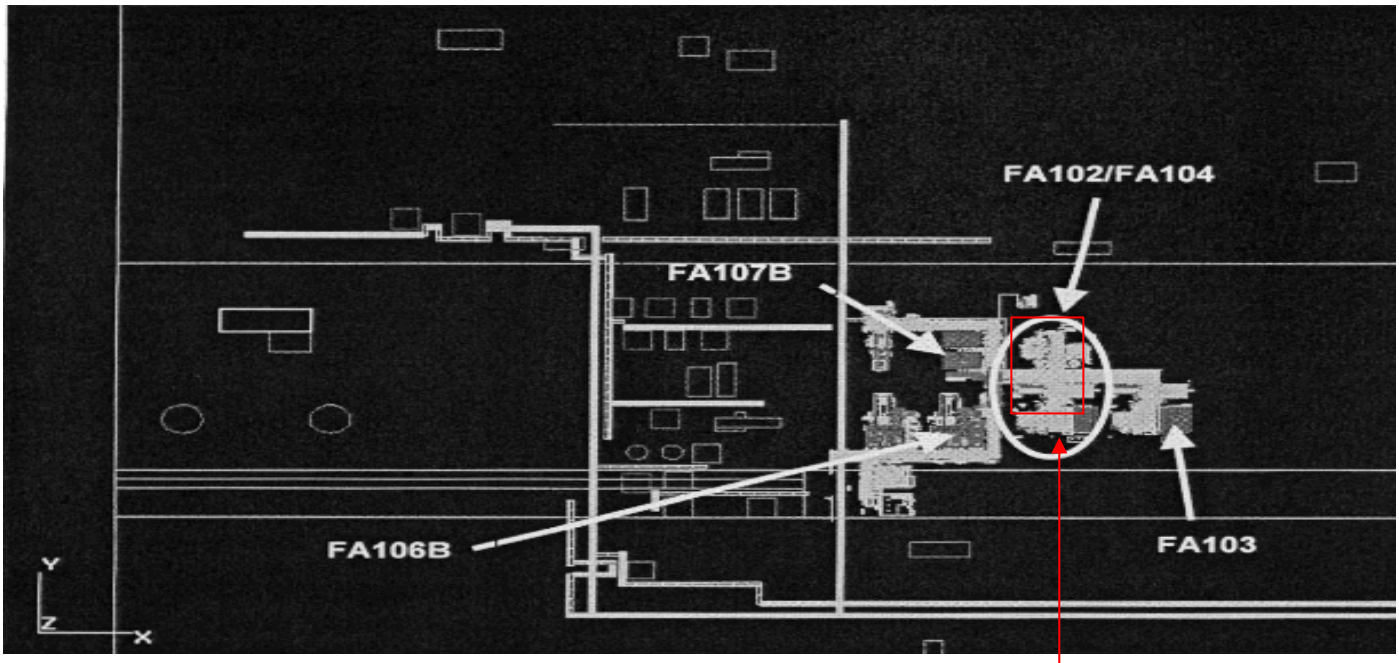

Case 3

Appendix 22: Simulation plots from Kårstø, Åsgard

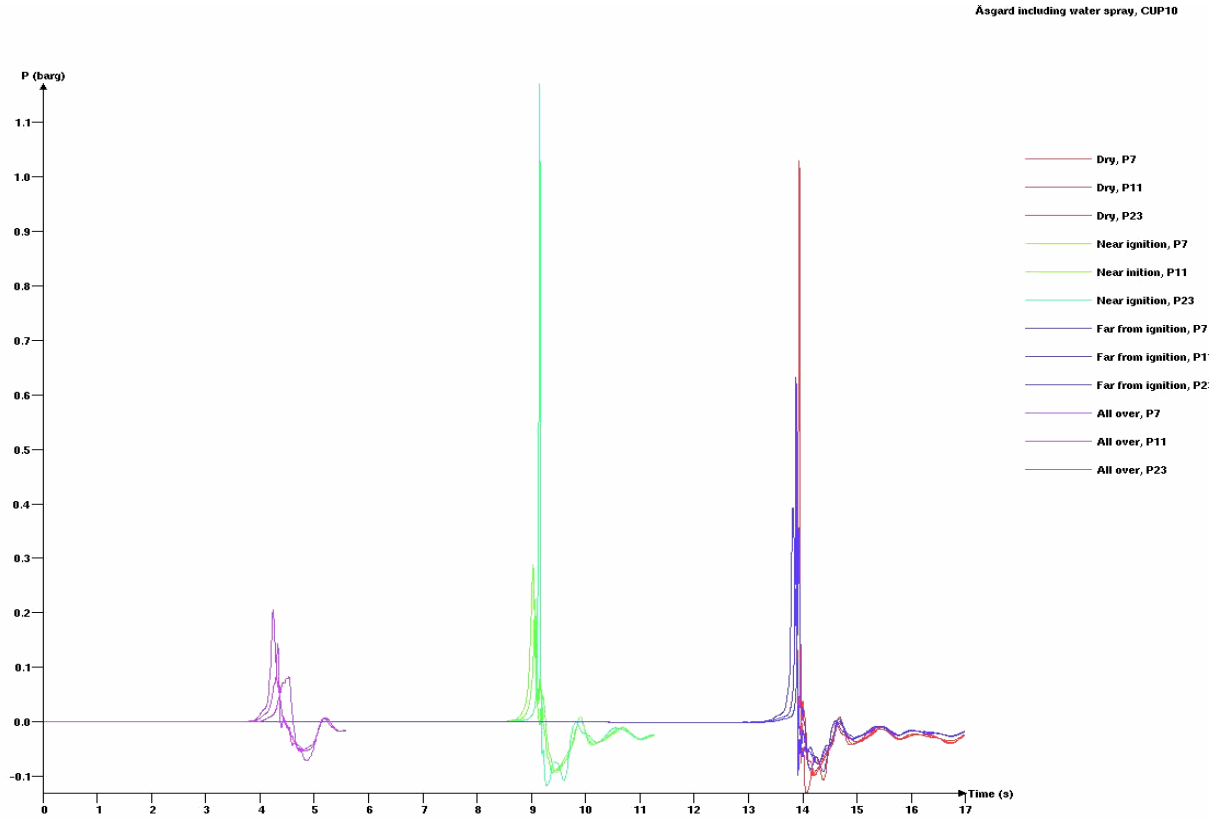

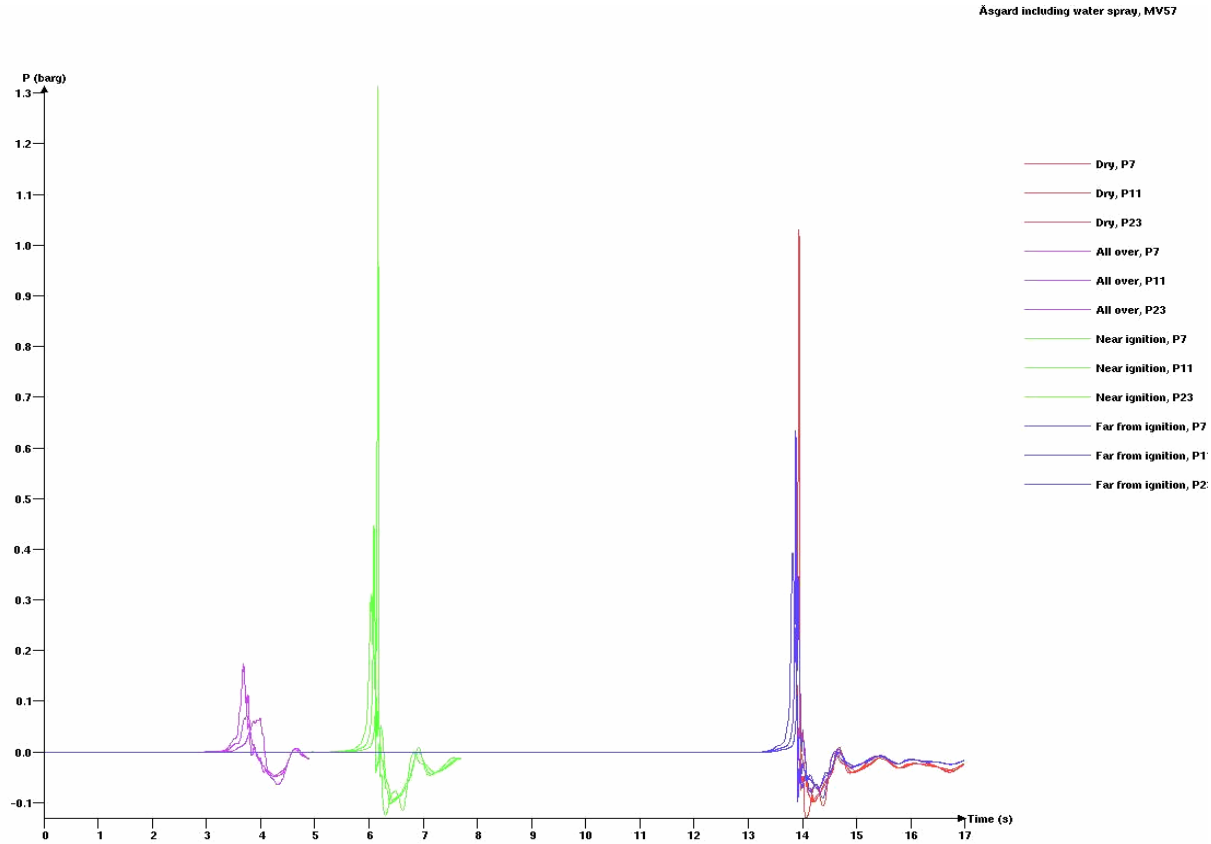

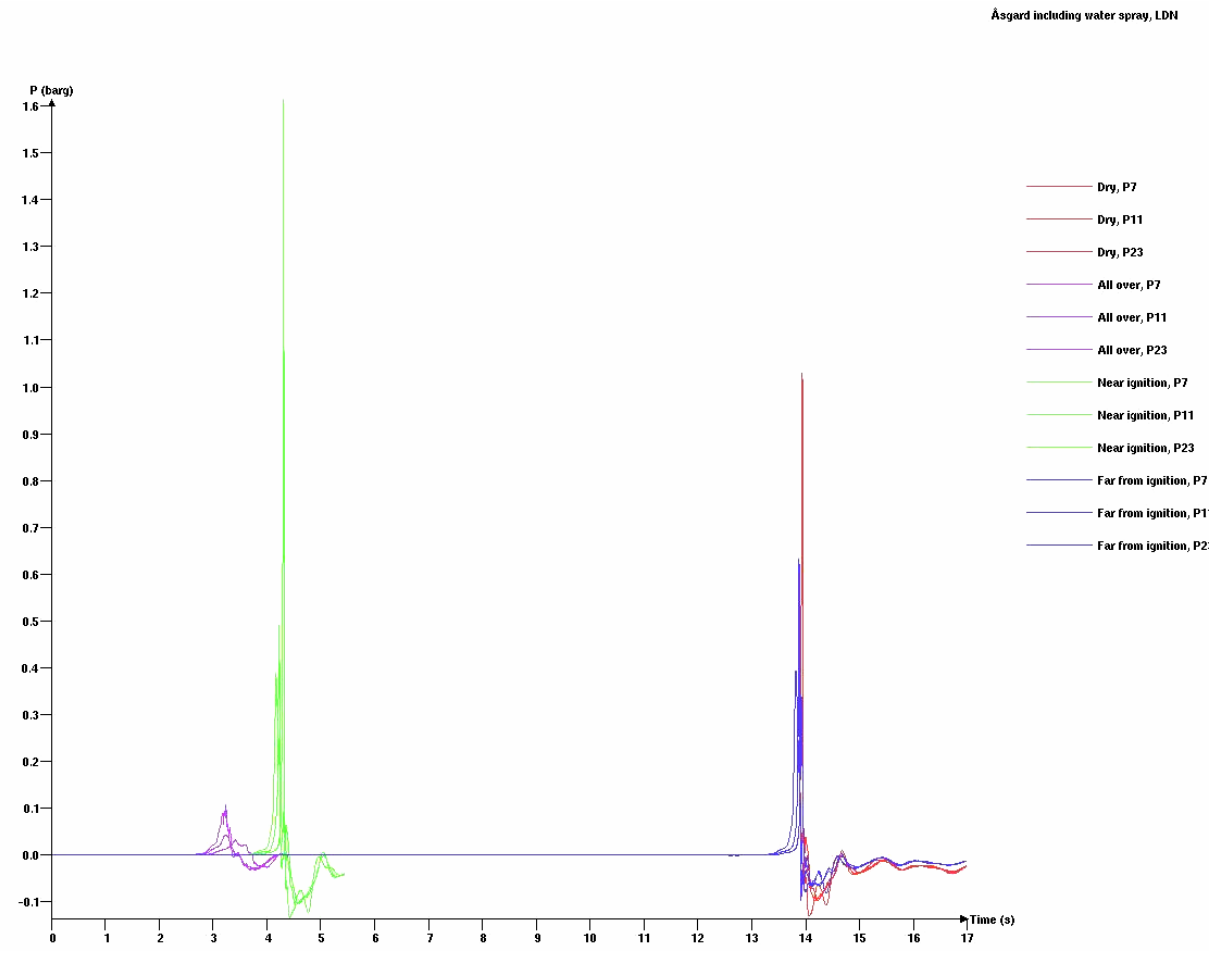
Åsgard including water spray, LDN
P (barg)
1.6
1.5
1.4
1.3
1.2
1.1
1.0
0.9
0.8
0.7
0.6
0.5
0.4
0.3
0.2
0.1
0.0
-0.1
0
1
2
3
4
5
6
7
8
9
10
11
12
13
14
15
16
17
Time (s)
Dry, P7
Dry, P11
Dry, P23
All over, P7
All over, P11
All over, P23
Near ignition, P7
Near ignition, P11
Near ignition, P23
Far from ignition, P7
Far from ignition, P1
Far from ignition, P2

Appendix 23: Scenario input for explosion box with FLACS 2.2.6*

- SINGLE FIELD SCALAR TIME AND 3D OUTPUT: Many new parameters related to the droplets can be chosen in addition to pressure (P), for example the area of particle class 1 (APART: 1) and volume of particle class 1(VPART: 1).

- SIMULATION AND OUTPUT CONTROL:
  Tmax =30, Tmax is set to 50 seconds to limit the simulation time.
  Modd = 5, the amount of data which is stored is increased to 5.

- BOUNDARY CONDITIONS: “Nozzle”

- INITIAL CONDITIONS:
  Ambient pressure: 100000Pa
  Air: “Normal”, the amount of oxygen in air is normal
  Pasquill class: None
  Ground roughness condition: “Rural”

- IGNITION:
  Time of ignition is set to 20 seconds to let the water spray build up before the gas cloud is ignited.

- LEAKS: 8 leaks are defined to represent the nozzles in explosion box.
  Type: “Jet”
  Position:

1.125	1.125	4.5
3.375	1.125	4.5
5.625	1.125	4.5
7.875	1.125	4.5
1.125	3.375	4.5
3.375	3.375	4.5
5.625	3.375	4.5
7.875	3.375	4.5

  Open sides: +-xyz
  Start time: 0
  Duration: 30

- MIXTURES:
  Name: “mixture-water”
  Fraction type: “Volume”
  Fractions: H_20 =1

- SOURCES:
  Name: “source-water”
  Mixture: “mixture-water”
  Diameter class [mm]

Class 1: 0.01
Class 2: 0.03
Class 3: 0.1
Class 4: 0.3
Class 5: 0.659 or 0.585

- REGIONS:
  Name: “region-water”
  Position: 1000 1000 1000, must be defined and is therefore placed outside the simulation area
  Source: “source-water”
  Fractions class (initial droplet diameter):
  Class 1: 0
  Class 2: 0
  Class 3: 0
  Class 4: 0
  Class 5: 1
  Temperature class:
  Class 1: 20
  Class 2: 20
  Class 3: 20
  Class 4: 20
  Class 5: 20
  Equivalence ratio: $1*10^{30}$
  Pressure: 1atm
  Temperature: 20

Appendix 24: Scenario input for dispersion simulations at Kårstø

- SINGLE FILED SCALAR TIME AND 3D OUTPUT: Some of the parameters we want to measure are fuel mass fraction (FUEL), fuel mole fraction (FMOLE), temperature (T), combustion product mass fraction (PROD) and the velocity vector (VVEC).

- SIMULATION AND OUTPUT CONTROL:
  Tmax: 60
  Last: 9999999
  CFLC: 5.0
  CFLV: 0.5
  Scale: 1
  Modd: 5
  NPLOT: Not active in gas dispersion simulations
  DTPLOT: 999999
  Grid: Cartesian
  Wallf: 1
  Heat switch: 0

- BOUNDARY CONDITIONS:
  XLO: “Wind”; wind speed = 3.2 m/s, wind direction: -1 0 0, relative turbulence intensity = 0.05, turbulence length scale = 0.5, wind build-up time = 3.
  XHI, YLO, YHI, ZLO, ZHI = “Nozzle”

- INITIAL CONDITION:
  Up-direction: 0 0 1
  Gravity constant. 9.8
  Temperature: 20
  Ground roughness condition: “Rural”

- GAS COMPOSITION AND VOLUME:
  Volume fractions: Methane: 1
  Equivalence ratios: 1E+30 0

- LEAKS:
  Edge leak:
  Insert: 1
  Type: “Jet”
  Position: 19790   4995   0
  Open sides: +Y
  Start time: 3
  Duration: 37
  Area:0. 38 m^2
  Mass flow: 878.6 kg/s
  RTI: 0.05
  TLS: 0.14

Water spray:
Insert: 2-21
Type: “Jet”
Position: see Table 5.4.3
Open sides: +-XYZ
Start time: 10
Duration: 50

- IGNITION:
  Must be defined and is thereby set outside the simulation time interval since no ignition is to occur.
  Time of ignition: 999999

  - MIXTURES:
    Name: “mixture-water”
    Fraction type: “Volume”
    Fractions: H_20 =1

  - SOURCES:
    Name: “source-water”
    Mixture: “mixture-water”
    Diameter class [mm]
    Class 1: 0.7
    Class 2: 0
    Class 3: 0
    Class 4: 0
    Class 5: 0

  - REGIONS:
    Name: “region-water”
    Position: 100000 100000 100000, must be defined and is therefore placed outside the simulation area.
    Source: “source-water”

    Fractions class (initial droplet diameter):
    Class 1: 1
    Class 2: 0
    Class 3: 0
    Class 4: 0
    Class 5: 0
    Temperature class:
    Class 1: 15
    Class 2: 15
    Class 3: 15
    Class 4: 15
    Class 5: 15
    Equivalence ratio: $1*10^{30}$
    Pressure: 1atm
    Temperature: 20

The position of the different nozzles is given in table 5.4.3.

Nozzle number	Position		
	X	Y	Z
1	19825	4950	5
2	19825	4954	5
3	19825	4958	5
4	19825	4962	5
5	19825	4966	5
6	19825	4970	5
7	19825	4974	5
8	19825	4978	5
9	19825	4982	5
10	19825	4986	5
11	19825	4990	5
12	19825	4994	5
13	19825	4998	5
14	19825	5002	5
15	19825	5006	5
16	19825	5010	5
17	19825	5014	5
18	19825	5018	5
19	19825	5022	5
20	19825	5026	5

Table 5.4.3: Position of the nozzles in the Statpipe/Sleipner area.